ER-7372

FINAL DESIGN AND QUALIFICATION OF A HYPERGOLIC ELECTRICAL POWER SYSTEM

•

FINAL REPORT
AUGUST 1969

NASA MANNED SPACECRAFT CENTER
HOUSTON, TEXAS

CONTRACT NAS 9-8247

FACILITY FORM 602
N69-37223
(ACCESSION NUMBER) (THRU)
265 1
(PAGES) (CODE)
NASA-CR 101909 26
(NASA CR OR TMX OR AD NUMBER) (CATEGORY)

TRW®
MECHANICAL PRODUCTS DIVISION

Reproduced by the CLEARINGHOUSE for Federal Scientific & Technical Information Springfield Va. 22151

NASA-CR-101909

ER-7372-1

SUPPLEMENT TO ER-7372

FINAL DESIGN AND QUALIFICATION OF A HYPERGOLIC ELECTRICAL POWER SYSTEM

•

DECEMBER 1969

NASA MANNED SPACECRAFT CENTER
HOUSTON, TEXAS

CONTRACT NAS 9-8247

TRW®
MECHANICAL PRODUCTS DIVISION

TABLE OF CONTENTS

Section	Title	Page
	LIST OF FIGURES	ii
	LIST OF TABLES	iii
1.0	INTRODUCTION	1
2.0	SUMMARY	2
3.0	CONCLUSIONS	4
4.0	ASSEMBLY	5
	4.1 Configuration	5
	4.2 Mass Properties	14
5.0	TEST PROGRAM	23
	5.1 Acceptance	23
	5.2 Development	23
6.0	TEST RESULTS	25
	6.1 Acceptance	25
	6.2 Development	25
7.0	TEST LOG (APPENDIX)	A-1

LIST OF FIGURES

Figure No.	Title	Page
2-1	HEPS Unit (Deployed)	3
4-1	HEPS Left Side (Stowed)	6
4-2	HEPS Rear View (Stowed)	7
4-3	HEPS Right Side View (Stowed) . . .	8
4-4	HEPS Front View (Stowed)	9
4-5	HEPS Right Side View (Stowed) . . .	10
4-6	HEPS Right/Rear View (Deployed) . .	11
4-7	HEPS Left/Rear View (Deployed) . .	12
4-8	HEPS Left Side View (Stowed) . . .	13
4-9	HEPS Front View (Stowed)	15
4-10	HEPS Right View (Stowed)	16
4-11	HEPS Front View (Partially Deployed) .	17
4-12	HEPS Rear View (Stowed)	18
4-13	View Looking Into "HEPS" Storage Bay .	19
4-14	View Looking at "HEPS" From the Right Side	20
4-15	HEPS Weight Breakdown	20
5-1	Acceptance Test Load Profile . . .	24
6-1	Specific Propellant Consumption - Low O/F - Phase II and Phase III Comparison (010-4.1-017, -018) (011-4.2-001, -002) .	28
6-2	Phase II & III Coast Time Comparison Data From Tests (010-4.1-017, -018) (011-4.2-001, -002)	29
6-3	HEPS Qualification Unit (After Test) .	32
6-4	HEPS Qualification Unit (After Test) .	33

LIST OF TABLES

Table No.	Title	Page
6-1	Acceptance Test	26&27
6-2	SPC Comparison, Lb/KW-Hr	30

PRECEDING PAGE BLANK NOT FILMED.

LIST OF FIGURES

Fig. No.	Title	Page
2.0-1	HEPS Qualification Unit Model (Deployed)	4
2.0-2	Hypergolic Electrical Power System	5
4.1-1	Valve Seat Configuration	11
4.1-2	DVR Gas Generator, Turboalternator, and Rectifier Cold Plate	14
4.1-3	DVR Gas Generator	15
4.2-1	Lubrication System Schematic	17
4.2-2	DVR Rear View	18
4.2-3	DVR Radiator Panels - Front View	19
4.2-4	DVR Right View	20
4.2-5	DVR Right Side View	21
4.2-6	DVR Right Top View	22
4.2-7	DVR Left Side View	23
4.2-8	Phase Separator	26
4.3-1	Block Diagram, Electrical System	33-34
4.3-2	Speed Control Schematic	35-36
4.3-3	Control Panel Schematic	37-38
4.3-4	Voltage Regulator Schematic	39-40
4.3-5	Rectifier Filter Schematic	41
5.2-1	DVR Speed Control	47
5.3-1	DVR Voltage Regulator	49
5.4-1	DVR Control Panel	50
6.1-1	Operating Location - Landing Strut Mounting	55
6.2-1	LM Descent Stage and View Looking Down	58

LIST OF FIGURES

Fig. No.	Title	Page
6.2-2	HEPS Envelope	59
6.3-1	Surveyor Spacecraft Model A-21 Equipment Specification 224832	63
6.3-2	Variation of Radiating Effectiveness with Fin Plate Length	67
6.5-1	HEPS Package - Stowed	77
6.5-2	HEPS Package - Deployed	78
6.5-3	HEPS Package - Deployed	79
6.5-4	HEPS - Turboalternator and Frame . . .	80
6.5-5	HEPS - Frame Extension Mechanism and Electronic Packages	81
6.5-6	HEPS - Turboalternator Heat Reflector and Frame	82
6.5-7	HEPS Package - Stowed	84
6.5-8	HEPS Package - Deployed	85
6.5-9	HEPS Package - Deployed	86
6.5-10	HEPS Qualification Unit Model	87
6.5-11	HEPS Qualification Unit Model	88
6.5-12	HEPS Qualification Unit Model	89
6.5-14	HEPS Qualification Unit Model	91
6.5-15	HEPS Qualification Unit Model	92
6.5-16	HEPS Qualification Unit Model	93
6.5-17	HEPS Package - Stowed Propellant Lines and Electrical Harnesses	94
6.5-18	HEPS Package - Deployed Propellant Lines and Electrical Harnesses	95

LIST OF FIGURES

Fig. No.	Title	Page
6.6-1	DVR Pin Connected Frame and Vibration Mount Location	99
6.6-2	Force Analysis of Pin Connection Frame for Load in ± X Direction Indicating the Major Forces	100
6.6-3	Force Analysis of Pin Connection Frame for Load in ± Y Direction Indicating the Major Forces	101
6.6-4	Force Analysis of Pin Connection Framd and Load in ± Z Direction Indicating the Major Forces	102
6.6-5	HEPS All-Welded Frame	105
6.6-6	Original Concept of Uniball Mountings	106
6.6-7	Final Concept for Mounting Turboalternator on the All-Welded Frame	108
6.6-8	Chassis Slides	109
6.7-1	HEPS Vibration Mounts	111
6.8-1	Extraction of HEPS Package from LM Equipment Bay	113
6.8-2	Deployment of Oil Radiator	114
6.8-3	Deployment of Rectifier Cold Plate	115
6.8-4	Deployment of Speed Control Box	117
7.3-1	Front Slide Oxygen-Free High Purity Copper Substrate After Exposure	124
7.3-2	Microprobe Analysis of Nickel in Fe_2TiO_5 Coated Hastelloy X	125
7.3-3	Microprobe Analysis of Nickel in Fe_2TiO_5 Coated Hastelloy X	126
7.3-4	Fe_2TiO_5 on Hastelloy X	127

LIST OF FIGURES

Fig. No.	Title	Page
7.3-5	Fe_2TiO_5 on Hastelloy X	128
8.1-1	Control Panel Layout	132
8.1-2	Altitude Chamber VPI Test Facility	134
8.1-3	HEPS Propellant Feed System	135
8.1-4	Chiller-Heater System	137
8.2-1	Pressure Drop Versus Flow	139
8.2-2	Pressure Drop Versus Flow	140
8.2-3	Thermal Data Presentation - DVR Gas Generator Component Tests (Test 013)	144
8.2-4	Thermal Data Presentation - DVR Gas Generator Component Tests (Test 027)	145
8.2-5	Flexure Tube Failure	146
8.3-1	HEPS Lubrication System Simulation	148
8.3-2	Alternator Mechanical Losses Versus Shaft Speed	150
8.3-3	Alternator/Lubrication Test Rig	151
8.3-4	Alternator Component Losses Versus Shaft Speed	152
8.3-5	Alternator Lubrication and Cooling Schematic	154
8.3-6	Alternator Mechanical Losses Versus Shaft Speed	155
8.3-7	Alternator Component Test Configuration	156
8.3-8	Modifications of Alternator Oil Jets	158
8.3-9	Alternator Mechanical Losses Versus Shaft Speed	159

LIST OF FIGURES

Fig. No.	Title	Page
8.3-10	Location of Thermocouples for the Alternator Component Tests	161
8.3-11	Temperature in Alternator During High Temperature Tests	162
8.3-12	Alternator Bearings After High Temperature Tests	163
8.3-13	Shaft Seal After High Temperature Tests	164
8.3-14	Alternator Components After High Temperature Tests	165
8.3-15	Lube System Temperature Profile	166
8.3-16	Density Versus Temperature for MIL-L-23699 Oil	168
8.3-17	Surface Tension Versus Temperature for MIL-L-23699 Oil	169
8.3-18	Pressure Drop Versus Flow Rate for MIL-L-23699 Oil and 35μ Screen	170
8.3-19	Pressure Drop Versus Flow Rate for MIL-L-23699 Oil and 60μ Screen	171
8.3-20	HEPS Oil Flow Simulation System	173
8.4-1	Voltage Regulator Drive Constant I_{FIELD} = 1.5 Amperes - DVR Unit 010	175
8.4-2	Pulse Width and Pulsing Period Variations with Temperature	176
8.4-3	Voltage Regulation Characteristic	177
8.5-1	DVR Rotating Assembly	178
8.5-2	DVR Unit - Right Side	179
8.5-3	DVR Unit - Left Side	180
8.5-4	DVR Unit - Left Bar	181
8.5.5	DVR Unit - Rear	182

LIST OF FIGURES

Fig. No.	Title	Page
8.5-6	DVR Unit - Right Front	183
8.5-7	Phase II & III Coast Time Comparison	185
8.5-8	Phase II & III Spc. Comparison	186
8.5-9	Specific Propellant Consumtption - Low O/F - DVR Tests	187
8.5-10	Specific Propellant Consumption - High O/F - DVR Tests	188
8.5-11	Lunar Staytime Versus Load, DVR - Phase III	189
8.5-12	Test 010-4.1-0.7 - 160°F Ambient - Oil Flow: 0.9-1.0 gpm	192
8.5-13	Oil Pressure and Temperature Versus Time	193
8.5-14	Oil Pressure and Temperature Versus Time	194
8.5-15	Radiator Inlet Pressure Versus Oil Temperature	195
8.5-16	Oil Temperature Versus Load	196
8.5-17	Oil Radiator Temperature Profile and Performance	197
8.5-18	T/A Temperature Versus Load	198
8.5-19	Temperature Versus Load	199
8.5-20	Alternator Mount and Mounting Rail Thermocouples	202
8.5-21	Alternator Mount and Rails Temperature Profile	203
8.5-22	Rectifier Cold Plate Thermocouple	204
8.5-23	Lower Diode Stud Temperature Versus Load	205
8.5-24	Temperature Versus Load	206
8.5-25	Heat Reflector Thermocouples	207
8.5-26	Reflector Temperature Versus Load	208

LIST OF FIGURES

Fig. No.	Title	Page
8.5-27	Frame Temperature at 3 KW	209
9.1-1	Power Profile	214
10.1-1	Percentages of Total Failure Modes for Various System Conditions	218
10.4-1	A Functional Block Diagram of a Modified Gas Generator Assembly	223
10.4-2	System Reliability Versus Time	224

PRECEDING PAGE BLANK NOT FILMED.

LIST OF TABLES

Table No.	Title	Page
4.1-1	Dribble Volume History	10
4.1-2	Gas Generator Design Data	12
4.2-1	Lubrication System Component Identification	24
5.1-1	HEPS Electrical System Performance Data	44,45,46
7.3-1	Selected Thermal Characteristics and Thermal Control Coatings for Radiating Surfaces	121
7.3-2	Emissivity of Calcium Titanate and Iron Titanate	122
8.2-1	DVR Gas Generator Test Data Summary	141,142
8.3-1	HEPS Oil Separator Simulation Test	172
8.5-1	HEPS Lubrication System Performance	191
8.5-2	DVR Test and Data Correlations	200
9.1-1	Startup Test Sequence	213
10.1-1	Summary of Type Failure for Various System Conditions	219
10.1-2	State of Indicator Lights for Various System Conditions	220

1.0 INTRODUCTION

This report describes the work performed from August 1969 to December 1969 in the development of a hypergolic electrical power system. Phase I of this work was performed previously under NASA Contract NASA Contract 9-4820 and was continued as Phase II under Contract NAS 9-6879. The NASA Contract NAS 9-8247 covers Phase III activity. The effort during the Phase III program was directed toward design finalization, fabrication and testing of a flight qualification system which could be used in conjunction with the LM providing electrical power for additional lunar stay time. The work described in this report includes the results of acceptance and system development tests.

2.0 SUMMARY

A Qualification Unit, incorporating the latest HEPS design improvements was fabricated and tested. The unit incorporated an all welded frame, an extension mechanism using Jonathan supplied slides, and all electrical subsystems. Approximately 14 hours of test time was accumulated on this unit including the 2.5 hour Acceptance Test. The Acceptance Test was conducted at a chamber wall temperature of 77°F with loads ranging from 0 to 3 KW with spikes to 4.5 KW. Thermal tests were conducted with 160°F chamber wall temperature to evaluate the thermal characteristics and limitations of the system. The HEPS Qualification Unit is shown in Figure 2-1.

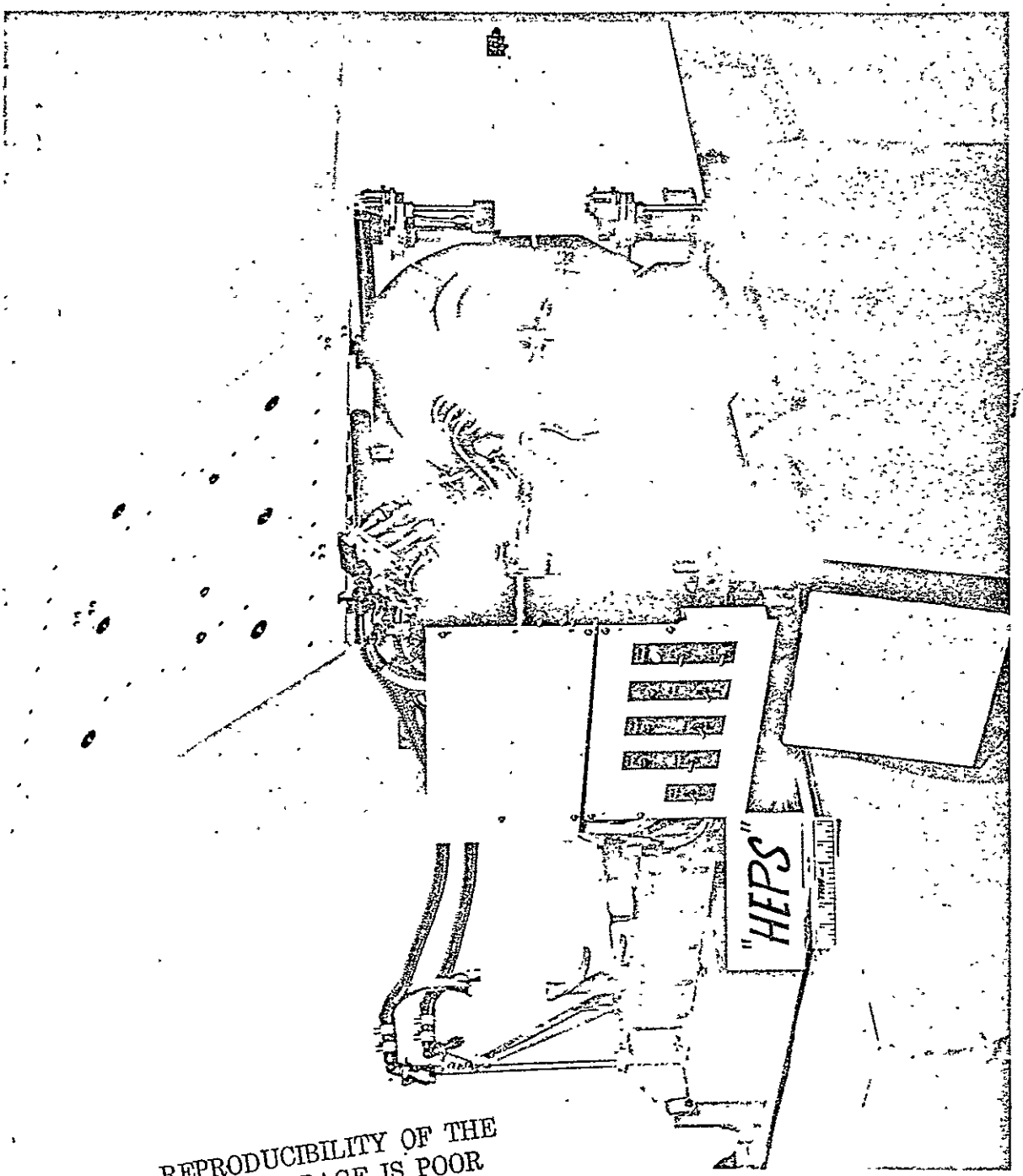


FIGURE 2-1 HEPS UNIT (DEPLOYED)

REPRODUCIBILITY OF THE
ORIGINAL PAGE IS POOR

3.0 CONCLUSIONS

Successful completion of the Acceptance Test demonstrated the system capability to operate over a typical load profile described in the Acceptance Test Plan, ER-7380. Subsequent testing revealed that the thermal limitations of the system could be exceeded if operated above 2.0 KW continuously with a heat sink temperature of 160°F. Additional thermal design considerations could eliminate this limitation.

Specific propellant consumption was increased by 15% but decreased 35% compared to the DVR and Phase II units respectively. The decrease in performance compared to the DVR unit, was caused by higher friction losses resulting from more positive lubrication to the roller bearing. The improvement over the Phase II unit performance was attributed to decreased frictional losses caused by generally lower oil flows directed to the bearings.

Performance improvement could be obtained by redirecting the roller bearing oil flow to the adjacent shaft area thus reducing oil churning losses.

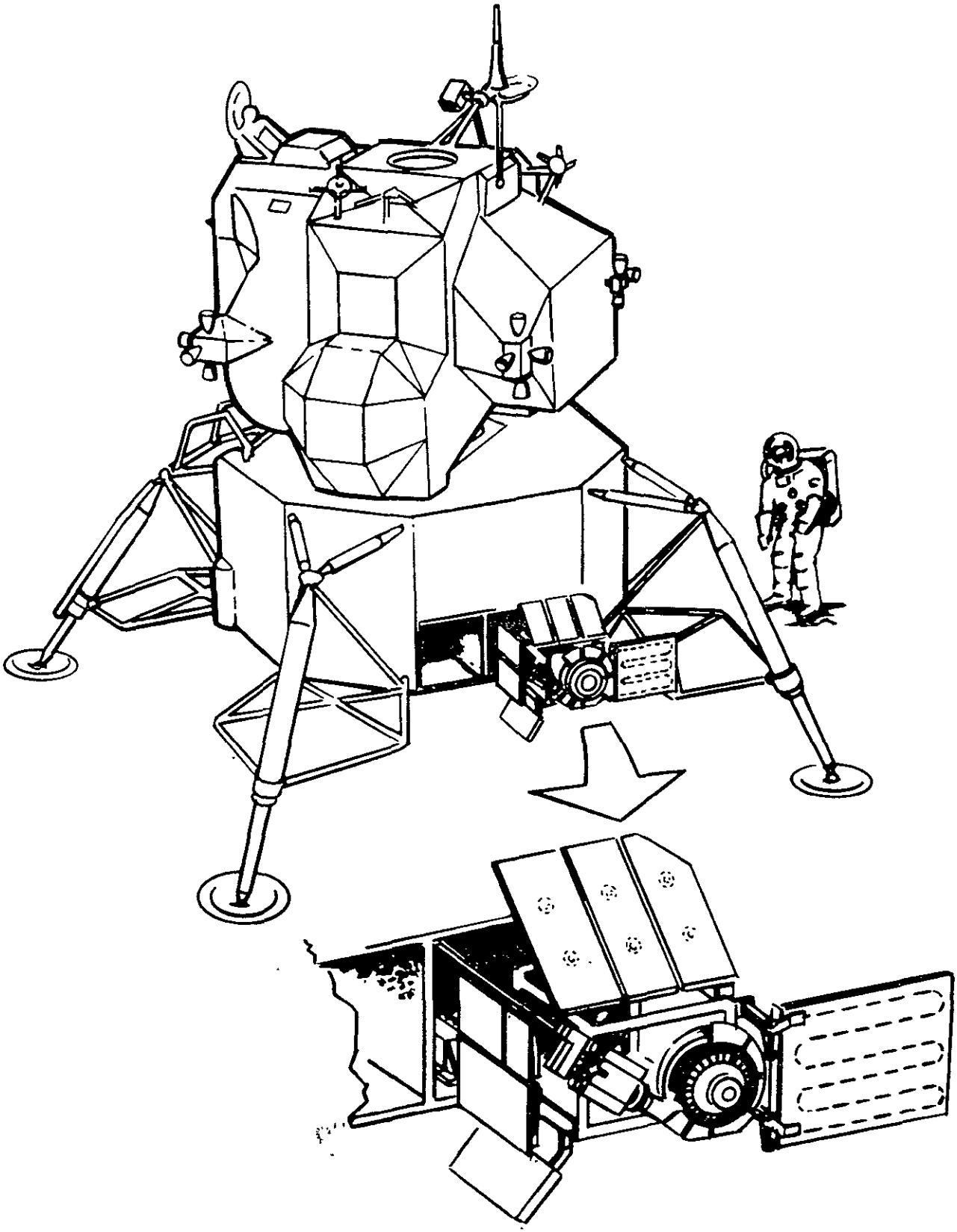


FIGURE 2.0-2 HYPERGOLIC ELECTRICAL POWER SYSTEM

REPRODUCIBILITY OF THE
ORIGINAL PAGE IS POOR

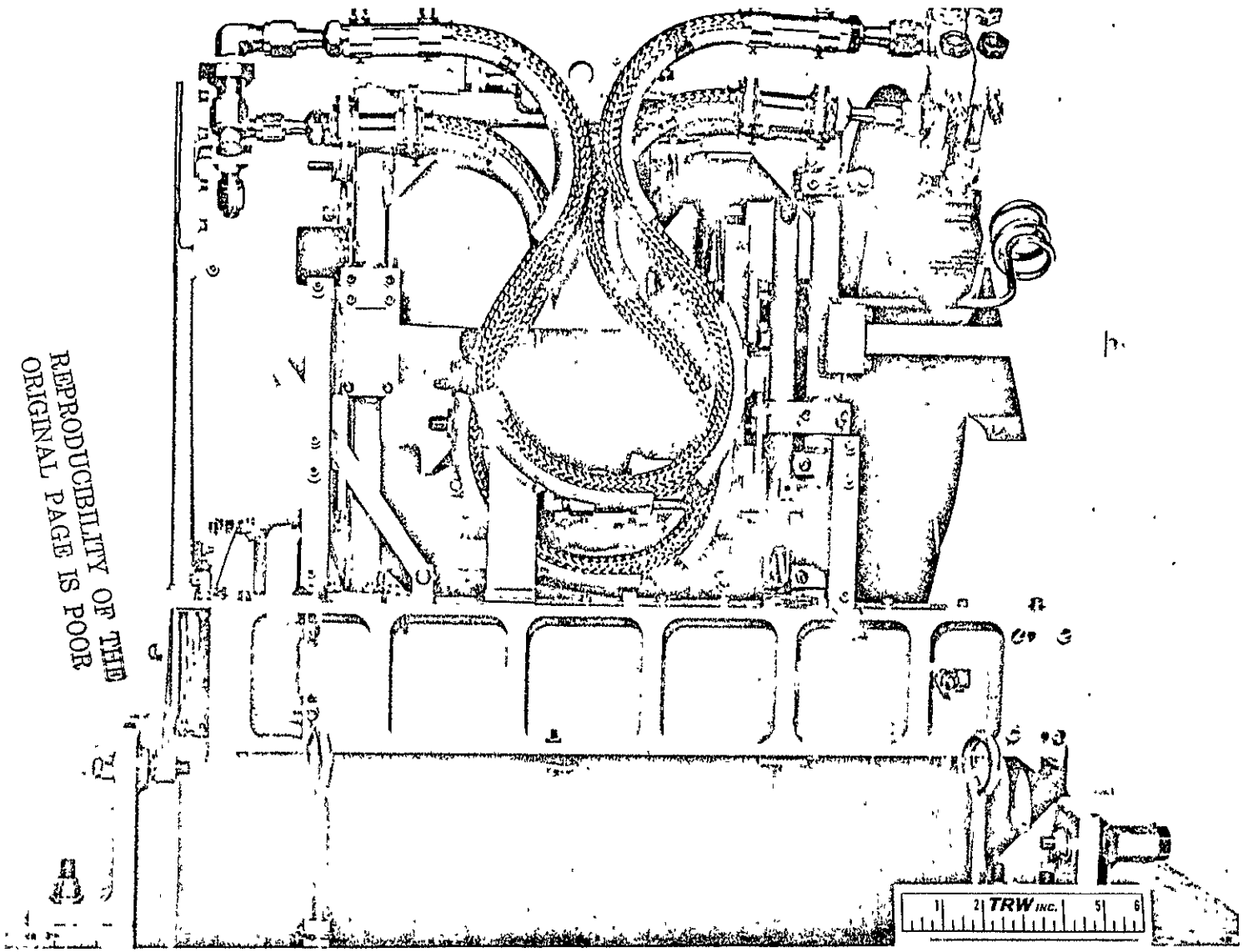


FIGURE 4-1 HEPS LEFT SIDE (STOWED)

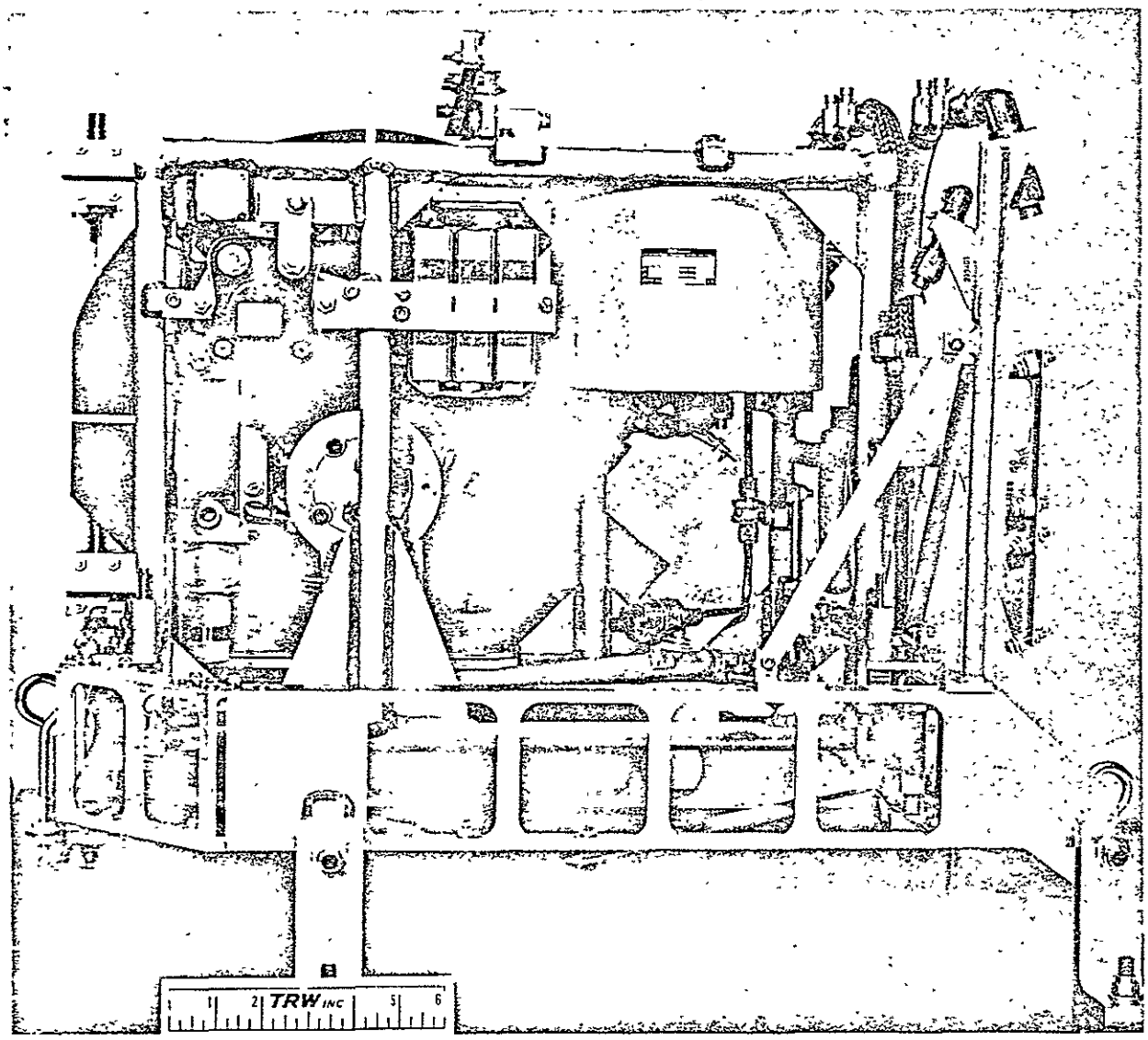


FIGURE 4-2 HEPS REAR VIEW (STOWED)

REPRODUCIBILITY OF THE
ORIGINAL PAGE IS POOR

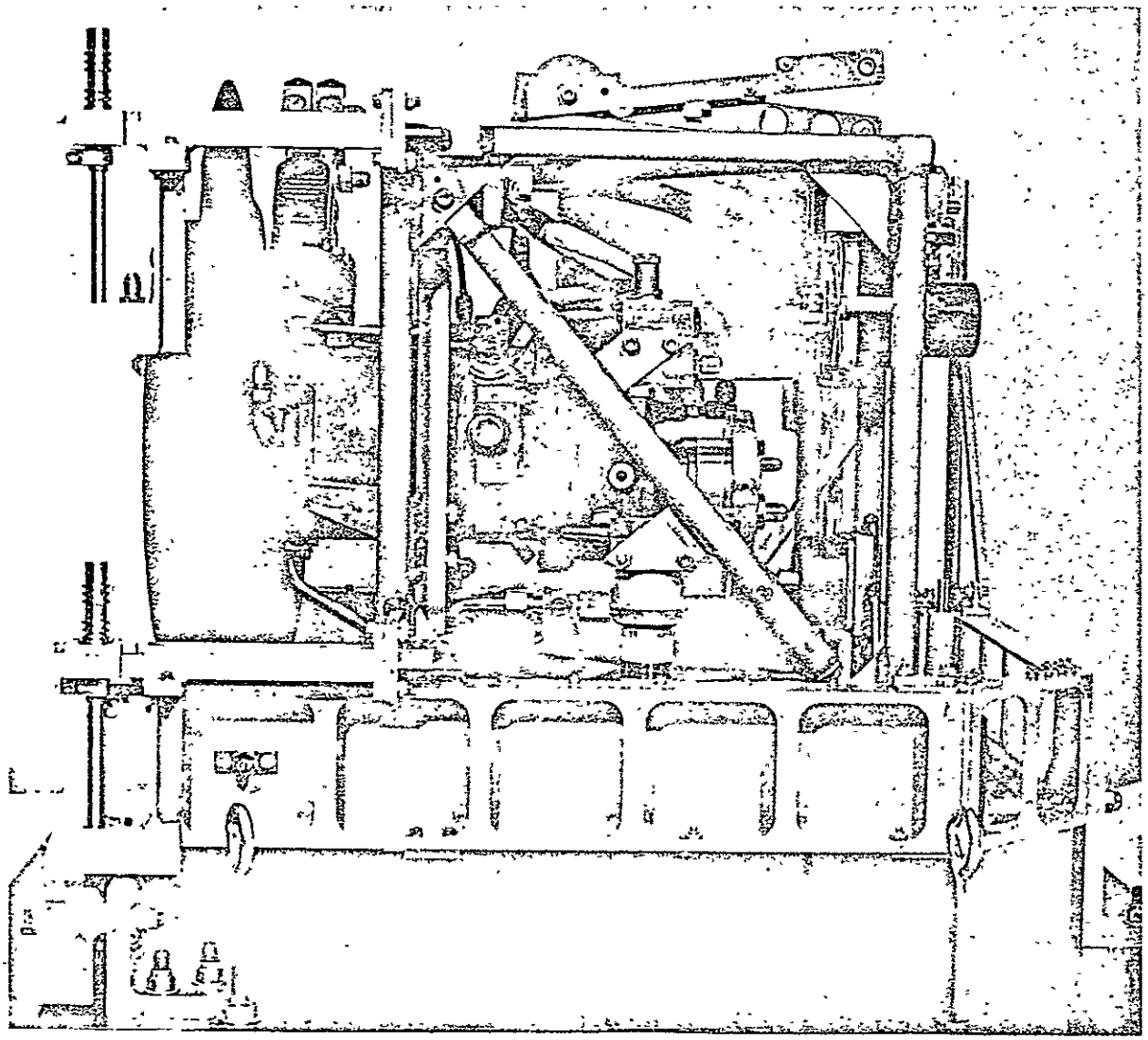


FIGURE 4-3 HEPS RIGHT SIDE VIEW (STOWED)

REPRODUCIBILITY OF THE
ORIGINAL PAGE IS POOR

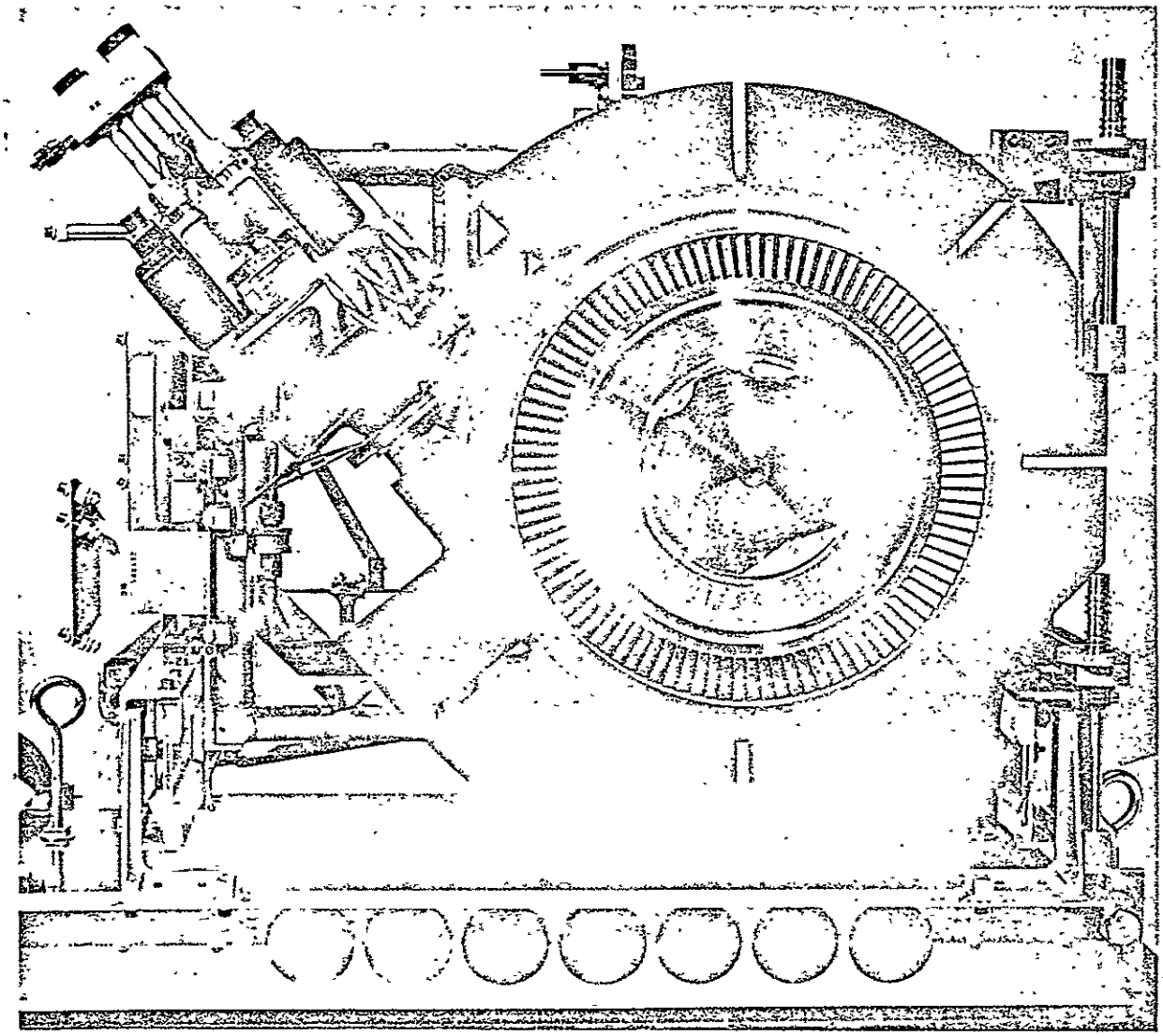
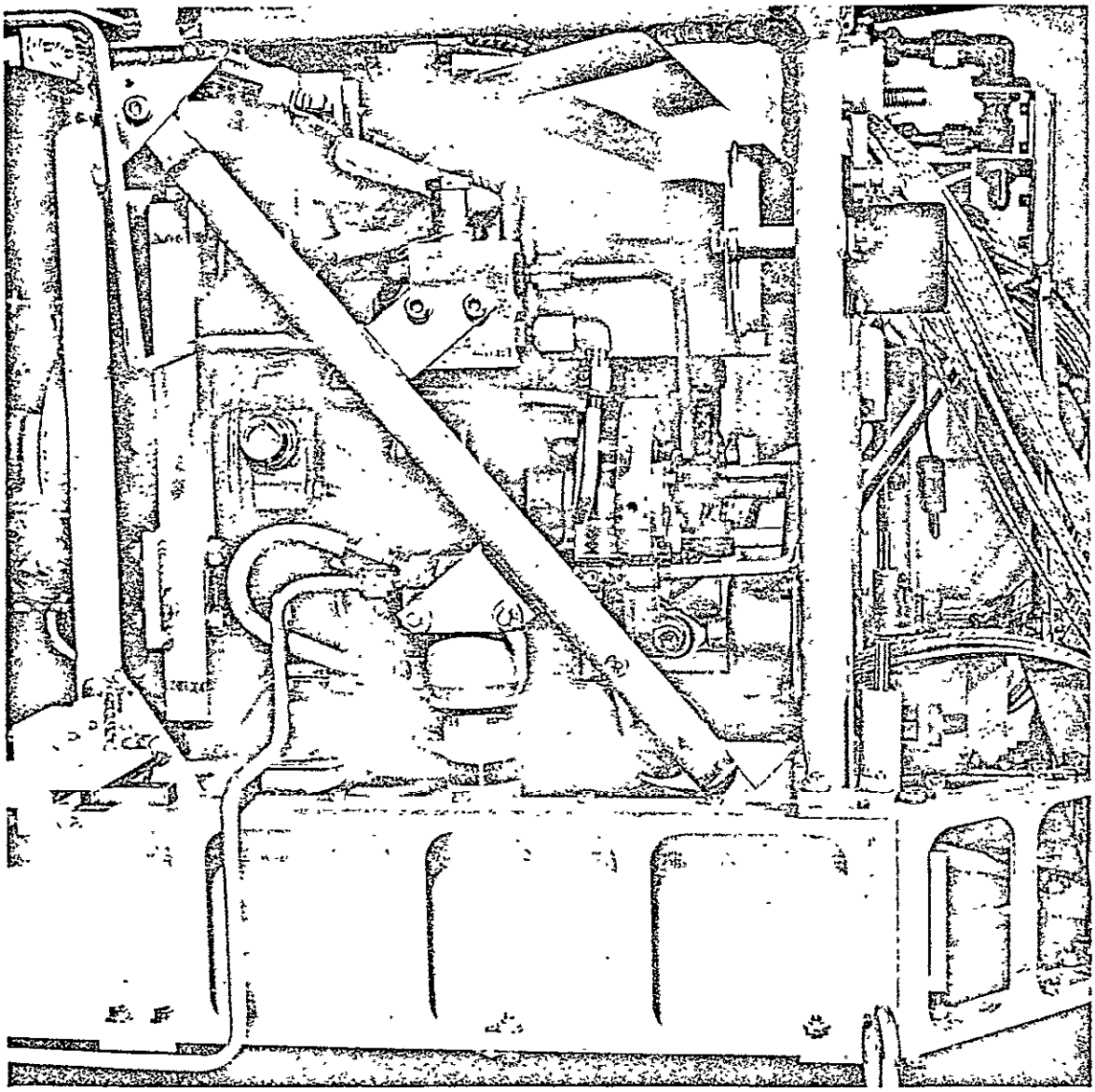


FIGURE 4-4 HEPS FRONT VIEW (STOWED)



REPRODUCIBILITY OF THE
ORIGINAL PAGE IS POOR

FIGURE 4-5 HEPS RIGHT SIDE VIEW (STOWED)

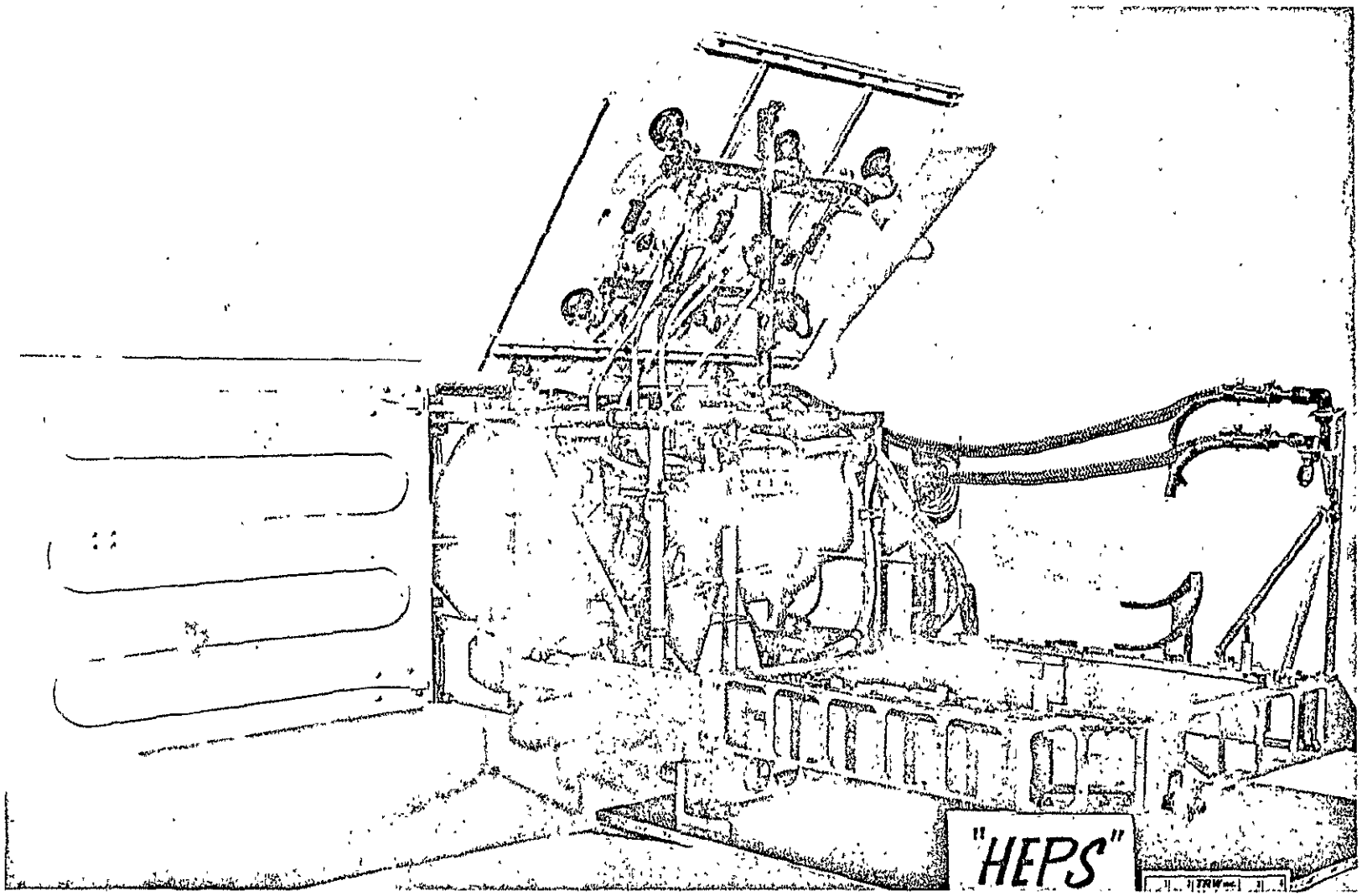


FIGURE 4-6 HEPS RIGHT/REAR VIEW (DEPLOYED)

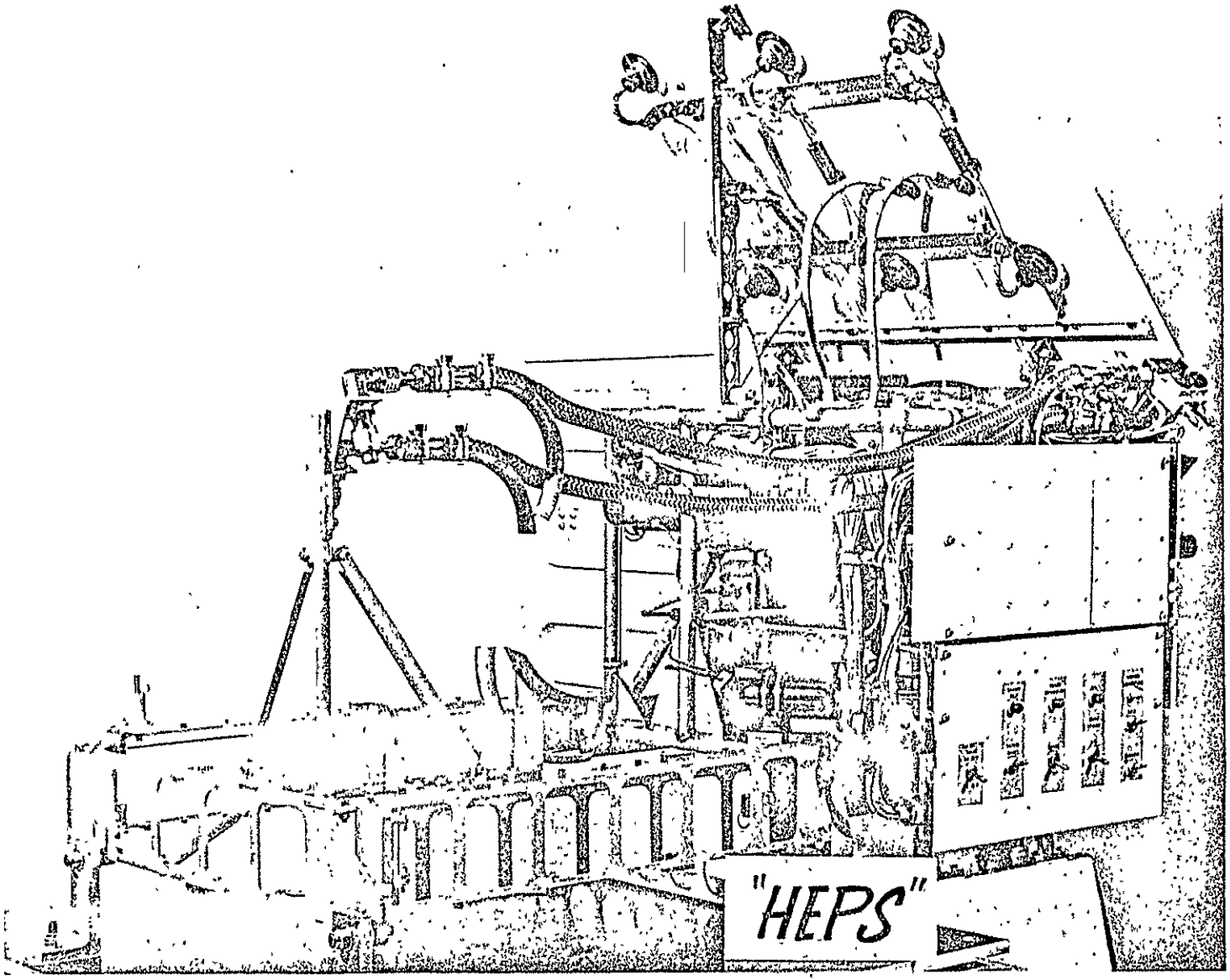


FIGURE 4-7 HEPS LEFT/REAR VIEW (DEPLOYED)

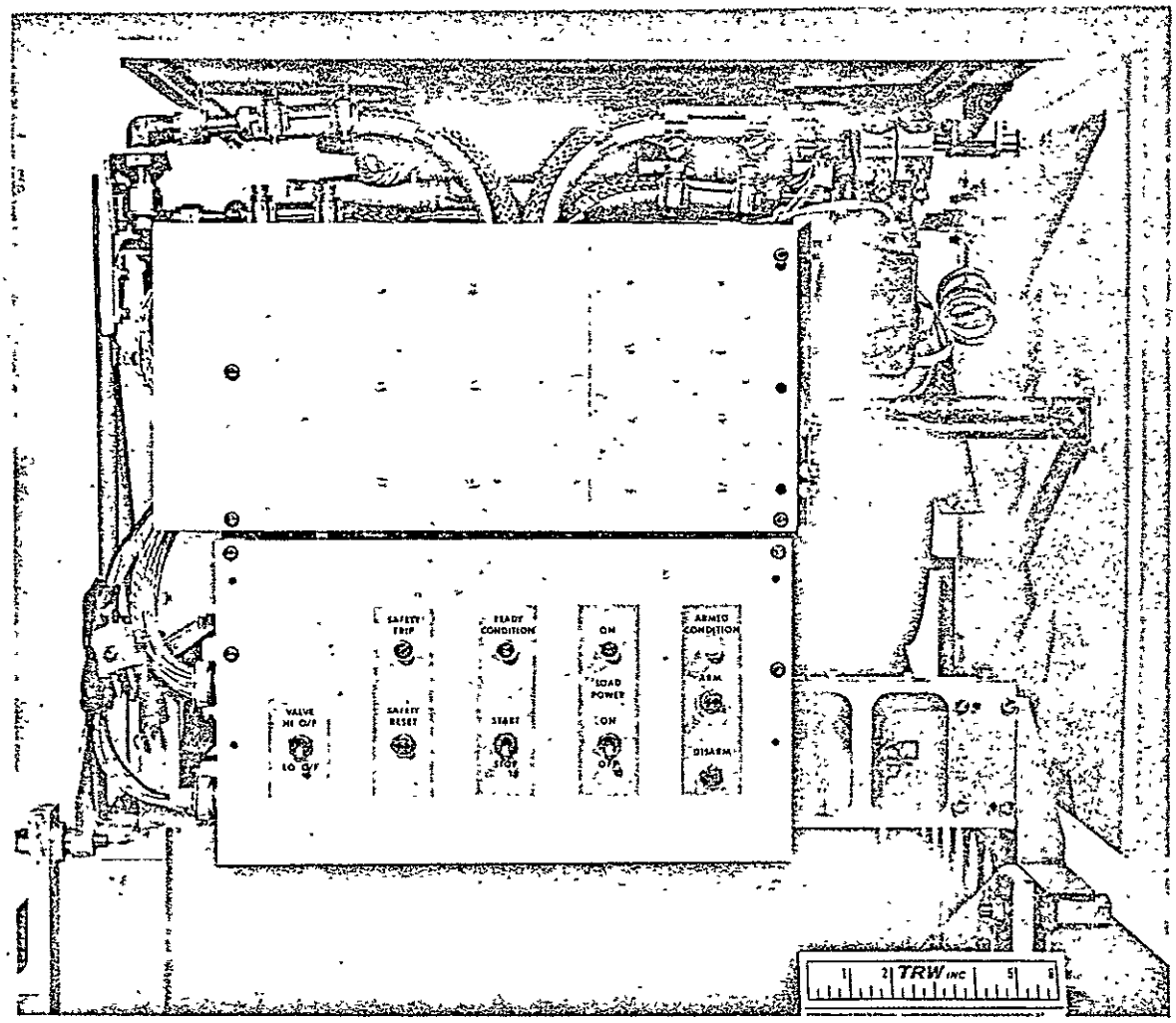


FIGURE 4-8 HEPS LEFT SIDE VIEW (STOWED)

REPRODUCIBILITY OF THE
ORIGINAL PAGE IS POOR

hard mount pins. Figure 4-9 and 4-10 show the front and right side view of the stowed HEPS. Also shown in Figure 4-10 are the details of the lubrication system associated with the oil radiator. The HEPS unit is shown in a stowed position with the oil radiator deployed in Figure 4-11. The heat reflector, used to prevent high scroll radiation to cooler components, is seen in Figure 4-11. The rear view of the HEPS in a stowed position is shown in Figure 4-12.

4.2 Mass Properties

The mass properties for the HEPS were measured prior to shipment to the test site. The coordinate system used is shown in Figures 4-13 and 4-14 and does not relate to the "LM" coordinate system because the sides of the SEQ Bay No. 2 envelope for the HEPS are at a 45° angle with the "LM" system. The coordinate system shown is identified with three mutually perpendicular datum planes on the "LM" and can therefore be translated and rotated to the "LM" system. In the data presented the x, y and z axes pass through the HEPS center of gravity.

The HEPS was weighed at 191.0 lb, exclusive of oil weight, which is 8.5 lb at 4 quarts inventory. A breakdown of various component weights is shown in Figure 4-15 so as to identify various weight concentrations in the package.

The center of gravity and moments of inertia about the three principal axes were measured by a standard gravity pendulum method. The center of gravity is shown located with respect to the three "LM" datum planes in Figures 4-13 and 4-14 and the moments of inertia are as follows:

A. $I_{x-x} = 53$ lb-in.-sec^2

B. $I_{y-y} = 54$ lb-in.-sec^2

C. $I_{z-z} = 33$ lb-in.-sec^2

The moments were calculated by substitution of the required parameters measured during the three different pendulum position motions.

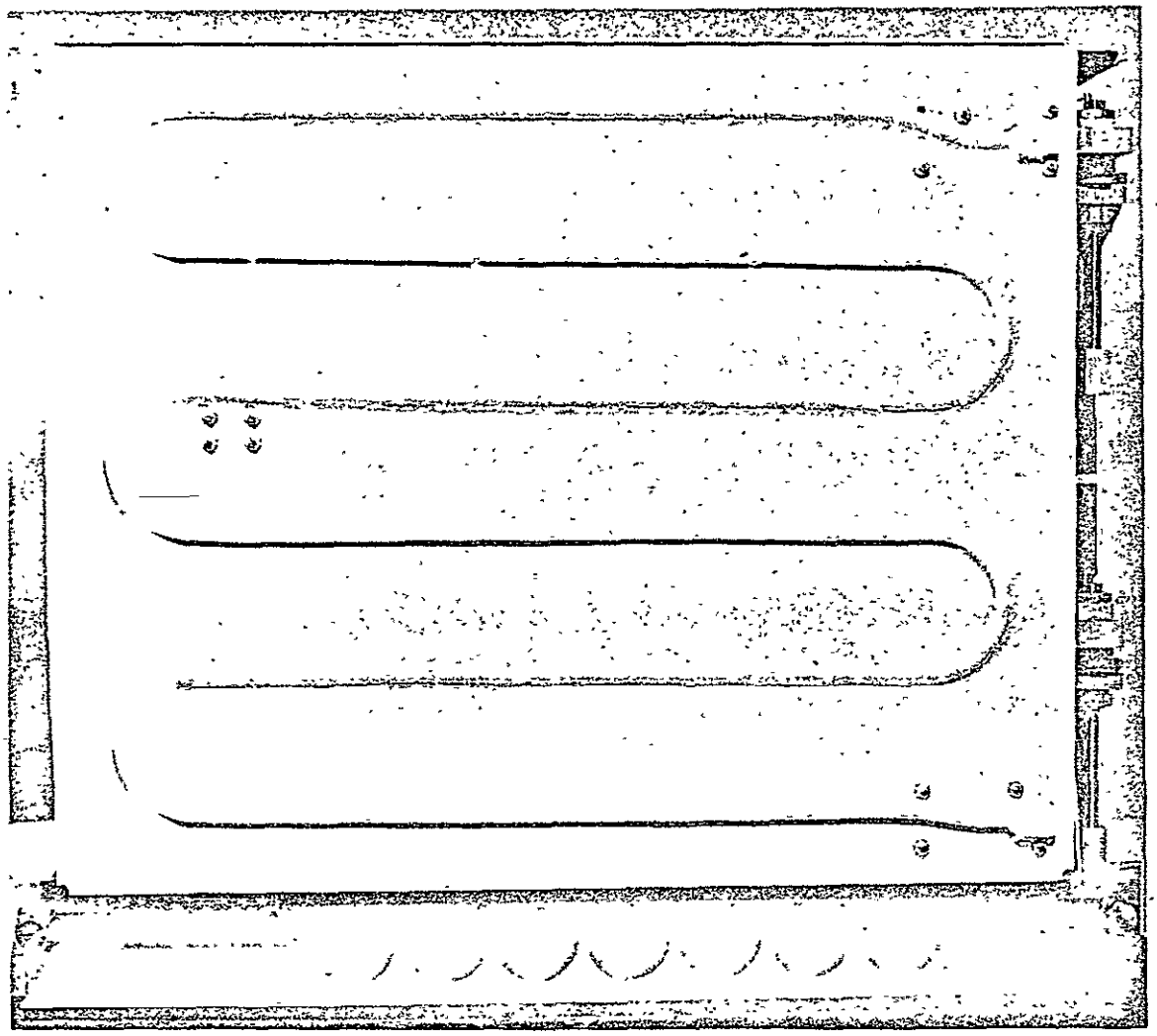
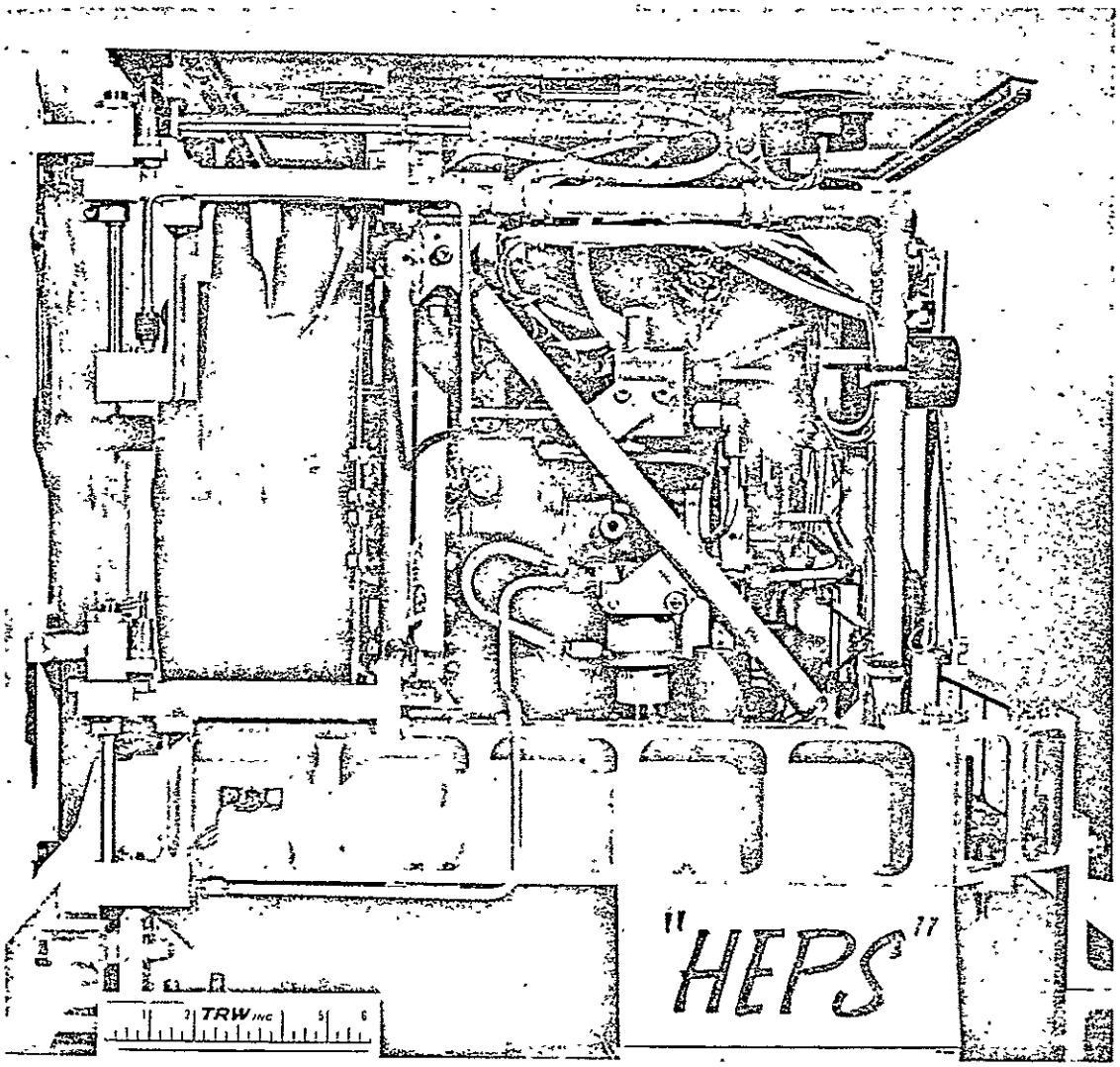


FIGURE 4-9 HEPS FRONT VIEW (STOWED)



REPRODUCIBILITY OF THE
ORIGINAL PAGE IS POOR

FIGURE 4-10 HEPS RIGHT VIEW (STOWED)

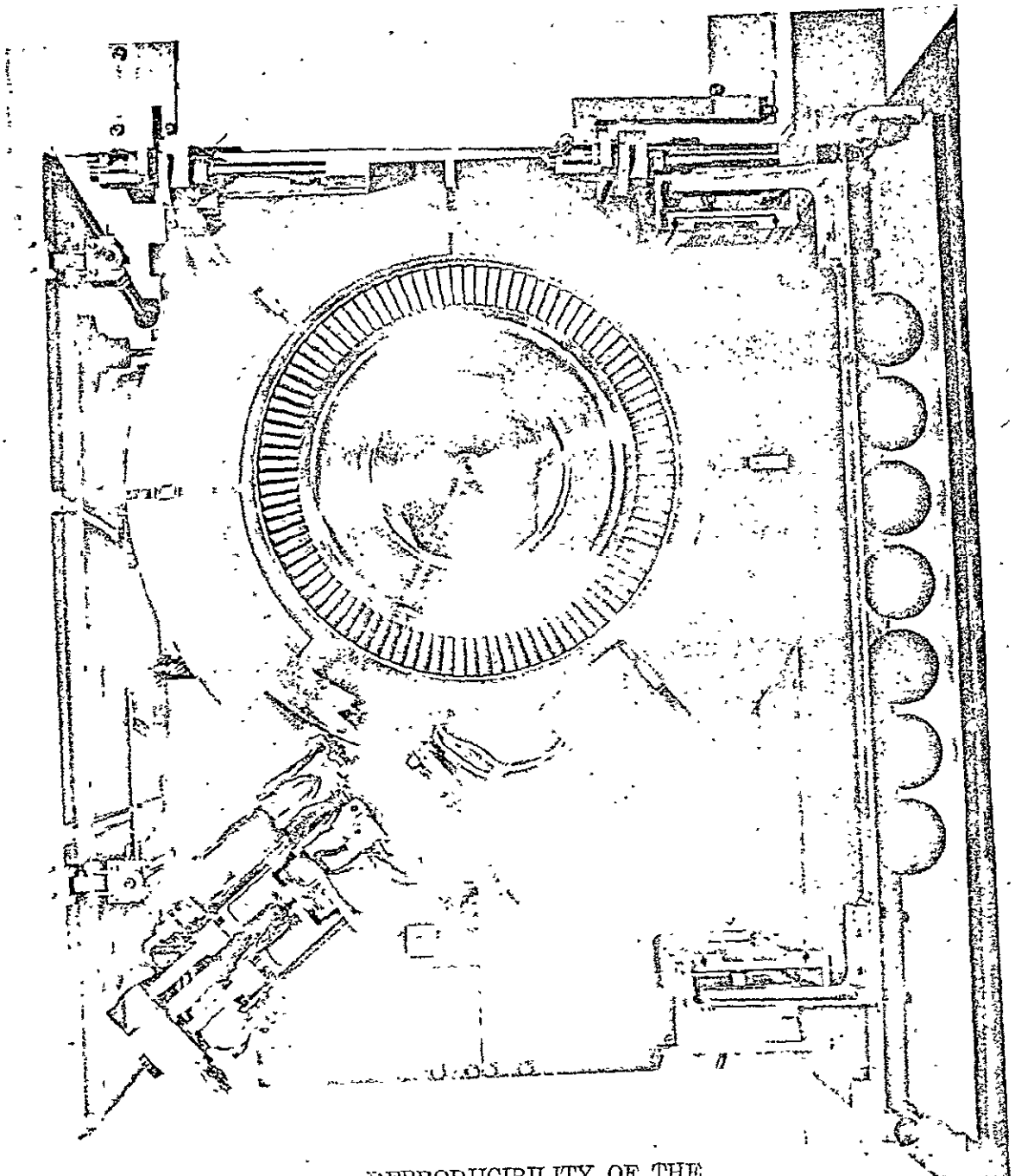


FIGURE 4-11 HEPS FRONT VIEW (PARTIALLY DEPLOYED)

REPRODUCIBILITY OF THE
ORIGINAL PAGE IS POOR

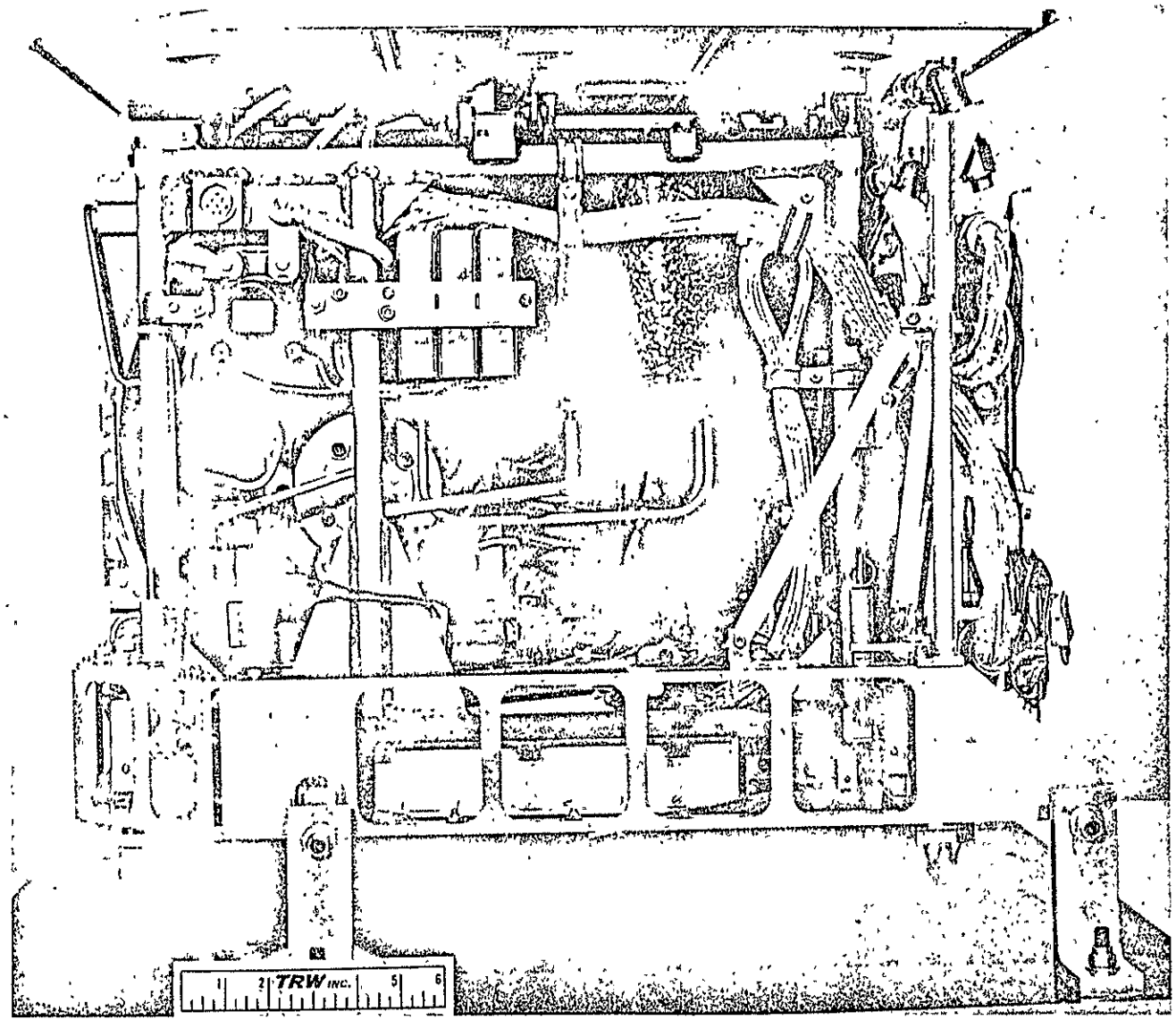


FIGURE 4-12 HEPS REAR VIEW (STOWED)

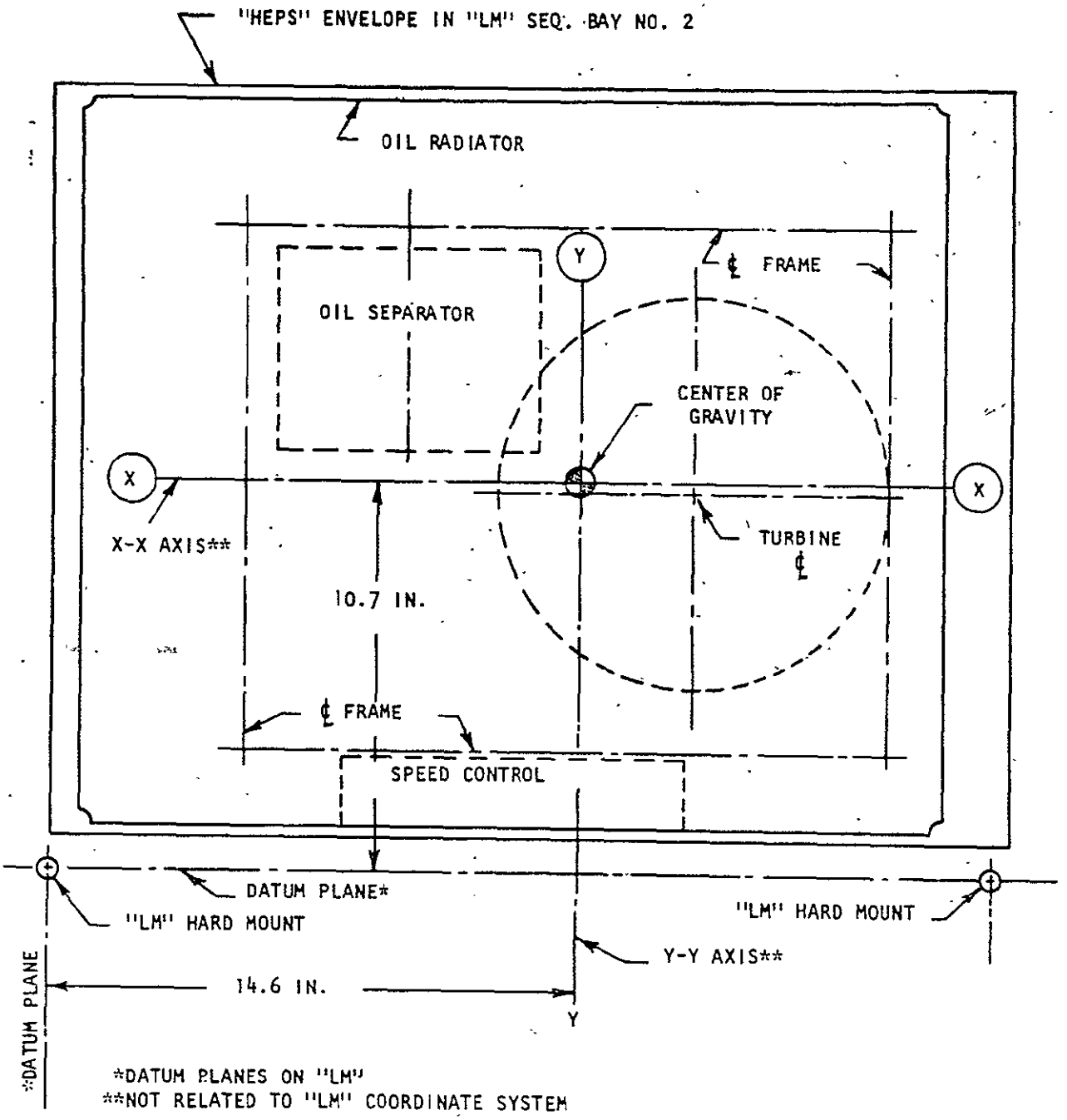


FIGURE 4-13 VIEW LOOKING INTO "HEPS" STORAGE BAY

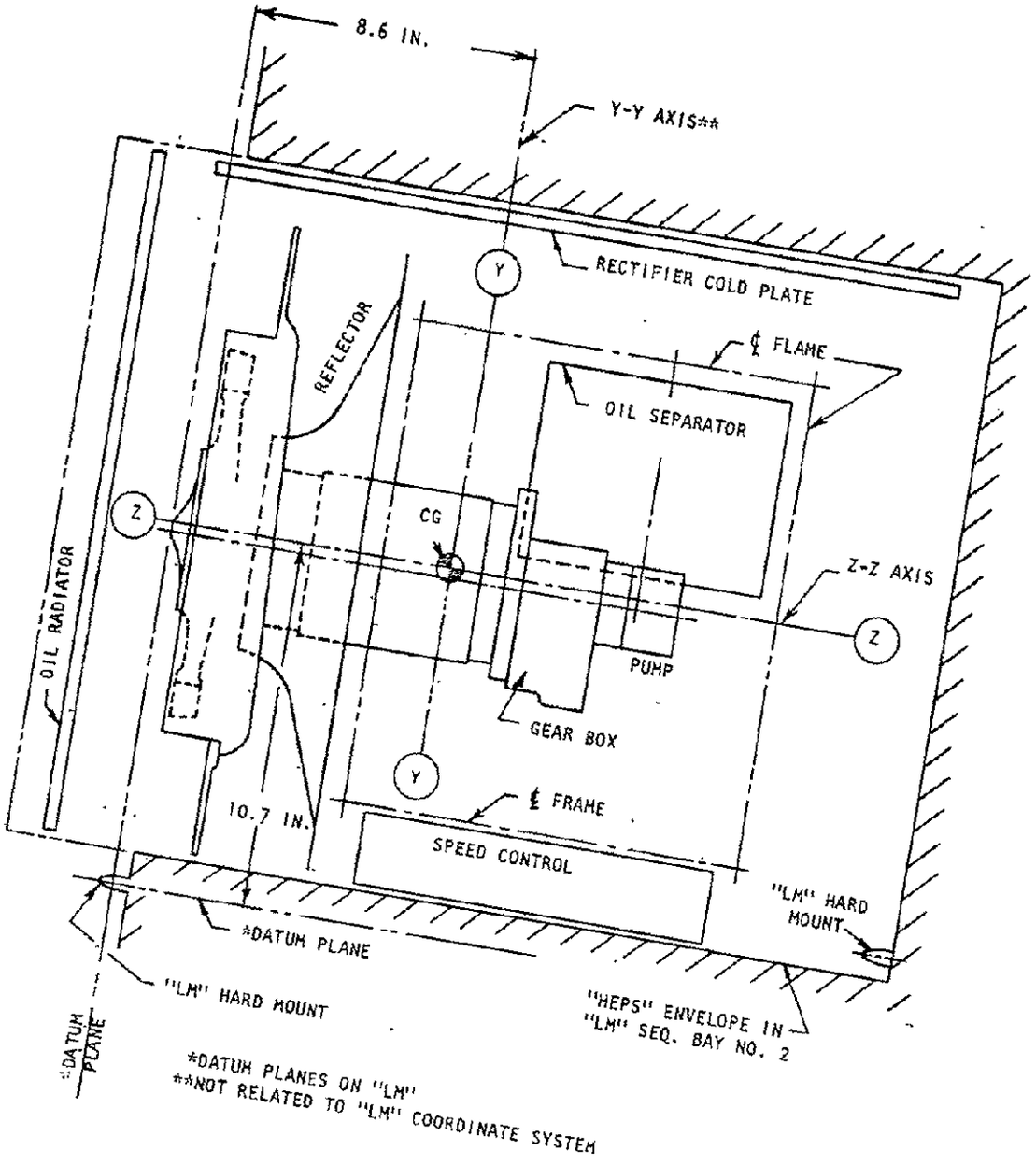


FIGURE 4-14 VIEW LOOKING AT "HEPS" FROM THE RIGHT SIDE

		Pounds
1.	Turboalternator Assembly (817801)	
	A. Alternator Assembly (213484)	16.99
	B. Turbine Wheel and Shaft (213111)	21.29
	C. Seal and Housing Assembly (817831)	0.72
	D. Scroll and Nozzle (817834)	20.74
	E. Gearbox, Pump and Miscellaneous Hardware	12.95
	Subtotal	72.69
2.	Lube System	
	A. Oil Radiator (213191)	4.37
	B. Radiator Hinges, Release Lock, Mounts	1.04
	C. Separator; Dry (213136)	5.40
	D. Lube Lines (estimate)	0.5
	E. Filter (212954)	0.65
	F. Relief Valve (212955)	1.28
	G. Low Pressure Switch (estimate)	0.2
	Subtotal	13.44
3.	Electrical Control System	
	A. Control Panel Assembly (212940)	5.07
	B. Speed Control Assembly (212941)	7.64
	C. Voltage Regulator Assembly (212918)	4.06
	D. Rectifier Cold Plate Assembly (213530) (Radiator Plates; 3 - 9.19 lb)	13.44
	E. Harnesses and Power Leads	Not Weighed
	F. Capacitors; 3 (817758)	2.74
	G. Power Relay (213381)	2.29
	H. Terminals, Receptacles, Miscellaneous	1.25
	Subtotal*	36.49

*Not including harnesses and power leads.

FIGURE 4-15 HEPS WEIGHT BREAKDOWN

		Pounds
4.	Gas Generator and Control System	
	A. Injector and Chamber (817948)	5.90
	B. Control Valves (817779)	3.31
	C. O/F Manifolds (213415 and 213428)	0.50
	D. O/F Hoses (213388 and 213389)	1.78
	E. Mounting Brackets and Miscellaneous	2.14
	F. Nitrogen Pressurization System	
	1) Tank, Safety Adapter and Fill Valve (90861-1, 213486 and 213487)	2.16
	2) Solenoid Valve (212984)	0.35
	3) Check Valve and Swivel Elbow (92416-4 and 213508-2)	0.15
	4) Tubes (estimate)	0.2
	Subtotal	16.49
5.	Flight Package (817800)	
	A. Extension Mechanism, Frame and LM Mount Structure (213220 and 213189)	21.45
	1) Two Slides (213286) - 5.58 lb	
	2) Frame (213189) - 9.5 Calc.	
	3) Five Vibration Mounts (213187) - 2.49 lb	
	B. Reflector (814099-31)	4.47
	C. Thermal Insulation Blankets	0.75
	D. Mounts and Miscellaneous for Control System Boxes (3)	2.68
	E. Cold Plate Deployment Hardware	1.99
	Subtotal	31.34
6.	HEPS Unit Weight, Dry (Measured)	191.0
7.	Total of Weights Measured in 1 to 5 above	170.45
8.*	Miscellaneous Parts Not Weighed (items 6 minus item 7)	20.45
9.	Oil at Four Quarts Inventory	8.5
10.	Final Heps Package Weight (item 6 plus item 9)	199.5

*A large share of this weight is probably in the harnesses, power leads and some turboalternator parts.

FIGURE 4-15 HEPS WEIGHT BREAKDOWN (Continued)

5.0 TEST PROGRAM

The test program for the Qualification Unit included Acceptance and Development tests. Leak and proof pressure tests were also conducted at various phases of the assembly and test program but because of their minor significance, they will not be discussed. Also, tests conducted for the sole purpose of setting O/F ratios and correcting electrical difficulties will not be reported except as noted in the Appendix.

5.1 Acceptance

The Acceptance Test that was conducted complied with the Acceptance Test Plan explained in detail in ER-7380, "Qualification Acceptance Test Plan - Hypergolic Electrical Power System". In Figure 5-1, the Acceptance test load profile is presented. The heat sink (wall) temperatures in the altitude chamber were regulated to 77 ± 5°F.

5.2 Development

Development testing was primarily conducted to evaluate and establish the thermal environmental upper limit for continuous operation. The thermal tests were conducted at 160 ± 5°F wall temperature at various power levels and the critical hardware temperatures were measured. A vibration investigation included reduced oil flow tests after the rotating assembly was dynamically rebalanced.

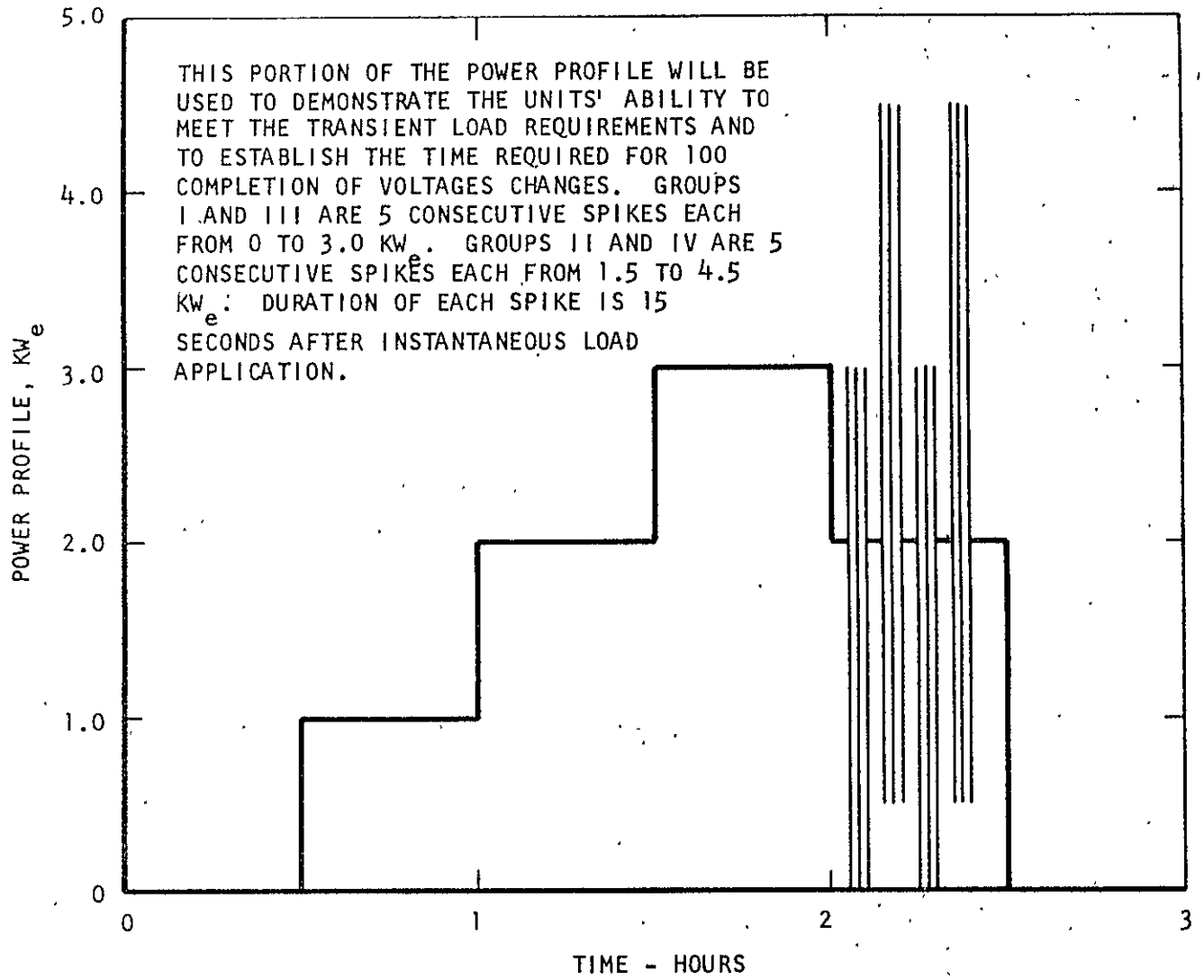


FIGURE 5-1 ACCEPTANCE TEST LOAD PROFILE

6.0 TEST RESULTS

Data available for steady state comparison of the Design Verification Retest Unit and the Qualification Unit was limited because of the general nature of the Qualification Unit tests. However, the Acceptance Test and subsequent Development Testing provided adequate data for performance comparison but not thermal characteristic comparisons.

6.1 Acceptance Test

The Acceptance Test as described in ER-7380 was conducted in accordance with the load profile as shown in Figure 5-1. Data was taken approximately every ten minutes throughout the test and is presented in Table 6-1. In Figure 6-1, the Specific Propellant Consumption (SPC) is shown in comparison with the Phase II and Phase III (DVR Unit) systems. The Phase III (Qualification Unit) data was gathered during transient oil temperatures varying from 292 to 360°F. However, it is important to note that the coast time did not vary significantly during this period of oil viscosity changes.

Tabulated values of SPC and percentage changes are listed in Table 6-2.

The Qualification Unit SPC was 12%-27% higher than DVR SPC. Performance change was attributed to higher internal losses due to friction. A Phase II and III unit coast time comparison is shown in Figure 6-2. The coast time curves verify the SPC results that the Qualification Unit performance was slightly lower than the DVR unit performance but greater than the Phase II unit performance. The maximum oil temperature was 362°F.

6.2 Development Test

Additional testing after the Acceptance Test was conducted to evaluate the load limitations of the HEPS with a 160°F heat sink temperature and to evaluate the vibration causes.

160°F Heat Sink Test

The altitude chamber wall temperature was elevated to 160° ± 5°F and maintained at that level throughout the test. After the unit transferred into the speed control mode, 1.0 KW load was applied utilizing the low O/F ratio valve. Thermal stabilization occurred after 3.3 hours of operation. The oil temperature was 359°F and the electrical control panel temperatures were 200-207°F. The high O/F ratio operation was initiated and the load was maintained at 1.0 KW. After 1.3 hours, thermal stability was achieved. The oil temperature was 370°F and the electrical

TEST NO. 011-4.2-001 (ACCEPTANCE)

TIME HOURS	O/F RATIO	LOAD KW	ALT RUN HR	COAST TIME SECONDS	OIL SEPARATOR PSIA	ALT OIL INLET PSIA	SCAVENGE PUMP INLET PSIA	OIL RAD INLET PSIA	OIL RAD INLET PSIA	OIL FLOW GPM	SEAL TEMP. °F	ROLLER BRG. TEMP °F	OIL TEMP °F	VIBRATION LEVEL, g FRAME	VERT	AXIAL	SCR STUD IN VR(2) °F	DIODE STUD RF (5) °F	BKT IN Q3 SC (10) TR BKT IN CP (11)	FIELD AMPS ALT AMPS	FIELD VDC ALT VDC	PLATE COILS TEMP °F
1332	LO	0	34		NORMAL START												AMBIENT 78°F					
1340	LO	0	45	26	16	39	3.5	79	64	1.10	158	149	133	22-10	57-44	86-50	1 / 1					82
1345	LO	0	45	26 5	16	39	3 4	71	62	1 14	192	188	158	24-13	56-46	85-46	2 / 2	3 /	68° / 67°	5.2 / 0	8.3 / 29.5	82
1350	LO	0	45	28	16	38 5	3.5	69	61	1 16	212	204	178	26-15	58-48	60-46	28 / 82°	27 / 90°		5.2 / 0	8.4 / 29.5	82
1355	LO	0	45	28.5	16	38	3.2	68	60	1 18	238	218	193	28-15	60-50	60-46	41 /	38 / 70°	72° /			85
1400	LO	0	4	28 5	16	38	3.2	64	58	1.2	252	230	206	29-17	64-53	60-48	45 / 98	41 / 86		5.7 / 0	8.6 / 29.5	73
1402	LO	1			APPLIED 1 KW LOAD																	
1405	LO	1	45	14 5	16	37 5	3 2	63	58	1 2	268	242	220	32-18	67-56	60-49	58 /	87 /		5.8 / 35.5	7.8 / 28.3	74
1410	LO	1	45	14 5	16	37	3 2	62	58	1.18	283	253	232	35-19	64-55	58-48	89 / 108	86 / 115	80° / 78°	5.9 / 35.5	7.95 / 28.3	75
1415	LO	1	45	14 5	16	37	3 2	62	57	1 16	300	262	242	38-18	64-55	58-48	78 / 112	103 / 122		5.8 / 35.5	8.1 / 28.3	76
1417	HI	1			CHANGED TO HI O/F RATIO																	
1420	HI	1	45	15	16	36 5	3 2	60	56	1.14	316	272	252	44-20	66-58	56-50	86 / 115	1 16 / 128	86 / 84	5.9 / 35.1	8.2 / 28.3	78
1425	HI	1	45	15.5	15 5	36	3 2	60	56	1 14	332	280	284	50-22	66-58	58-48	93 / 118	1 28 / 133		5.8 / 35.1	8.2 / 28.2	80
1430	HI	1	45	15 5	15 5	38	3 2	60	55	1 12	348	288	274	59-23	67-58	56-47	1 01 / 122	1 36 / 136		5.2 / 35	8.3 / 28.2	83
1432	LO	2			CHANGED TO LO O/F AND APPLIED 2 KW LOAD																	
1440	LO	2	5	10	15 5	35	3 2	58	54	1.10	372	386	292	53-24	67-58	52-47	1 22 /	1 81 /	100 / 95	6.3 / 69	9.8 / 28.5	78
1447	HI	2			CHANGED TO HI O/F RATIO																	
1450	HI	2	6	10 4	15	37	3.2	56	52	1 10	392	320	310	50-26	70-58	58-50	1 39 / 137	2 21 / 171	108 / 100	6.5 / 69	8.7 / 28.6	82
1500	HI	2	6	10 4	14 5	34	3.2	54	50	1.08	412	338	326	62-25	70-56	57-48	1 57 / 145	2 43 / 179	112 / 108	6.3 / 69	9.8 / 28.6	83
1502	LO	3			CHANGED TO LO O/F AND APPLIED 3 KW LOAD																	
1510	LO	3	6	7.8	14	32	3 2	52	48	1 04	430	346	340	49-25	66-56	60-50	1 81 / 154	2 81 / 196	120 / 145	7.4 / 103	11.4 / 28.5	78
1520	LO	3	6	7 8	14	30	3 2	50	47	9	438	382	352	46-25	68-44	62-44	1 94 / 186	3 11 / 206	125 / 120	7.4 / 102.5	11.4 / 28.4	80
1525	LO	3	6	7.8	13 5	30	3.2	50	46	84	444	364	356	50-25	68-56	62-54						
1530	LO	3	6	7 8	13 5	30	3 2	48	46	8	450	398	382	56-28	68-57	63-57	2 06 / 185	3 22 / 210	130 / 124			76
1532	LO	2			REDUCED LOAD TO 2 KW IN PREPARATION FOR SPIKES																	

TABLE 8-1 ACCEPTANCE TEST

&REPRODUCIBILITY OF THE ORIGINAL PAGE IS POOR

TEST NO. 011-4 2-001 (ACCEPTANCE)

TIME HOURS	O/F RATIO	LOAD KW	ALT mm Hg	COAST TIME SECONDS	OIL SEPARATOR PSIA	ALT OIL INLET PSIA	SCAVENGE PUMP INLET PSIA	OIL RAD INLET PSIA	OIL RAD INLET PSIA	OIL FLOW GPM	SEAL TEMP. °F	ROLLER BRG. TEMP. °F	OIL TEMP. °F	VIBRATION LEVEL, g FRAME,	VERT	AXIAL	SCR STUD IN VR (2) °F	DIODE STUD RF (5) °F	BKT IN 03 SC (10) TR BKT IN OP (11)	FIELD AMPS ALT AMPS	FIELD VDC ALT VDC	PLATE COILS TEMP °F
1538	LO			SPIKE 0 KW TO 3 KW						15 SEC DEVIATION			5 TIMES									
				SPIKE 1-1/2 KW TO 4-1/2 KW						15 SEC DEVIATION			5 TIMES									
				SPIKE 0 KW TO 3 KW						15 SEC DEVIATION			5 TIMES									
				SPIKE 1-1/2 KW TO 4-1/2 KW						15 SEC DEVIATION			5 TIMES							15X	28.9	
1548				COMPLETED SPIKING - APPLIED 2 KW LOAD LO O/F RATIO																		
1550	LO	2	6	10	13	30	3.2	49	46	1.0	442	370	362	54-32	66-54	62-42	2.12 / 187	2.92 / 199	135 / 129	6.3 / 69	9.9 / 28.7	78
1600	LO	2	6	10	12.5	29.5	3.2	49	46	1.02	440	370	362	58-33	70-54	63-52	2.13	2.79	138 / 130	6.2 / 69	9.8 / 28.7	80
1602	LO	0		REDUCED TO 0 KW LOAD																		
1608	LO	0	65	29.5	12.5	29.5	3.2	49	46	1.0	430	362	358	59-28	70-56	56-50	2.02	2.10	138 / 132	4.7	7.3 / 28.8	82
1615	LO	0	65	29.5	11.7	29	3.2	49	45	1.04	414	358	353	56-35	70-54	56-48						82
1616				NORMAL SHUTDOWN								829 PULSES	2 HOURS AND 44 MIN			RUN TIME						

TABLE 6-1 ACCEPTANCE TEST (CONTINUED)

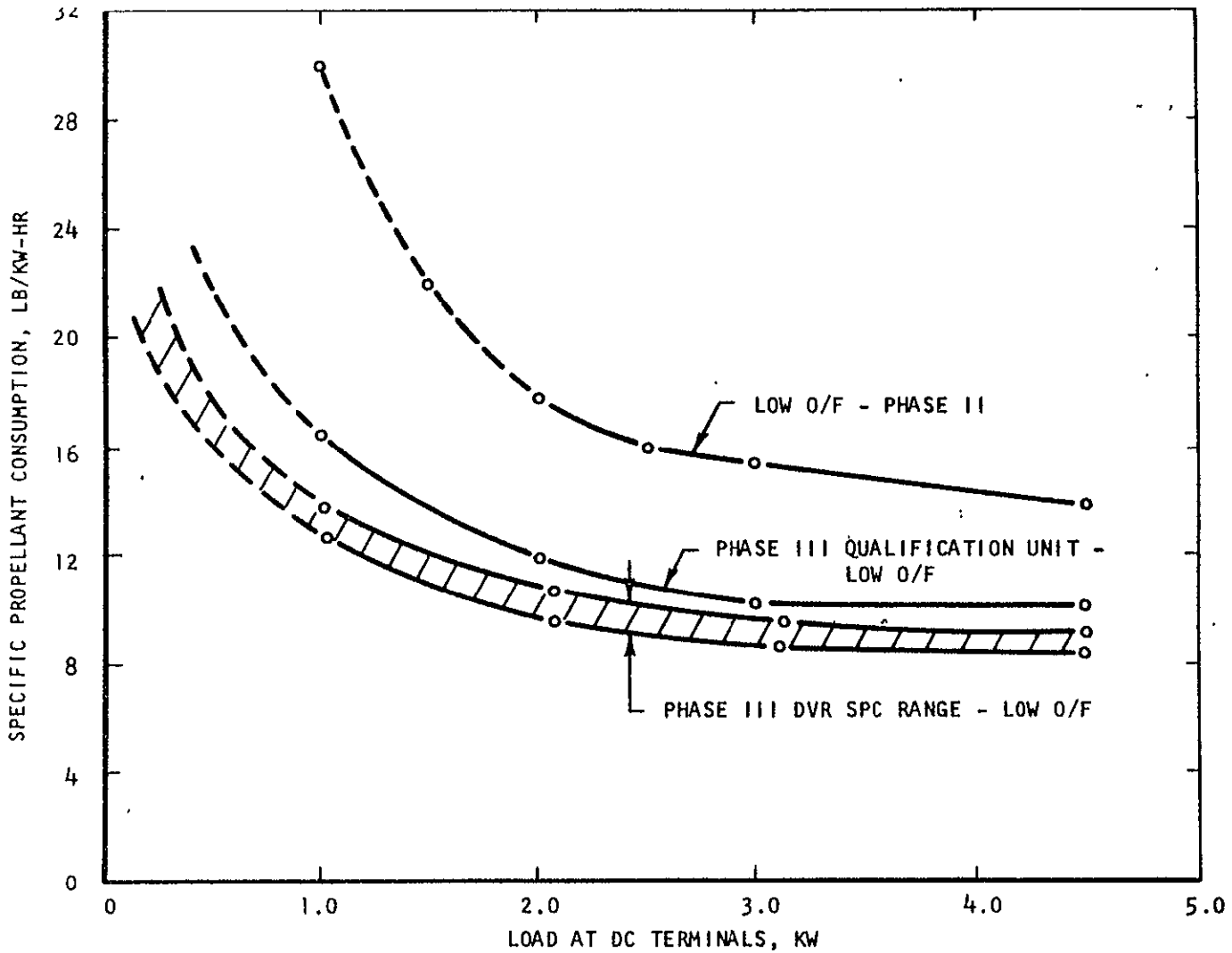


FIGURE 6-1 SPECIFIC PROPELLANT CONSUMPTION - LOW O/F - PHASE II AND PHASE III COMPARISON
(010-4.1-017,-018)
(011-4.2-001,-002)

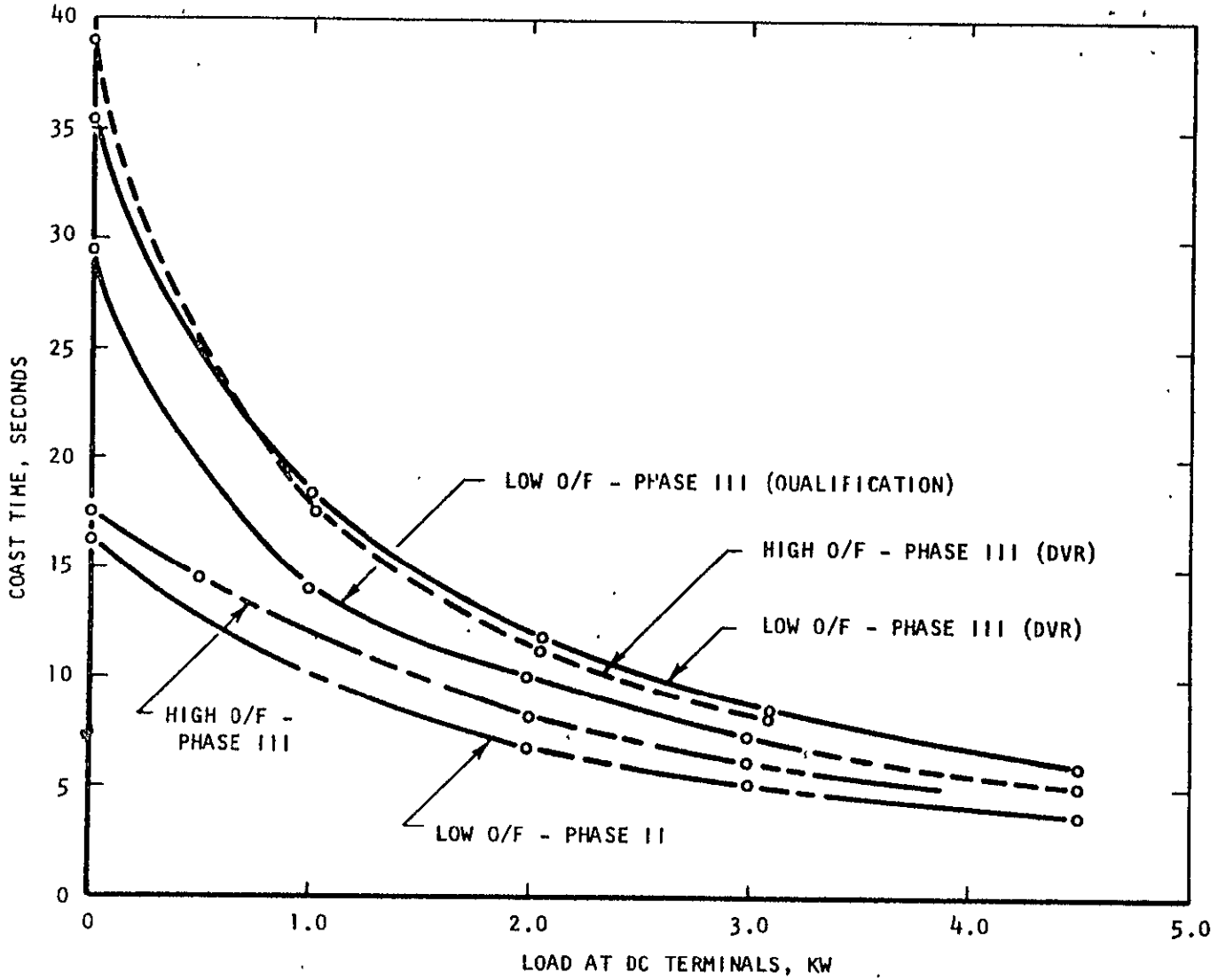


FIGURE 6-2 PHASE II & III COAST TIME COMPARISON
DATA FROM TESTS (010-4.1-017,-018)
(011-4.2-001,-002)

control panel temperatures were 211-215°F. The testing was concluded after this test because some of the electrical components were at their maximum allowable temperature. This test proved that the HEPS could operate continuously at 1.0 KW in a 160°F environment: at both low and high O/F ratios. However, for greater load application, system redesign would be required.

TABLE 6-2 SPC COMPARISON, LB/KW-HR.

	1.0 KW	2.0 KW	3.0 KW	4.5 KW	
Qualification Unit	16.7	11.9	10.2	10.15	
DVR Unit	13.2	10.0	9.1	8.9	(Average Values)
Phase II Unit	30.0	18.0	15.5	14.0	
% Difference From DVR Unit	+26.5%	+19.0%	+12.1%	+14.0%	
% Difference From Phase II Unit	-44.3%	-34.0%	-34.2%	-27.4%	

Vibration Investigation

Preliminary testing indicated that the vibration levels on the pump end of the rotating assembly were 80 g. The accelerometers were mounted in such a manner that two radial components and one axial component were measured. The two radial components were 90° apart. An accelerometer placed on a structural frame member showed the vibration level to be 28 g. The accelerometer outputs were scanned on a spectral analyzer for frequency content. The results showed that the rotating speed was the main source with minor contributions from the shaft speed harmonics. The problem was attributed to imbalance and the HEPS unit was returned to Cleveland for rework. The unit was disassembled and the rotating assembly was rebalanced in the alternator housing. This represented an improved technique for final balancing since the rotating assembly did not require any further disassembly. The balancing was done on a Bear Balancing Machine at 3500 rpm. After complete assembly, the unit was run up to 15,000 rpm using 400°F air. The accelerometer outputs revealed that the imbalance was 7.8 g at 15,000 rpm. The predicted vibration level at a shaft speed of 33,000 rpm was 38 g; less than half the previous imbalance. Further hot gas testing at VPI/Roanoke resulted in the following vibration levels after 45 minutes of operation:

REPRODUCIBILITY OF THE
ORIGINAL PAGE IS POOR

		Max.	Min.
1.	Radial Component on the Rotating Assembly	56 g	38 g
2.	Axial Component on the Rotating Assembly	64 g	50 g
3.	Structural Frame	28 g	12 g

The maximum values occurred at the instant of the pulse after which they decayed to the minimum values. The primary frequency of vibration was 550 Hz, the shaft speed.

The vibration level was sufficient to cause fatigue failure to occur in one of the lubrication lines. All the lubrication lines connecting the frame and the rotating assembly were replaced with flexible steel braided teflon hoses except for the pump inlet and scavenge discharge line.

The Qualification Unit is shown after testing in Figures 6-3 and 6-4.

A revised balancing technique using a concentric stub on the turbine outboard end for turbine radial location during balancing should be incorporated to correct the unbalance problem.

The Qualification Unit is shown in Figures 6-3 and 6-4.

REPRODUCIBILITY OF THE
ORIGINAL PAGE IS POOR

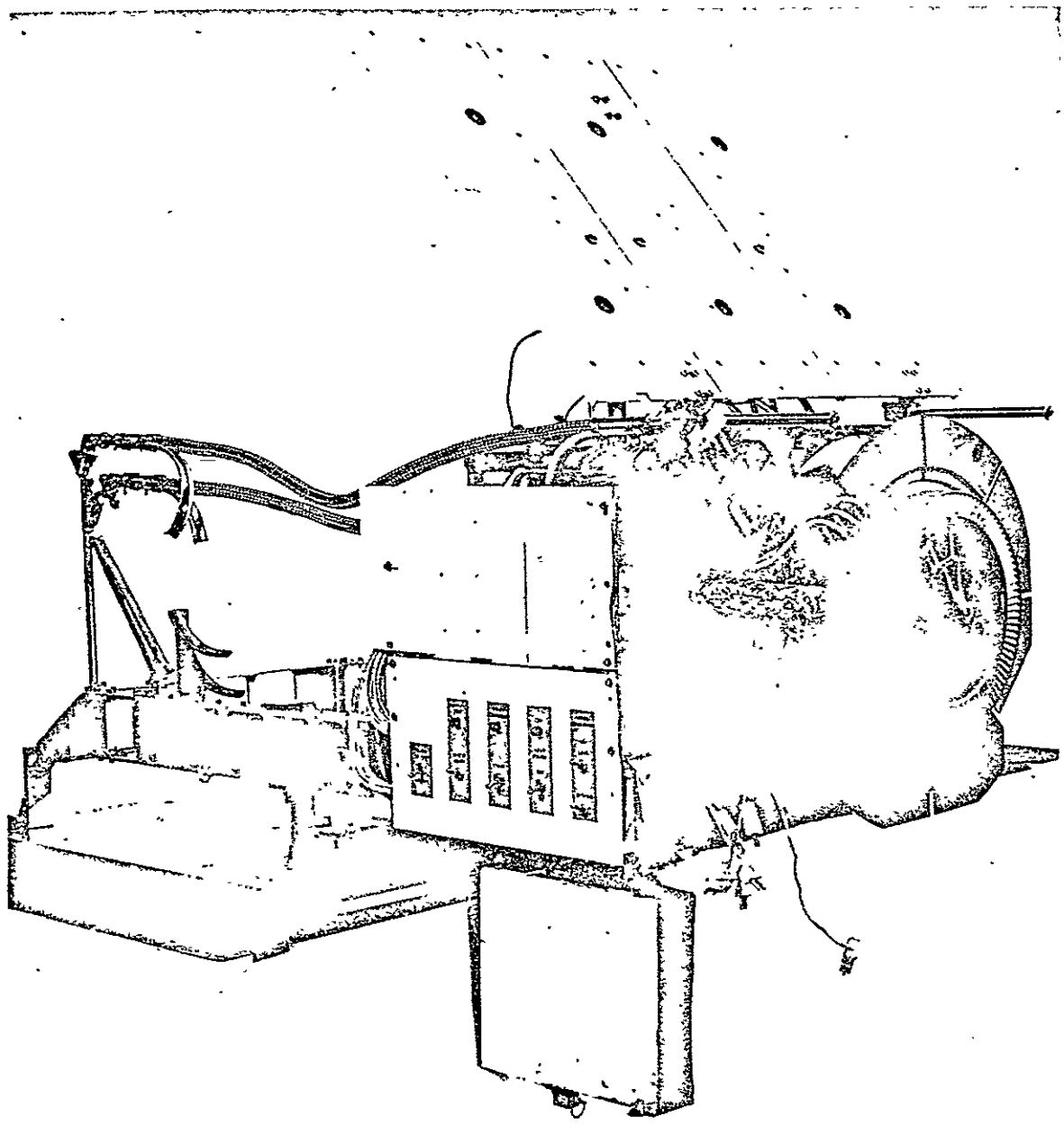


FIGURE 6-3 HEPS QUALIFICATION UNIT (AFTER TEST)

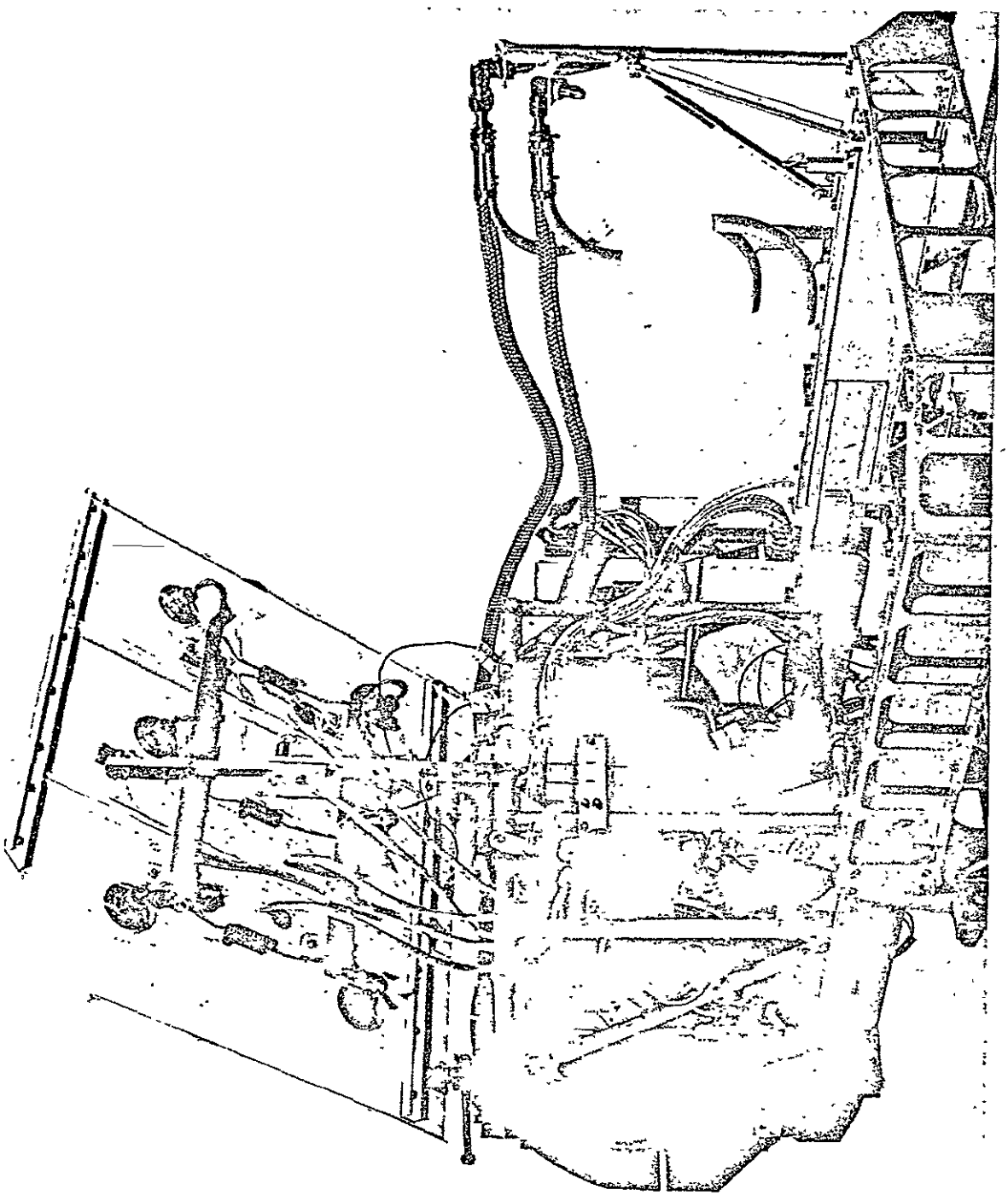


FIGURE 6-4 HEPS QUALIFICATION UNIT (AFTER TEST)

REPRODUCIBILITY OF THE
ORIGINAL PAGE IS POOR

The data listed in Table 6-1 verified the compliance of the Acceptance Test with the Specification ER-7380. The following personnel witnessed and hereby approve the Acceptnace Test conducted November 5, 1969 at VPI/Roanoke:

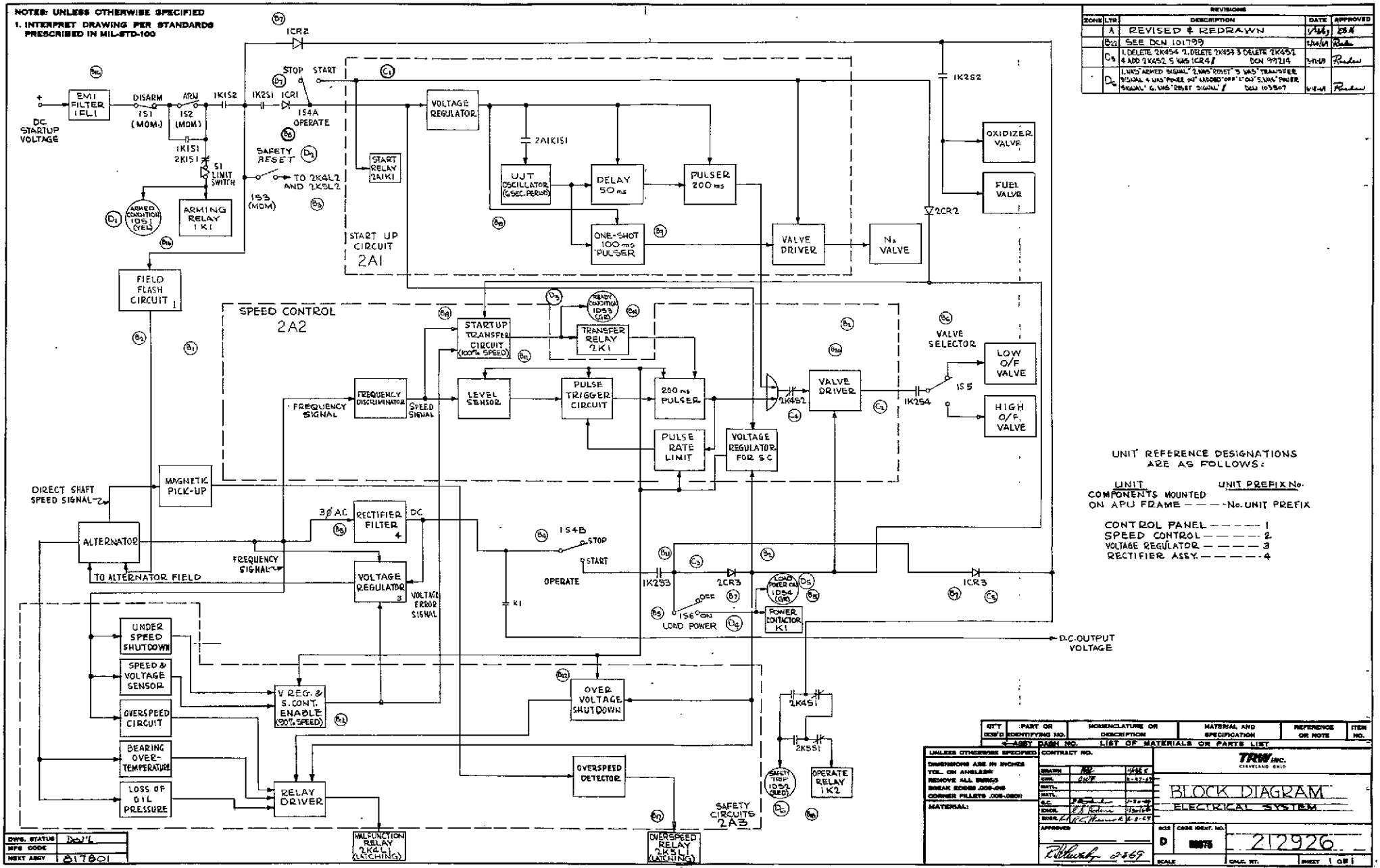
SIGNATURE OF WITNESS

G. E. Bernard
TRW/Engineering

E. C. Parker
TRW/Quality Assurance

R. Scaggs
DCAS/Quality Assurance

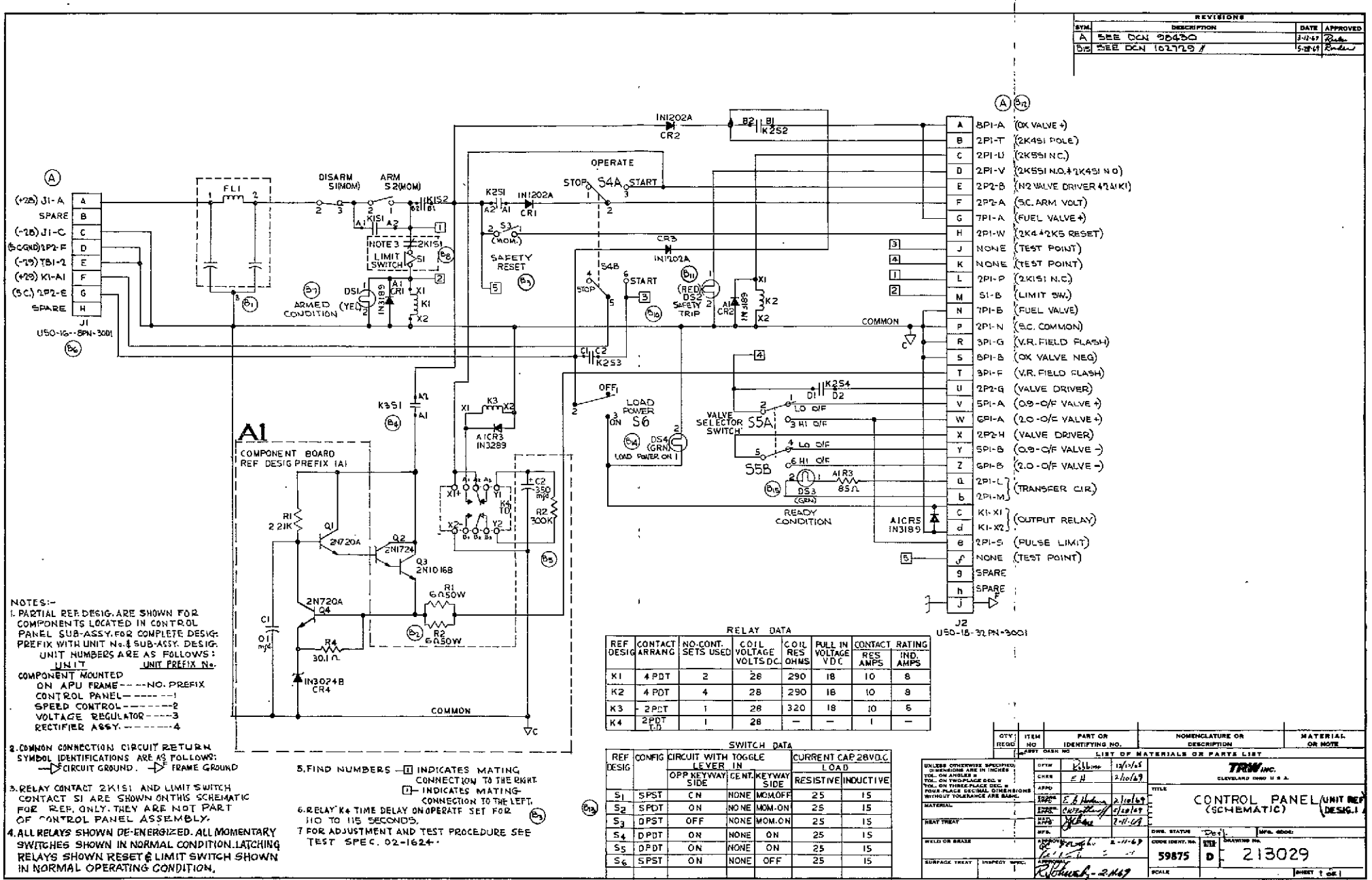
R. E. Elbel
TRW/HEPS Program Manager



FOLDOUT FRAME #1

FOLDOUT FRAME #2

FIGURE 4.3-1



NOTES:-

1. PARTIAL REF. DESIG. ARE SHOWN FOR COMPONENTS LOCATED IN CONTROL PANEL SUB-ASSY. FOR COMPLETE DESIG: PREFIX WITH UNIT No. & SUB-ASSY. DESIG: UNIT NUMBERS ARE AS FOLLOWS:

UNIT	UNIT PREFIX No.
COMPONENT MOUNTED ON APU FRAME	NO. PREFIX
CONTROL PANEL	1
SPEED CONTROL	2
VOLTAGE REGULATOR	3
RECTIFIER ASSY.	4

2. COMMON CONNECTION CIRCUIT RETURN. SYMBOL IDENTIFICATIONS ARE AS FOLLOWS: —▷ CIRCUIT GROUND. —▷ FRAME GROUND

3. RELAY CONTACT 2K1S1 AND LIMIT SWITCH CONTACT S1 ARE SHOWN ON THIS SCHEMATIC FOR REF. ONLY. THEY ARE NOT PART OF CONTROL PANEL ASSEMBLY.

4. ALL RELAYS SHOWN DE-ENERGIZED. ALL MOMENTARY SWITCHES SHOWN IN NORMAL CONDITION. LATCHING RELAYS SHOWN RESET & LIMIT SWITCH SHOWN IN NORMAL OPERATING CONDITION.

5. FIND NUMBERS —[1]— INDICATES MATING CONNECTION TO THE RIGHT. —[1]— INDICATES MATING CONNECTION TO THE LEFT.

6. RELAY K4 TIME DELAY ON OPERATE SET FOR 110 TO 115 SECONDS.

7. FOR ADJUSTMENT AND TEST PROCEDURE SEE TEST SPEC. 02-1624.

RELAY DATA

REF DESIG	CONTACT ARRANG	NO. CONT. SETS USED	COIL VOLTAGE VOLTS DC.	COIL RES OHMS	PULL IN VOLTAGE VDC	CONTACT RATING RES AMPS	CONTACT RATING IND. AMPS
K1	4 PDT	2	28	290	18	10	8
K2	4 PDT	4	28	290	18	10	8
K3	2 PDT	1	28	320	18	10	6
K4	2 PDT T.D.	1	28	—	—	1	—

SWITCH DATA

REF DESIG	CONFIG	CIRCUIT WITH TOGGLE LEVER IN: OPP KEYWAY SIDE	CENT.	KEYWAY SIDE	CURRENT CAP. 28 V.D.C. LOAD: RESISTIVE	INDUCTIVE
S1	SPST	ON	NONE	MOM.OFF	25	15
S2	SPDT	ON	NONE	MOM-ON	25	15
S3	DPST	OFF	NONE	MOM.ON	25	15
S4	DPDT	ON	NONE	ON	25	15
S5	DPDT	ON	NONE	ON	25	15
S6	SPST	ON	NONE	OFF	25	15

QTY REQD	ITEM NO	PART OR IDENTIFYING NO.	NOMENCLATURE OR DESCRIPTION	MATERIAL OR NOTE
ASSY GASK NO		LIST OF MATERIALS OR PARTS LIST		

UNLESS OTHERWISE SPECIFIED: DIMENSIONS ARE IN INCHES; TOL. ON ANGLES ±; TOL. ON TWO-PLACE DEC. ± .02; TOL. ON THREE-PLACE DEC. ± .010; FOUR-PLACE DECIMAL DIMENSIONS WITHOUT TOLERANCE ARE BASIC.

MATERIAL | HEAT TREAT | WELD OR BRAZE | SURFACE TREAT | INSPECT. SPEC.

DRWN K. Williams 12-1-68
CHKR E H 2-10-69
APPD
ENGR E. E. Hedges 2-10-69
ENGR C. W. Hastings 2-10-69
MFG APPD J. Kline 2-11-69
MFG.
APPROVED R. Rinker 2-11-69
APPROVED R. Schuck 2-11-69

TRW INC. CLEVELAND OHIO U.S.A.

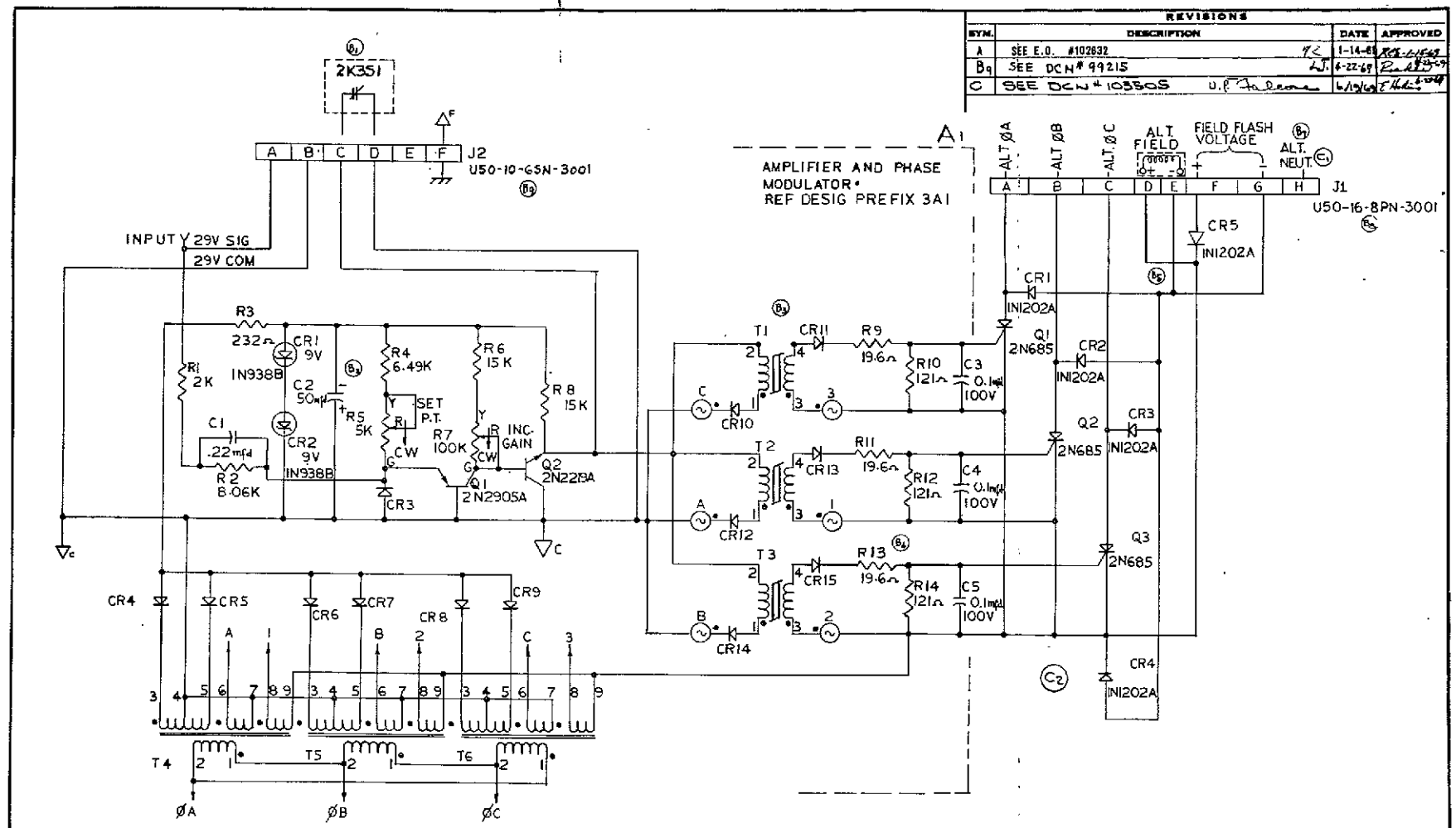
TITLE: CONTROL PANEL (SCHEMATIC) (UNIT REF DESIG. 1)

OWG. STATUS: Rel. | MFG. ECOC:
CODE IDENT. NO. 59875 | SIZE D | DRAWING NO. 213029
SCALE | SHEET 1 OF 1

FOLDOUT FRAME #1

FOLDOUT FRAME #2

FIGURE 4.3-3



NOTES:

1. PARTIAL REFERENCE DESIGNATIONS ARE SHOWN FOR COMPONENTS LOCATED IN VOLTAGE REGULATOR ASSEMBLY. FOR COMPLETE DESIGNATION, PREFIX WITH UNIT NUMBER AND SUBASSEMBLY DESIGNATION. UNIT NUMBERS ARE AS FOLLOWS:

	NO. PREFIX
COMPONENTS MOUNTED ON APU FRAME	
CONTROL PANEL	1
SPEED CONTROL	2
VOLTAGE REGULATOR	3
RECTIFIER ASSEMBLY	4

2. COMMON CONNECTION CIRCUIT RETURN SYMBOL IDENTIFICATIONS ARE AS FOLLOWS:
   - C — CIRCUIT GROUND
   - F — FRAME GROUND
3. ALL DIODES 1N645 UNLESS OTHERWISE SPECIFIED
4. FOR ASSEMBLY SEE TRW DWG. # 212918
5. REQUIRES ABC ALTERNATOR ROTATION (SEE ADJUSTMENT PROCEDURE 02-1623) B6

QTY REQD	ITEM NO.	PART OR IDENTIFYING NO.	NOMENCLATURE OR DESCRIPTION	MATERIAL OR NOTE

ASSY. DASH NO. — LIST OF MATERIALS OR PARTS LIST

UNLESS OTHERWISE SPECIFIED DIMENSIONS ARE IN INCHES
TOL ON ANGLES ±
TOL ON TWO-PLACE DEC ±
TOL ON THREE-PLACE DEC ±
FOUR-PLACE DECIMAL DIMENSIONS WITHOUT TOLERANCE ARE BASIC.
MATERIAL
HEAT TREAT
WELD OR BRAZE
SURFACE TREAT. INSPECT. SPEC.

DFTM	Robbins	8/1/68
CHKR	EH	11-22-68
APPD		
ENGRG. APPD.	E.J. Hudson	8/1/68
ENGRG. APPD.		
MATL. APPD.		11-25-68
MFG.		
APPROVED		11-21-68
APPROVED		12/5/67
APPROVED		11-25-68

TRW INC. CLEVELAND, OHIO, U.S.A.

TITLE: SCHEMATIC VOLTAGE REGULATOR (UNIT REF DESIG 3)

DWG. STATUS DEVL. MFG. CODE

CODE IDENT. No. 59875 | DWG. SIZE C | DRAWING No. 817770

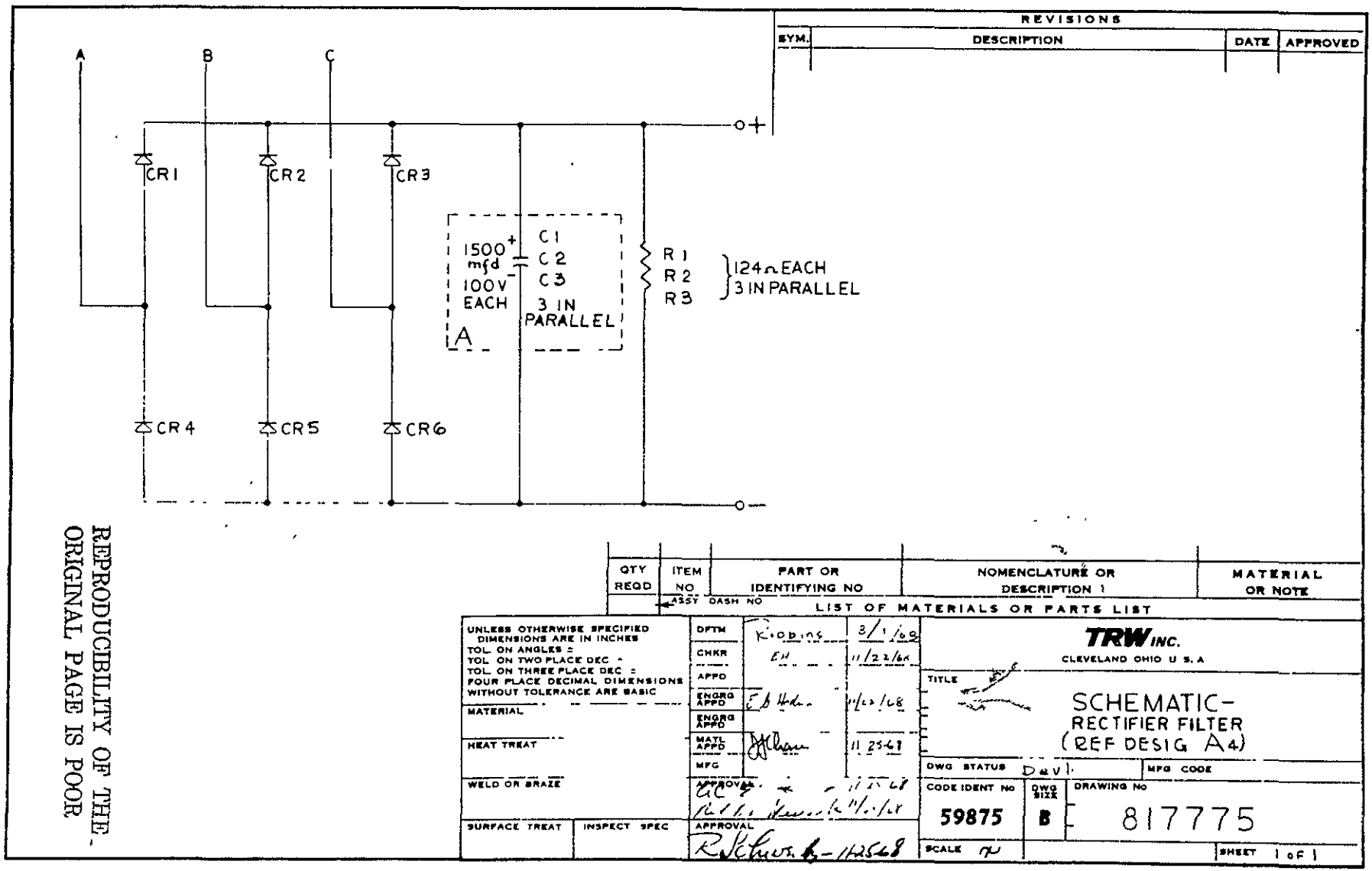
SCALE | SHEET CF

FOLDOUT FRAME #1

39 - 40

FOLDOUT FRAME #2

FIGURE 4.3-4



REPRODUCIBILITY OF THE ORIGINAL PAGE IS POOR

FIGURE 4.3-5

PRECEDING PAGE BLANK NOT FILMED.

5.0 ELECTRICAL SYSTEM DESIGN

5.1 Design Requirements and System Considerations

The design of the electronic package was based on a number of parameters, the most important of which were its temperature limitations and the space available for mounting the packages. No external cooling methods were provided and, therefore, all heat generated by the controls must be removed by radiation. The thermal design of the electrical system is discussed in Section 6.3. The power losses used to determine radiating areas for semiconductors are manufacturers' published data. As a result, there is an additional margin of safety built into the radiator sizing.

The electrical packages discussed in this section were designed using component parts selected in accordance with NASA document MSC-A-66-7, Parts Reliability Program Requirements and specification control drawings. Performance data and operating temperature limits of the control system are listed in Table 5.1-1.

5.2 Speed Control

The startup programmer, speed control and safety circuits are contained in the speed control package. The speed control package is shown in Figure 5.2-1. The speed control package generates the least amount of heat (it dissipates only 12 watts under worst conditions). When the HEPS unit is deployed, the speed control swings down 105 degrees and views space. The radiating surface contains 0.71 ft^2 of radiating area and is coated with a thermal control paint. This assembly should maintain a maximum component temperature of 210°F which provides a 20°F safety margin. Thermal data will be obtained to verify the design when the assemblies are tested with the first HEPS Qualification Unit. The exact shape of the speed control was governed by the available space under the HEPS frame and the space requirements for all the internal components.

5.3 Voltage Regulator

The voltage regulator package has two primary heat generating components and they are the semiconductors which make up the output power stage. The heat sink radiator for this package was built in two sections because the components have different limiting temperatures. The diodes have the highest allowable operating junction temperature, in this case 350°F, hence, require a smaller radiating surface. The SCR's have an upper temperature limit of 260°F and, therefore, require more radiating area. The SCR chosen was not a JAN-type component since units with higher temperature limits were only available on non-JAN units.

TABLE 5.1-1

HEPS ELECTRICAL SYSTEM PERFORMANCE DATA

Output Voltage	29v DC nominal
Voltage Regulation	±2% no load to full load
Transient Recovery Time	70 msec max for 4.5 KW load removal
	20 msec max for 4.5 KW load application
Transient Voltage Deviation	10 v maximum
Ripple Voltage	1.5v peak - peak maximum
Output Power	2 KW continuous at high O/F
	3 KW continuous at low O/F
	4.5 KW intermittent at low O/F
Electrical System Efficiency	80%
Operating Ambient Temperature Range	20°F to 160°F
Component Maximum Temperature Limits:	
Rectifier Cold Plates	Diode Stud Limit 320°F
Filter Capacitors	210°F
Voltage Regulator - Internal	210°F (circuit designed for 230°F)
Cold Plate Surface 4.5 KW Load	
Diode Radiator	350°F diode stud limit,
	311°F radiator limit
SCR Radiator	260°F SCR stud limit,
	238°F radiator limit

TABLE 5.1-1 (continued)

Speed Control	210°F internal limit (circuit designed for 230°F)

Component Characteristics:

Voltage Regulator

Input:	
Voltage	23v AC ±10 volts line-line (3 phase)
Frequency	1100 HZ ±300 Hz
Error Signal	29v DC ±2v DC
Output Voltage	0-24v DC maximum. Nominal operating range 4 to 12v DC depending on alternator load condition.

Controls

Input Voltage	28v DC nominal (22 to 33v) for approximately 3 minutes during startup.
Input Power	Average 18 watts @28v DC Peak current 3 amp each 6 seconds for 0.2 seconds. Maximum 125 watts for 30 seconds.

Startup Programmer

Startup Programmer Pulsing Rate	0.2 seconds on, 5.8 seconds off
Nitrogen Pulse	100 msec from T = 0 (first pulse of startup sequence only)
Gas Generator Pulse	200 msec first occurring at T = 50 msec

TABLE 5.1-1 (continued)

Transfer Circuits	
Voltage Regulator Turned On - - - -	90 to 95% rated speed
Speed Control Turned On - - - - - -	100% rated speed
Startup Programmer and Input Power Turned Off - - - - - - - - - - -	100% rated speed
Speed Control	
Input Voltage - - - - - - - - - - - -	28v DC from startup power 29v DC from HEPS power
Control Circuit Operating Voltage -	Regulated to 24 DC
Speed Signal - - - - - - - - - - - - -	Sense alternator frequency (nominal 1100 Hz)
Trigger Point - - - - - - - - - - - -	1089 Hz nominal (1% decrease in speed)
Gas Generator Pulse - - - - - - - -	200 msec on
Coast Time - - - - - - - - - - - - - -	Varies with load (3 sec min to 40 sec)
Pulse Rate Limit - - - - - - - - - -	3 sec minimum at low O/F ratio 5 sec minimum at high O/F ratio
Safety Circuits	
Overspeed (alternator frequency) - -	35,000 rpm (approx.)
Overspeed (shaft speed - - - - - - -	35,500 rpm
Underspeed - - - - - - - - - - - - -	Approximately 80%
Bearing Overtemperature - - - - - -	500°F
Low Oil Pressure - - - - - - - - - -	10 psia
Overvoltage - - - - - - - - - - - - -	45v DC for 1 millisecond



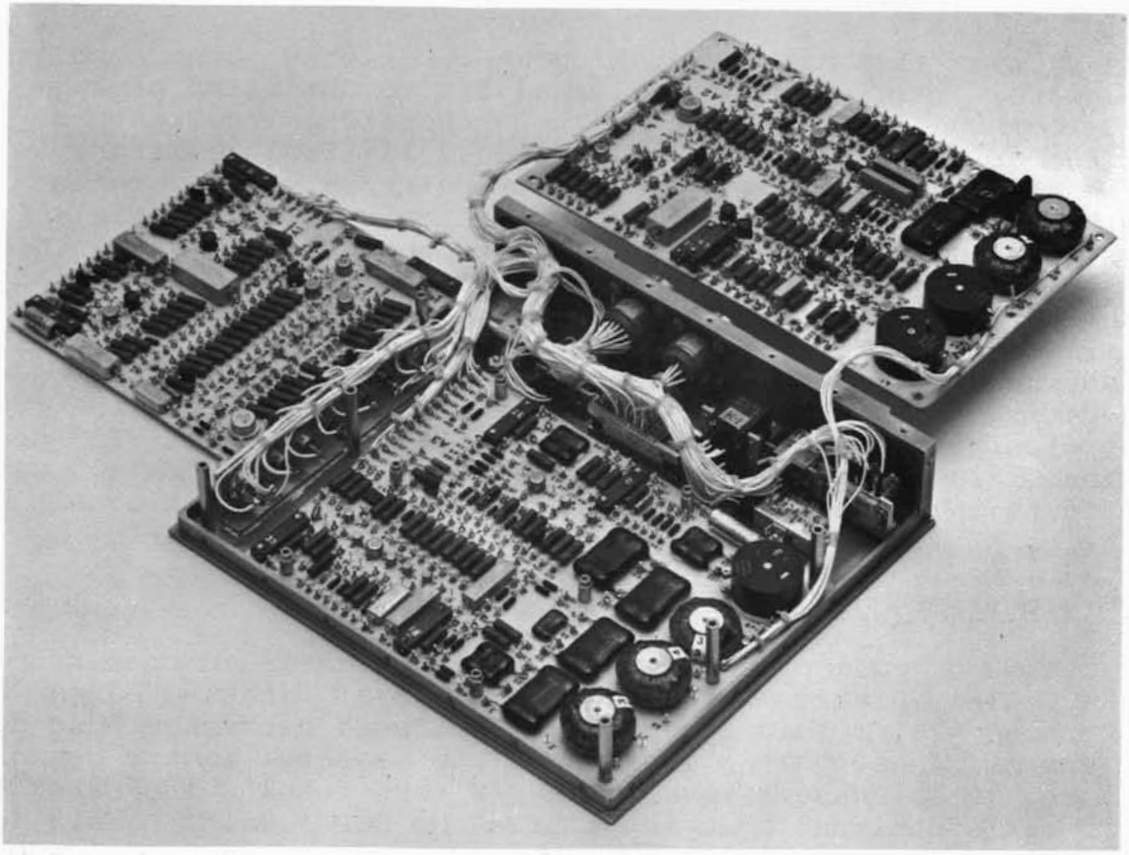


FIGURE 5.2-1 DVR SPEED CONTROL

REPRODUCIBILITY OF THE ORIGINAL PAGE IS POOR

The diodes and SCR were mounted on heat sinks which were in turn connected to the radiating panels. These brackets were electrically isolated from the panels and located such that the heat input was uniformly distributed over the entire panel. The diode is mounted directly to the bracket without electrical insulation. This improved the thermal distribution over a larger area before the electrical insulation was encountered. The voltage regulator is shown in Figure 5.3-1.

The voltage regulator is mounted on the left side of the HEPS unit where it has a view to space. The back side of the voltage regulator is insulated while the radiator surface is painted with a thermal control paint. The physical shape of the package was limited by the volume available along the side area.

5.4 Control Panel

The control panel is mounted on the left side of the HEPS unit under the voltage regulator. This package contains the manual control switches necessary to operate the system as well as the time delay and constant current circuits used to flash the alternator field.

This package also has several heat-generating components and, therefore, requires a thermal analysis to establish package size and location. The basic heat generating components are auctioneering diodes in power lines, limiting resistors in the field flash circuit and two power transistors. The temperature limiting component is the control transistor in the field flash constant current circuit. This component is required to dissipate 49 watts for a period of 30 seconds. Thermal analysis resulted in a heat sink design that contained one cubic inch of material to help absorb this heat input until it could be transferred to the radiating panel. The other major heat generating component is the resistors in series with the field. They dissipate an additional 41 watts for the same 30 second period. The total power dissipated in this unit is 104 watts. Lab tests indicated that the estimated power dissipation was 6-10 watts high. The control panel is shown in Figure 5.4-1.

5.5 Rectifier Cold Plate

The rectifier cold plate was designed for sustained operation at 3 KW. The plates were sized for heat inputs based on a continuous 4.5 KW load level using published rectifier loss data. The use of these data increased the safety factor slightly because it is conservative. The DVR test results indicated that there was additional heat input from the HEPS unit. This heat input was a result of conduction through the AC leads and radiation from the scroll. The panels were relocated on the unit to reduce the amount of radiated heat input from the scroll.

REPRODUCIBILITY OF THE
ORIGINAL PAGE IS POOR

FIGURE 5.3-1 DVR VOLTAGE REGULATOR

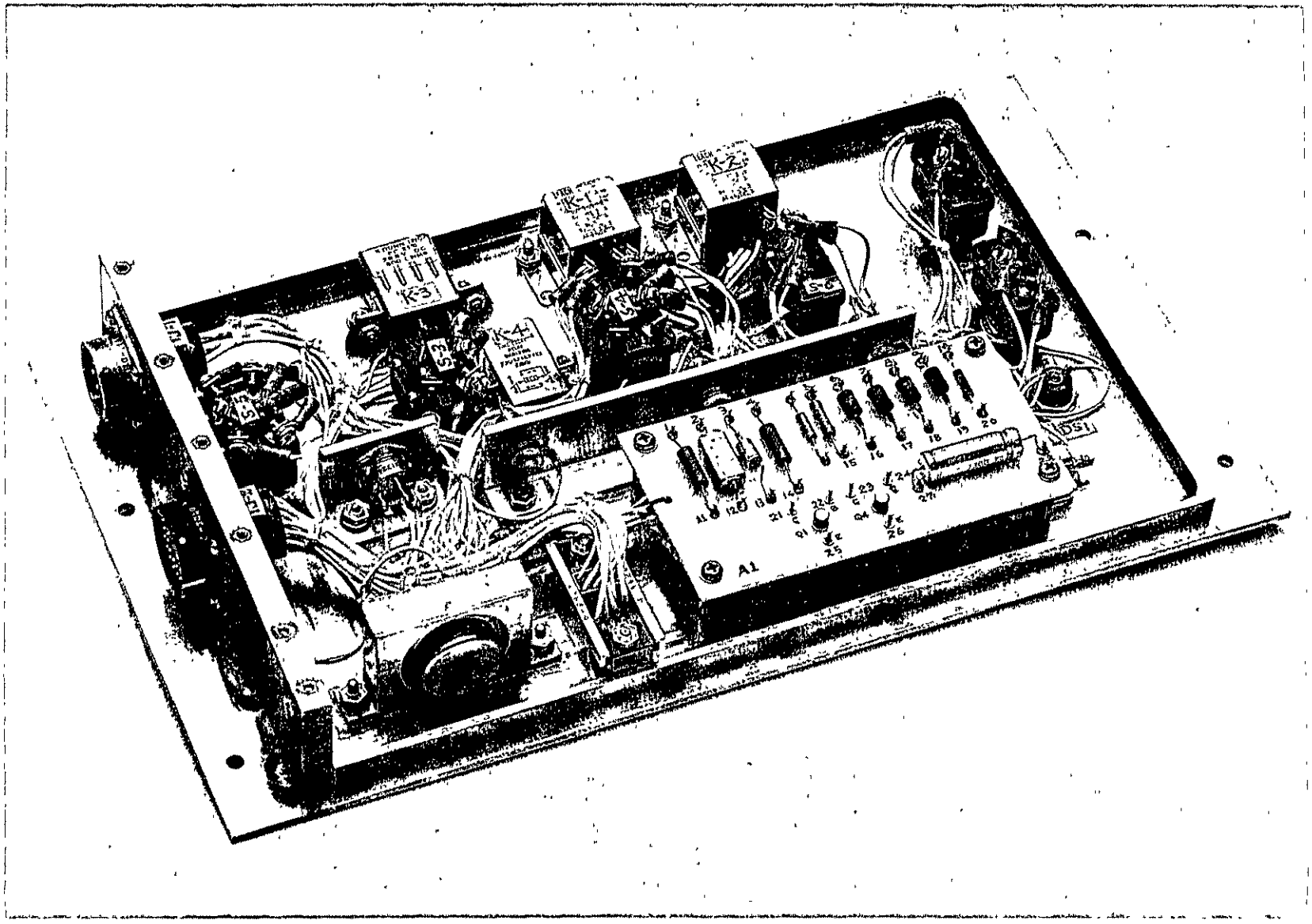


FIGURE 5.4-1 DVR CONTROL PANEL

Test data indicated that the panel sizes were adequate for the load levels required. A multiple layer radiation barrier was to be used on the back side of the panels but was removed to increase the cooling efficiency.

Weight of the DVR rectifier cold plate is 15 pounds. Some weight reduction was realized on the Qualification rectifier cold plate when relocated bus bars and supports permitted a reduction in panel size.

5.6 Input/Output Circuit and Filter

The input startup power connector, the power output terminal block, the power output relay, and filter capacitors were located on a panel at the rear of the unit. The power relay provided a method of isolating the output from the load until load was applied to the unit. This panel also provided a convenient place to mount the filter capacitors since the connecting leads to the DC bus are critical and should be maintained as short as possible.

5.7 Alternator

The alternator electrical design remained unchanged from Phases I and II except for improved ouput terminals. However, the terminals are still susceptible to breakage and future designs would include a supermica and O-ring type of construction which would not require welding.

Some additional work was done on insulating materials, and the new alternator made during Phase III was upgraded in several areas.

The field coil assembly used Fiberglas spacers along the inside of the field coil spool instead of mica which is subject to cracking and chipping. The field coil was also impregnated with a Stycast epoxy to improve the heat transfer of the coil. Phase I field coils were varnish impregnated. The stator assembly used a new high temperature varnish which is similar to epoxy and improved the thermal transfer. Polyimide film was used as insulation between end-turns instead of the mica used in Phase I. Another improvement was the elimination of the neutral power lead. This lead was located in a vulnerable position on the alternator housing and was not needed as a power lead because the alternator output is delta connected. This lead, used only for alternator testing, was brought out through the field connector. The field connector was also improved by increasing the pin size and allowing each lead to be connected to a single pin. Phase I alternators required splitting each lead and connecting it to three pins in the connector.

PRECEDING PAGE BLANK NOT FILMED.

6.0 FLIGHT PACKAGE DESIGN

6.1 Technical Requirements

General

The technical requirements for the HEPS were established by two criteria - the customer specification and the internal system configuration. The primary influence on design was the customer specification which established performance requirements and environmental constraints. The internal aspects inherent to the HEPS system influenced the optimization of the design and intercomponent performance. All of these aspects have been manipulated, sometimes through several iterations, in order to arrive at a satisfactory Qualification Unit design. The structural and thermal design considerations were the primary factors influencing package design.

Launch Environment

The launch vibration environment places the package in the most severe structural loading mode. When all types of inertial loads, including those due to launch, acceleration, shock, vibration, deployment and operations, were considered, the launch vibration environment was the most severe. Therefore, the package components, and especially primary structure, were sized for a 20 g vibrational load applied in any of three mutually perpendicular directions. While the design specification did not set the vibrational g level that high, it was justified based on two factors:

1. The random and sinusoidal spectrums were superimposed with a magnification factor of four applied to the sinusoidal input and proper vibration factors applied to both spectrums.

2. LM test experience wherein 20 g design levels have been required in some components.

This design limit level is expected to be adequate for all loads including anticipated 30 g shock levels during transportation when proper shock mounts are used in the shipping container. In general, the structural materials have been chosen with consideration given to a high elongation rate to meet the safety factor of 1.5 for the ultimate limit.

Lunar Environment

The lunar environment exposes the package to the most severe thermal environment, especially when the HEPS is operating.

Thermal design complexity was attributed to: LM/HEPS proximity, worst case incident solar and lunar radiation, and intercomponent exchange. In particular, the 1250°F turbine scroll had to be efficiently isolated from all other package components and the LM. The thermal requirements necessitated the use of hybrid thermal coatings to optimize net heat rejection from the HEPS. In this manner, smaller panels and reduced weight and reduced intercomponent heat exchange were realized.

Of secondary importance in the package design was the lunar vacuum. All components that have sliding contact during the deployment sequences are made of dissimilar metals and are dry lubricated to avoid cold welding. Also, the thermal control coatings on the heat rejection panels have been selected based on previous vacuum tests to confirm space compatibility or an actual space experience. Because of the lunar vacuum condition, the efficient multiple radiation layer type of thermal barrier was used extensively to minimize HEPS to LM and HEPS intercomponent thermal transfer.

Intercomponent Considerations

Design of the package has required considerable attention regarding component placement. Primary effort has been in placing the heat rejection panels in an optimum deployed configuration while still allowing adequate deployment kinematics to avoid interferences. The gas generator and oil separator were required to be above the turboalternator centerline to allow gravity drainage of the dribble volume and to provide a head of oil on the rotating unit, respectively. Minor components, such as the lube system accessories, the nitrogen pressurization system and the propellant lines and electrical harness stowage, were then placed where space remained. In the midst of the various component positions, a basic frame was provided as a common attachment place for all components. Finally, a combination extension device and adapter member was provided for frame attachment and to carry package inertial loads into the LM and for deployment out of the SEQ Bay. The placement of vibration mounts between the turboalternator and the frame isolated the LM from the HEPS vibration.

LM Vehicle

The initial design specification required that the HEPS package be stowed in SEQ Bay No. 2. Upon lunar landing, the package was to be removed from the bay and carried by one astronaut and mounted on the landing strut (Figure 6.1-1). A preliminary model which simulated the lunar weight and attachment sections was fabricated to verify this approach. It was immediately apparent that this was too difficult a task for an astronaut because of

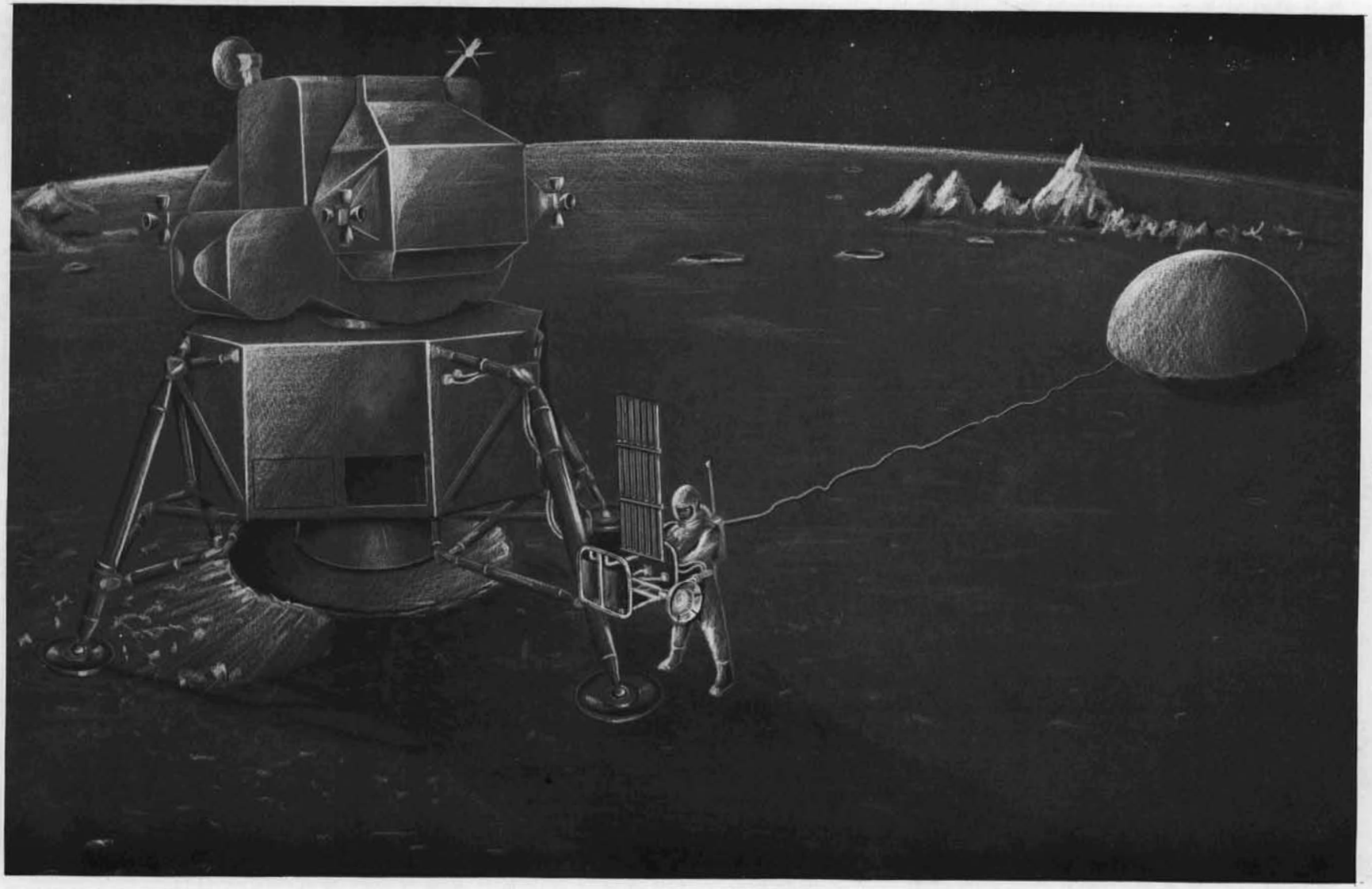


FIGURE 6.1-1 OPERATING LOCATION - LANDING STRUT MOUNTING

REPRODUCIBILITY OF THE ORIGINAL PAGE IS POOR

the bulky nature of the unit. The specification was revised to allow stowing the HEPS in the same bay and then extending it from the bay aperture to be operated as shown in Figure 2.0-2. The major package design task was then changed from astronaut compatibility to providing adequate heat rejection because of the LM proximity. All deployment and interface connections have been made within the confines of Scientific Equipment Bay No. 2 and the four hard mounts.

Weight

The proposed weight for the Phase III HEPS was estimated at 190 pounds. Early in the program, a request to reduce weight resulted in a design goal of 150 pounds which was considered attainable even without changing the turboalternator unit significantly. Under the reduced level of effort that was placed on the later portion of the program, the estimated weight of the Qualification Unit is 180 pounds. However, the design goal of 150 pounds without reducing the turboalternator weight appears achievable if a higher level of weight reduction effort were to be established. If the turboalternator were resized for actual 1.0 KW output, a 65 pound weight reduction could be achieved.

Life

The HEPS package has been designed for an operating life of 100 continuous hours under lunar environment conditions. The primary package design consideration for this life was the thermal coating durability under space vacuum and electromagnetic or particulate bombardment; in particular, the ultraviolet degradation. Any degradation factor in either the emittance or absorptance had to be considered in the sizing of the heat rejection panels. The low α/ϵ coating applied to the 400°F or lower heat rejection panels was tested at 400°F in vacuum and under one sun UV. Tests showed a significant increase in solar absorptance, which indicated a requirement for larger panels than anticipated or possibly a reduced operating temperature.

Design of the deployment mechanisms is not stringent with regard to life since it is deployed only once on the lunar surface and a limited number of times while on earth. The design of these mechanisms incorporated the use of dissimilar metals and dry lubricants on sliding surfaces in order to avoid cold welding under high vacuum conditions.

6.2 Integration into LM Vehicle

General

Efforts made toward integrating the HEPS package into the LM descent stage included detail discussions with personnel from GAEC and NASA/ MSC at two meetings prior to and during the critical design review. The first meeting was a TRW presentation of the initial concept. This was the first exposure of HEPS to the GAEC personnel and several design changes appeared necessary. The second meeting at GAEC was held to indicate the package changes that were jointly established after a detailed review by GAEC and TRW. The changes were agreed upon and appeared in the critical design review presentation where general satisfaction was expressed by the review team. The HEPS concept was essentially frozen at that time, except for minor modifications that were necessary because of more detailed treatment which followed.

Location

The HEPS package is designed to be located in the LM descent stage SEQ Bay No. 2, which is defined in Figure 6.2-1. The HEPS utilizes residual oxidizer and fuel and electrical startup power from that stage.

Envelope and Hard Points

The envelope and hard points specified for the HEPS are shown in Figure 6.2-2. The volume is a simple shape and is well defined because of its use for the ALSEP package. The volume is a right angle parallelepiped with a bevel at the right rear corner. The front 3.935-inch portion extends outside the metal equipment bay of the descent stage and is enclosed in retractable thermal barrier layers during flight.

The four hard points provide pin type support for the HEPS package. It should be noted that the front two hard points are outside the envelope; therefore, the adapter member from the HEPS-to-hard points is outside the package. An evaluation of this envelope violation showed no interference with other equipment as long as the ALSEP release mechanism is not in place. This mechanism would not be used for the HEPS deployment and is, therefore, not needed.

Structural

The various inertial and operating loads due to the HEPS are carried into the LM via the four hard points only. The unit is not rigidly fastened to the mount pins but is pin supported.

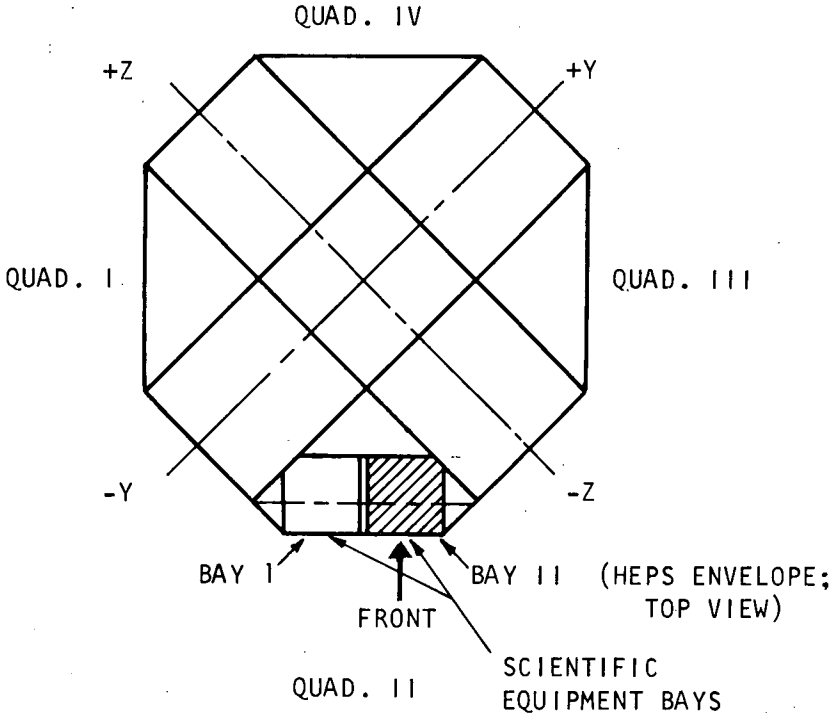


FIGURE 6.2-1 LM DESCENT STAGE AND VIEW LOOKING DOWN (- X COORDINATE IS LOOKING INTO PLANE OF PAPER)

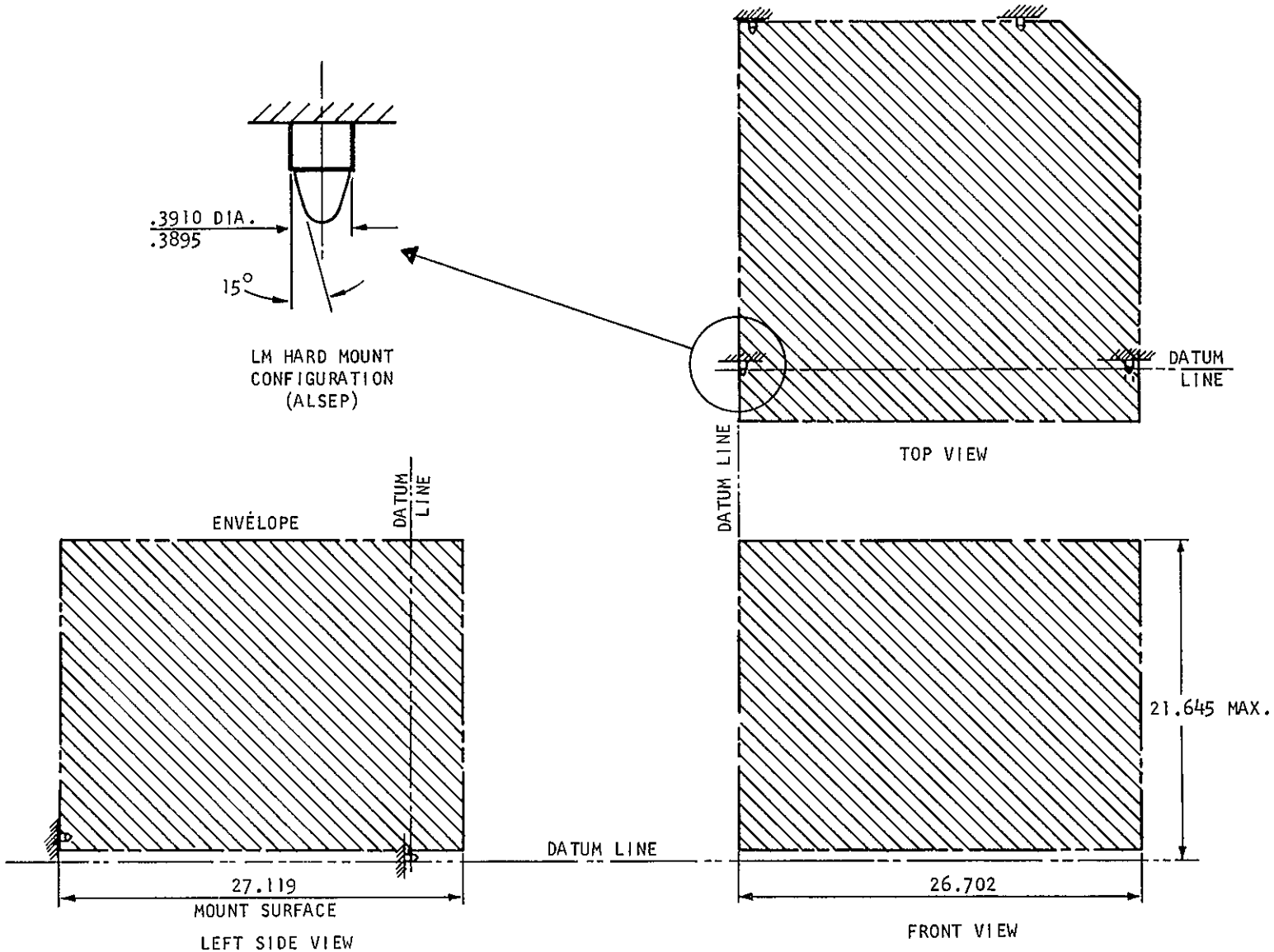


FIGURE 6.2-2 HEPS ENVELOPE

Shear or tension loads, but no torsion loads, are applied to the LM support structure as in the case of the ALSEP design. The rear two pins can experience shear only while the front two can experience shear and tension. The front two hard points for the HEPS differ from the ALSEP in that the HEPS requires shoulder bolts in place of plain pins in order to resist inertial loads applied in the forward or rear direction.

Points where the propellant and electrical lines enter the LM will be subjected to small inertial loads which are not large compared to the HEPS package loads. However, some minor form of local reinforcement will be required on the rear surface of the Scientific Equipment Bay.

Thermal

The LM and HEPS will interchange significant thermal energy because of their proximity, and the transfer occurs by conduction and radiation. While the heat transferred by conduction is less than the heat transferred to the LM by radiation, the conduction to the LM has a greater effect on LM. Conductive transfer places the heat energy internal to the LM which causes the interior temperature to rise since there is an efficient thermal barrier around the LM that resists transfer out to space. The greater radiant energy incident on the LM from the HEPS is efficiently buffered from the interior by the LM shielding. Both transfer modes have been studied to minimize the effect on LM temperatures. Radiant interchange is at a minimum because the HEPS heat rejection panels have been geometrically placed to minimize the view factors to the LM and the lunar surface. This minimized radiator panel sizes because of maximum view factors to cold space.

Mechanical Interfaces

The mechanical interfaces that exist between the HEPS and the LM vehicle are as follows:

1. Propellant hose connections
2. DC electrical power bus to LM
3. Startup electrical power to the HEPS
4. Structural attachment to the LM
5. Thermal interchange

The oxidizer and fuel lines interface at the rear surface of the HEPS envelope. The hose connections to the HEPS are such that

the interface location can be made almost anywhere on this rear surface which is 20.750 inches high by 21.702 inches long. The preferred location is in the lower half of the surface since the hose connections are in the lower left hand corner, and the electrical interface panel is in the upper right corner of the package. It is known that no reinforced sections exist in the rear surface of the SEQ, and they would have to be added to accommodate the interface. The DC power bus lines and HEPS startup power harness would also be interfaced on the rear surface of the bay and require reinforcing. The loads imposed on the propellant and electrical connections would be low and sized primarily for handling loads. Loads due to launch or deployment are small.

Structural attachment of the HEPS to the LM is well established because the ALSEP mount points are specified for use. Interfaces are straightforward and the only area of was the weight and center of gravity of the HEPS which differ somewhat from the ALSEP.

Thermal interchange was a more difficult interface to consider because of the proximity of the HEPS and LM. In order to minimize radiant thermal energy transfer, the HEPS heat rejection panels were designed with minimum view factors between LM and HEPS. It can only be qualitatively stated that 1) radiant interchange between LM and HEPS is minimized, 2) that the HEPS to LM interchange is significant and 3) that specific thermal barriers may have to be provided on the LM external surfaces to prevent temperature excursions on the LM beyond design points.

Conductive heat transfer between the HEPS and LM is toward the LM and is smaller by an order of magnitude than the incident radiant energy. However, the conducted heat enters the interior of the LM and can only escape by transfer through very efficient thermal barriers surrounding LM. For this reason, the conduction path from HEPS to LM is one of high resistance.

Astronaut Interface

Astronaut participation is of prime importance in the design. The objective has been to avoid overburdening the astronaut with operation of the HEPS so that valuable time may be spent on scientific information gathering. The major task involving HEPS is deployment where four separate sequences must occur. Operation of the unit is more simply performed because of the control panel which was designed for visual and manual convenience. The astronaut will control the four sequences by lanyard manipulation similar to ALSEP. This manual manipulation includes triggering the four events and provides deployment power. The

present design includes the following components used for deployment.

1. Release devices for deployment initiation.

2. Mechanisms for rotating and translating components.

3. Locks to maintain deployed positions.

An additional design feature being considered for deployment is the utilization of springs. The springs would provide the force required to deploy the HEPS.

The control panel for unit operation is presently located on the unit so that it can be qualified as part of the package. It is recognized that it would eventually be located elsewhere and most likely in the LM. This would eventually require a wire harness to interface with the LM and in the same location and manner as the electrical power and startup power harnesses.

6.3 Thermal Analysis

Environmental Considerations

The HEPS unit was designed to operate at the worst possible conditions that could be encountered in the lunar environment. The specifications require operation with a lunar surface temperature between 0°F and 260°F. This corresponds to a solar inclination between 10° and 90° above the horizon. The variation of the lunar surface temperature with solar inclination is shown in Figure 6.3-1 (see reference 2). The worst operating environment is nct necessarily at the subsolar point even though that is when the lunar surface is hottest. Actually, a combination of thermal emission from the lunar surface and solar absorption is more severe slightly below the subsolar point. The worst condition is merely a function of the individual component's orientation with respect to the sun and the lunar surface. Each component in the package, therefore, was designed to operate under its own worst environment.

The lunar albedo effects on the HEPS unit operation were found to be negligible. The albedo factor of the moon is approximately 0.07, thus the incident heat flux is very small. Conversely, the surface of the LM and other HEPS components were found to have a significant effect on the unit. These effects were included in the analysis when applicable.

The environmental ground tests do not entirely duplicate the lunar environment. The test specifications require operation at 20°F and 160°F ambient temperatures. The environmental

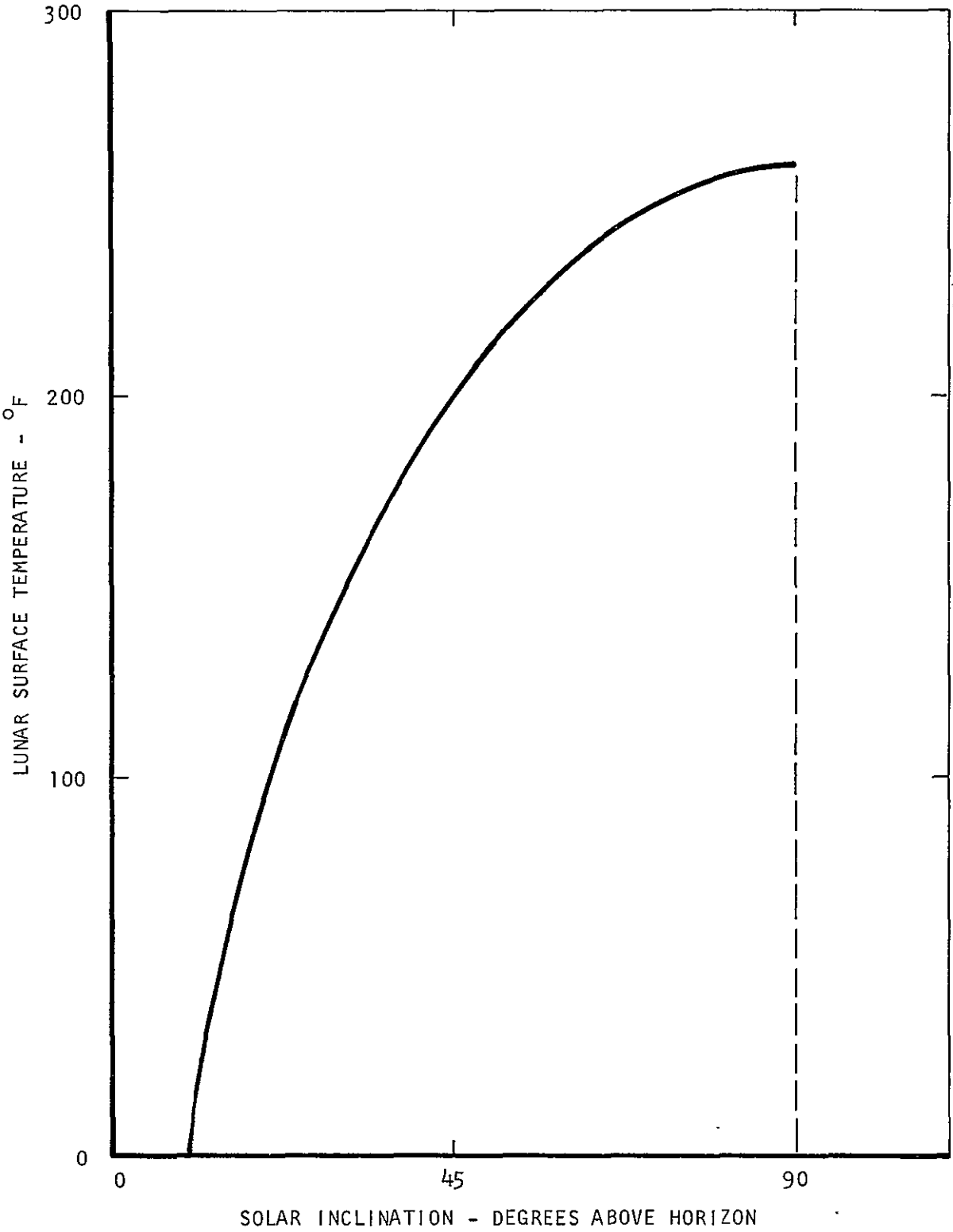


FIGURE 6.3-1 SURVEYOR SPACECRAFT MODEL A-21 EQUIPMENT SPECIFICATION 224832 (SEE REFERENCE 2, SECTION 6.3)

temperatures for the various HEPS components during their operation on the moon do not correspond to these required ambients. However, the 160°F ambient requirement is generally more severe than the anticipated lunar environment. Therefore, a design that operates in the vacuum chamber at 160°F will be conservative for most of the components. Operation at 20°F is ideal for HEPS because the reduced heat sink temperature promotes heat transfer by radiation. However, oxidizer and fuel freezing, which occurs at 12°F and 18°F, respectively, could prevent ignition of the gas generator.

The pressure level in the vacuum chamber is not as low as the pressure on the lunar surface. The vacuum chamber runs at a pressure of approximately 0.6 mm Hg as compared to 10^{-16} torr on the moon. As a result, there will be additional convective cooling in the chamber. However, calculations show that the convection effects account for less than 1% of the total heat rejection by radiation.

The vacuum chamber pressure also has an effect on the insulating value of the multilayer radiation barriers that are used on the unit. The super-insulation manufacturers recommend that the pressure during operation be less than 10^{-4} mm Hg. Therefore, it was concluded that if the insulation performance was satisfactory in the chamber then it would certainly be adequate for lunar application.

Each component in the HEPS unit will have its own environment on the moon which is chiefly a function of its orientation and surface properties. The effective sink temperature (T_S) of a particular component represents the combined effect of all solar and thermal energy that can influence its performance. For the HEPS, the thermal energy comes from the lunar surface, the LM surfaces and from other parts of the HEPS unit. The rate of incident energy on a component depends on the temperature and surface characteristics of the energy source and the view factor to the energy source. This is true of both solar and thermal radiation. Incident energy is defined as:

$$(Q/A)_{INCIDENT} = F \times I \left[\frac{BTU}{hr\text{-}ft^2}\right]$$

where F is the view factor and I is the emitted energy from the source.

The emitted energy is defined as:

$$(I)_{THERMAL} = \sigma_1 \epsilon_1 T^4 \left[\frac{BTU}{hr\text{-}ft^2}\right]$$

where σ_1 is the Stefan-Boltzmann constant $0.171 \times 10^{-8} \left[\frac{BTU}{hr\text{-}ft^2}\right] {}^{o}R^4$ ϵ_1 is the surface emissivity of the source and T is surface temperature of the source (^{o}R).

$$(I)_{SOLAR} = 442 \left[\frac{BTU}{hr\text{-}ft^2}\right] \quad \text{(reference 3)}$$

The resulting definition of the effective sink temperature is:

$$T_S = \left\{\frac{1}{\sigma_1}\left[\frac{\alpha_S}{\epsilon_{th_1}}\left(\frac{Q}{A}\right)_{INCIDENT\text{-}SOLAR} + \left(\frac{Q}{A}\right)_{INCIDENT\text{-}THERMAL}\right]\right\}^{1/4} {}^{o}R$$

where α_S and ϵ_{th_1} are the solar absorptivity and thermal emissivity, respectively, of a particular component surface.

The most difficult task in calculating the effective sink temperature was determining the view factors. The majority of the view factors were based on configuration P-2 (see reference 4) along with an extensive geometrical analysis.

The view factor to the sun is merely the cosine of the solar inclination angle above the lunar horizon. Various component geometries with their resultant view factors are shown in Appendix C.

Thermal Design of Electrical Components

The thermal requirements for the rectifier cold plate were very severe because the total heat rejection rate for the panel was 1200 Btu/hr (peak power) with a maximum diode stud temperature limitation of 320°F. A temperature drop exists between the diode stud and the radiating panel due to the electrical insulation. The radiator was designed to run cooler than the stud in order to maintain the required stud temperature. The magnitude of this temperature drop depends on the insulation characteristics and the power dissipated from the diodes. Typically, it varies between 0.2 °C/watt and 0.3 °C/watt. At 55 watts dissipation per diode, the temperature drop varies between 20°F and 30°F. Therefore, the radiator was designed to operate at approximately 290°F to maintain the proper diode stud temperature. In the lunar environment, the cold plate is exposed to an effective sink temperature of 124°F (see Appendix C for view factors and orientation). The difference between the root temperature (290°F) and this sink temperature is small enough that the

REPRODUCIBILITY OF THE
ORIGINAL PAGE IS POOR

radiator must be reasonably large and very efficient. The radiator efficiency or effectiveness depends largely on the material thickness, conductivity and the conduction path length from the source of heat to the fin edge. The basic curve used for fin effectiveness determination is presented in Figure 6.3-2 (see reference 5). The generalized length parameter is defined by the following equation (see reference 5):

$$L = l\sqrt{\frac{\sigma_1 \epsilon_1 (10^9)}{kt}\left(\frac{T_R}{1000}\right)^3}$$

where l is the representative plate length from source to edge (ft), σ_1 is the Stefan-Boltzmann constant where:

$\sigma_1 = 0.171 \times 10^{-8}$ (Btu/hr-ft^2-^{0}R^4)

is the surface emissivity of the plate, k is the thermal conductivity of the plate (Btu/hr-ft-^{0}R), t is the plate thickness (ft), and T_R is the source temperature (^{0}R).

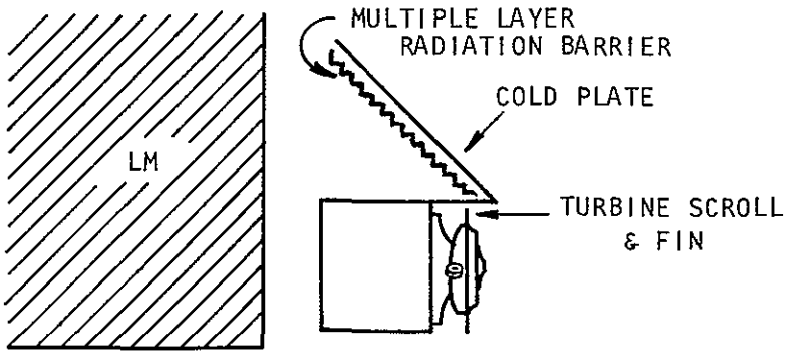
With an aluminum panel, a thickness of 1/8 inch was a reasonable tradeoff between radiator weight and radiator efficiency. This yielded a radiator effectiveness of approximately 0.91.

With the root temperature and fin effectiveness established, the following equation was used to determine the required area:

$$A = \frac{Q_{REj}}{\sigma_1 \epsilon_1 \eta \left(T_R^4 - T_S^4\right)} (ft^2)$$

where Q_{REj} is the required heat rejection rate (Btu/hr), σ_1 is the Stefan-Boltzmann constant 0.171 x 10^{-8} (Btu/hr-ft2-^{0}R^4), ϵ_1 is the surface emissivity, η is the fin effectiveness, T_R is the source temperature (^{0}R) and T_S is the effective sink temperature (^{0}R).

The required area for the rectifier cold plate was approximately 4.0 ft^2 with radiation from one side only. Originally, the backside of the cold plate was to be insulated as shown below.



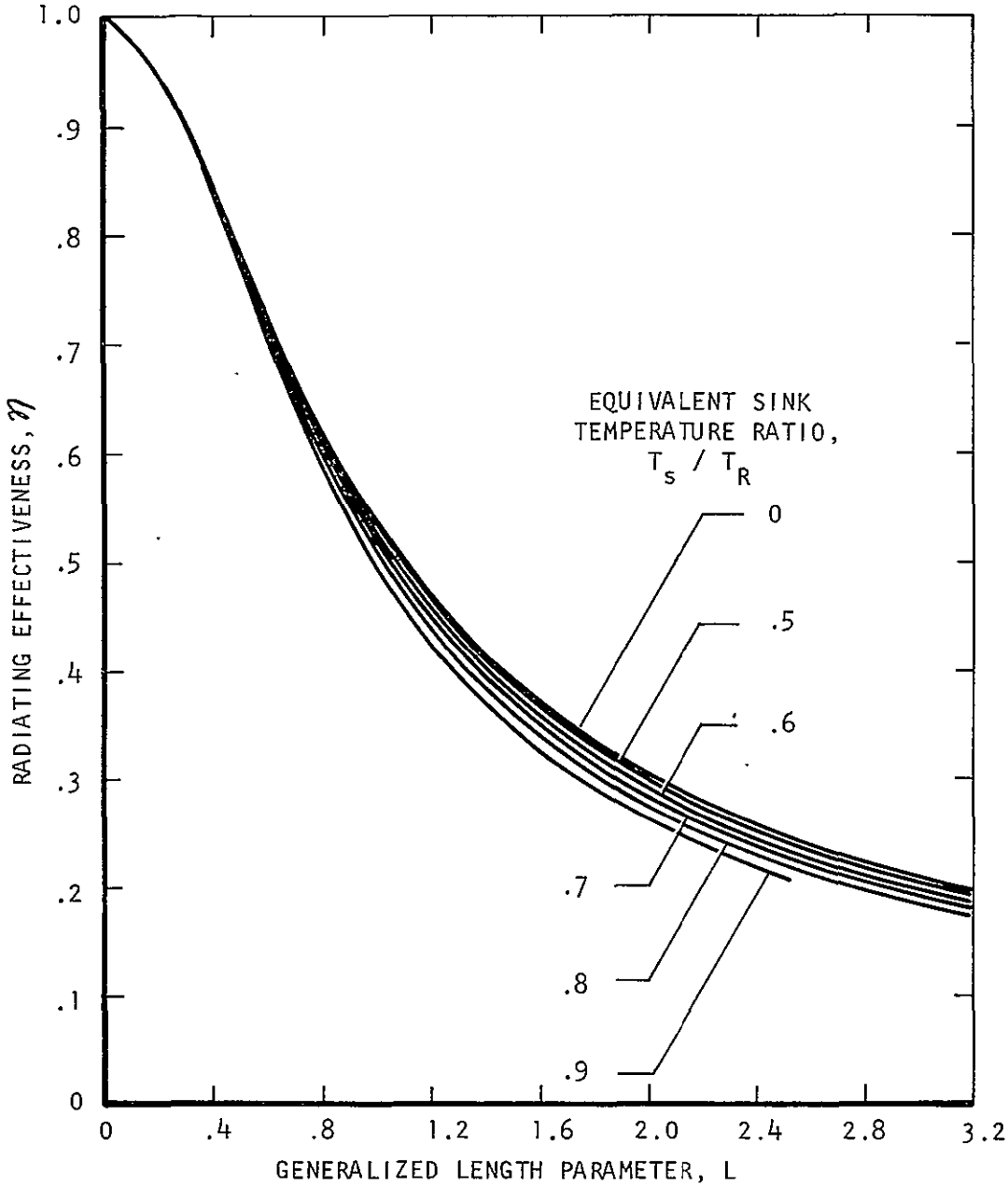
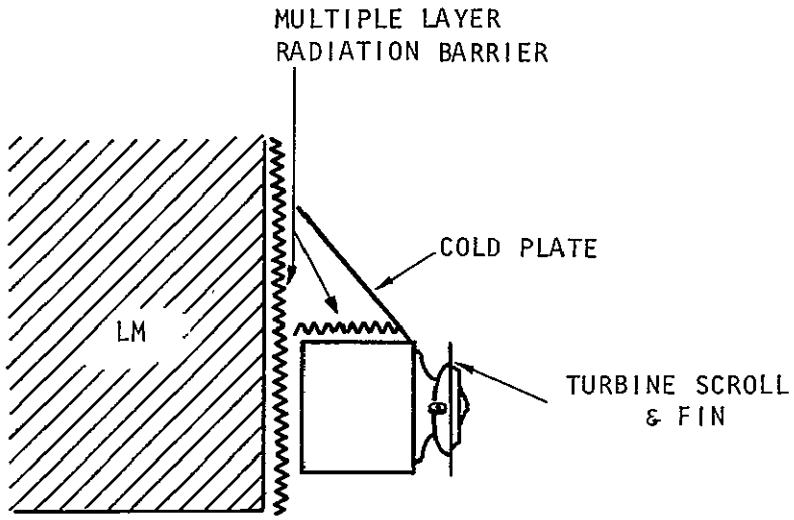


FIGURE 6.3-2 VARIATION OF RADIATING EFFECTIVENESS WITH FIN PLATE LENGTH

This would have eliminated the heat transferred from the turbine scroll and fin to the cold plate, and it would have also minimized the heat radiated from the cold plate to the lunar module. This concept, however, was not feasible for vacuum chamber use when the ambient temperature in the test chamber was 160°F which is much more severe than the 124°F lunar environment. The cold plate would run too hot with radiation from one side only; therefore, some of the insulation was removed from the back side. Testing revealed that this was not sufficient and the cold plate was then moved back to avoid any view of the scroll. In addition, all of the insulation was removed from the backside and a layer of insulation was placed on top of the HEPS unit to avoid any view to other components, such as the alternator and oil separator. The following sketch shows the resulting orientation and insulation. This approach was incorporated in the Qualification Unit after successful testing.



Since the backside of the diode panel was uninsulated, it also contributed toward heat removal; therefore, the design was slightly conservative for lunar operation.

The voltage regulator consists of two basic heat emitting components, the diodes and the SCR's. The temperature limitation on the diodes is not as severe as it is on the SCR's. The diodes can run as hot as 350°F as compared to 260°F for the SCR's. In order to maximize the heat radiated from the voltage regulator radiator, it was made in two pieces. One part of the radiator cooled the diodes while a second part cooled the SCR's at a lower

temperature. These components were also electrically insulated from the radiator surface. Therefore, the radiators were required to operate at a lower temperature than the electrical components. In order to stay within the maximum temperature limitations, the diode and SCR radiators were designed to operate below 311°F and 238°F, respectively. The radiators, made of aluminum, operate at approximately 0.92 effectiveness, and the effective sink temperature in the lunar environment is 178°F (refer to Appendix C for the radiator orientation). The required areas needed to maintain the proper temperature levels were 0.22ft² for the diodes and 0.55 ft² for the SCR's. The required heat rejection rates were 54.6 Btu/hr for the diodes and 51.2 Btu/hr for the SCR's.

The speed control radiator must remove 40.9 Btu/hr and maintain a component temperature less than 210°F. In the worst lunar environment, the effective sink temperature is 162°F. The radiating panel effectiveness is approximately 0.90. The electrical insulation between the electrical components and the radiator accounted for an 11°F temperature difference. Therefore, the radiator, also made of aluminum, was designed to operate at approximately 200°F. The required area for the radiator to reject the proper amount of heat was 0.71 ft. (See Appendix C for the speed control radiator orientation and view factors.)

The thermal requirements of the control panel were different from the other electrical components. The critical item is a large silicon transistor that dissipates 167.3 Btu/hr. However, it only operates for 30 seconds during the startup cycle. The maximum allowable temperature for the transistor is approximately 256°F (125°C). Therefore, a conductive heat sink large enough to absorb the heat and keep the temperature within limits was required. Since the duration of operation is so short, radiation to the lunar environment is negligible. The amount of heat removed in 30 seconds is 1.4 Btu and, therefore, an aluminum heat sink volume must be at least 0.83 in³ to adequately cool the transistor. The sink was designed as a mounting bracket between the transistor and the control panel radiator with a volume of 1.0 in³. The transistor was directly mounted to the heat sink with electrical insulation between the heat sink and the radiator. This eliminated the conductive barrier between the transistor and the sink.

After the initial startup cycle, the control panel must reject approximately 24 Btu/hr and maintain component temperatures below 210°F. The effective sink temperature for this radiator is 178°F (see Appendix C for the orientation). As with the speed control, this panel operated at approximately 0.90 fin effectiveness and 200°F fin temperature and was made of aluminum. The area

required to remove the heat was 0.65 ft²; however, the panel was made larger to accommodate mounting the various components. The resulting area was 0.78 ft².

Thermal Design of Scroll-Fin-Reflector Arrangement

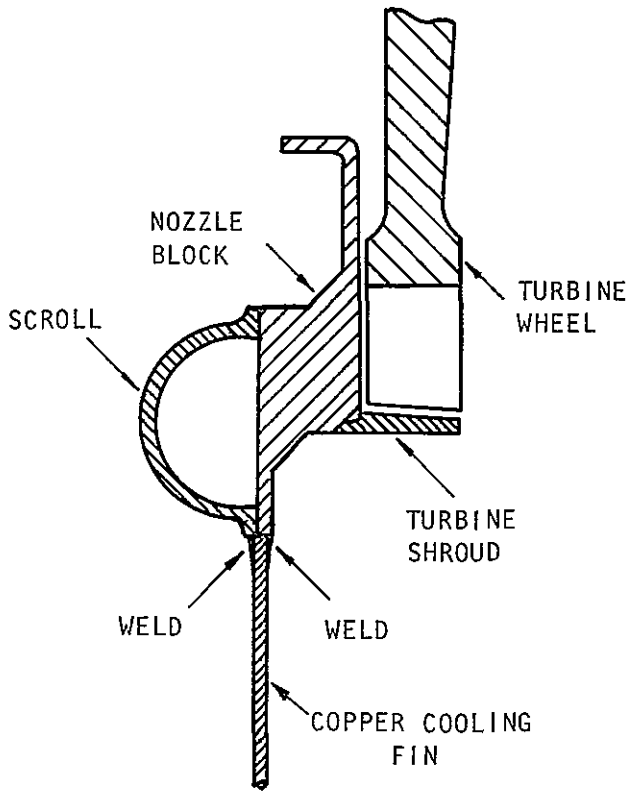
The gaseous combustion products that drive the turbine would cause the turbine scroll to reach intolerably high temperature levels if cooling was not provided. The concept of adding radiating fins to the scroll was proven in the previous phases on the HEPS program. However, a need still existed for improvement. Some modifications made during Phase III were the addition of a combustion reflector and heat shield, improved conduction path between the scroll and the scroll fin and the use of emissivity coatings. The thermal coatings are discussed in more detail in Section 7.3.

Initially, the heat reflector was to be a parabolic, highly reflective surface; however, restrictions within the package limited the available space and a different shape had to be used. The geometry that was used consisted of a 2-inch radius section on the inside, followed by a conical section and a straight section. The surface of the reflector was gold plated to improve the reflectivity.

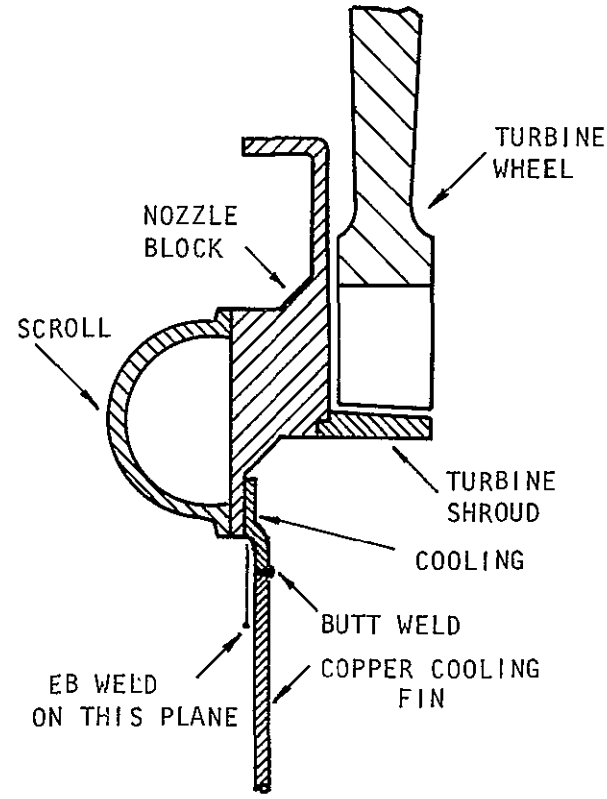
The copper cooling fins on the scroll were sized to remove approximately 20,000 Btu/hr. This heat rejection rate was based on performance and temperature levels from previous testing. The fins were located around the circumference of the scroll. The first sections covered approximately one-third of the scroll with a 4-inch fin width. The remaining fins had a width of 3 inches. Since the cooling fins were 1/8 inch thick, they had an effectiveness of 0.54 and 0.65, respectively, for the 4-inch and 3-inch widths. The total fin area was 0.84 ft². If the fins operate at a temperature near the design scroll temperature of 1350°F, the calculated heat rejection rate is 23,400 Btu/hr.

One major change in the new fin design was an improved conduction path between the scroll and the fin. Previously, the fin was welded onto the end of the scroll flange with very little surface area in contact. The Phase III fin was welded along the flange so that there was much more area in contact. This conduction path, as illustrated below, was designed to improve fin effectiveness and heat rejection rate through higher fin temperature operation.

Testing of the development unit in the vacuum chamber indicated that the qualification unit design was somewhat conservative. The DVR unit had a heat reflector of the same geometry as the final design; however, it did not have a high reflectivity surface. The conduction path between the scroll and the cooling fin for the DVR unit was the Phase II design. In addition, the fin area was only 0.6 ft².



PHASE II — FIN ATTACHMENT



PHASE III — FIN ATTACHMENT

With this combination of fin size and attachment and reflector design, the temperature levels stayed within the acceptable limits; therefore, the qualification unit design was conservative. Further weight reduction and less hardware complexity could be achieved without hampering the operation.

Thermal Control of Flight Package

There is a significant amount of thermal interaction between the various HEPS components and between the HEPS package and the Lunar Module. Within the package, there are components that operate at temperatures as high as 1350°F in close proximity to components whose temperature cannot exceed 200°F. In addition, the amount of heat that is transferred into the LM had to be minimized or eliminated wherever possible. Therefore, much effort was given to package arrangement and heat transfer paths.

The most important thermal considerations in package arrangement were the component view factors. Cool components were not allowed to "see" hot components. The deployed oil radiator, for example, was designed to be in the same plane as the scroll fins. Therefore, the view factor from the radiator to the fins was essentially zero, and the view factor to the scroll and shroud was minimized. In addition, a heat barrier was also used to eliminate any direct view of the scroll and shroud. A scroll reflector served as a heat shield protecting the frame and electronics from the hot scroll.

Two modes of heat transfer were controlled. The first of these, radiation, was minimized through the use of multiple layer radiation barriers. This super-insulation was used on the back of the scroll heat reflector to make it a true heat shield as well. If the heat shield operates at 1000°F, components on the other side of the foil will be at 200°F when 25 layers of the insulating foil are used. These components may be hotter due to other components near them, but the effect from the heat shield, scroll and shroud will be very small. Super-insulation is used on the backside of all of the electronic boxes to minimize radiation effects. It is also used between the gas generator and the scroll heat reflector and on the top of the frame to minimize the interaction between the package and the rectifier cold plate. The second type of heat transfer is conduction. Conductive paths within the package were minimized through the use of thin members and nonconductive insulating material. These high strength insulators, such as Supramica, are extremely effective in reducing the heat transferred between components.

In order to minimize the heat input to the LM, radiation barriers such as super-insulation were used between the HEPS package and the LM. Some components, such as the oil radiator, were positioned such that the radiation to the LM was minimized. With the oil radiator deployed, the heat input to the LM was only 255 Btu/hr. The use of nonconductive insulators between the HEPS frame and the LM SEQ bay is essential.

Another aspect of thermal control was the thermal coatings that were applied to the radiating surfaces. A combination of high thermal emissivity and low solar adsorptance is required for best performance. The aluminum radiating panels, such as the oil radiator, and the rectifier cold plate and the electronic boxes have a surface emissivity of approximately 0.1 to 0.2. Therefore, only 10% to 20% of the heat within the aluminum will be radiated to its surroundings. By applying a thermal coating, this emissivity was increased to approximately 0.85. Therefore, with the coating, 85% of the heat can be radiated. The same is true with the scroll and fin arrangement; however, the effect is not as strong on the scroll since Hastelloy has an emissivity of approximately 0.5. The copper is greatly improved from 0.1 to 0.85.

6.4 Oil Radiator Design

The radiator location with its view factors is shown in Appendix C. In the lunar environment, the radiator "sees" an effective sink temperature of 135°F. As with some of the electronics radiators, the vacuum chamber test at 160°F is more severe than the lunar environment. Therefore, operation in the vacuum chamber proves that the design is slightly conservative with the

exception that the radiator was not located in its final position for the vacuum chamber tests. Due to the size of the chamber, the radiator was mounted behind the unit instead of on the side near the scroll; therefore, care was taken to provide adequate insulation to eliminate any effect from the scroll and the other hot components.

The thermal analysis for the oil radiator was more complex than for the electronic packages because there is a two-dimensional temperature gradient in the oil radiator. The aluminum fin temperature decreases from the heat source (oil) to the edge, and in addition, the oil temperature decreases throughout the radiator from inlet to outlet. There is also a temperature gradient between the oil itself and the tubing which is brazed to the radiator. The first gradient in the fin from the source to the edge is accounted for as a fin effectiveness. This is defined the same as it was for the electronic packages in Section 6.3. For a 1/16-inch thick aluminum fin the effectiveness is approximately 0.95.

The decrease in oil temperature from inlet to outlet was 10°F. This calculation was based on the total heat rejection rate of 2470 Btu/hr, an oil flow rate of 0.9 gpm, oil specific heat of 0.74 Btu/lbm-°F and oil density of 0.0313 lbm/in³. The following equation defines the temperature gradient:

$$\Delta T = \frac{Q_{REj}}{\dot{m}\, C_p (60)} \ (^{o}F)$$

where Q_{REj} is the heat rejection flow rate in Btu/hr; $\dot{m}$ is the mass flow rate in lbm/min and c_p is the oil specific heat in Btu/lbm-°F Testing showed this temperature drop to be 12°F as compared to a calculated value of 10°F.

The temperature drop from the oil to the radiator fin was determined using the Prandtl number, the Nusselt number and the Reynold's number to find the heat transfer coefficient. The following equation defines the temperature gradient:

$$\Delta T = Q_{REj}/hA \ (^{o}F)$$

where Q_{REj} is the heat rejection rate in Btu/hr, h is the heat transfer coefficient in Btu/hr-ft²-°F and A is the total surface area of the inside of the tubing in ft².

The heat transfer coefficient is defined as:

$$h = \frac{N_{Nu}k}{D}$$

where N_{Nu} is the Nusselt number, k is the thermal conductivity of the oil in Btu/hr-ft-F and D is the inside diameter of the tubing in ft.

The Nusselt number is defined as:

$$N_{Nu} = 0.0265 \ (N_{Re})^{0.8} \ (N_{PR})^{0.3}$$

where N_{RE} is the Reynold's number and N_{PR} is the Prandtl number.

A definition of the Reynold's number is:

$$N_{RE} = \frac{\rho V D}{\mu}$$

where ρ is the density of the oil in lbm/ft^3, V is the oil velocity in the radiator in ft/sec, D is the outside diameter of the tubing in ft and μ is the oil viscosity in lbm/ft-sec.

The Prandtl number is defined as:

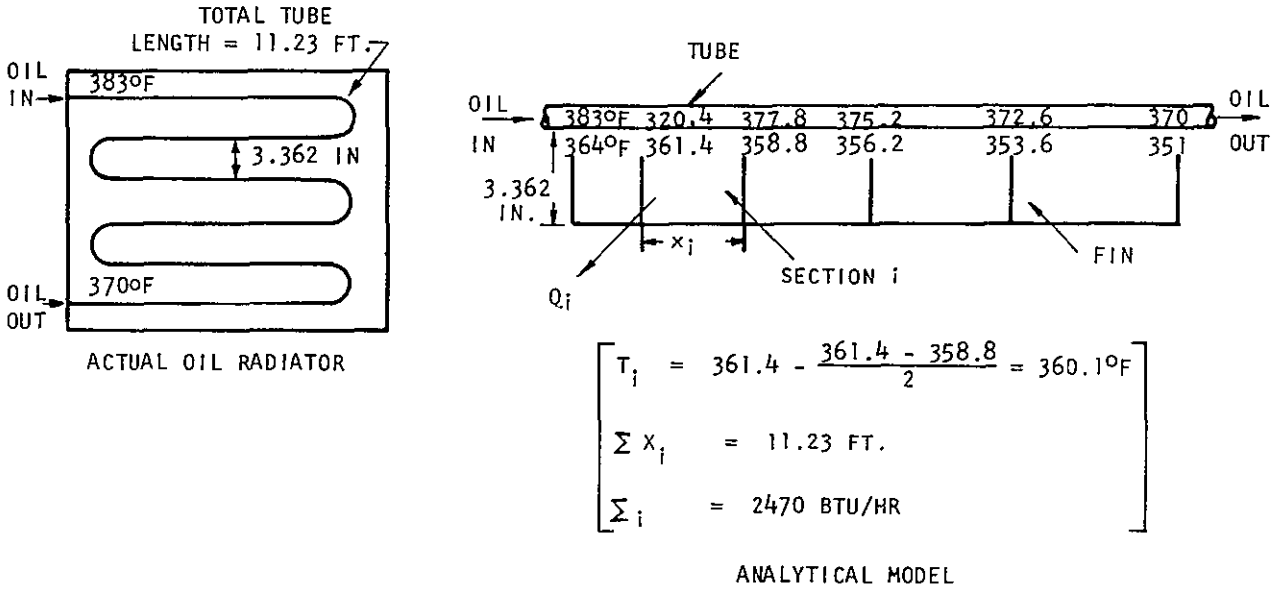
$$N_{PR} = \frac{C_P \mu}{k} \quad (3600)$$

where c_p is the specific heat of the oil in Btu/lbm-F, μ is the viscosity of the oil in lbm/ft-sec, and k is the thermal conductivity of the oil in Btu/hr-ft-F.

The resulting temperature drop from the oil to the radiator was calculated as 18.5°F. Testing revealed that the drop in temperature was actually 19°F. A complete temperature profile of the oil radiator at the worst vacuum chamber ambient temperature can be seen in Figure 8.5-17.

A two-dimensional analysis of the radiator was required. A model was defined which closely simulated the actual radiator. The model was then broken down into increments, and a sectional analysis was made assuming that the same amount of heat was rejected from each section. The model was made merely by unwrapping the tubing that is used on the oil radiator as shown in the following figure.

It was found that five increments were sufficient for a meaningful result. The addition of more sections did not change the required area. The analysis consisted of first defining the anticipated temperature profile and heat rejection rates. The numbers that appear in the sketch above are real temperatures as



derived from actual testing. These temperatures, of course, were not known at the time the radiators were sized. The numbers that were estimated at that time were as follows:

Estimated: $T_{OIL} = 400°F$

$Q_{REj} = 4500$ Btu/hr

This heat rejection rate was based on previous testing in Phases I and II on the HEPS program. Although allowances were made for the improved performance of the unit, it actually worked better than anticipated. Based on a heat rejection rate of 4500 Btu/hr, two oil radiator panels were required; however, testing in the vacuum chamber showed that one panel would be sufficient. A back calculation then showed that the actual required heat rejection rate was only 2470 Btu/hr with only a single radiator.

Once the heat rejection rate and temperature profile were established, an average temperature ($T_{}$) was found for each section. Using this temperature, the previously calculated fin effectiveness and the heat rejection rate for each section, the required area for that section can be calculated. The same equations that were used in Section 6.3 for determining radiator area also applied. The total radiator area is merely the summation of each of the incremental areas. The resulting area for the radiator, after eliminating one panel, was 3.38 ft^2.

The primary mechanical design requirement of the oil radiator was to minimize the line pressure drop. The tubing size on the panel was thus increased from 1/4 inch O.D. to 5/16 inch O.D. with a resulting change in pressure drop from 2.25 psi to 0.70 psi at 400°F and from 42.7 psi to 15.2 psi at 20°F operation (cold start). The stress on the tubing at these pressure levels was 1250 psi which is well within the material limits.

6.5 Package Arrangement

General

The package arrangement proceeded by setting priorities in the following descending order of importance:

1. Place components that have a mandatory position relative to other components.
2. Place deployable components in an advantageous posit tion, primarily the outer volume of the package.
3. Place components that interface with LM in preferred positions.
4. Place the main structural member.
5. Place components with no preferred position.
6. Place routing of tubes and harnesses.

To aid in package visualization, Figures 4.1-2, 6.5-1 through 6.5-18 and 8.5-14 provide considerable detail.

Turboalternator

The turboalternator is the heaviest portion of the HEPS system and should preferably be centrally located in the envelope. However, two factors placed the rotational axis to the lower right direction. First, the gas generator has a preferred location above the turbine centerline to provide gravity drain. Second, the oil separator has a preferred location above the turbine centerline to provide a lube head at the supply pump inlet. The large diameter turbine scroll and heat rejection fins prevented the unit from being located further to the lower right. In fact, the fin height was reduced as required to fit the turboalternator into the package. This detail is shown in Figures 6.5-7 and 6.5-8.

The turbine was isolated from other components by placing it in the forward volume of the envelope because of its high temperature and hot exhaust gases.

Heat Rejection Panels

The heat rejection panels were located in the outermost volume of the package (Figures 6.5-1, 6.5-2 and 6.5-3) since they consist of large areas and, in three cases, require deployment. An additional primary requirement was that the view factors between

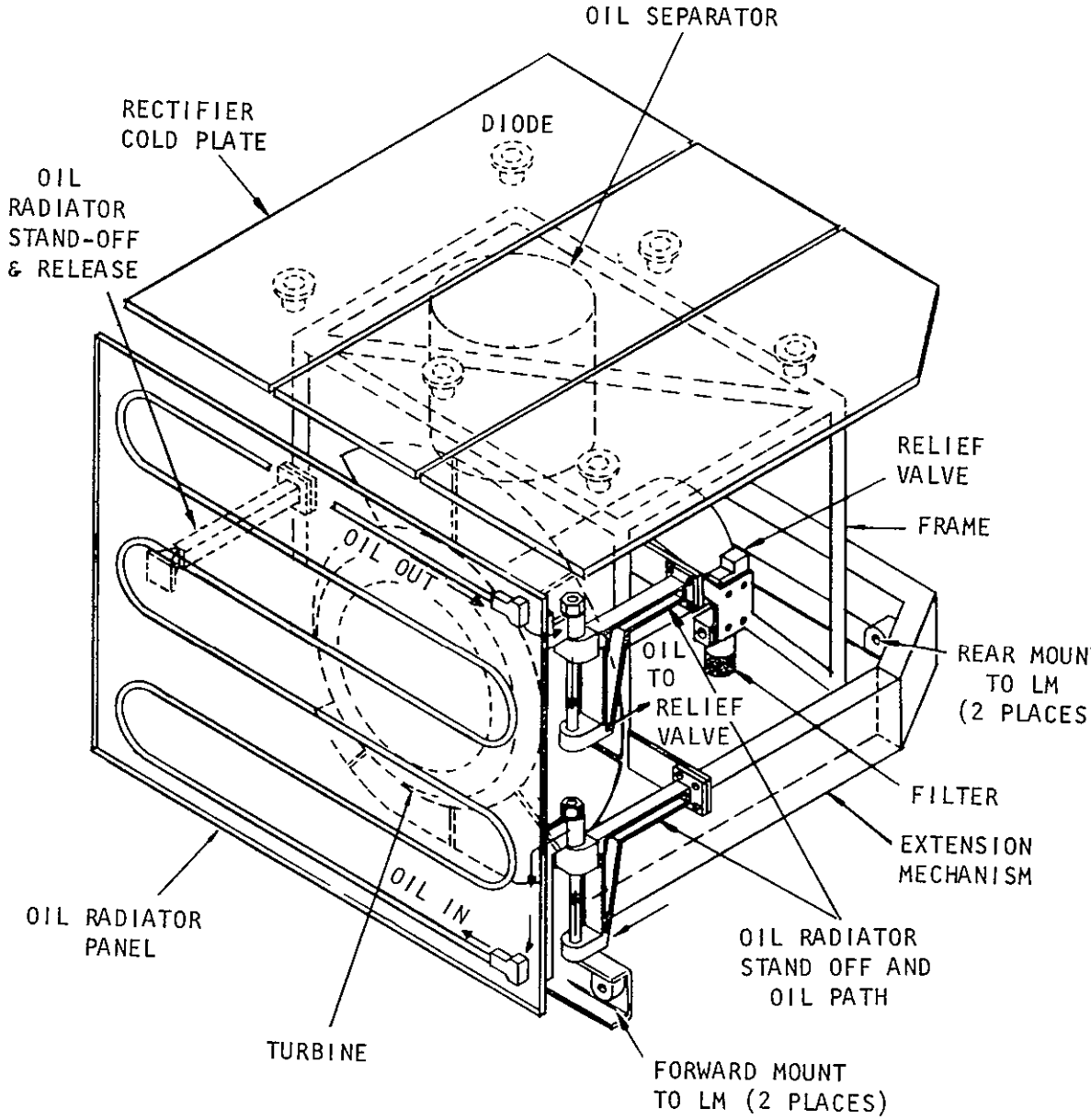


FIGURE 6.5-1 HEPS PACKAGE - STOWED

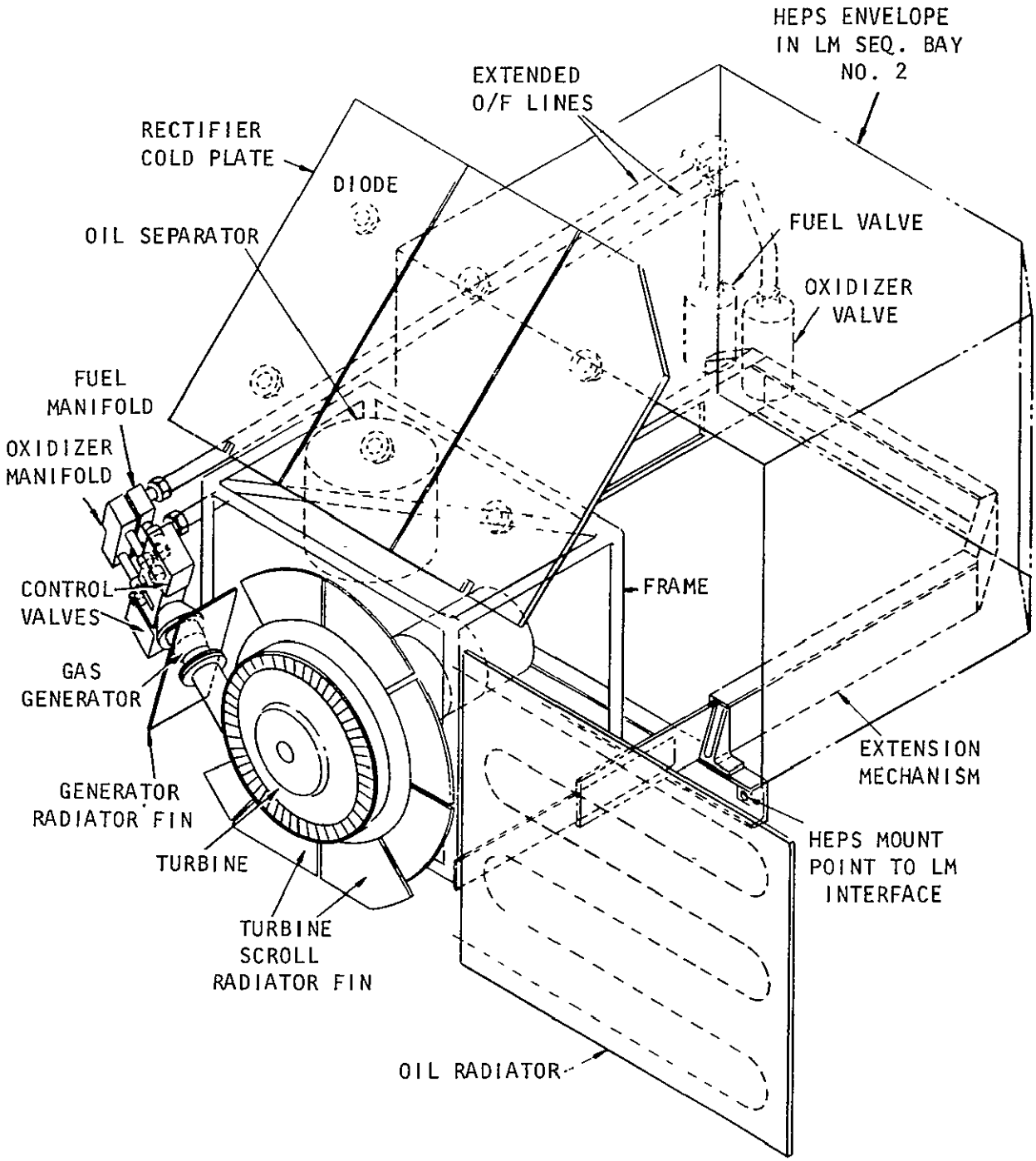


FIGURE 6.5-2 HEPS PACKAGE - DEPLOYED

FIGURE 6.5-3 HEPS PACKAGE - DEPLOYED

REPRODUCIBILITY OF THE
ORIGINAL PAGE IS POOR

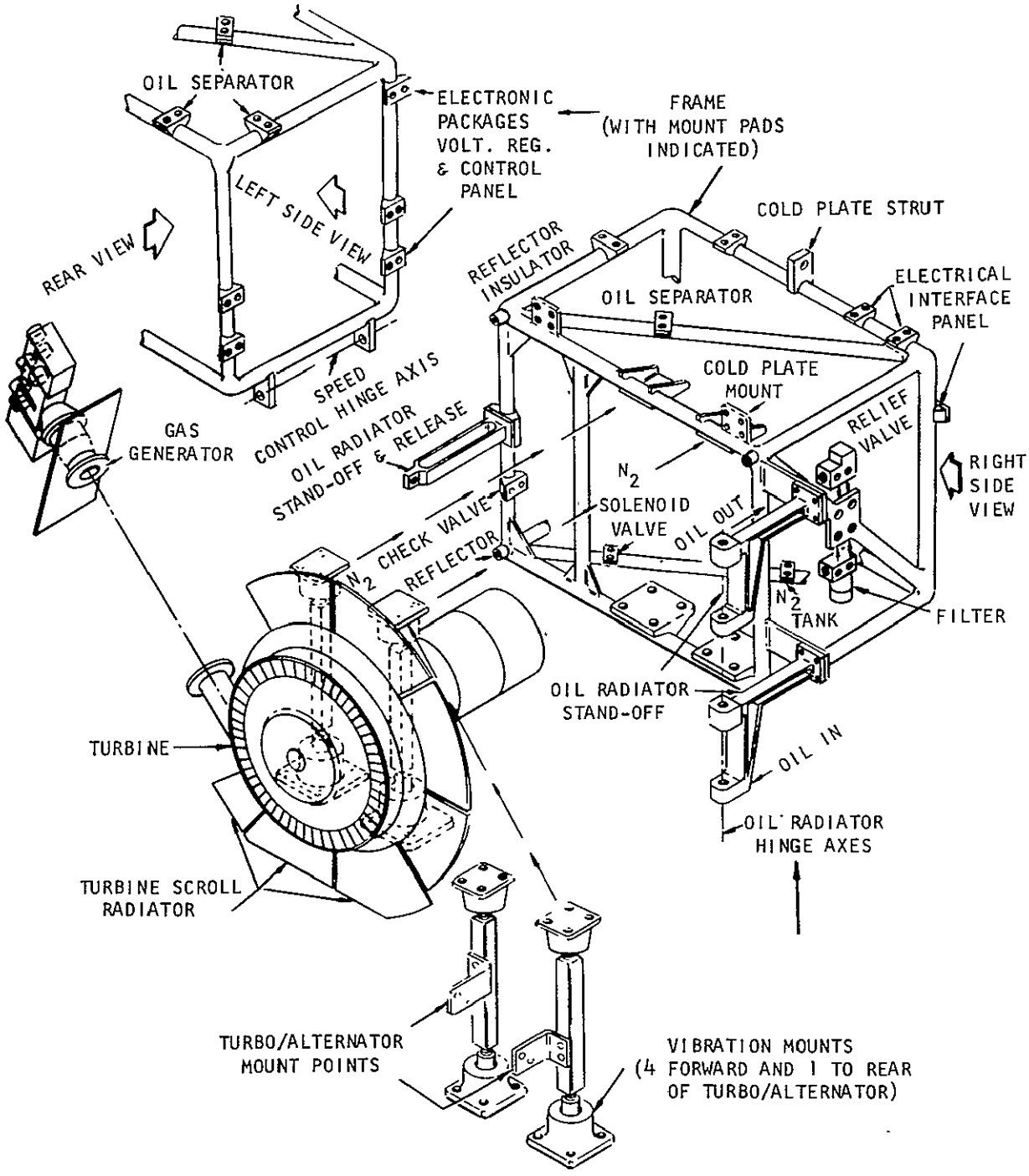


FIGURE 6.5-4 HEPS-TURBOALTERNATOR AND FRAME

REPRODUCIBILITY OF THE
ORIGINAL PAGE IS POOR

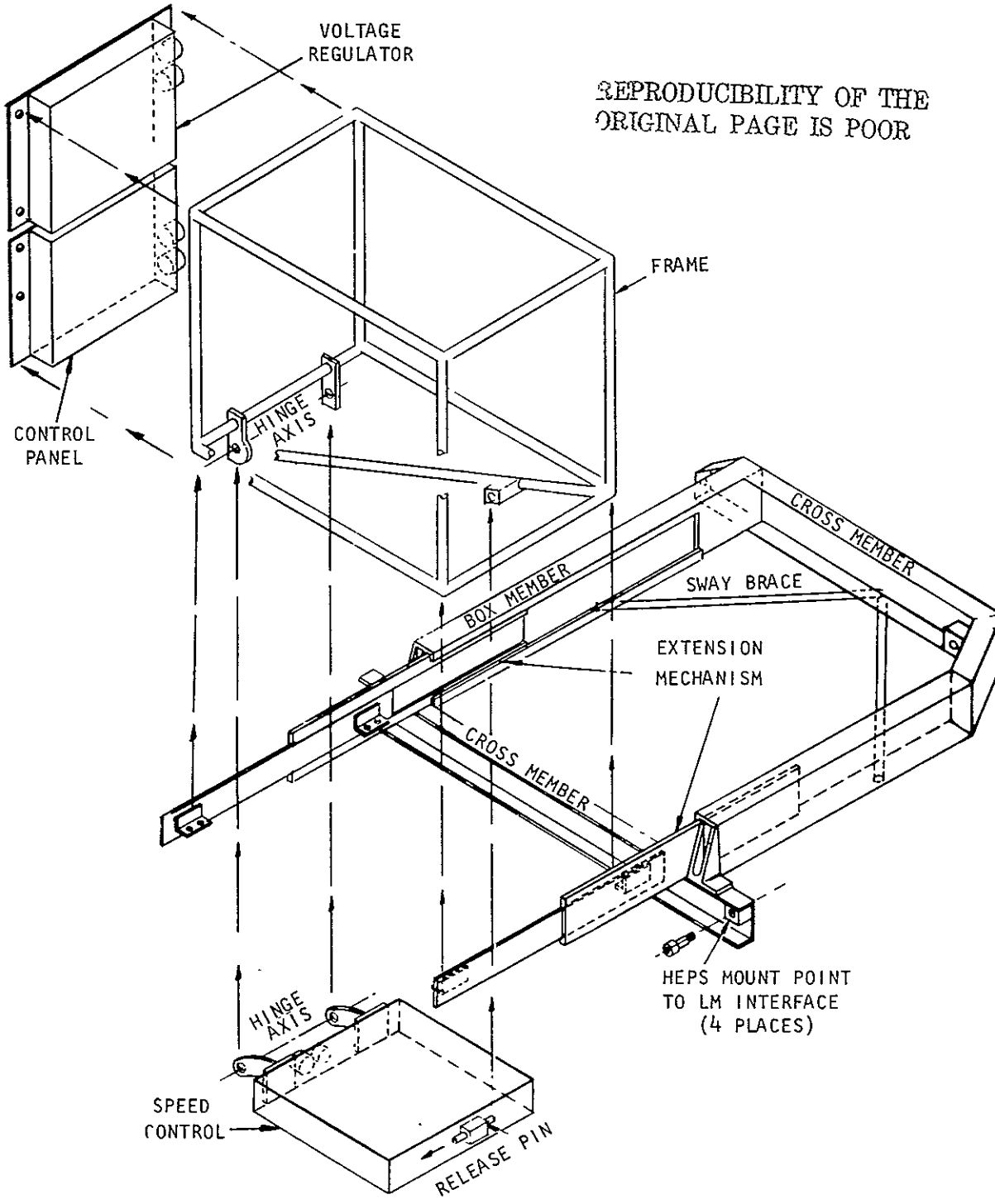


FIGURE 6.5-5 HEPS - FRAME EXTENSION MECHANISM AND ELECTRONIC PACKAGES

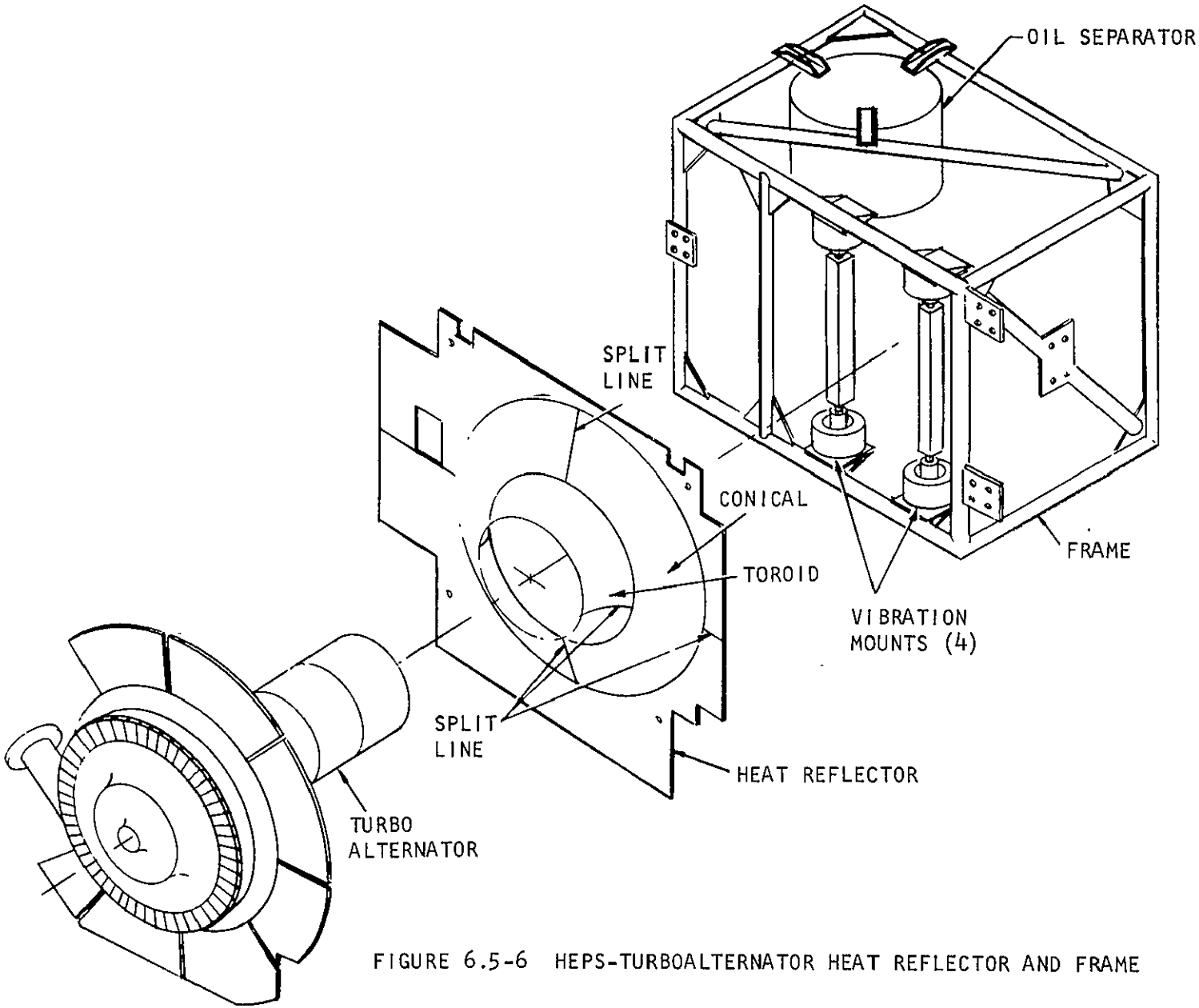


FIGURE 6.5-6 HEPS-TURBOALTERNATOR HEAT REFLECTOR AND FRAME

the four panels and the turbine scroll area be an absolute minimum. The panel-to-panel view factors and panel-to-LM and lunar view factors were minimized so that the total net heat rejected required as small a set of panels as possible.

A heat reflector-insulator panel (Figure 6.5-6) was inserted between the turbine scroll and other rearward components. It is a shaped specularly reflecting gold-coated surface used to remove heat from the partially enclosed inner region of the scroll. The rear of the panel is composed of multiple radiation layers to minimize heat flow to the frame and other components. Thus its purpose is twofold: to insulate other components from the high temperature surface and to reduce the high local temperature at the scroll to alternator housing interface.

Lube System

The oil separator was located in the upper left portion of the envelope (Figure 6.5-6) to provide a lube head on the turbo-alternator and accessibility to the fill fitting. All other lube accessories, including lines, were positioned after most of the other components were located. The lube lines which run directly from the turboalternator to components attached to the frame have flexibility designed into their configurations. This was necessary because the pulsed turboalternator moves slightly in the vibration mounts relative to components fixed to the frame.

Propellant System

The gas generator has been located in the upper left part of the envelope (Figure 6.5-8) to provide dribble volume drainage. This located the propellant lines which extend to the LM interface in the left side of the envelope. These lines stow in an omega form, Figure 6.5-17, and extend as shown in Figure 6.5-18. They have a high degree of flexibility due to the internal bellows construction and the type of external braiding. The particular stowed form is maintained by guides which are fixed to the extension mechanism and the frame. The hoses merely disengage from the guides, which have a half circle cross-section, as the front and rear guide sets move away from each other. The rear set is attached to the fixed part of the extension mechanism and the front set is attached to the moveable frame. The guides, therefore, provide proper shaping of the stowed hoses to avoid overstressing at local points, especially at the end points. In addition, the guides restrain the hoses from uncontrolled motions due to vibration input during flight.

The propellant shutoff valves are located toward the rear of the envelope (Figures 6.5-2, 6.5-3 and 6.5-9) as close to the LM interface connection as possible. Manifold blocks for the

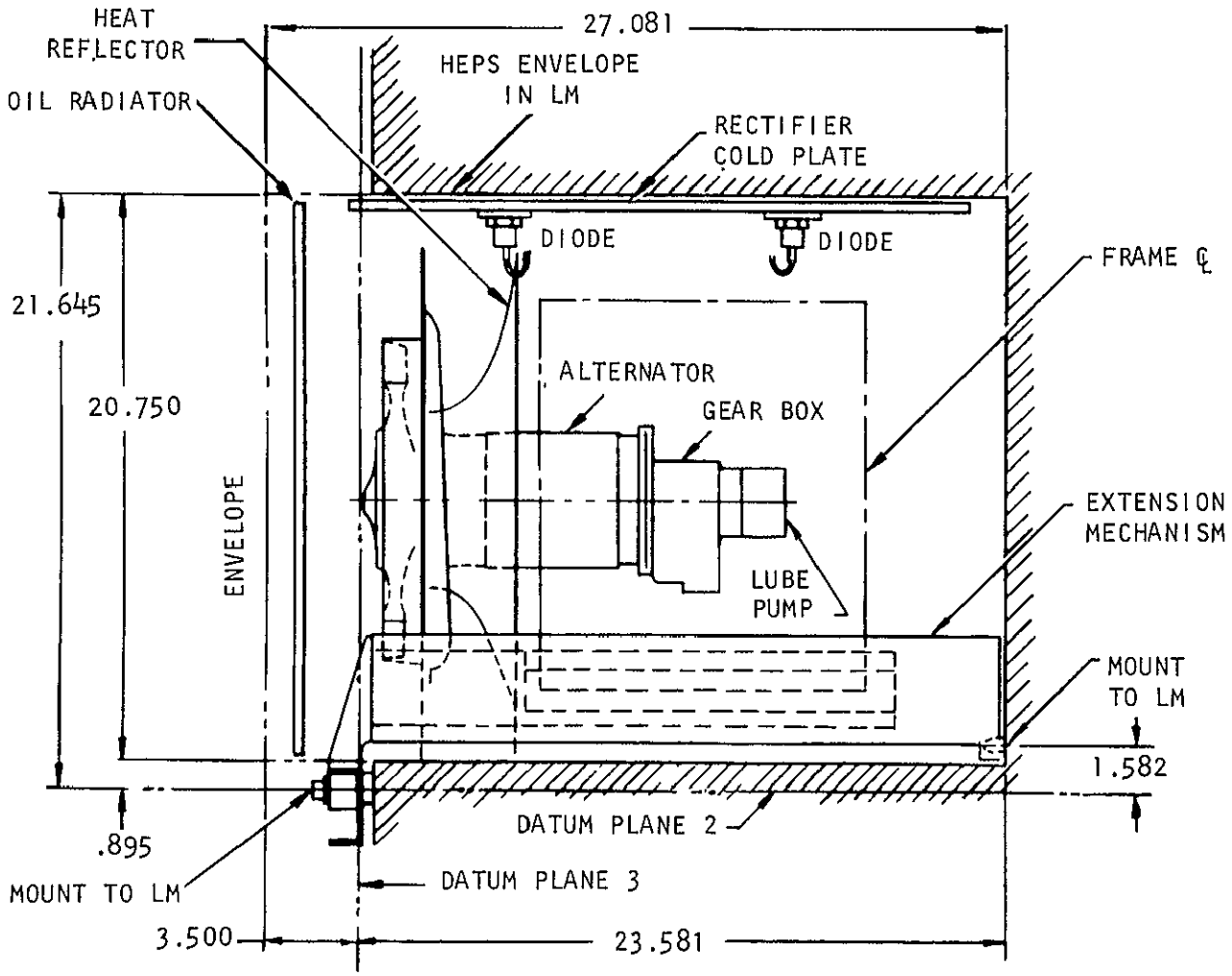


FIGURE 6.5-7 HEPS PACKAGE - STOWED

10 IN.

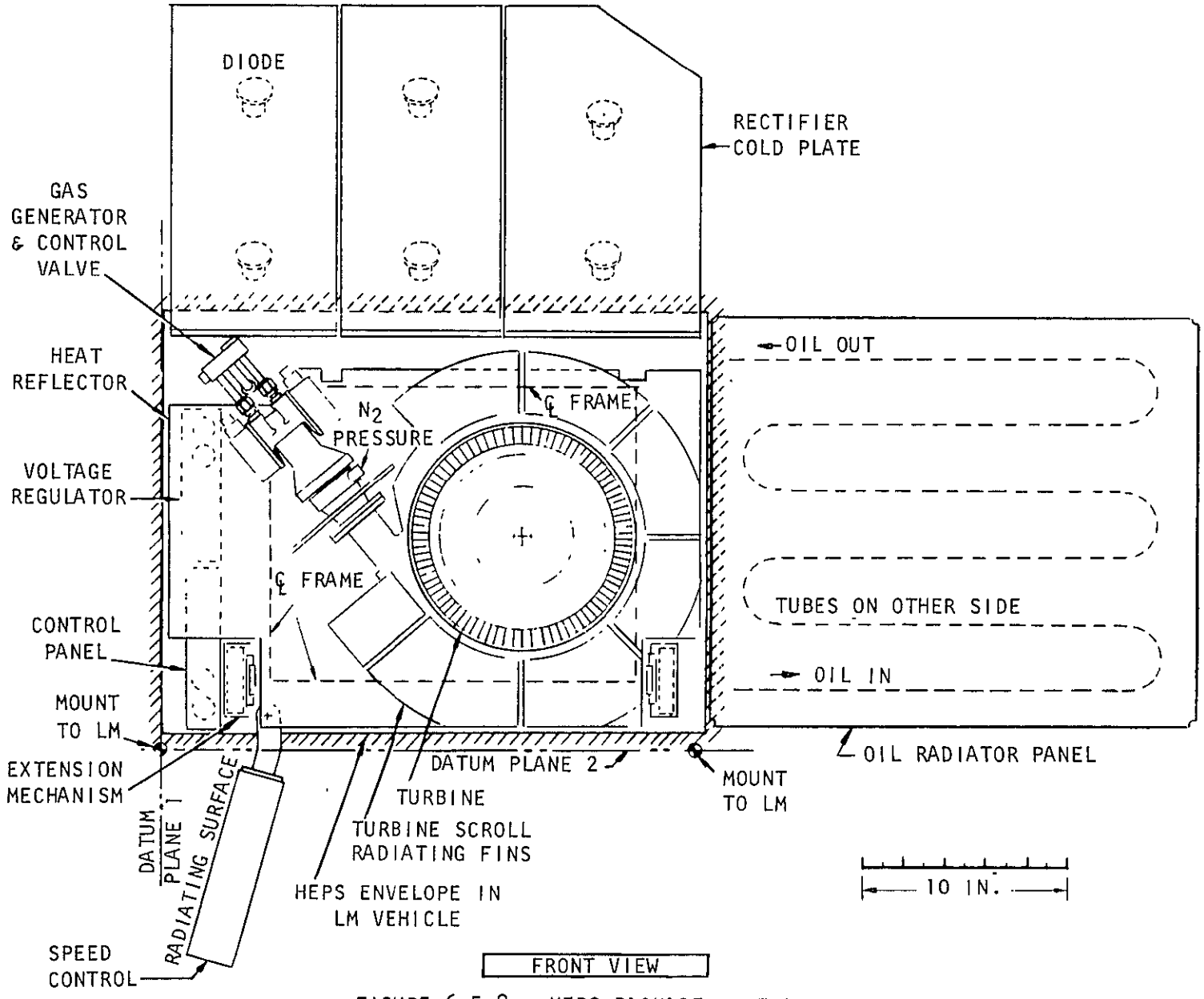


FIGURE 6.5-8 HEPS PACKAGE - DEPLOYED

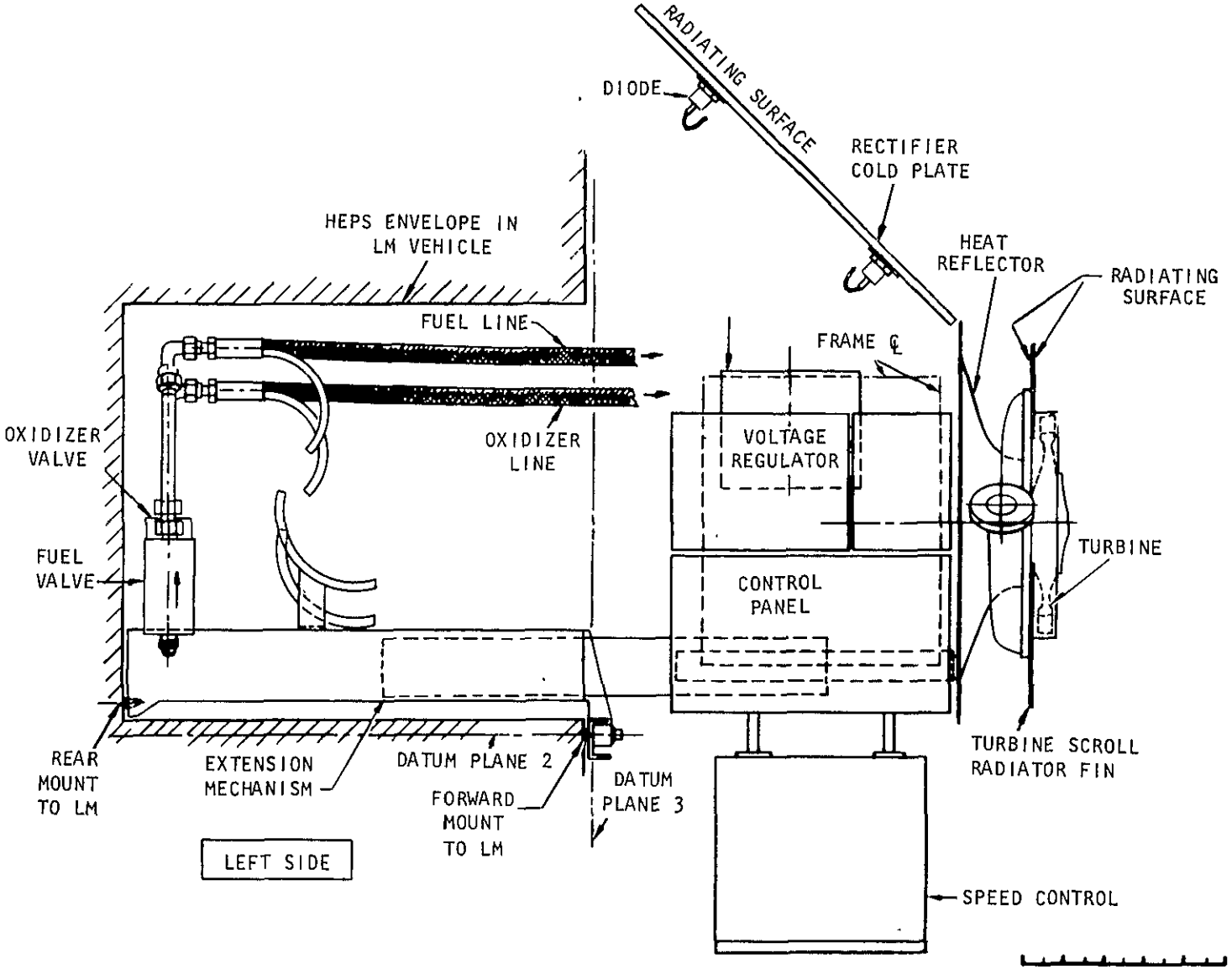


FIGURE 6.5-9 HEPS PACKAGE - DEPLOYED

REPRODUCIBILITY OF THE
ORIGINAL PAGE IS POOR

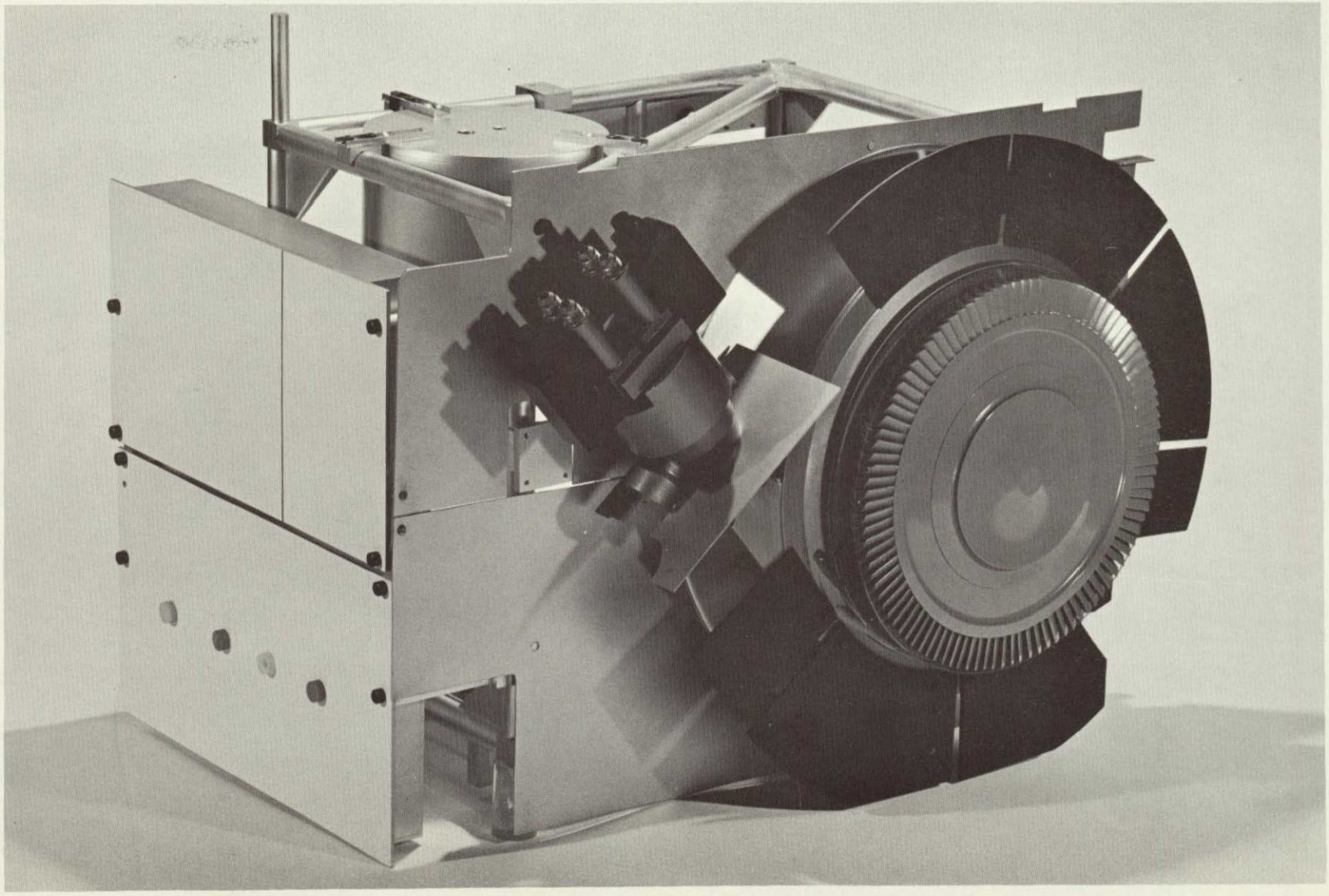


FIGURE 6.5-12 HEPS QUALIFICATION UNIT MODEL (TURBOALTERNATOR, REFLECTOR, GAS GENERATOR AND ELECTRONIC PACKAGES)

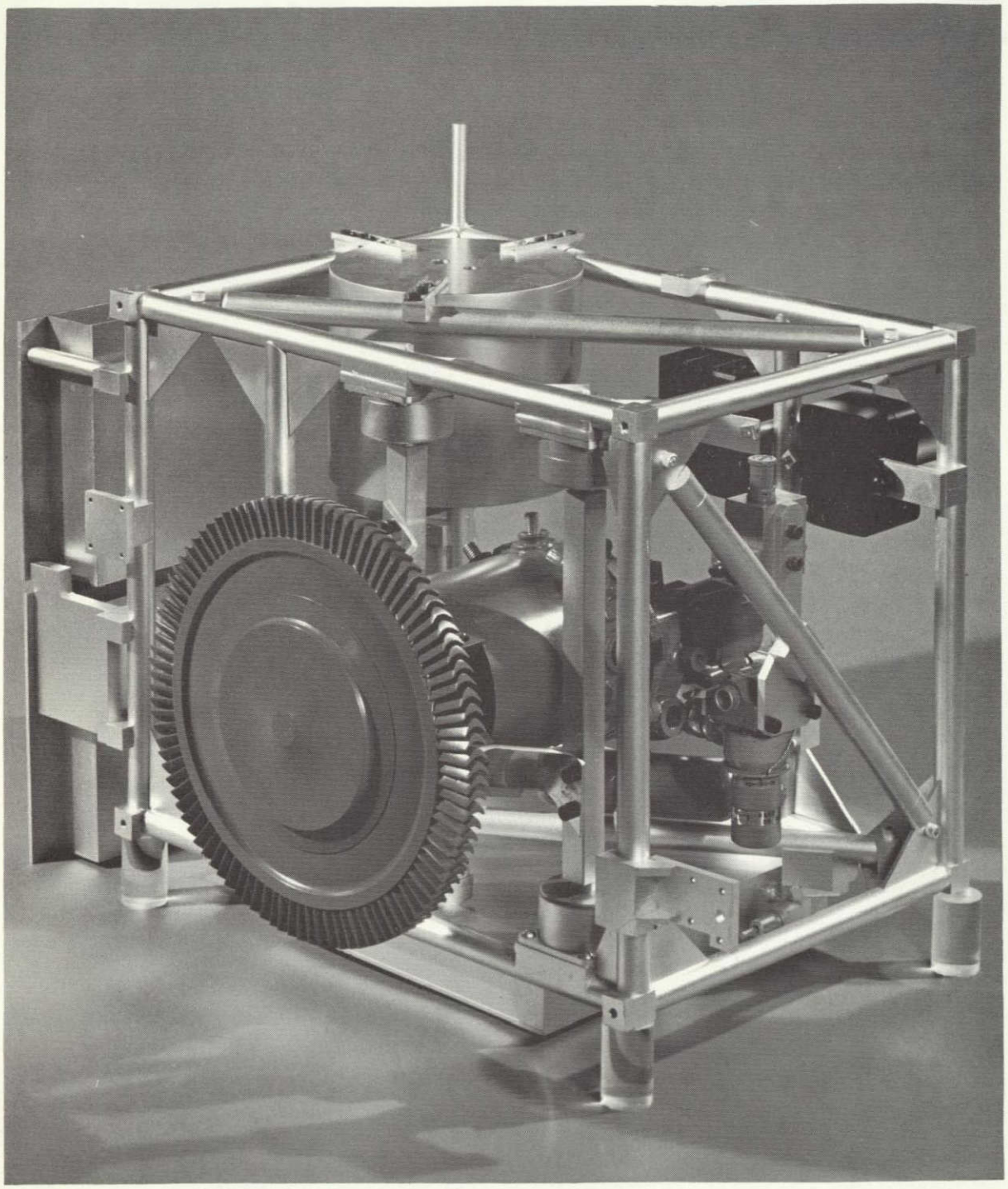


FIGURE 6.5-13 HEPS QUALIFICATION UNIT MODEL (TURBOALTERNATOR, FRAME AND LUBE SYSTEM ACCESSORIES)

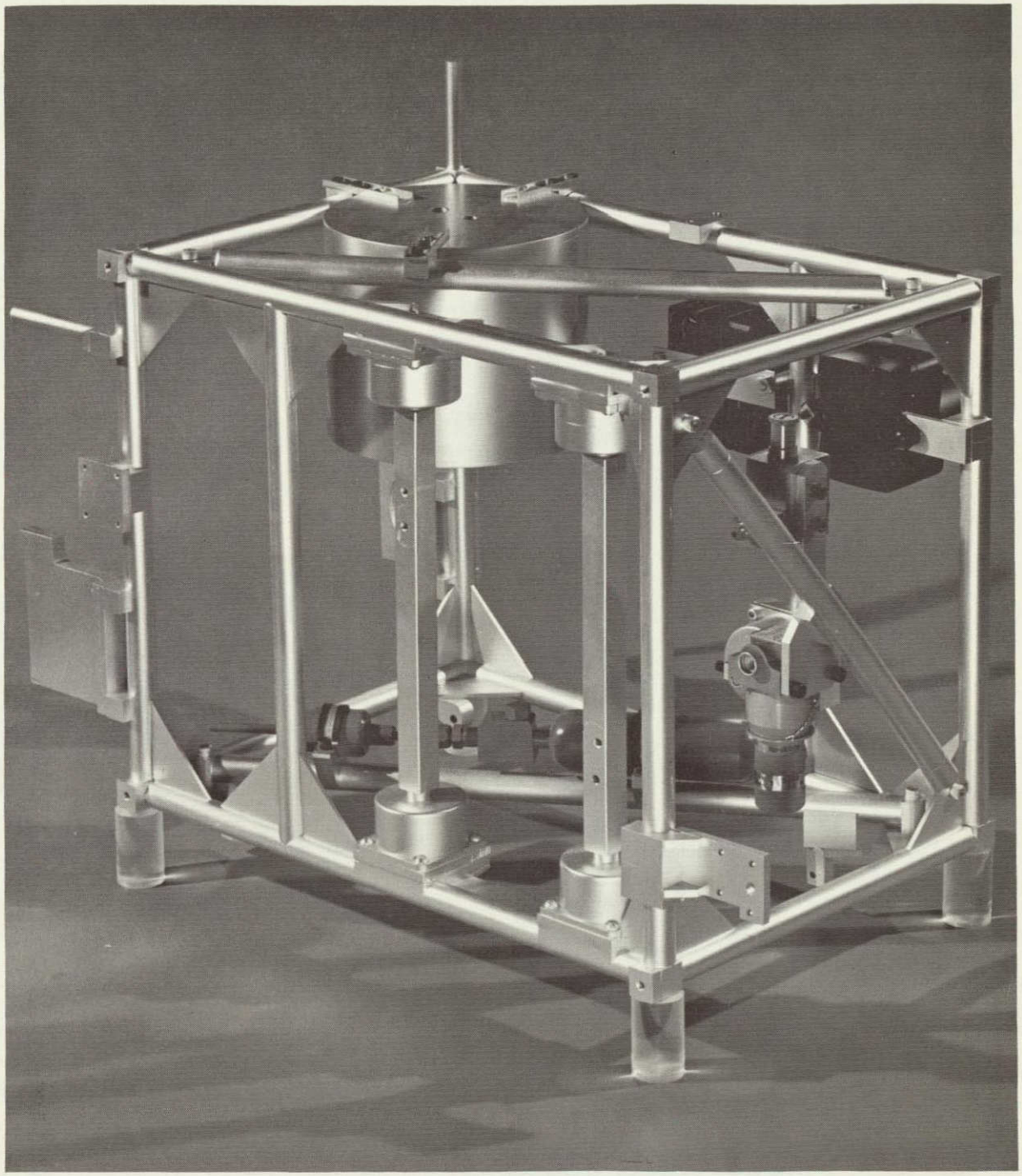


FIGURE 6.5-14 HEPS QUALIFICATION UNIT MODEL (FRAME, LUBE SYSTEM ACCESSORIES AND ELECTRICAL INTERFACE PANEL)

REPRODUCIBILITY OF THE
ORIGINAL PAGE IS POOR

2020

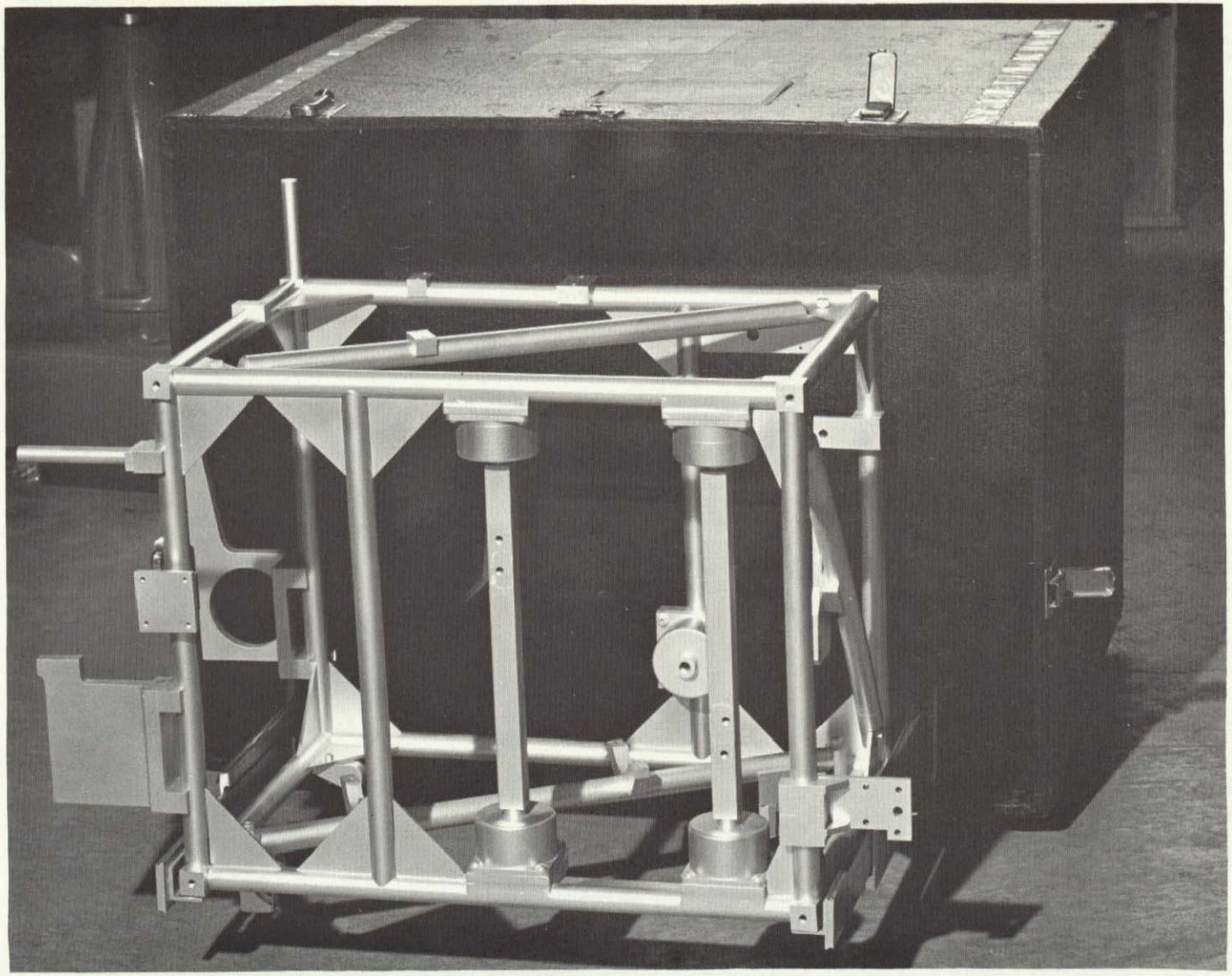


FIGURE 6.5-15 HEPS QUALIFICATION UNIT MODEL (FRAME, EXTENSION MECHANISM AND SEQ. BAY NO. 2)

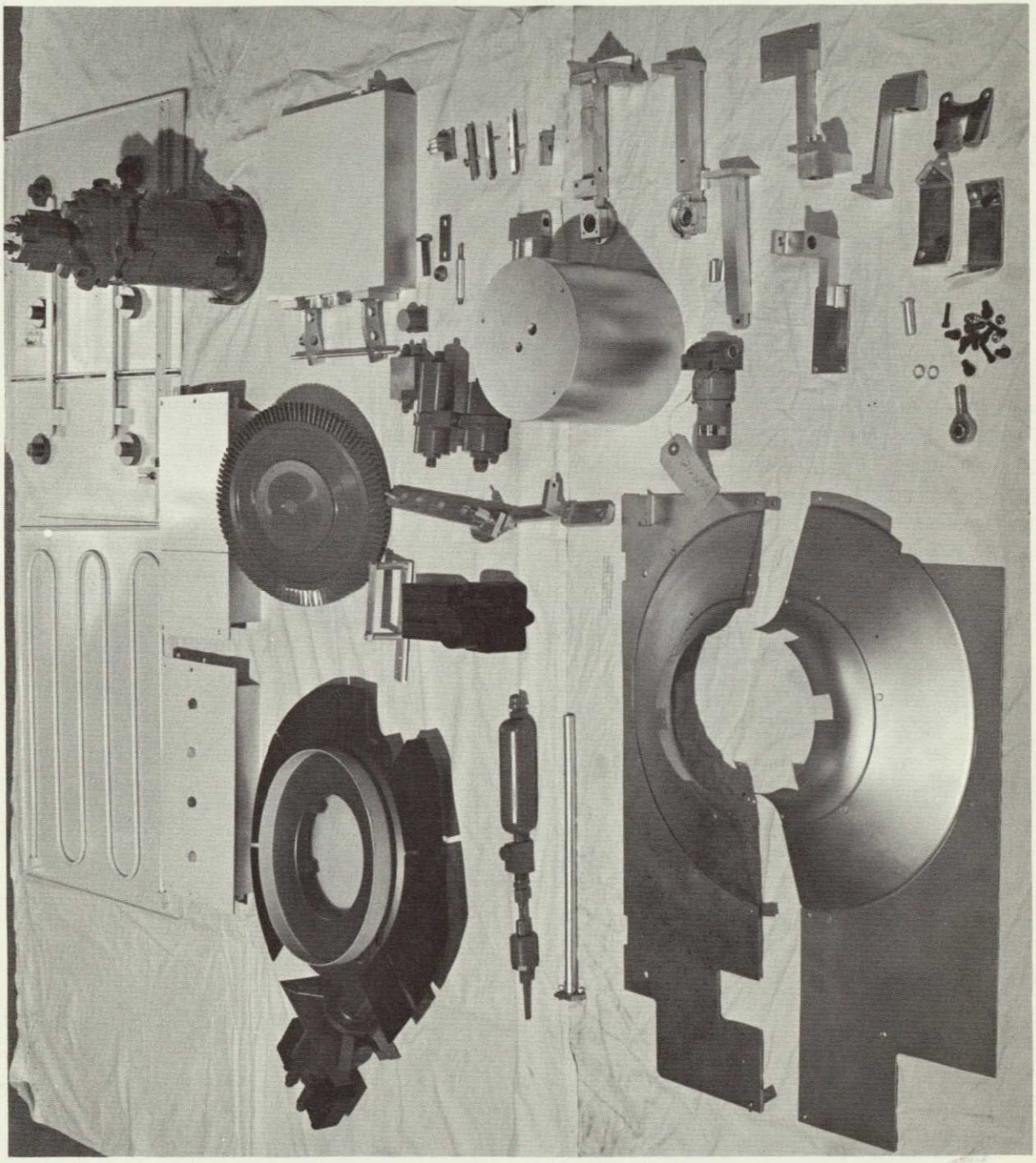


FIGURE 6.5-16 HEPS QUALIFICATION UNIT MODEL (DISPLAY OF PARTS)

PRODUCIBILITY OF THE
RIGINAL PAGE IS POOR

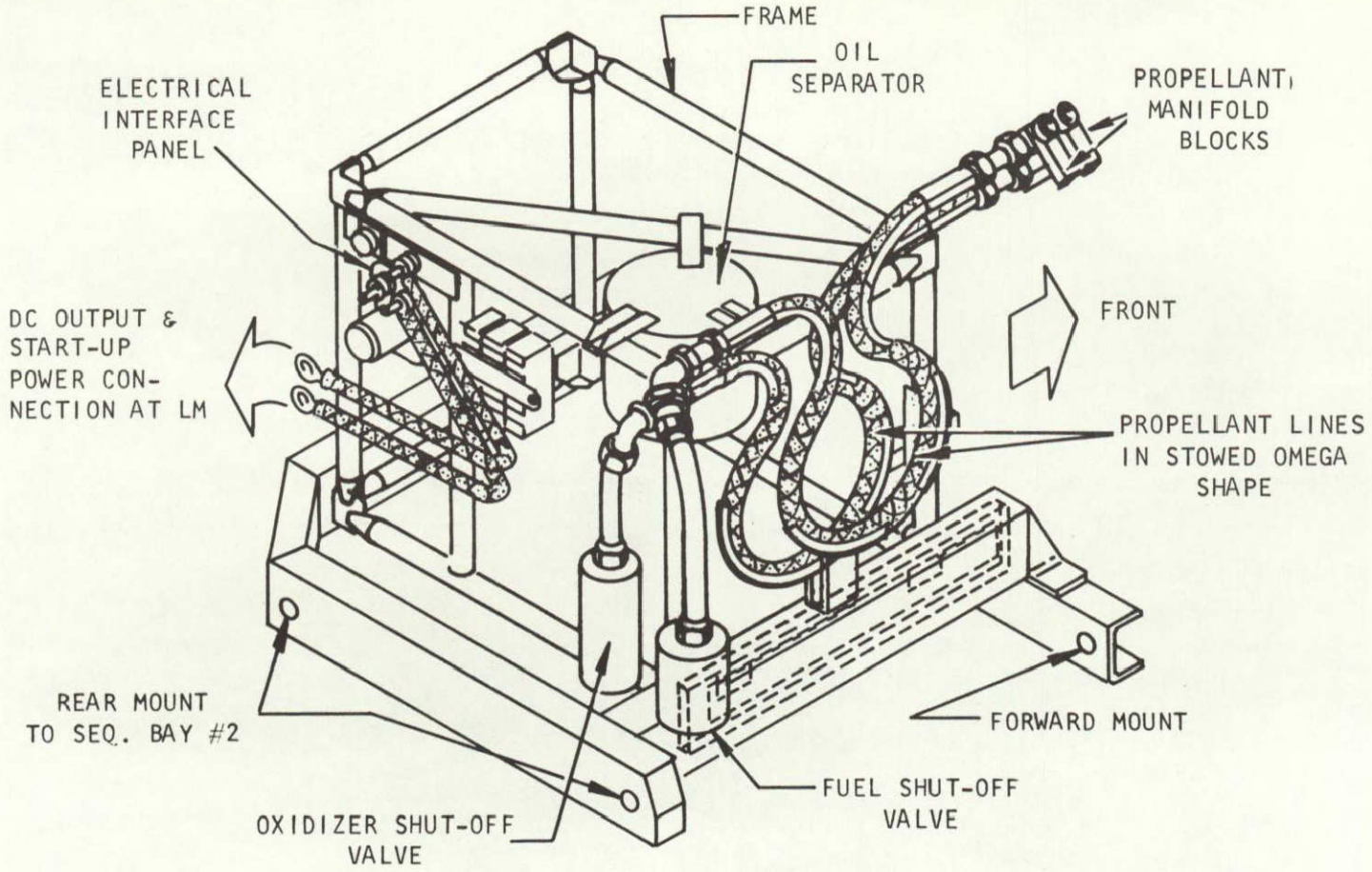


FIGURE 6.5-17 HEPS PACKAGE - STOWED PROPELLANT LINES AND ELECTRICAL HARNESSES

The oil radiator and speed control are rotated to their operating positions. Spherical type bearings are used in both cases to avoid the more precise alignment required of journal or ball bearings. Oil flow paths to and from the radiator are provided by rotating seals that are in alignment with the rotational axis. This avoids the more cumbersome and heavy flexible hose-type connections. O-rings are used as seals, and an extra set is added for reliability.

The rectifier cold plate deployment involves two motions. First, the rear edge is rotated about two forward bearings to a 45° angle by means of a scissors-type strut attached to the upper rear tube on the frame. The forward edge is moved horizontally (7 inches) toward the rear by means of two split linear ball bushings, and the resultant panel angle is 49° from horizontal. The second motion moves the forward edge away from the hot scroll region and allows more efficient rejection of diode heat. All stowed and deployed position locks for the deployable panels are operated manually and are retractable. Dissimilar metals and dry lubricants are to be used on all sliding surfaces to avoid cold welding.

Interfaces

The LM mount point locations are the same as for the ALSEP package. The ALSEP release mechanism could not be used for the HEPS because of the complicated and heavier structural arrangement that would be required. Two shoulder bolts replace the tapered pins at the front mount points as a substitute for the ALSEP release mechanism. The rear two mount pins are as presently defined for ALSEP.

There are no specific details for the method of interfacing the propellant lines or the electrical harnesses except that they pass through the rear wall of the SEQ Bay and that local, minor reinforcing will be required.

Thermal control interface details are not defined except that a thermal barrier will be required between the HEPS rear surfaces and the SEQ Bay walls to minimize net radiant heat exchange into the LM. The barrier is difficult to establish because the thermal details are more dependent on local LM construction, which comes under cognizance of GAEC. The qualification unit will operate with a barrier at the rear surface to simulate low heat transfer in that direction.

6.6 Structural Design

The DVR unit was tested with a pin-connected frame but was replaced with an all-welded frame on the Qualification Unit. This was done to improve the structural integrity of the frame. Both designs are discussed in this section.

Pin Connection Frame

The frame that was used on the DVR unit is shown in Figure 6.6-1. It was comprised of tubular members with welded ends to accommodate pin connections at the joints. The existing tube locations were established to efficiently transfer the load of the turboalternator to the chassis slides and extension mechanism. Cross members were added for additional rigidity. They also served as mounting points for various components within the package.

Since the turboalternator weighed approximately 90 lb, it accounted for the majority of the weight of the unit. It, therefore, was the major area of concern in the design of the frame. The turboalternator was supported by three vibration mounts. The mount locations are shown in Figure 6.6-1. The mounts marked A and B were located just outside the plane of the turboalternator center of gravity. These two front mounts, therefore, carried the majority of the weight of the turboalternator. The side mount (C) was included for stability. It was assumed for the stress analysis that each of the two front mounts carried half of the turboalternator load, namely, 45 lb. The lower front mount (B) was tied directly to a corner of the frame. As a result, any imposed load was directly transmitted to the chassis slide and was not carried by any of the frame structural members.

The frame was designed to withstand the large launch loads that will be applied. The launch and flight loads are a combination of sinuscidal and random vibration and shock loads. A 20g applied load approximates the net effect of the shock and vibration loads. Previous experience indicated that a 20g load applied in all directions was slightly more severe than the maximum sinusoidal and random vibration combination. For that reason, the stress analysis was conducted assuming a 20g load applied to the turboalternator in all directions. This produced an effective total force due to the turboalternator of 1800 lb. The forces that the tubular members of the frame will carry when loaded in each of the three major axes are shown in Figures 6.6-2 through 6.6-4.

Once the force levels in the tubes were established, the stress was calculated and tube sizes were chosen. The stresses for each

REPRODUCIBILITY OF THE
ORIGINAL PAGE IS POOR

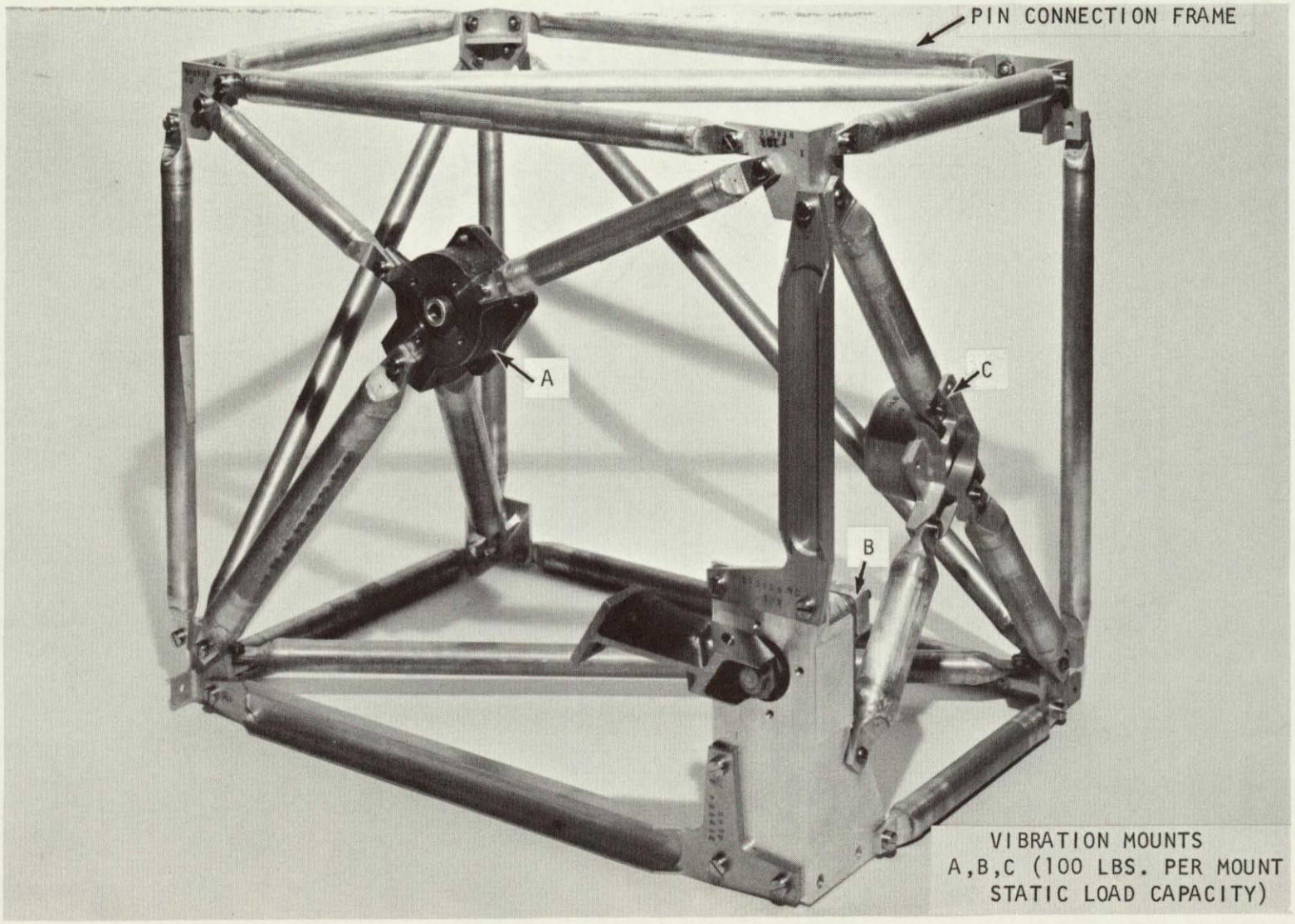


FIGURE 6.6-1 DVR PIN CONNECTED FRAME AND VIBRATION MOUNT LOCATION

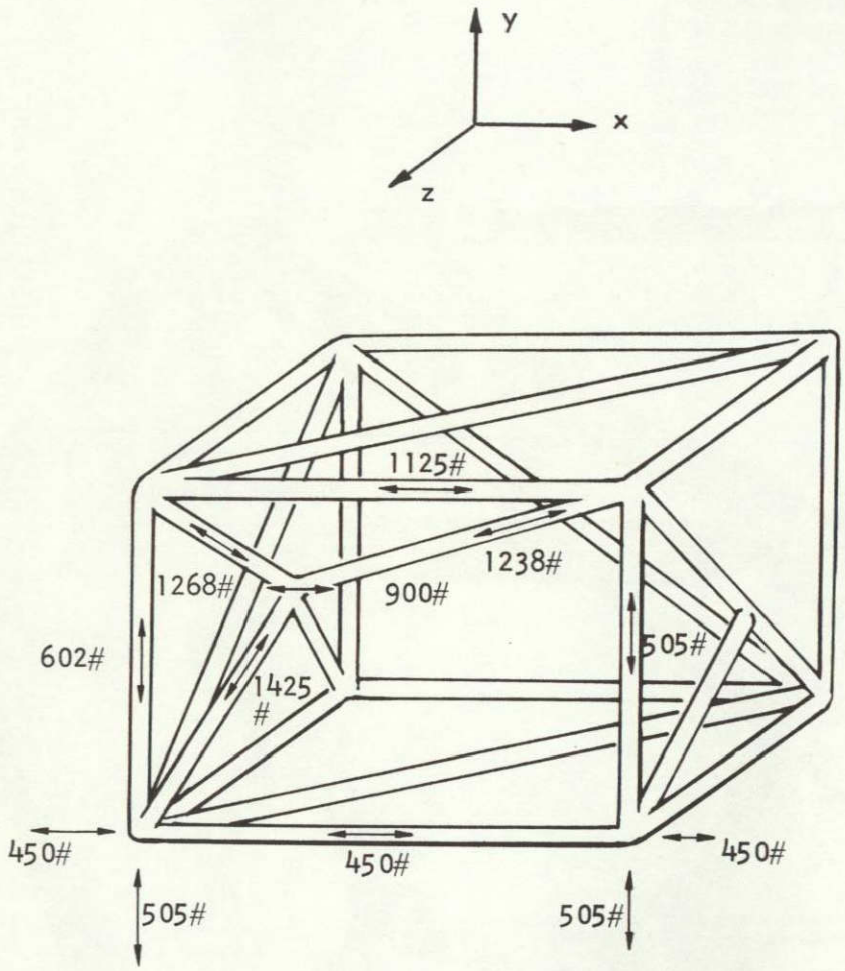


FIGURE 6.6-2 FORCE ANALYSIS OF PIN CONNECTION FRAME FOR LOAD IN ± X DIRECTION INDICATING THE MAJOR FORCES

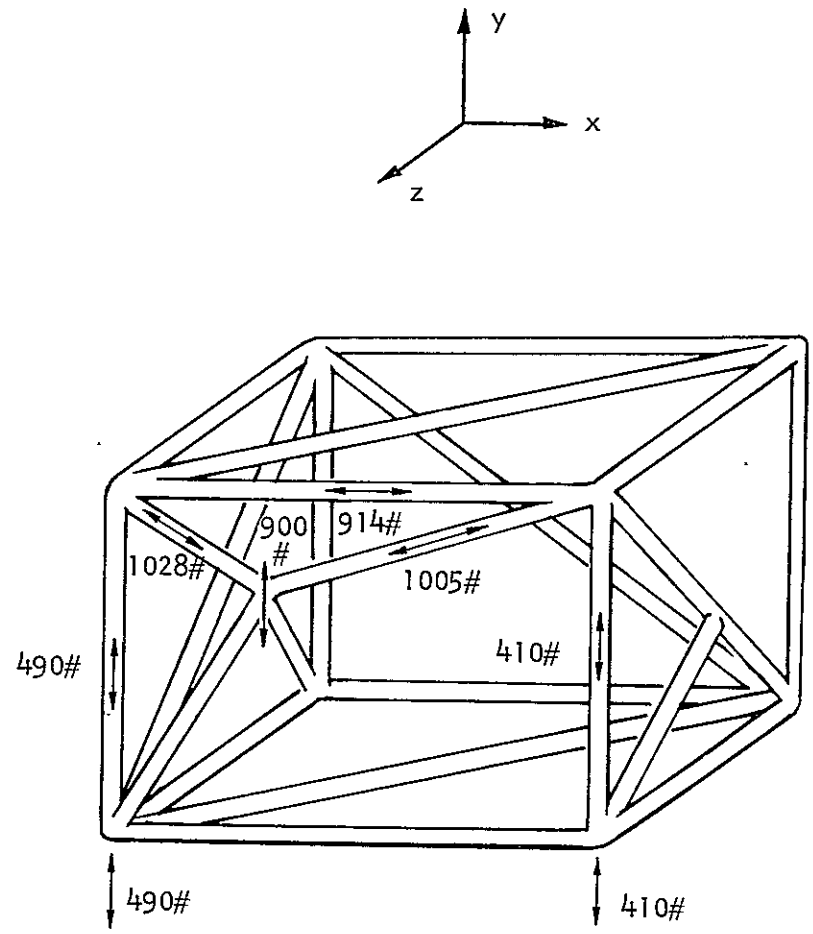


FIGURE 6.6-3 FORCE ANALYSIS OF PIN CONNECTION FRAME FOR LOAD IN ± Y DIRECTION INDICATING THE MAJOR FORCES

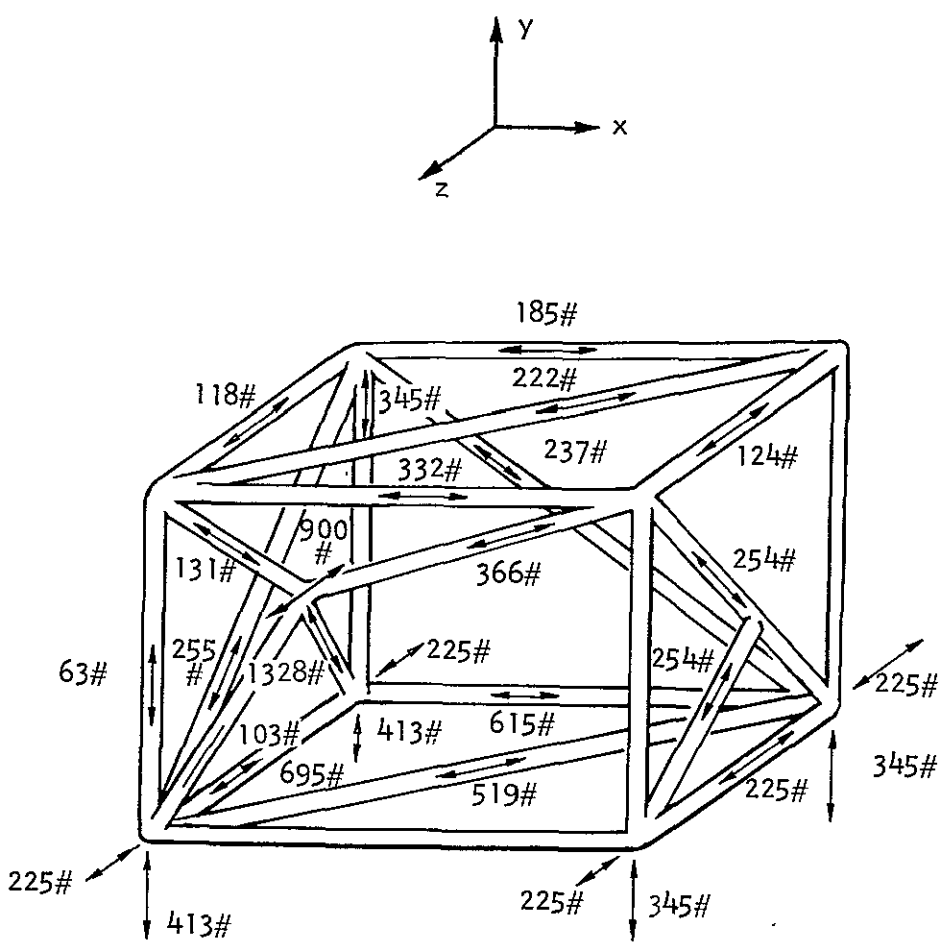


FIGURE 6.6-4 FORCE ANALYSIS OF PIN CONNECTION FRAME FOR LOAD IN ± Z DIRECTION INDICATING THE MAJOR FORCES

member were calculated using 3/4 inch O.D. with .035 inch wall aluminum tubing. This size was adequate for the majority of the members; however, a few members required a 1 inch O.D. with .035 inch wall tubing. (See Figure 6.6-1 for the locations of the 1 inch O.D. tubing and the 3/4 inch O.D. tubing.)

The tubular members were made with welded inserts on each end to accommodate the pin connections. They were heat treated after welding to increase the yield strength. The end connections were sized for the force levels that were anticipated. Milled corner pieces and shoulder bolts were used to tie the frame together.

The tubular members were statically tested separately and as an assembled frame. It was discovered in the pull tests on the tubes that the inserts in the ends were not strong enough for the design loads. The cross-sectional area around the hole was not large enough for the force levels that were expected. The end pieces showed definite signs of yielding with the holes significantly elongated.

The complete frame was statically loaded to simulate the turbo-alternator applied load. These tests revealed that the frame deflected significantly under load. The deflections, although not unreasonably high, were higher than predicted. In addition, the frame showed signs of a permanent set after the load was released. This was attributed to pin movement within the tolerance of the holes. There was no indication of yielding during these tests; however, the applied load was not as high as the predicted launch loads. The test results showed that the pin connection frame was not adequate for the high "g" launch loads that were expected. Several courses of corrective action were available. The existing frame could be redesigned to add strength wherever necessary. The inserts at the ends of the tubes could be made larger in cross-section to carry the required loads. It was not felt that the tubes themselves should be enlarged since they showed no signs of yielding. In addition to strengthening the frame members, an improved method was needed for fastening. The movement that was obtained with the bolted connections was not desirable; therefore, another method of attachment was required. One possibility was the addition of rivets in the end connections to backup the bolts; however, thermal expansion and contraction of the members would still tend to loosen the joints.

In addition to the changes that were required, the pin connection frame was very difficult to assemble. It required many bolted connections which inevitably caused many interference problems. It was decided that an all-welded frame should be used instead of a pin connection frame because a majority of the problems that were encountered with the old frame could be eliminated.

All-Welded Frame

The all-welded frame did not require the same arrangement of tubular members as did the pin connection frame. A view of the frame showing the location of the vibration mounts is shown in Figure 6.6-5. Five vibration mounts are used instead of three mounts as in the previous design. The mock-up of the new frame with the attachment points for the various components is shown in Figure 6.5-16. The all-welded frame was designed to be interchangeable with the pin connection frame in order to minimize the changes required within the package. Component mounting locations, therefore, were unchanged.

Since the all-welded frame actually has fewer structural members than the pinned frame, each member carries a larger load. However, the corners and tube ends are considerably stronger. The gussets, alone, add considerable strength and rigidity. A tubing O.D. of 3/4 inch was used throughout the entire frame. All of the members, with the exception of the upper and lower horizontal front members, have a wall thickness of .065 inches as compared to the .035-inch wall thickness used for the pinned frame members. The remaining two front members have a wall thickness of .083 inch. These tubes were made stronger since they carry nearly the entire weight of the turboalternator. An additional vertical member was installed in the front plane to help support the turboalternator as well as one in the back for the rear vibration mount. Since the rear vibration mount is so far back, it carries a very small portion of the turboalternator weight; however, it provides increased stability. The turboalternator weight is carried primarily by the four front vibration mounts since they are located near the turboalternator center of gravity.

The turboalternator is mounted to the two vertical members that are shown in Figure 6.6-5. Originally, there was to be a uniball between the turboalternator and each vibration mount. However, the two front uniballs provided no resistance to rotation of the vertical members and the only resistance would come from the restoring force of the rubber in the vibration mounts. Under launch loads, the mounts offer virtually no resistance to rotation. As a result, the vertical members would be free to rotate which would permit the turboalternator to move back and forth between them. The addition of a stiffening cross member helps restrict this motion, but it is not very effective. The uniball attachment method is shown in Figure 6.6-6. Also shown are the two stiffeners added to strengthen the vertical box members to resist bending. A combination of analysis and static load testing indicated that the vertical box members would not be strong enough. The most effective remedy without adding a lot of

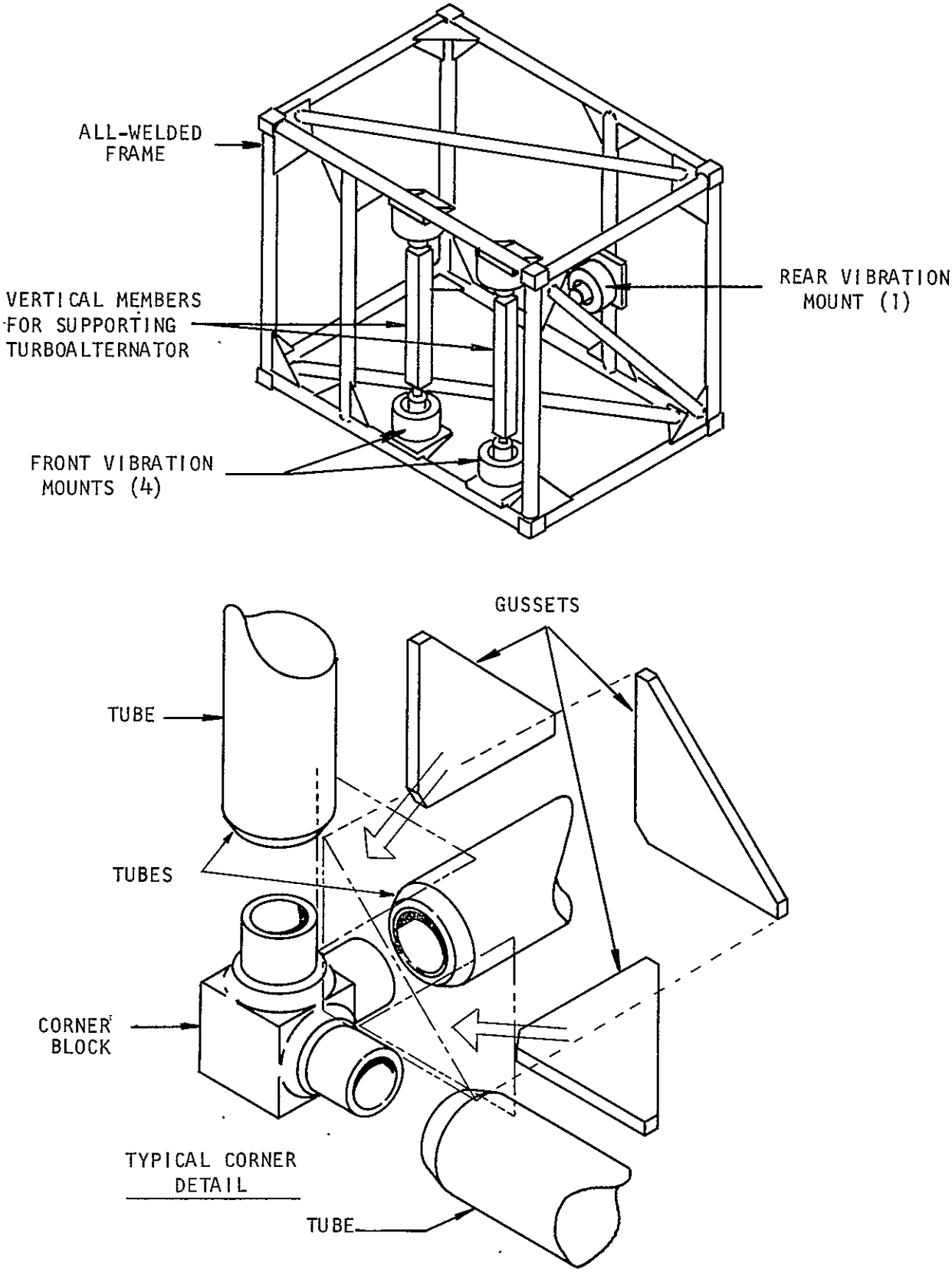


FIGURE 6.6-5 HEPS ALL-WELDED FRAME

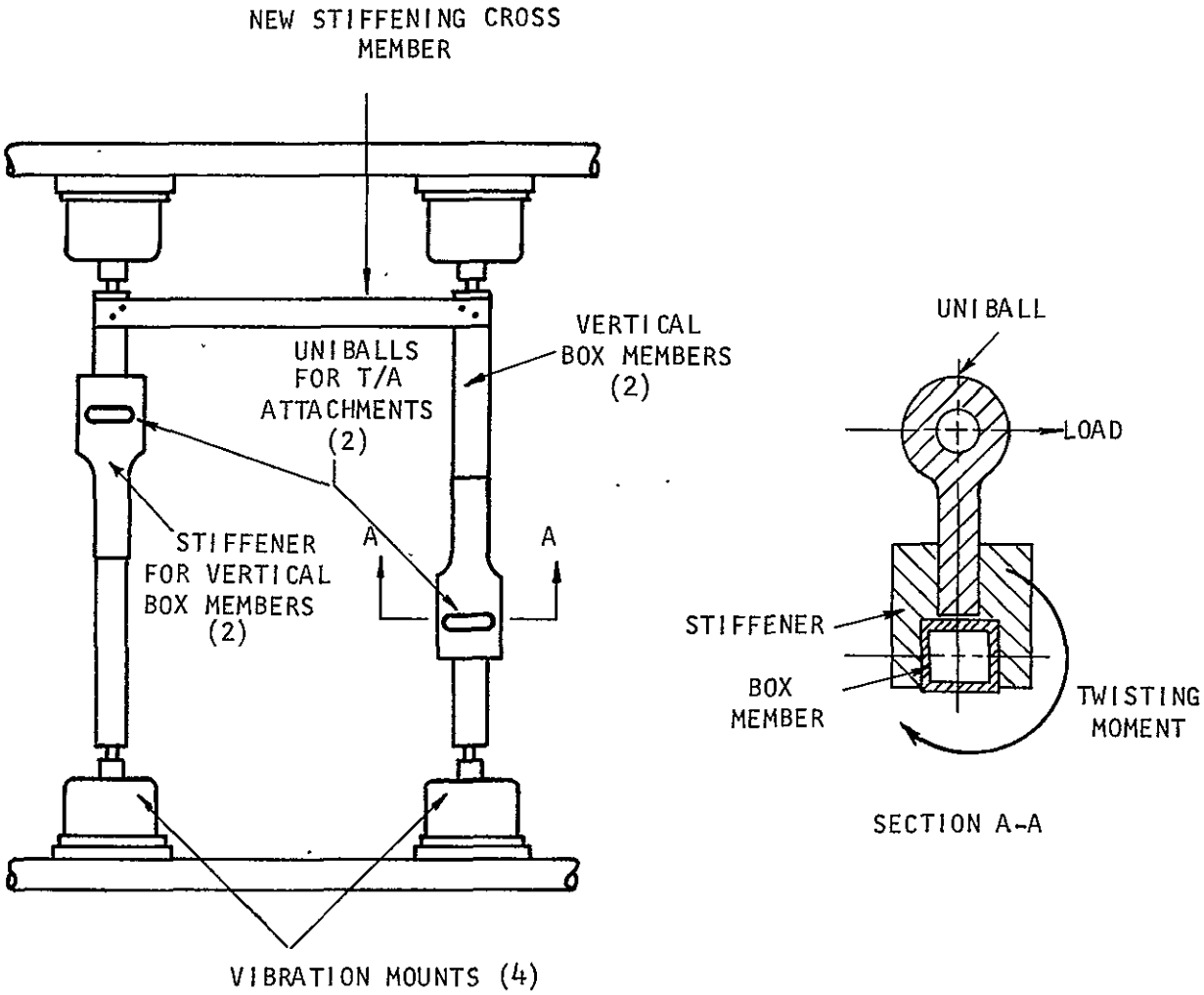


FIGURE 6.6-6 ORIGINAL CONCEPT OF UNIBALL MOUNTINGS FOR THE TURBOALTERNATOR ON THE ALL-WELDED FRAME

weight was the addition of stiffeners in the region near the point of load application.

Due to the twisting problem, the two front uniballs were eliminated from the design. The rear uniball was utilized as a means of taking up any tolerance stackup that might hamper assembly. Two rigid mounting brackets were used in place of the front uniballs for attaching the turboalternator to the vertical box members. A small stiffener pad on each member was used for added strength. This finalized concept is shown in Figure 6.6-7.

Several diagonal tubular members were added to the frame, not for structural support, but for component attachment. The diagonal on the top of the package was added to support the oil separator.

The nitrogen purge system is mounted on a diagonal member on the bottom of the package. The oil filter and oil check valve are mounted on a diagonal member on the right side of the package. Other components, such as the oil radiator, the rectifier cold plate and the electronic packages, are mounted on stand-offs that extend from the frame. These stand-offs are mounted to the frame corners.

Extension Mechanism

The HEPS frame is mounted on two chassis slides which provide the means for removing the package from the LM. The chassis slide is shown in Figure 6.6-8. It is an aluminum slide with ball bearing rollers to provide almost friction free movement. Shock blocks were added to carry the large launch loads instead of transmitting them through the balls. The blocks consist of a pin and a receptacle hole. The front shock blocks are slightly more complicated because the inner member of the slide is shorter than the other two members.

The chassis slides are very strong in the vertical direction and weakest in the horizontal direction as shown in Figure 6.6-8. External support was provided for the thin cross-sectional slide members because of the high launch loads expected. The extension mechanism which was designed to meet this requirement is shown in Figure 6.5-5. Since the horizontal direction is critical, a box constructed base was designed. The channel members can carry extremely high loads in the horizontal direction. The extension mechanism also provides a simple chassis slide support. In addition, the extension mechanism is designed to match the hard point location within the LM SEQ Bay.

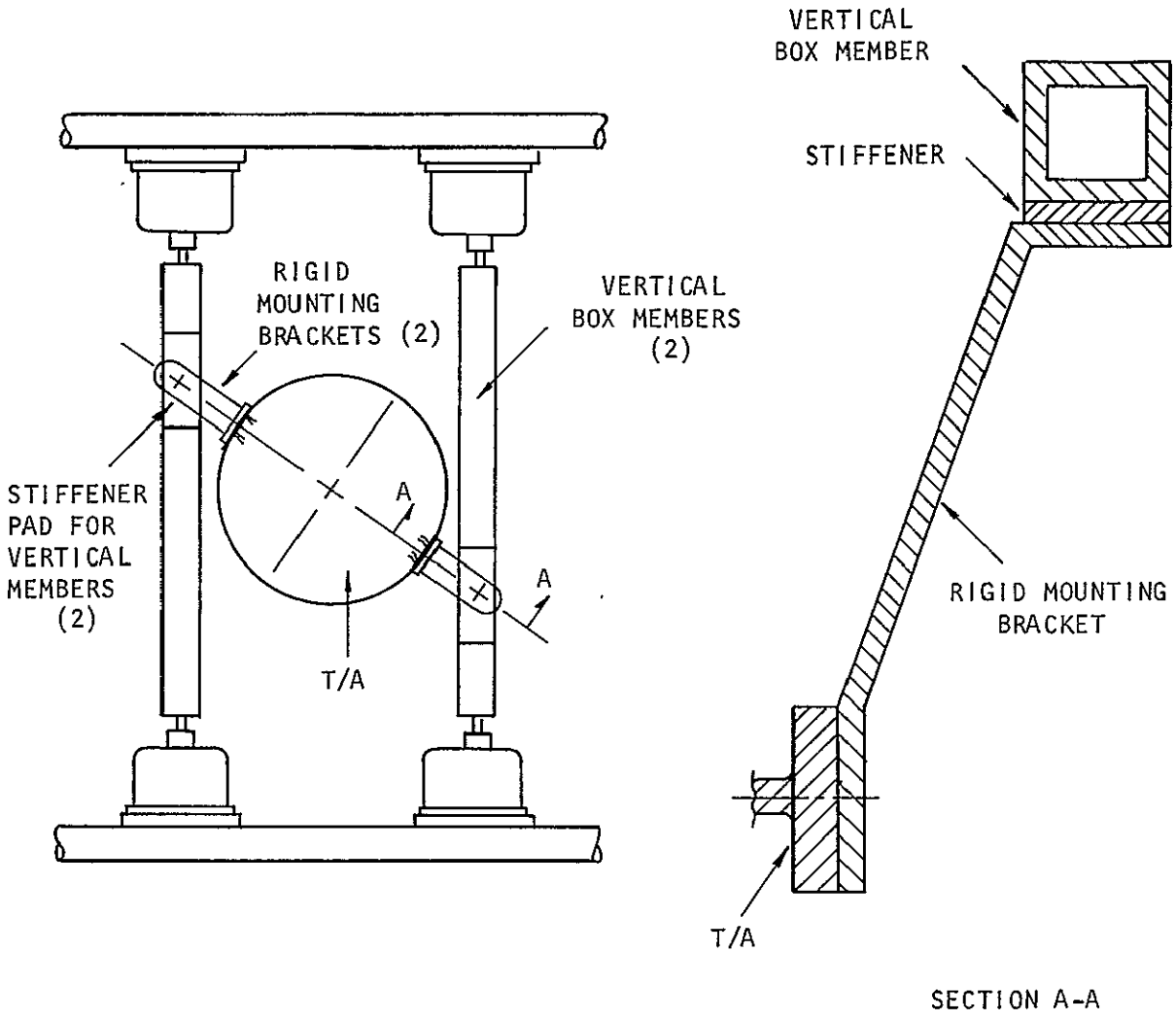
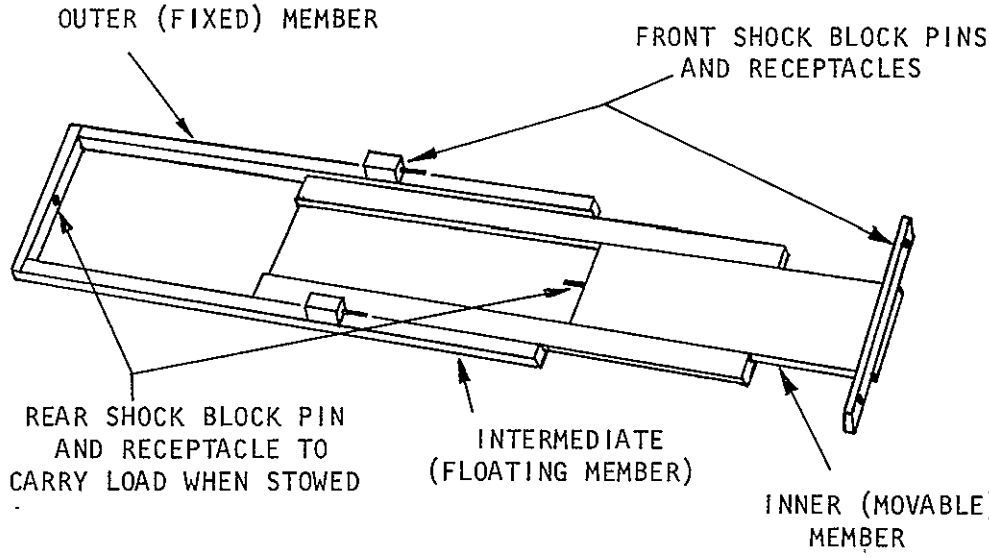
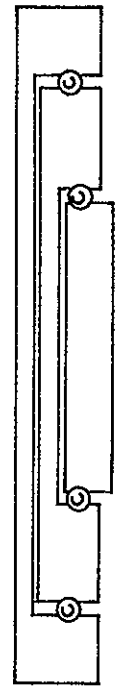


FIGURE 6.6-7· FINAL CONCEPT FOR MOUNTING TURBOALTERNATOR ON THE ALL-WELDED FRAME





SECTIONAL VIEW WITHOUT SHOCK BLOCKS

FIGURE 6.6-8 CHASSIS SLIDES

6.7 Shock and Vibration Isolation

Shock Mount Requirements

Since the turboalternator is driven with a pulsed turbine, there is a cyclic torque applied to the entire package of approximately 360 in-lb. The vibration isolators were used between the turboalternator and the frame to dampen out this imposed torque. This would ease the loading on the frame when subjected to long endurance testing and ultimately long term operation. In addition, these isolators would dampen any vibration and mechanical noise that might otherwise be transmitted into the LM.

It was felt that the addition of vibration isolators between the HEPS fixed frame members and the LM would not offer significant improvement to warrant their use. It is true that they could dampen out some of the launch loads, but the force levels would be so high that the isolators required would be very large and heavy.

Vibration Mount Selection

The HT2 series BTR elastomeric mount that was chosen is shown in Figure 6.7-1. Also shown are typical load-deflection curves for these mounts. The HT2-100 mount that was chosen can carry a maximum static load of 100 lb. The turboalternator itself weighs approximately 90 lb; therefore, the use of several HT2-100 mounts was conservative. Since the mounts do not weigh very much, this conservatism does not significantly contribute to the system weight.

The temperature limitations of the vibration mounts are not severe. The manufacturer indicated that the mounts will operate properly between -65°F and +300°F. However, tests conducted at TRW revealed no significant change in characteristics at 400°F. The thermal control of the package was aimed at maintaining a mount temperature of approximately 200°F.

Since the mounts are designed to carry a maximum of 100 lb, the launch loads are much too severe. These loads would certainly exceed the recommended maximum deflections of approximately 0.3 inches; therefore, mechanical stops were provided which will limit the travel and carry the high loads that are expected.

6.8 Deployment

Extending Package from LM SEQ Bay

The HEPS unit is mounted on chassis slides in order to provide a means for extraction from its launch and flight location. After



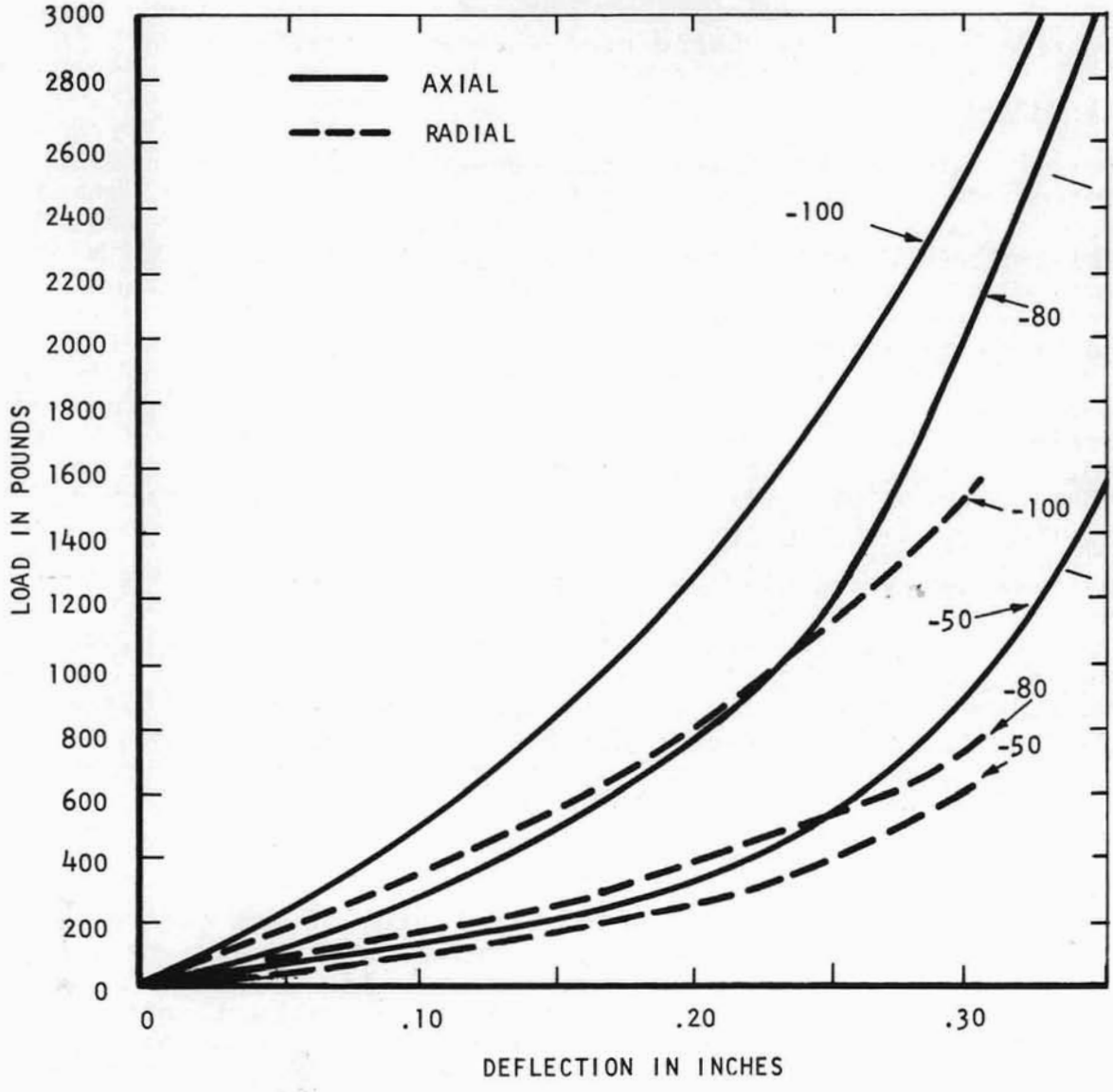


FIGURE 6.7-1 HEPS VIBRATION MOUNTS (SEE REFERENCE 6)

landing on the moon, the unit must be removed from the equipment bay so that the various radiating surfaces can be erected for operation. Due to its weight, it is not practical to physically remove the unit from the LM. For this reason, the chassis slides were chosen as a simple means for extending the unit out and supporting it during operation.

Pin-type locks are provided to keep the unit from moving within the equipment bay during launch and flight. These pins would be released when it was time to deploy the unit. It would then be pulled out of the bay to the full extent of the chassis slide travel and be locked in place by another set of locking pins. These pins would keep the unit from moving in the deployed position while it was being used (see Figure 6.8-1).

Oil Radiator

The oil radiator is shown in the stowed and deployed positions in Figure 6-8-2. The stowed position locking pin and stand-off support the radiator during launch and flight. When released the radiator will be rotated to its deployed location, and separate locking pins are used to prevent movement during operation.

The hinge mechanism also functions as the oil flow manifold. A tube, rigidly attached to the radiator, turns on uniball hinges in the two hinge point stand-offs. The tube has rotating seals consisting of two O-rings. The hinge axis is off-set from the radiator panel so that the radiator can be positioned in the same plane as the scroll fins when it is deployed. This minimizes the view factors between the radiator and the hot scroll components.

Rectifier Cold Plate

The stowed and deployed positions for the cold plate are illustrated in Figure 6.8-3. This panel can be pivoted up to a new position and also slides back as shown. The cold is pivoted back so that the radiator would not be subjected to the heat from the scroll components. As with the oil radiator, the panel locks in both the stowed and the deployed positions.

Speed Control

The speed control box hangs on the bottom of the package. When the stowed position locking pin is released, the box drops down to the new position and locks as shown. The radiator deploys to an angle of 15° past vertical to insure that it will not be aimed down toward the lunar surface since there is a possibility that the LM could land with as much as a 15° tilt. Therefore, at the worst position, the speed control will be perpendicular to the

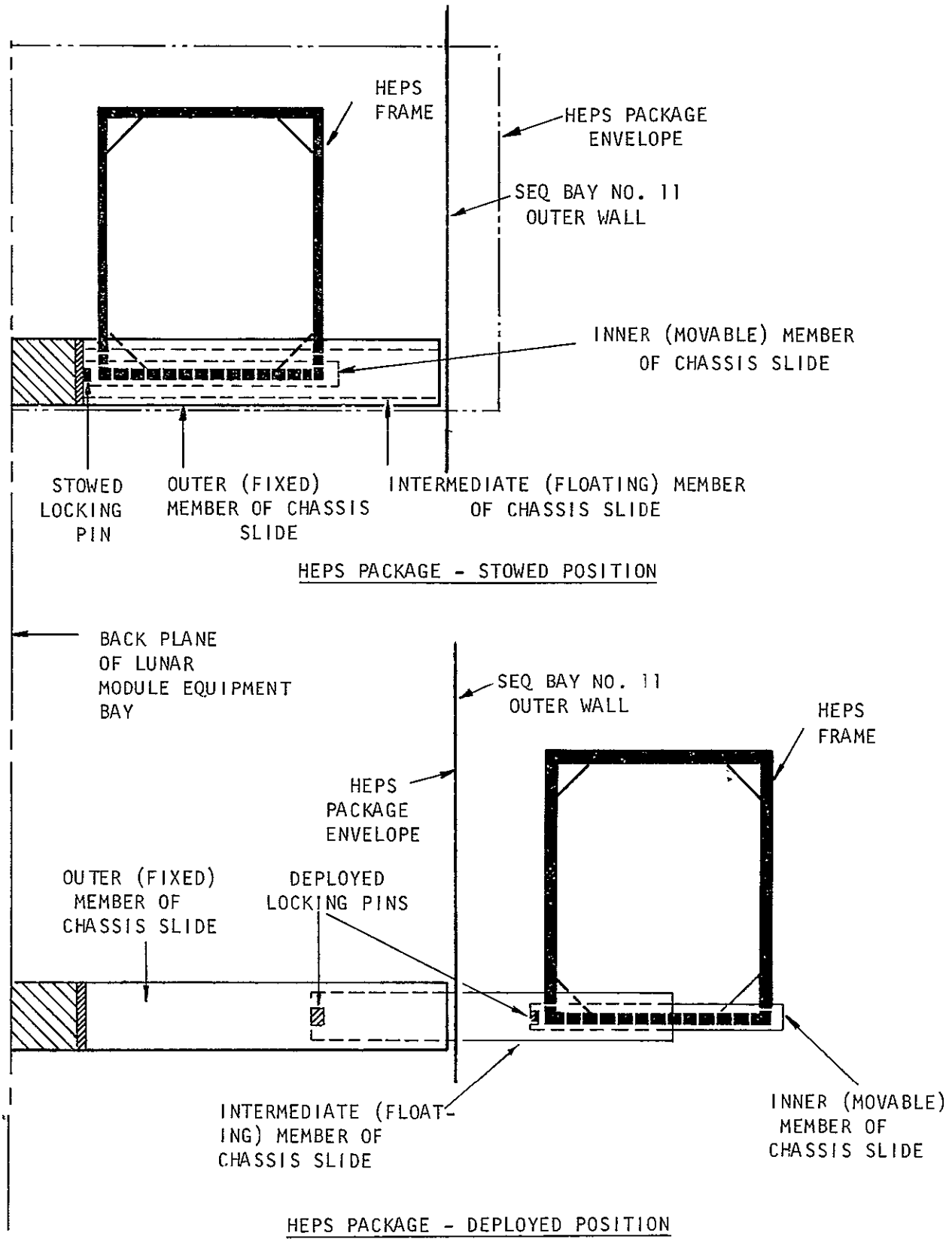
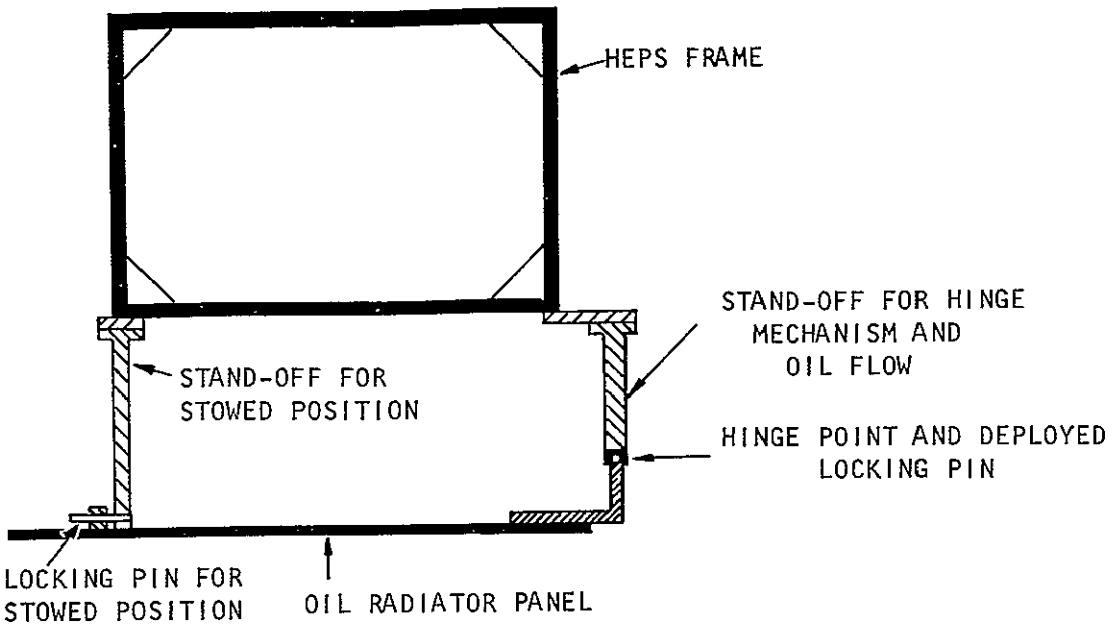
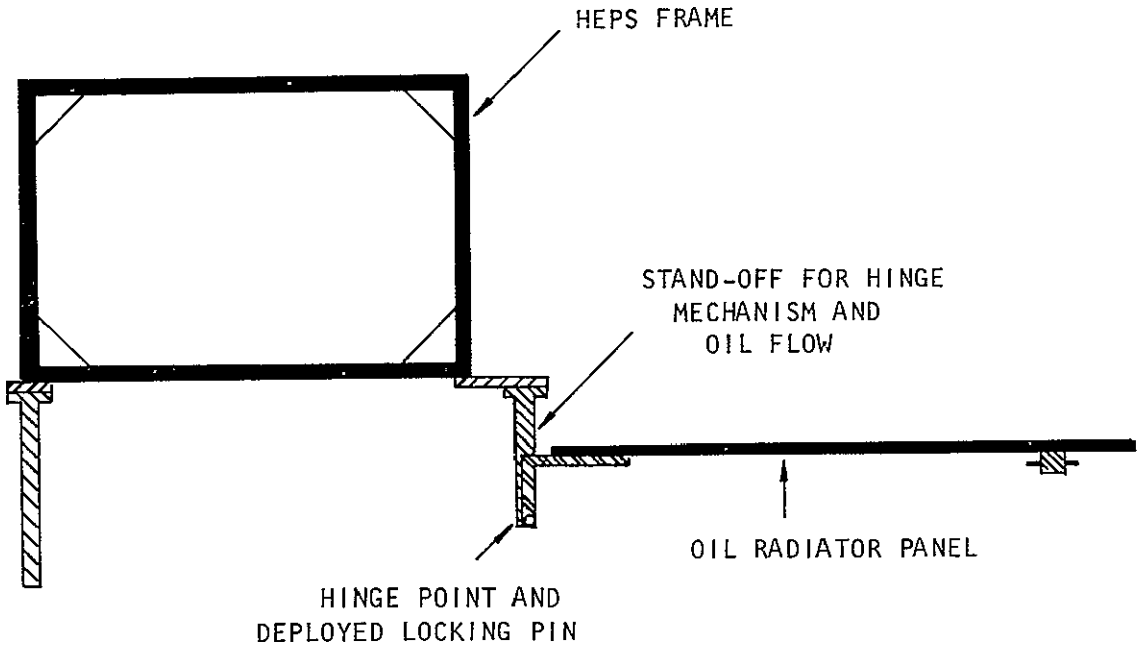


FIGURE 6.8-1 EXTRACTION OF HEPS PACKAGE FROM LM EQUIPMENT BAY

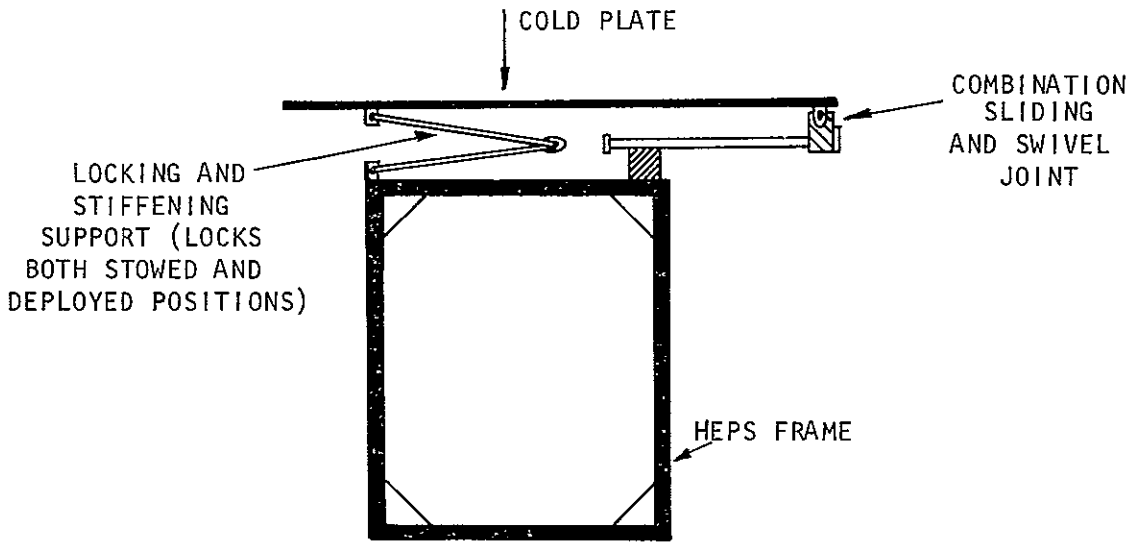


TOP VIEW OF PACKAGE - OIL RADIATOR STOWED

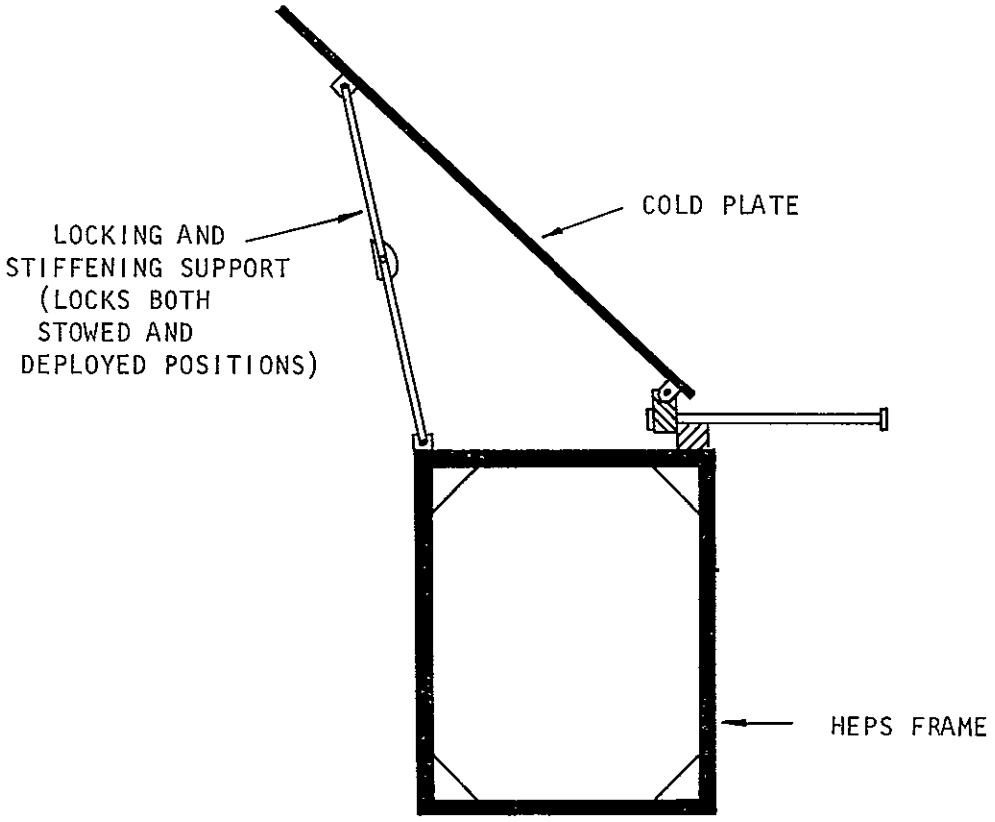


TOP VIEW OF PACKAGE - OIL RADIATOR DEPLOYED

FIGURE 6.8-2 DEPLOYMENT OF OIL RADIATOR



LEFT SIDE VIEW OF PACKAGE - COLD PLATE STOWED



LEFT SIDE VIEW OF PACKAGE - COLD PLATE DEPLOYED

FIGURE 6.8-3 DEPLOYMENT OF RECTIFIER COLD PLATE

lunar surface. See Figure 6.8-4 for views of the speed control box deployment.

Methods of Deployment

The outline presented below lists all of the basic methods of deployment that were considered for the HEPS unit. The Qualification Unit will be equipped with all of the hinge and sliding mechanisms and with all of the locking pins.

I Manual - with no mechanical advantage

A. Guided cable - not reversible

B. Guided cable - reversible

II Manual - with mechanical advantage

A. Pulley system - reversible or not reversible

B. Screw system - reversible or not reversible

C. Ratchet - reversible or not reversible

III Automatic

A. Piston - reversible or not reversible

1. Using LM pressure

2. Using HEPS pressure

B. Spring - not reversible

1. Compression

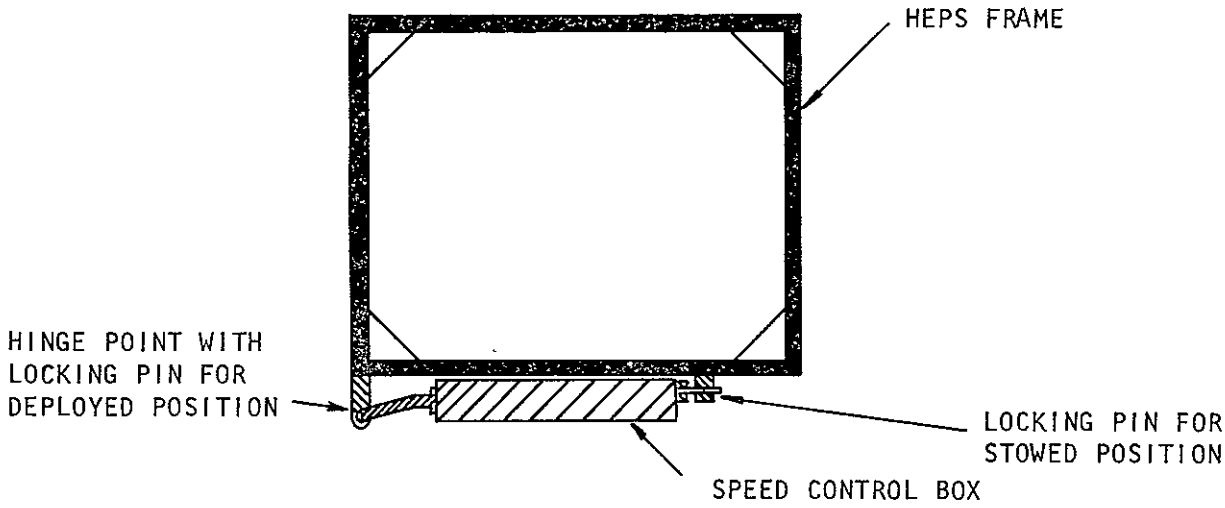
2. Negator

C. Electrical motor driven versions of I or II

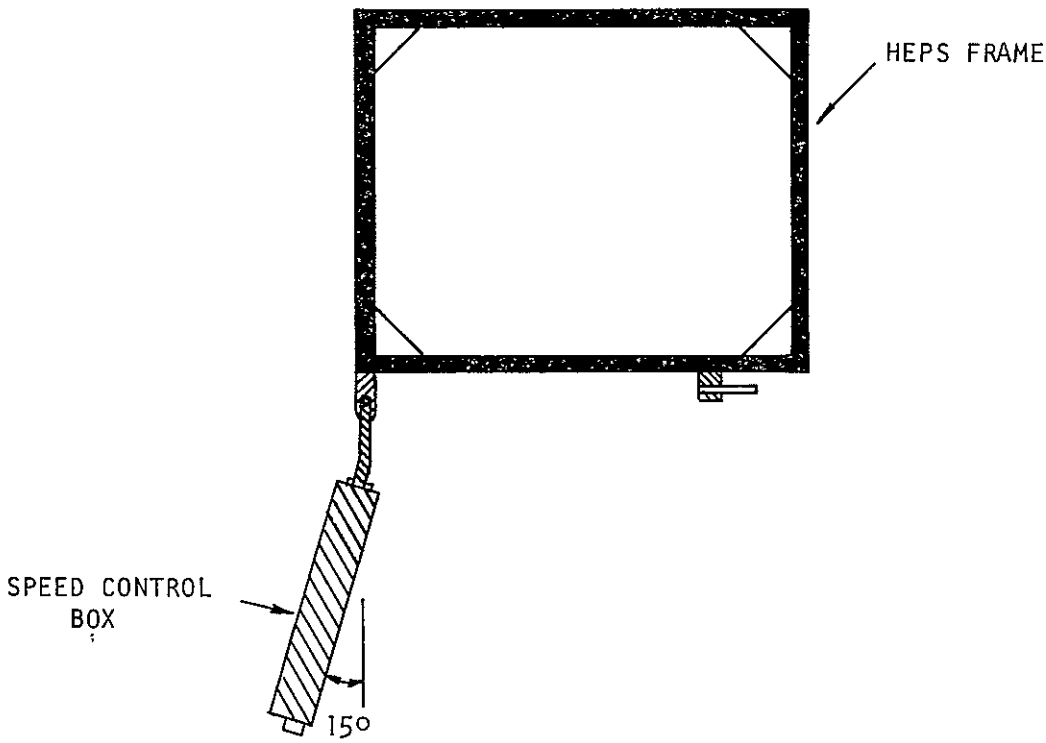
D. Lunar gravity

The HEPS is shown in the stowed position in Figures 6.5-1 and 6.5-10 and in the deployed position in Figures 6.5-2, 6.5-3, 6.5-11 and 6.5-12.

After design evaluation, the automatic spring method was selected to provide deployment power because of its simplicity, light weight, and reliability.



FRONT VIEW OF PACKAGE - SPEED CONTROL STOWED



FRONT VIEW OF PACKAGE - SPEED CONTROL DEPLOYED

FIGURE 6.8-4 DEPLOYMENT OF SPEED CONTROL BOX

PRECEDING PAGE BLANK NOT FILMED.

7.0 MATERIALS AND PROCESSES

In addition to providing process specifications, material selection, and recommendations, the Materials Group evaluated and selected candidate thermal coatings applicable for HEPS use. A major portion of this section is devoted to the thermal coating program.

7.1 Materials and Processes Selection Criteria

Materials selected for Phase III were nearly the same as the Phase II components with the exception of materials required for new parts. Materials and processes were selected in accordance with MIL-STD-143. A weight reduction program resulted in a greater utilization of lightweight materials, consistent with thermal and stress considerations. Nonmetallic materials were selected in accordance with NAA specification MC-999-0058D, "Approved Materials for Use in the Apollo Spacecraft."

7.2 Material and Process Changes and Additions

Materials chosen for the frame assembly were aluminum alloys, 6061-T6, used for welded members, and 2024-T851 used for unwelded parts where higher strength was required.

Aluminum was used for the phase separator construction and to replace some steel in the lubrication pump housing.

In Phase II a portion of the combustion chamber was flame sprayed with copper after the fin was welded to the chamber. Since the adherence of the copper was found to be poor after testing of the unit, the Phase III combustion chamber was electroplated with copper in the desired area, the copper was machined, then the fin was welded to the chamber.

The copper fins were butt welded to the Hastelloy X scroll using electron beam welding in Phase II. The joint configuration was changed in Phase III to insure better heat flow from the Hastelloy X to the copper. The fins were lapped over the nozzle plate and welded, which provided a much larger area of Hastelloy X in contact with the copper than was the case with the butt weld.

The oil radiator was made of 6061 aluminum sheet. The aluminum tubing and sheet were dip brazed using 718 aluminum braze alloy. All mounting hardware and tube fittings were also brazed to the sheet at the same time as the tubing.

The electrical system structural parts (rectifier cold plate, control box and speed control) were made of 6061-T6 aluminum. The rectifier cold plate was hard-coat anodized and painted with a thermal control coating to provide electrical insulation and heat rejection improvement.

To insulate the frame assembly from heat produced at the turbine and scroll assembly, a stainless steel shield, which was electro-polished and gold plated, was used to reflect heat. In addition, "Kapton," a polyimide film coated with aluminum was used in multiple layers to reflect heat away from critical areas (see reference 17).

7.3 Thermal Control Coatings

The prevention of excessive equipment temperatures in a lunar environment was immediately recognized as a major task in this program. A number of adequately sized radiating surfaces, which provide a sound means of energy dissipation, were incorporated in the system design. The temperatures of these radiating surfaces were determined by their net energy gain or loss rate and by their absorptance and emittance characteristics. Thermal control coatings were utilized to provide improved radiation performance. Table 7.3-1 lists the various radiating surfaces, their materials of construction, operational ambient temperature ranges and thermal gradients, and the selected thermal control coatings. The indicated thermal environments of the radiating surfaces suggested a desirability for two thermal control coatings systems; one for the high temperature requirement (>950°F) and another for the lower temperature (<400°F) components. Other factors that were considered in the coating selection include total hemispherical emittance stability, solar absorptivity stability, adherence and substrate compatibility in a lunar environment.

High Temperature Thermal Control Coating

Only two high temperature (>950°F) and high emissivity coatings have been established for space use (see reference 7). These coatings, iron titanate (Fe_2TiO_5) and calcium titanate ($CaTiO_3$) which were previously evaluated on substrates of 310 stainless steel and columbium-1% zirconium, exhibited emittance stability, adherence and substrate compatibility. The iron titanate coating exhibited exceptional stability after long-term exposure at 1800°F under vacuum while the calcium titanate experienced a chemical breakdown after short exposure at 1650°F while under vacuum. The emissivity of calcium titanate and iron titanate are reported in Table 7.3-2.

3

TABLE 7.3-1

SELECTED THERMAL CHARACTERISTICS AND THERMAL CONTROL COATINGS FOR RADIATING SURFACES

	Component	Materials of Construction	Operational Ambient Temp., °F Min.	Max.	Maximum Operational Thermal Gradient ΔT, °F	Thermal Control Coating
1)	Scroll and Fin Assembly	Hastelloy X	950	1350	<50	Iron Titanate (Fe_2TiO_5)
2)	Gas Generator and Fin	Oxygen-free high purity copper	200	875		Iron Titanate (Fe_2TiO_5)
3)	Rectifier-Filter Panel (Cold Plate)	6061 Aluminum	200 (E)	325 (E)	<50 (E)	Dow Corning 92-007
4)	Oil Radiator Panel	6061 Aluminum	350 (E)	400 (E)	400 (E)	Dow Corning 92-007
5)	Speed Control	6061 Aluminum	180 (E)	210 (E)	<20 (E)	Dow Corning 92-007
6)	Voltage Regulator	6061 Aluminum	210 (E)	240 (E)	<30 (E)	Dow Corning 92-007

(E) Estimated

TABLE 7.3-2

EMISSIVITY OF CALCIUM TITANATE AND IRON TITANATE (see reference 7)

Thermal Control Coating	Total Hemispherical Emittance (E_{tn})	Test Temp. (°F)	Test Duration (Hours)	Thermally Cycled	Test Vacuum (mm Hg)	Substrate	Remarks
Calcium Titanate ($CaTiO_3$)	0.88-0.91	1350	20,000	112 times at Room Temperature	1×10^{-7}	Type 310	Slight darkening on Coating, no apparent texture change also no indication of cracking or spalling.
Iron Titanate (Fe_2TiO_5)	0.87-0.89	1350	20,000	114 times at Room Temperature	2×10^{-8}	Type 310 SS	Slight change in coating color, texture and integrity of coating unchanged.
Iron Titanate (Fe_2TiO_5)	0.88	1500-1800	5,000	3,125 times (1500-1800°F)	1×10^{-7}	columbium -1% zirconium	Slight hairline crack appeared after 3500 hours test. There was no texture or color change and no indication of separation or spalling.

Various test samples were made to evaluate the candidate coatings. The test samples consisted of three base materials: Hastelloy X, OFC copper and type 310 stainless steel. Some test samples were plasma sprayed with iron titanate and others with calcium titanate. Prior to coating, 50% of the test samples were nickel plated. A number of the specimens from each base material group were exposed to a temperature of 1400°F for one hour in a vacuum. Visual examination revealed that both of the coatings adhered to all of the substrates, but the nickel plating exhibited blistering tendencies on the copper substrate. Representative samples subjected to a thermal vacuum test are shown in Figure 7.3-1. Microprobe analyses were made on all test specimens to evaluate the relative stability of the coating-substrate systems. The evaluation compared the "as coated" specimens with the "as coated and thermally exposed" specimens for common coating substrate systems.

Figures 7.3-2 and 7.3-3 are representative data for the microprobe analyses. A summary of the microprobe analyses follows:

1. There was no diffusion into either the coating or substrate of as-coated, plated or unplated specimens of any element checked (Ni, Cr, Fe, Cu or Ti).

2. There was little (<1 micron) or no diffusion into either the coating or substrate of unplated specimens after thermal exposure at 1400°F.

3. There was little (<1 micron) or no diffusion into or out of the coating on plated specimens after thermal exposure at 1400°F.

4. Copper diffused into the nickel plate and nickel diffused into the copper in plated copper substrate specimens during thermal exposure at 1400°F.

5. Nickel from the nickel plate diffused into the Hastelloy X and chromium from the Hastelloy X diffused into the nickel plate in nickel plated Hastelloy X specimens during thermal exposure at 1400°F.

6. Little (<1 micron) or no diffusion into or out of the coating of nickel plated Hastelloy X specimens occurred during thermal exposure at 1400°F.

Figures 7.3-4 and 7.3-5 are photomicrographs showing the Fe TiO_5 coating on unplated Hastelloy X before and after thermal exposure.

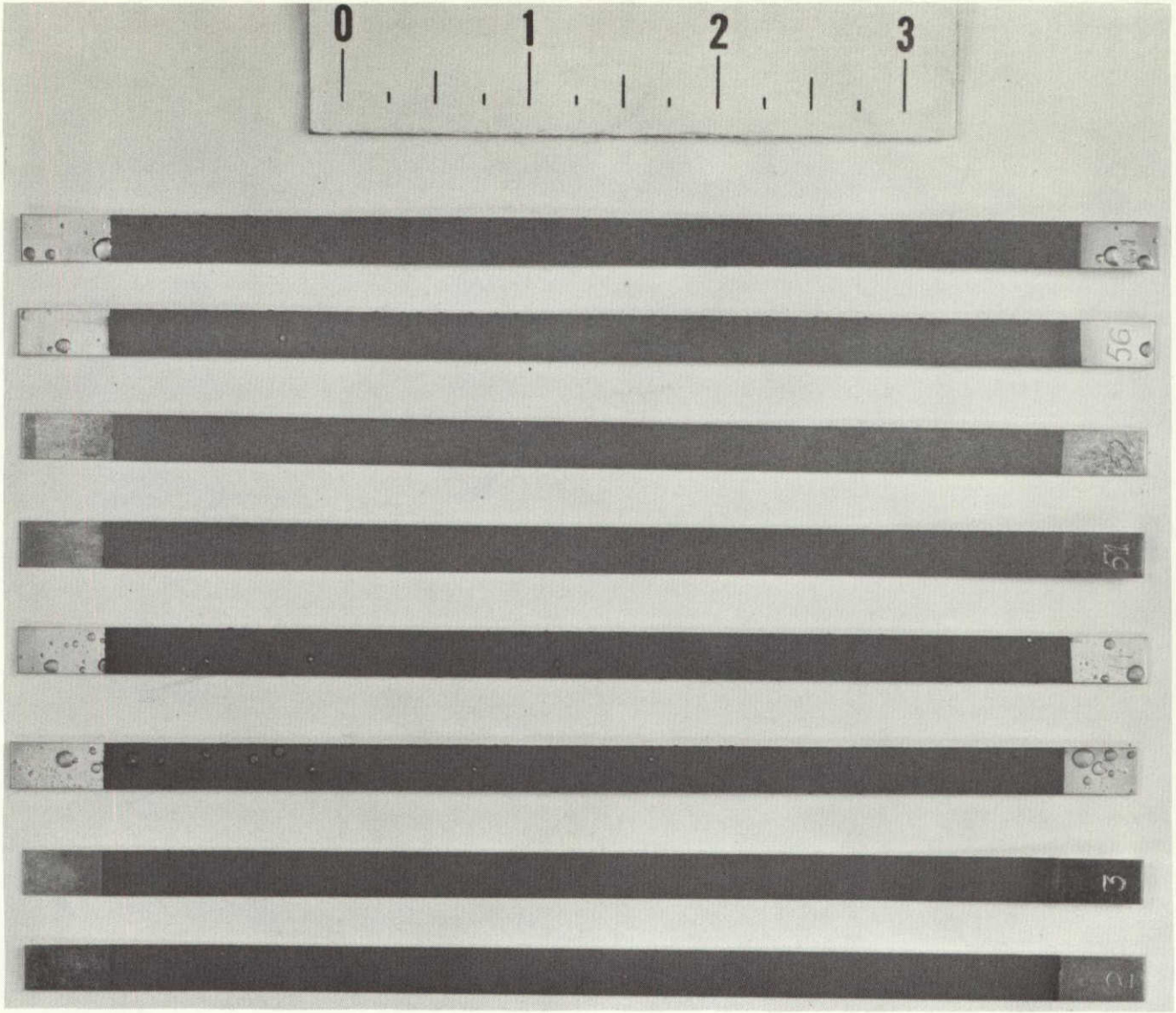


FIGURE 7.3-1 FRONT SIDE OXYGEN-FREE HIGH PURITY COPPER SUBSTRATE AFTER EXPOSURE (1400°F FOR 1 HR. IN VACUUM)

REPRODUCIBILITY OF THE ORIGINAL PAGE IS POOR

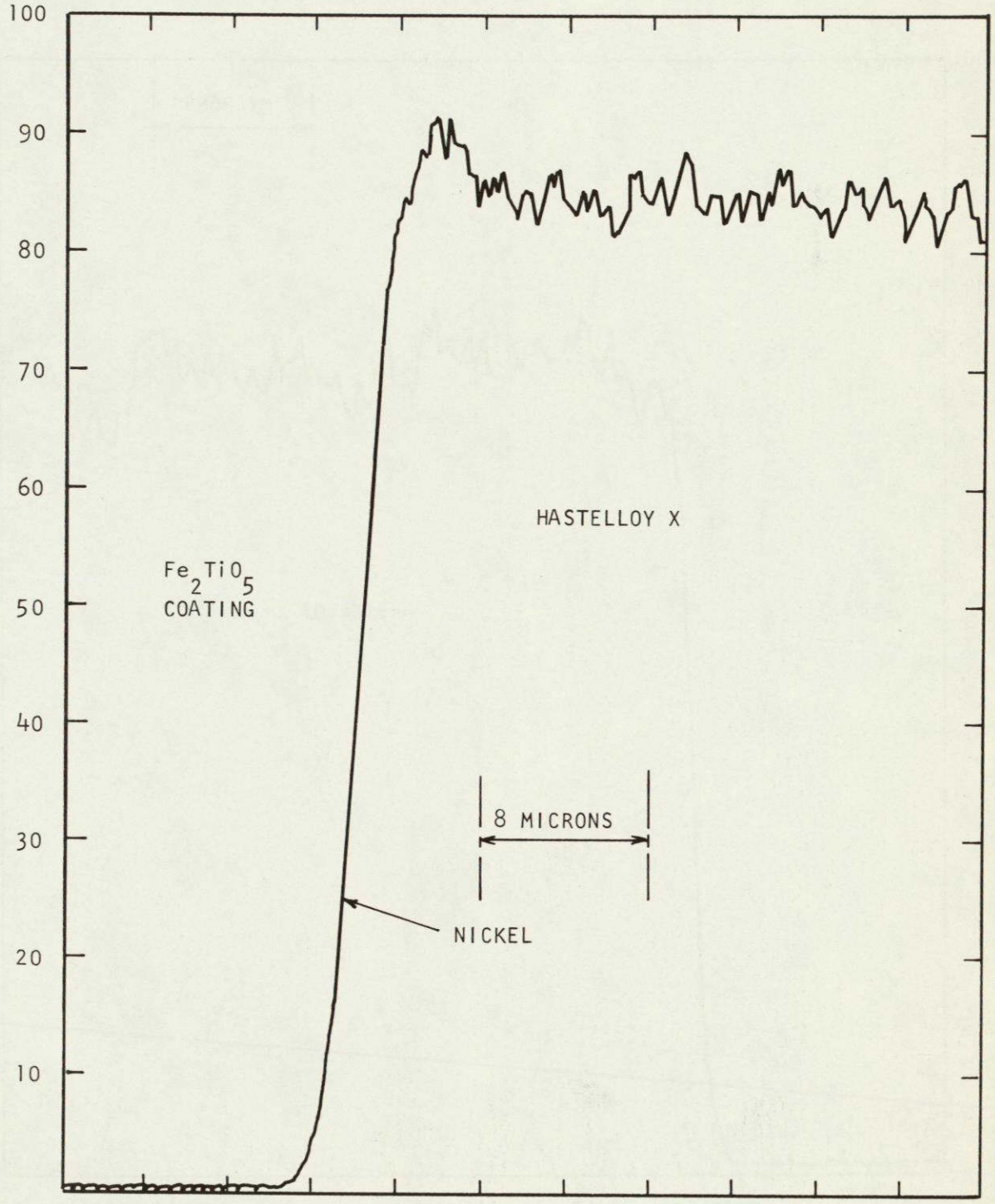


FIGURE 7.3-2 MICROPROBE ANALYSIS OF NICKEL IN Fe_2TiO_5 COATED HASTELLOY X (AS COATED)

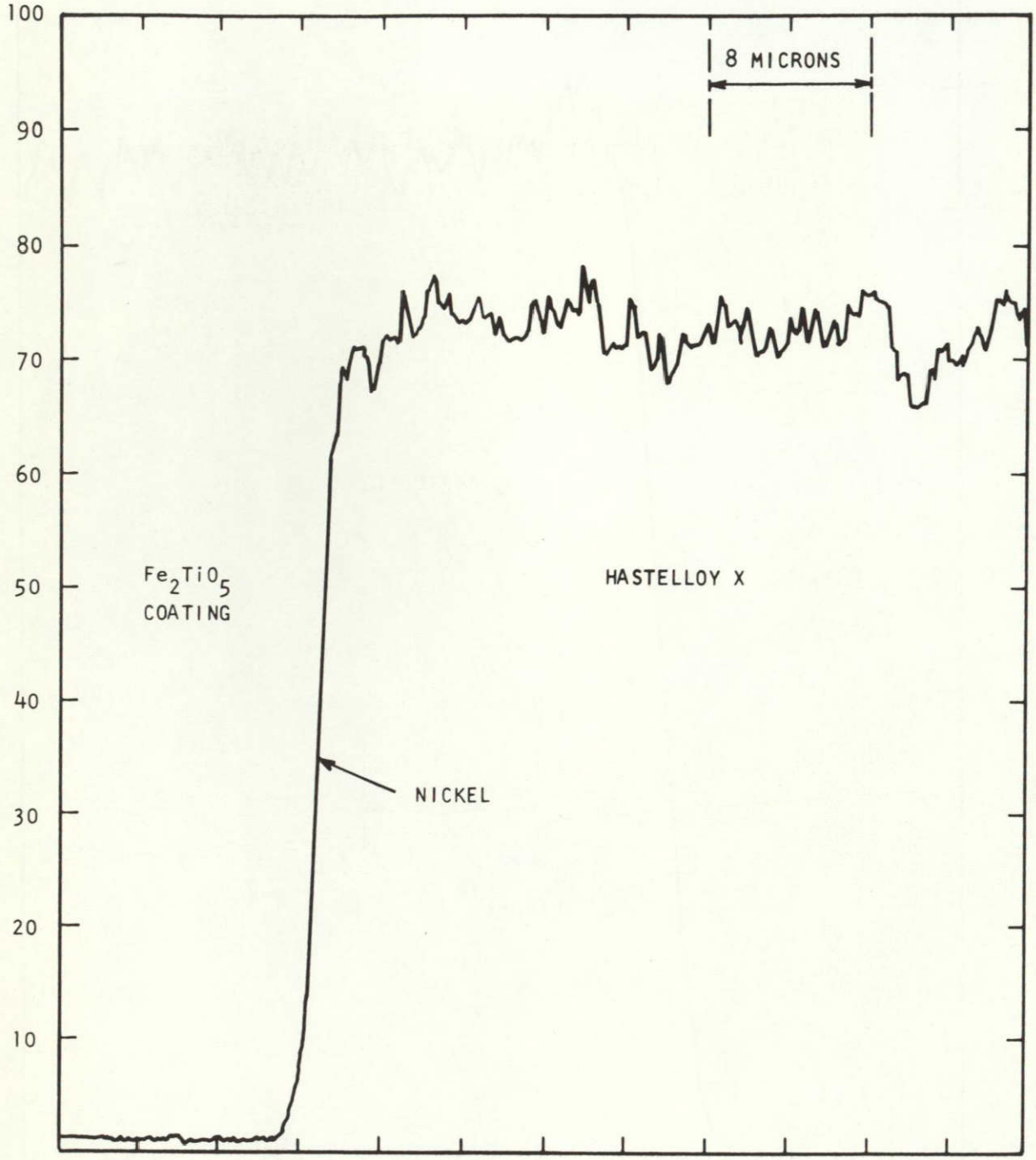
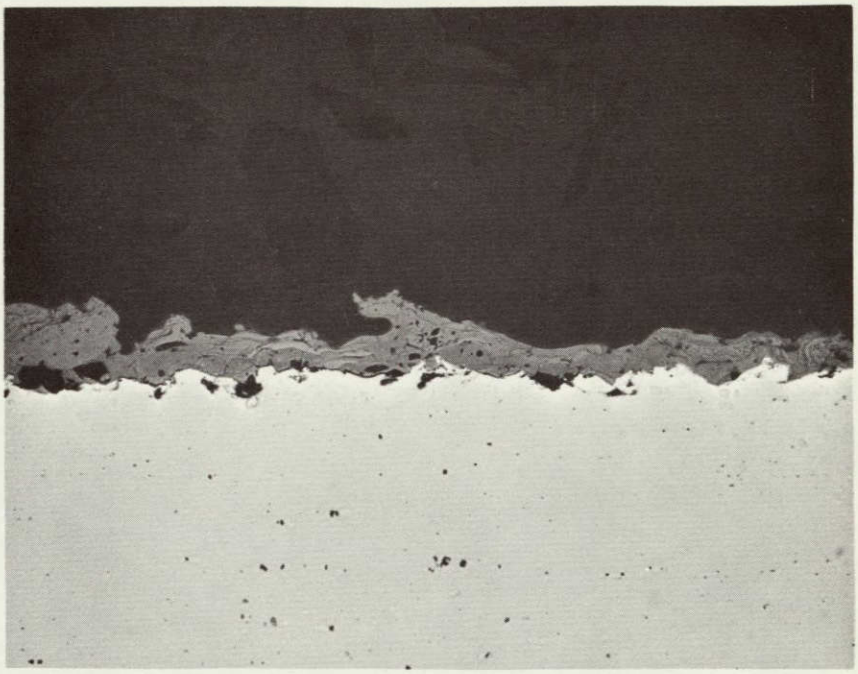
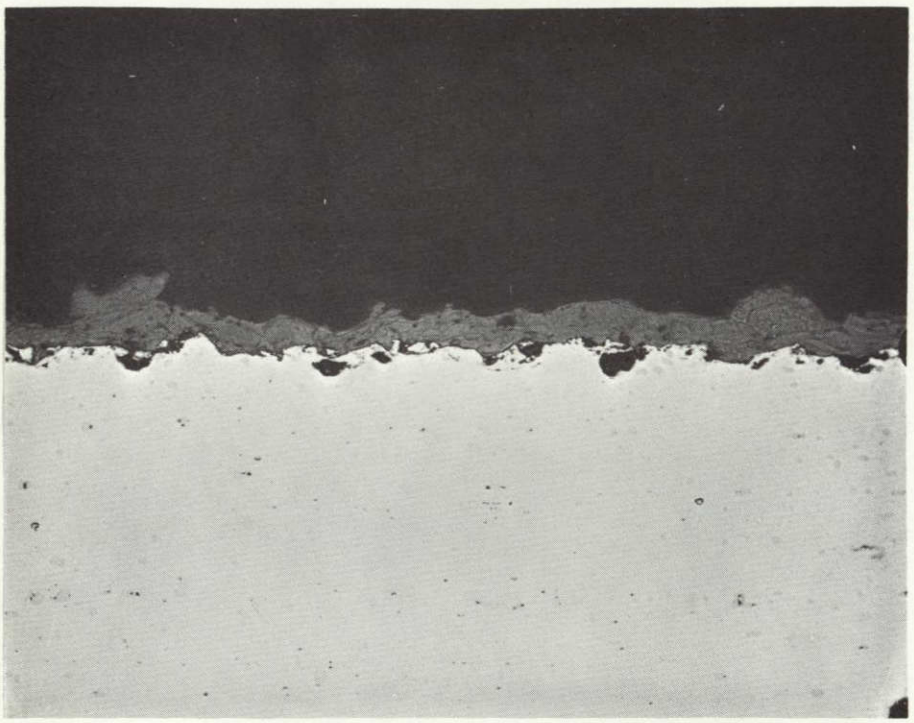


FIGURE 7.3-3 MICROPROBE ANALYSIS OF NICKEL IN Fe_2TiO_5 COATED HASTELLOY X (AS COATED AND THERMALLY EXPOSED)



250X

FIGURE 7.3-4 Fe_2TiO_5 ON HASTELLOY X (AS COATED)



250X

FIGURE 7.3-5 Fe_2TiO_5 ON HASTELLOY X (AS COATED AND THERMALLY EXPOSED)

The optimum coating-substrate combination selected for the high temperature application was an iron titanate coating on a bare substrate. After DVR testing, the coating was visually inspected and was found to be uniform in appearance and adherent to all scroll areas.

Low Temperature Thermal Control Coating

Two low temperature (<400°F) coatings (DC 92-007 and IITRI-293) were found to be suitable for the HEPS low temperature application. The IITRI-Z93 coating presented unique handling problems and was eliminated as a candidate coating. DC 92-007 coating had been used previously at TRW with excellent results. However, sufficient emissivity and absorptivity data was unavailable; therefore, a test program was conducted using coated specimens. The solar absorptance as a function of ultra-violet irradiation and the hemispherical emittance were measured for DC92-007 coated type 6061 aluminum specimens. The material was maintained at an elevated temperature during ultra-violet irradiation and during hemispherical emittance measurement. The results are presented below.

Solar Absorptance Following Ultraviolet Irradiance
(1 UV Sun) on Sample at 401°F, DC 92-007

	Solar Absorptance
Initial	0.22
After 50 hours	0.30
After 100 hours	0.44

Hemispherical Emittance During and Following
Elevated Temperature (401°F) Maintenance
in Vacuum, DC 92-007

Following Indicated Hours at Elevated Temperature	Temperature of Measurement	Hemispherical Emittance
Initial	196°F	0.847
Initial	347°F	0.793
50 Hours	397°F	0.787
100 Hours	394°F	0.790

PRECEDING PAGE BLANK NOT FILMED.

8.0 DEVELOPMENT TEST PROGRAM

The test program was divided into three parts: 1) component tests, 2) DVR system tests, and 3) Qualification Unit acceptance tests. The component tests were conducted on the following subsystems: gas generator, lubrication system, lubrication system and alternator, phase separator, lubrication system with phase separator and alternator, and electrical system bench tests. The component tests were conducted to evaluate the redesigned components. The DVR test program objective was to demonstrate the design feasibility of the complete system. The acceptance test program for the Qualification Unit was to be conducted at a later date and, therefore, will not be discussed in this report.

8.1 Test Facility

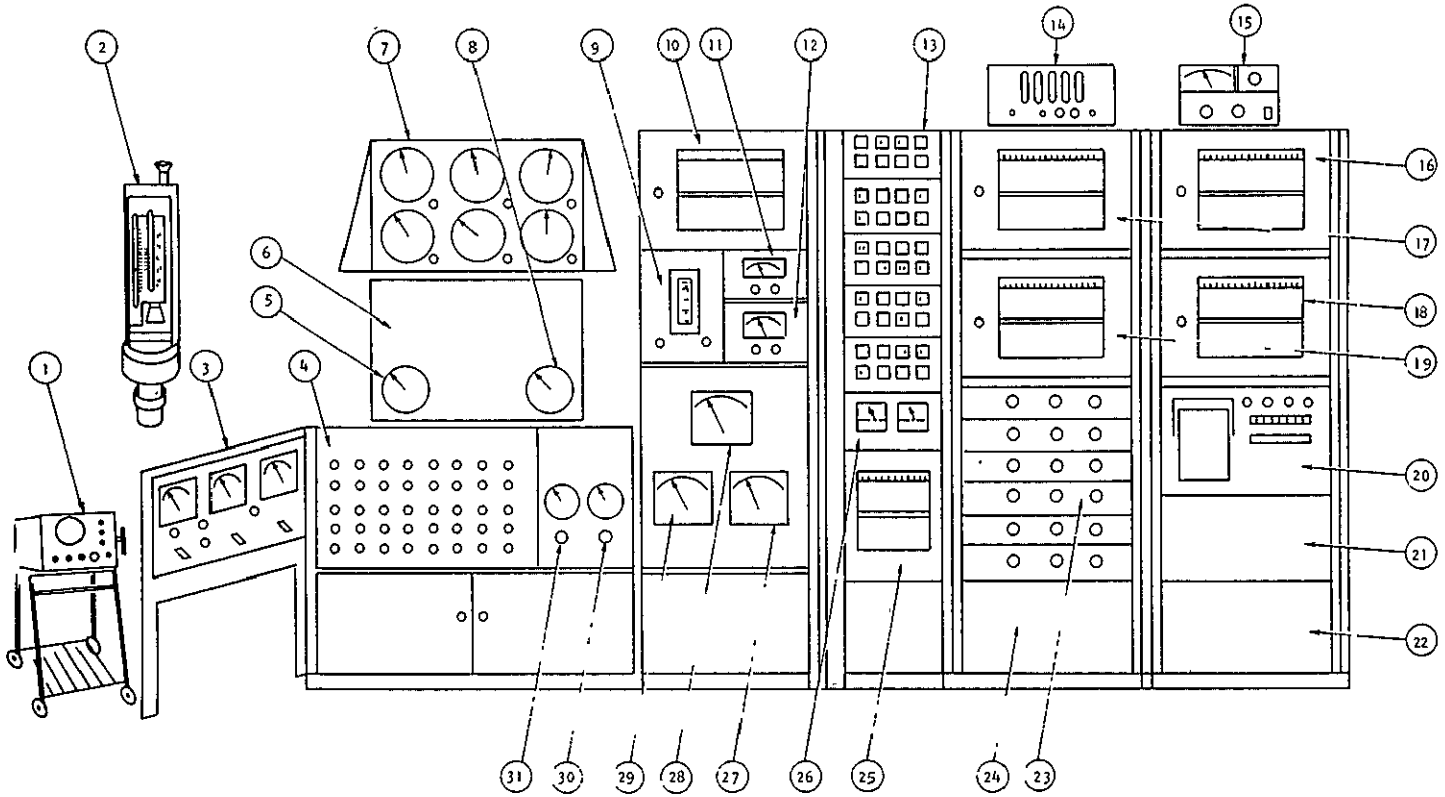
The system DVR tests and component gas generator tests were conducted in the Virginia Polytechnic Institute Altitude Test Facility located at Rocky Mount, Virginia. The system is designed and arranged specifically for liquid propellant turboalternator power system testing.

Control Panel and Instrumentation

A control room located adjacent to the test cell and opposite the earth-mound barricade houses a control console and all the instrumentation. Power system operation and data monitoring are performed in this room thereby eliminating the necessity for any personnel to enter the test cell while the turboalternator is running or while the propellant systems are pressurized. A bullet-proof glass window provides the capability of visual surveillance of the test cell during test operations.

An optical pyrometer for measuring turbine blade temperatures was mounted to the outside of the altitude chamber as shown in Figure 8.1-2. A remote actuator with a position indicator which was visible from the control room rotates the pyrometer to scan the turbine blade and disk temperatures. Temperature readout was located at the control console.

See Figure 8.1-1 for the control console layout. All instrumentation was consolidated and grouped by sections to assist in readouts while testing the DVR unit. All thermocouple readouts and the CEC recorder were on the right side, electric meters and oil flow meter in the center, and the more sophisticated electrical controls and readouts on the left of the control console. The manual pressure readout gages were located on a sloping panel just above the cell window. Directly below the cell window are located all the switches, buttons, and lights



NO.	DESCRIPTION
1	OSCILLOSCOPE
2	MCLEOD VACUUM GAGE
3	BREADBOARD-SPEED CONTROL & VOLTAGE REGULATOR PANEL
4	CONTROL PANEL
5	OXIDIZER TANK PRESS. GAGE
6	CELL WINDOW
7	OIL PRESSURE GAGES (6)
8	FUEL TANK PRESSURE GAGE
9	OIL FLOW METER
10	TEMPERATURE RECORDER I/C
11	OVER-TEMPERATURE CONTROL
12	OVER-SPEED CONTROL
13	T/C JACK PANELS (5)
14	EPUT COUNTER
15	FREQUENCY METER
16	TEMPERATURE RECORDER C/C
17	TEMPERATURE RECORDER C/A
18	TEMPERATURE RECORDER I/C
19	TEMPERATURE RECORDER C/A
20	CEC RECORDER
21	BALANCE BOX & POWER SUPPLY
22	BALANCE BOX & POWER SUPPLY
23	AMPLIFIERS
24	D.C. POWER SUPPLY
25	TEMPERATURE RECORDER C/C
26	FIELD VOLTS AND AMPS
27	D.C. VOLTMETER
28	D.C AMMETER
29	A.C. VOLTMETER
30	GROVE N_2 PRESS. REGULATOR
31	GROVE He PRESS. REGULATOR

FIGURE 8.1-1 CONTROL PANEL LAYOUT

for controlling the propellant feed systems and controls for stopping and starting the unit.

Altitude Chamber and Operation

The altitude chamber shown in Figure 8.1-2 is 6 feet in diameter and 9 feet long. A three-stage steam ejector barometric condenser system provides the altitude capability. Steam is supplied by a 40,000 lb/hr boiler and three 1000 gpm pumps provide condensing water. A 22-inch diameter exhaust duct connects the altitude chamber to the ejection system. This system is rated at an altitude of 100,000 feet at a gas flow of 0.5 lb/sec. During the DVR test program, altitudes up to 170,000 feet were attained.

The altitude chamber itself is located in a test cell having three one-foot thick reinforced concrete walls with a retractable overhead door on the fourth side which opens to an outside concrete pad. The concrete pad is bounded on the side opposite the test cell by an earth-mound type barricade.

Propellant Feed System

The propellant feed system schematic is shown in Figure 8.1-3. The feed system that was used is similar to the Phase II system except secondary tanks were added between the main propellant tanks and the altitude chamber. The secondary tanks had a 12 gallon capacity and were pressurized with nitrogen. The liquid level in the tanks was controlled by sight gage measurement. The secondary tanks were located approximately 18 feet from the gas generator in the altitude chamber and provided LM propellant system simulation. The main tanks were remotely pressurized and regulated with Grove regulators. All system pressurizing, venting, and purging operations were performed remotely from the control panel which was electrically connected to the solenoid valves in the propellant system. All flow passages in the system were one-half inch diameter stainless tubing. A line which bypassed the secondary tanks was installed so that the secondary tank influence on propellant dynamics could be analyzed. Two oxidizer and two fuel main tanks were installed in a piggyback manner. Each propellant tank was housed in a thermally insulated and temperature controlled enclosure. The enclosures were provided with 2.5 KW electric, explosion proof heaters for maintaining propellant temperatures in the range of 60° to 90°F during the winter months. Since the enclosures were shaded and insulated, no provisions for cooling were necessary.

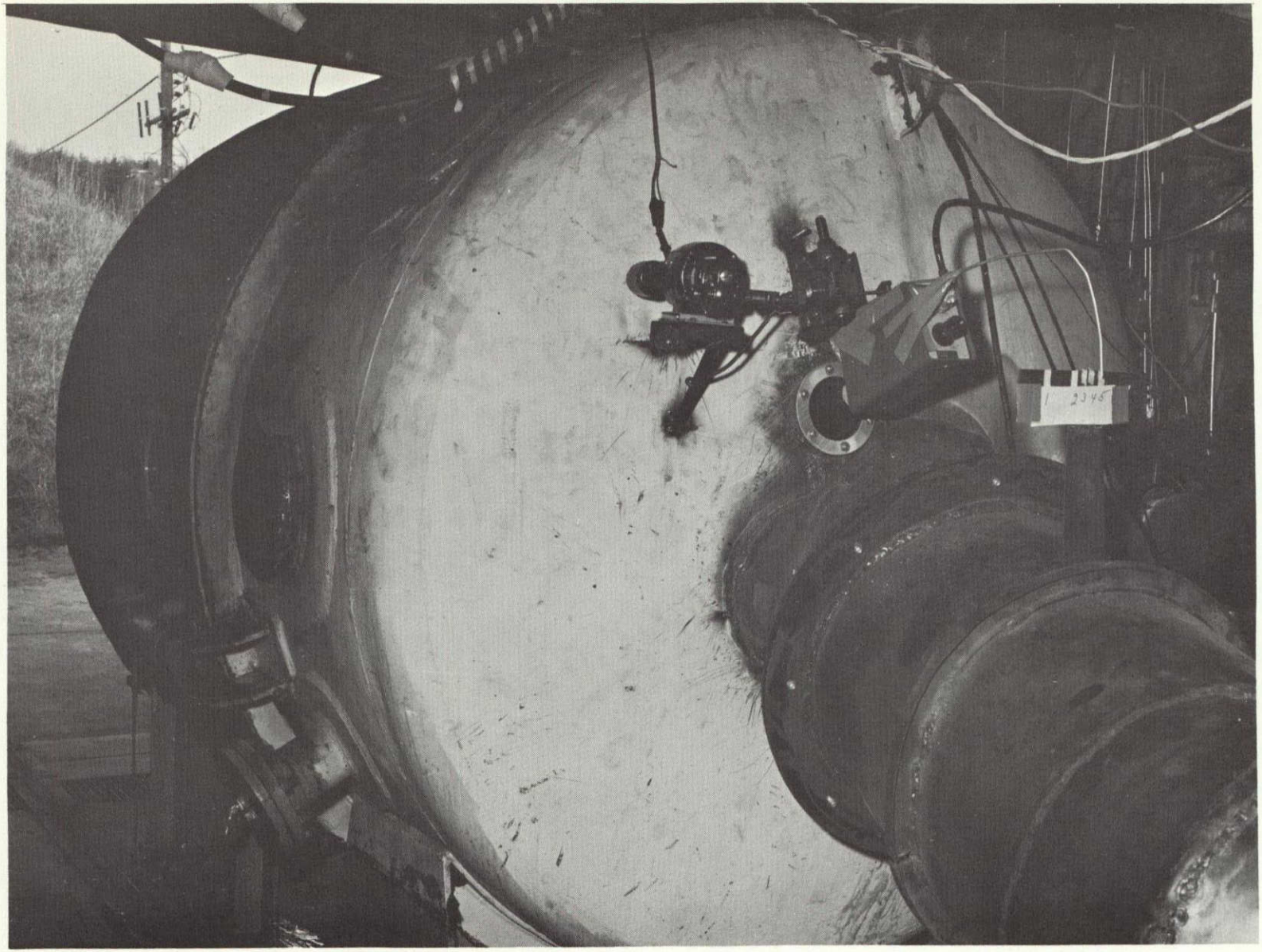


FIGURE 8.1-2 ALTITUDE CHAMBER VPI TEST FACILITY

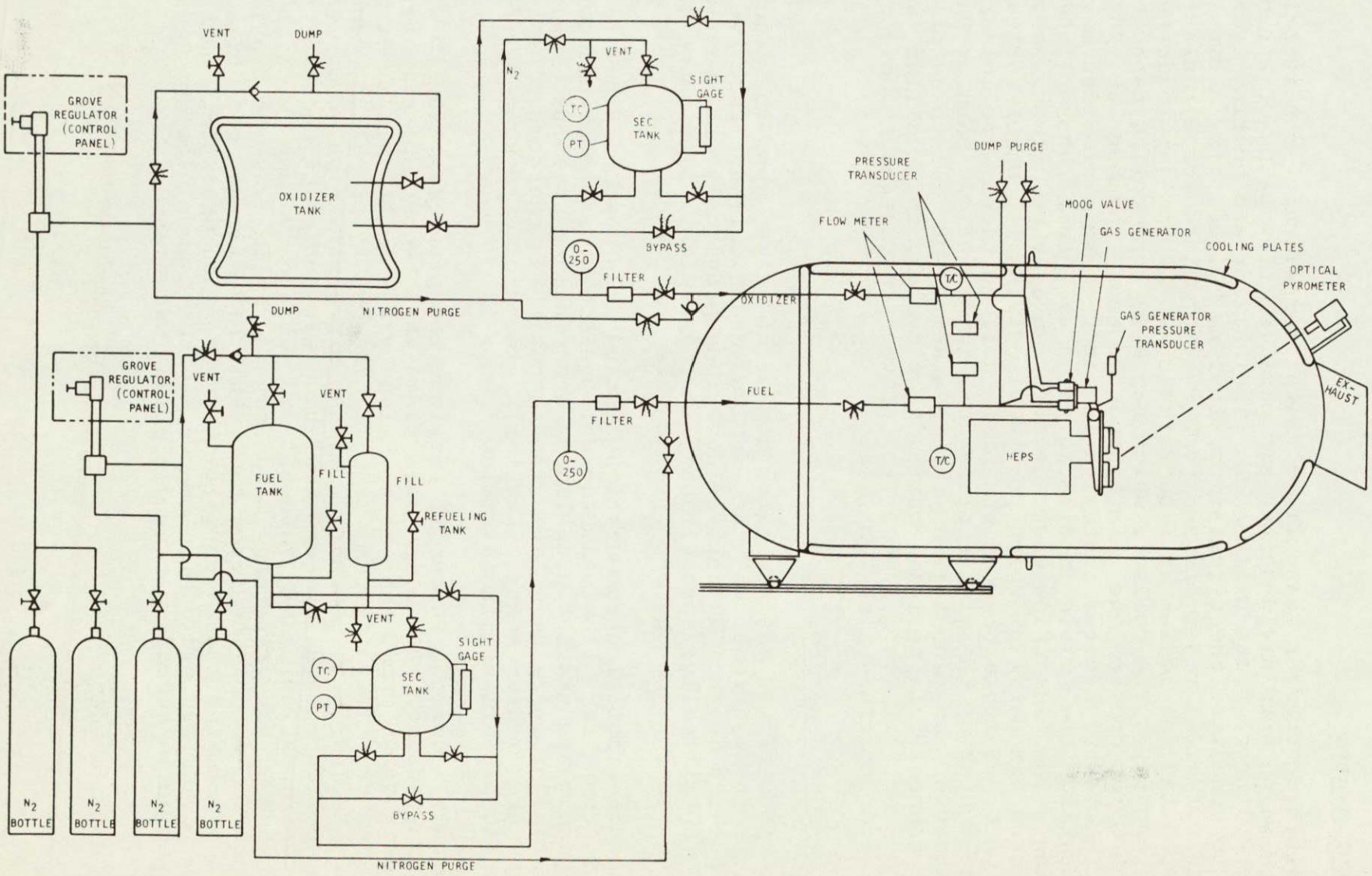


FIGURE 8.1-3 HEPS PROPELLANT FEED SYSTEM

Chiller System

The altitude chamber was lined with temperature conditioning plates which were divided into six parallel flow paths of approximately three plate coils each. The chiller and heating system used to condition the circulating ethylene glycol is shown in Figure 8.1-4. A reservoir and pump were provided for circulating the conditioning medium at flow rates up to 60 gpm (approximately 10 gpm/path). The chiller, which had a 10 ton cooling capacity, was used for cooling and maintaining the test chamber at 20°F. A 24 KW electric heater installed in the reservoir provided means of heating the fluid medium for high wall temperature (160°F) testing. The fluid flow was regulated manually by globe valves connected in parallel which provided individual control for each flow path. Temperatures of the plate coil surfaces were measured at the center of the middle plate coil in each flow path. This temperature was considered representative of all three plate coils connected in series. During heat cycles, the chiller was valved out of the system to prevent overpressure of the evaporator portion of the chiller.

8.2 DVR Gas Generator Test

The purpose of the gas generator component test was to demonstrate the effect of the design modifications that were incorporated in the DVR unit as described previously in Section 4.1. Specifically, propellant line dynamics, flow, thermal characteristics and chamber spiking were evaluated.

The gas generator instrumentation included: Flowcon flowmeters (0-2.5 gpm) for flow measurement; Dynisco pressure transducers for dynamic and static propellant and chamber pressure measurement; chromel/alumel and iron/constantan thermocouples for temperature measurement; Kistler pressure transducer for measuring propellant line dynamics.

Previously, during Phase II testing, the propellant supply was pressure-fed from 100 gallon main tanks that were approximately 40 feet away from the bipropellant valve inlet. In order to simulate the LM feed system, 12 gallon secondary propellant tanks were installed 18 feet upstream of the bipropellant valves. The LM propellant feed system simulation was not exact because the tank configuration, tank volume, and ullage volume were not duplicated. However, the main consideration was to provide pressure-fed propellants from tanks that had a large gas ullage and approximated the LM propellant system line distance. During system dynamics evaluation tests, water-hammer effect was observed while secondary tank gas ullage was varied.

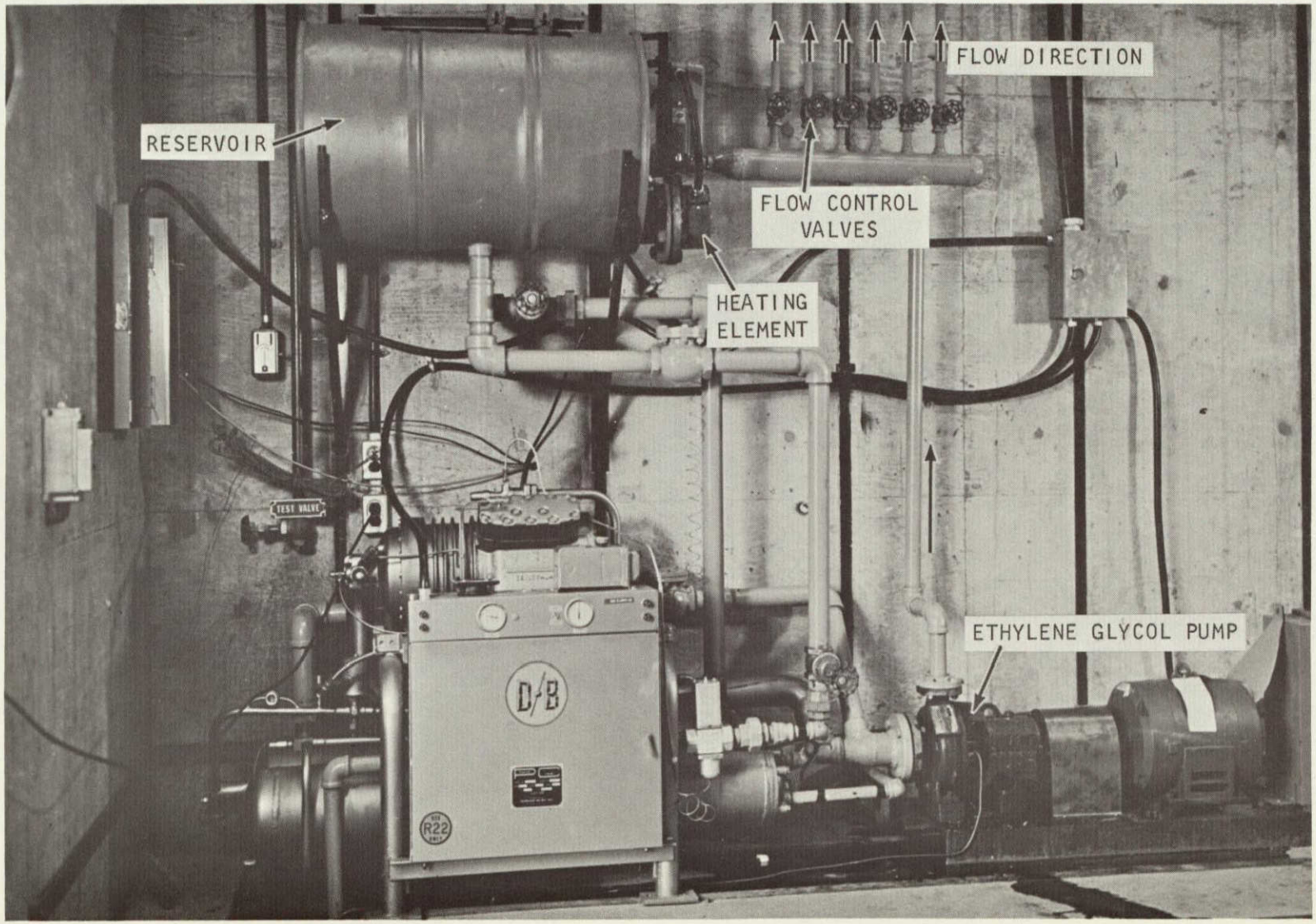


FIGURE 8.1-4 CHILLER-HEATER SYSTEM

In Table 8.2-1, chamber pressure, O/F ratios, flow rates and orifice diameters are presented. Tests 001 through 013 were conducted with no ullage volume in the secondary tank. During tests 014 through 027, the secondary tanks were pressurizecd to 100 psig with nitrogen prior to liquid propellant pressurization. This was done in order to evaluate the system response with increased ullage volume.

After Test 013 it was suspected that the valve and inlet manifold subassembly of the gas generator contributed an excessive pressure drop during hot gas testing and thus limited the maximum flow capability. The unit was returned to Cleveland for further testing utilizing water as a fluid. The results of these tests are shown in Figures 8.2-1 and 8.2-2. Shown in Figure 8.2-1 is the flow vs. pressure drop data that resulted when only the valve assembly and inlet manifold lines were used. The pressure drops on the high O/F oxidizer side and low O/F fuel side were not excessive as expected. Additional water flow testing was conducted with the entire gas generator assembly. These data are presented in Figure 8.2-2. The pressure drop across the gas generator assembly at the critical flow conditions are as follows:

0.9 O/F Fuel -- 98 psi

2.0 O/F Oxidizer -- 82 psi

The water flow data was density corrected to correspond to the density of N_2O_4 and Aerozine-50. Because the results of these tests showed no excessive flow restrictions in the gas generator assembly, the propellant feed system was suspected. The test data revealed that the system response was too slow after pulse initiation. The inlet pressure traces showed that the pressure level immediately dropped 40 psi when the valve was opened and remained at this level for approximately 150 milliseconds at which time it slowly increased. This problem was eliminated by prepressurizing the secondary tanks with nitrogen.

During DVR system testing, the ullage volume was controlled by adjusting the nitrogen gas volume which was observed in liquid-level sight glasses. An ullage volume of 75% yielded the fastest responding system. After 20 milliseconds, 100% line pressure recovery was achieved. A more efficient pulse resulted as was indicated by the rise and decay time of the chamber pressure.

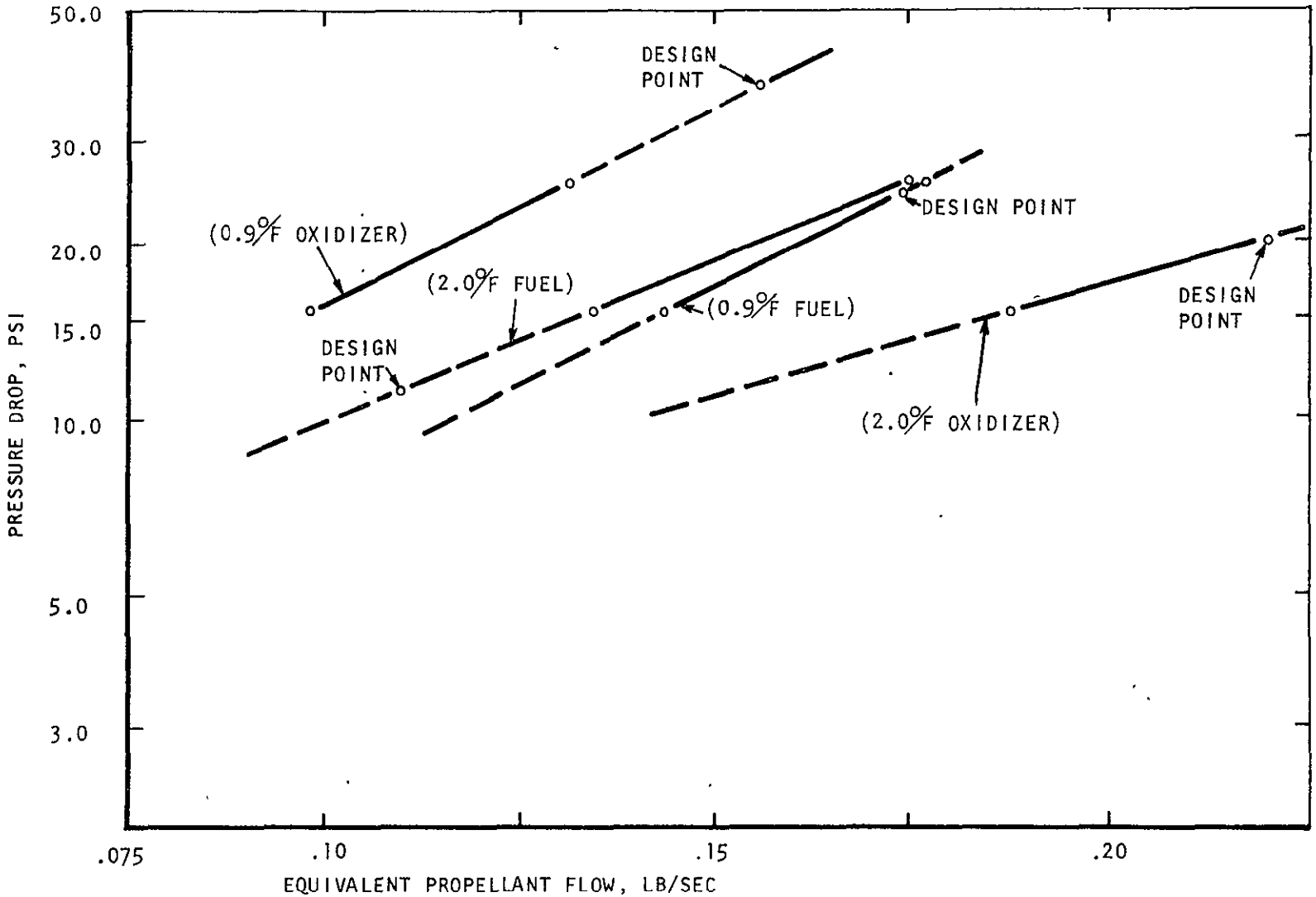


FIGURE 8.2-1 PRESSURE DROP VERSUS FLOW (FOR VALVE ASSEMBLY AND INLET MANIFOLDS)
(T_{water}= 76°F)

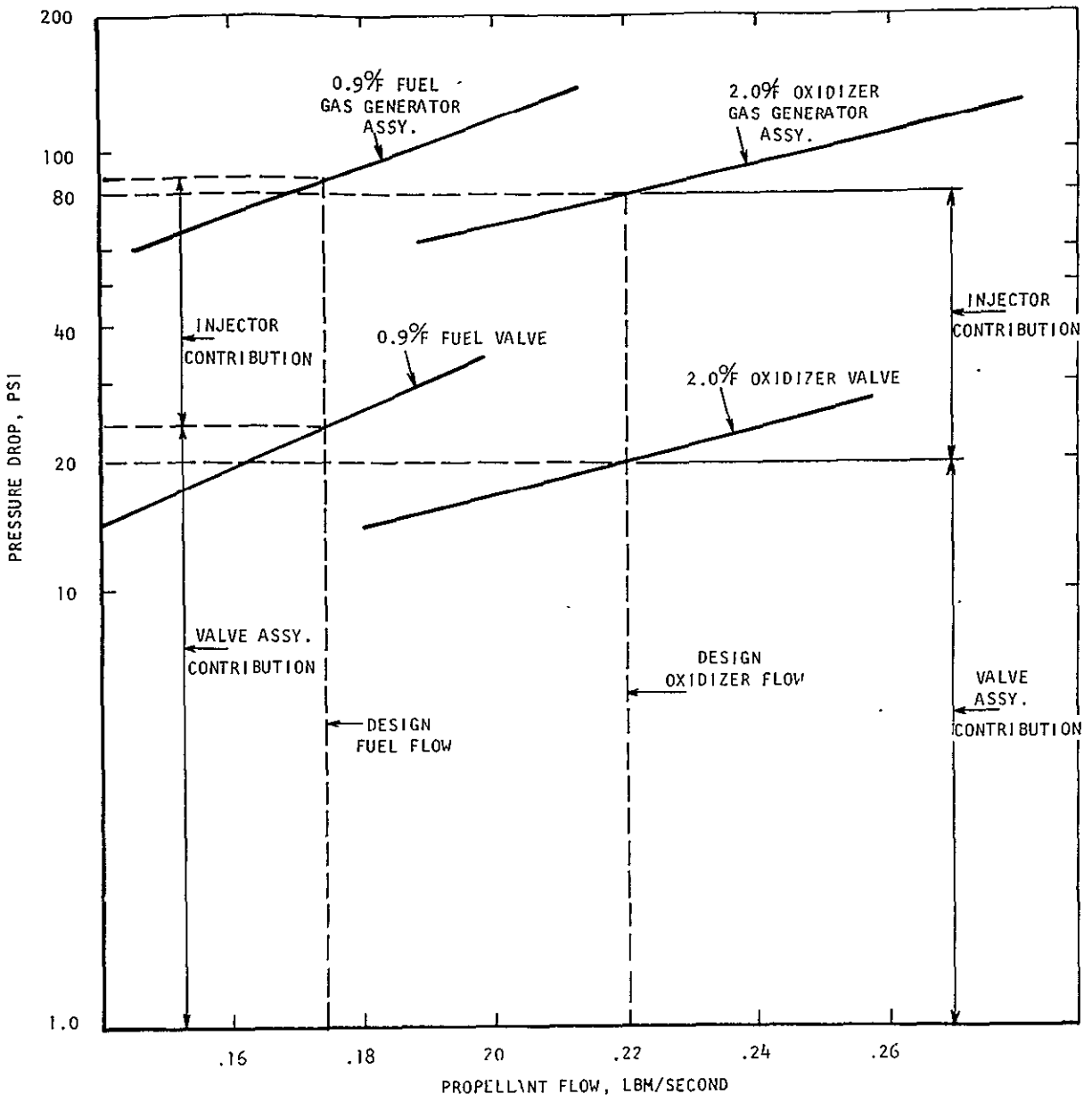


FIGURE 8.2-2 PRESSURE DROP VERSUS FLOW
(T_{WATER} = 74°F)

TABLE 8.2-1

DVR GAS GENERATOR TEST DATA SUMMARY

Port A - Low O/F Valve (Oxidizer)
Port B - Low O/F Valve (Fuel)
Port C - High O/F Valve (Oxidizer)
Port D - High O/F Valve (Fuel)

Test	Propellant Flow, lb/sec				Orifice Diameters, inch				Chamber Pressure, psia		O/F Ratio	
	Port A	Port B	Port C	Port D	Port A	Port B	Port C	Port D	Low O/F	High O/F	Low O/F	High O/F
001	.1500	.1710	.2210	.1015	.0730	.2010	.2210	.0700	115	125	.878	2.080
002	.1500	.1670	.2210	.1085	.0730	.2010	.2210	.0700	111	125	.898	1.945
003	--	.1020	.2050	.1136	.0470	.2210	.1610	.0820	130	113	--	1.805
004	.1530	.1470	.2200	.077	.0890	.1610	.1360	.1470	89	90	1.04	2.860
005	.1645	.1505	.1800	.1270	.1360	.1405	.0890	.1285	103	107	1.09	1.420
006	.1620	.1575	--	.1220	.1060	.2340	.0730	.0890	103	99	1.03	--
007 (200) psig	.1620	.1540	--	--	.1060	.2340	.0730	.0890	127	103	1.05	--
007 (215) psig	.1645	.1605	--	--	.1060	.2340	.0730	.0890	103	--	1.03	--
008	.1440	.1625	.2025	.1195	.0700	*	*	.1060	96	123	.886	1.700
009	.1420	.1550	.2025	.1170	.0700	*	*	.1060	88	114	.930	1.730
010 (200) psig	.1660	.1450	.2080	.1060	.1610	.2210	.2340	.0730	101	110	1.145	1.930
010 (230) psig	.1800	.1605	.2225	.1145	.1610	.2210	.2340	.0730	111	122	1.120	1.945
011	.1530	.1435	.2080	.1075	.0890	*	.2340	.0730	97	103	1.065	1.945
012	.1620	.1440	.2250	.0750	.1360	.1610	.2210	.0470	95	85	1.125	3.00
013	.1400	.1510	--	--	.0700	.2010	.2210	.0730	87	--	.927	--

*No Orifice

TABLE 8.2-1

DVR GAS GENERATOR TEST DATA SUMMARY (Continued)

Test	Propellant Flow, lb/sec				Orifice Diameters, inch				Chamber Pressure, psia		0/F Ratio	
	Port A	Port B	Port C	Port D	Port A	Port B	Port C	Port D	Low 0/F	High 0/F	Low 0/F	High 0/F
014	.1515	.1715	.2380	.1110	.0730	.1610	*	.0760	99.5	123	.883	2.145
015	.1515	.1695	.2355	.1110	.0890	.1610	*	.0760	98	117	.895	2.120
016	.1515	.1675	.2355	.1110	.0890	.1610	*	.0760	93	117	.905	2.120
017	.1580	.1695	--	--	.0890	.1610	*	.0760	101	--	.932	--
018	.1515	.1730	.2310	.1145	.0890	.1610	*	.0760	97	126	.876	2.02
019	.1515	.1710	.2330	.1110	.0890	.1610	*	.0760	97	122	.886	2.10
020	.1505	.1750	.2303	.1120	.0730	.1610	*	.0760	97	123	.86	2.06
021	.1669	.1580	.2344	.1100	.0890	.1405	.1610	.0760	--	--	1.055	2.13
022	.1387	.1740	.2296	.1120	.0820	.1610	.1405	.1760	--	--	.796	2.05
023	.1400	.1740	.2250	.1120	.0820	.1610	.1405	.0760	--	--	.805	2.01
024	.1495	.1695	.2272	.1140	.0860	.1610	.1405	.0760	--	--	.822	1.995
025	.1506	.1525	.2180	.1055	.0860	.1610	.1405	.0760	--	--	.987	2.077
026	.1605	.1760	.2338	.1120	.0860	.1610	.1405	.0760	--	--	.913	2.090
027	--	--	.2260	.1105	.0860	.1610	.1405	.0760	--	--	--	2.050

*No Orifice

Numerous instrumentation malfunctions resulted from the longer high temperature tests. The turbine-type flowmeters had bearing failures. The probable cause of the bearing failures was overspeeding during purging. The water-cooled chamber pressure transducer failed because of overheating. The strain-gage element pressure transducers used in the propellant lines were subjected to 250°F temperatures which resulted in a thermal calibration shift. A Kistler pressure transducer (Model 606) was used to measure pressure surges resulting from valve closure. The largest pressure pulse observed was 200 psia. This evaluation led to the conclusion that sufficient overpressure to damage the valve flexure tubes did not exist. During system testing, 40 inch flexible metal hoses were installed upstream of the bipropellant valves. The flex hoses provided propellants to the deployed unit and also dissipated the shock energy generated by the valve closure.

Test 013 was a temperature stabilization test during which time the gas generator was pulsed at a frequency of 0.200 seconds on and 8.8 seconds off utilizing the low O/F valve. The data presented in Figure 8.2-3 shows that, after 76 minutes of operation, the metal temperatures were stabilized. At that time, the unit was shut off and allowed to cool at a simulated altitude of 1.3 mm Hg. This simulated the worst condition for the soakback effect. The injector temperature reached a maximum of 230°F five minutes after shutdown. Test 027 temperature data is shown in Figure 8.2-4. This test was also a temperature stabilization test but was conducted with the high O/F valve. The pulsing frequency was 0.200 seconds on and 8.8 seconds off. The metal temperatures were stabilized after 60 minutes of operation. The injector temperature reached a maximum value of 222°F ten minutes after shutdown. These tests indicated that adequate thermal control was provided for the gas generator during the most severe mode of thermal soakback.

During the gas generator test program, the only failure that occurred was a bipropellant valve flexure tube. The failure was observed at the end of Test 027. After examination, it was concluded that the flexure tube, which had 0.003-inch wall thickness, failed due to a superimposed torsional stress on a bending stress. The torsional stress occurred because the fuel and oxidizer flexure tubes were of different diameters. These flexure tubes are an integral part of a common armature which imparts the opening and closing valve movement to the flexure tubes resulting in repeated bending. The estimated life of the valve was 75,000 cycles minimum. A forty times size of the failed tube section is shown in Figure 8.2-5. As a result of the failure, the following design changes were incorporated:

1. Soft poppet replacing a soft seat.

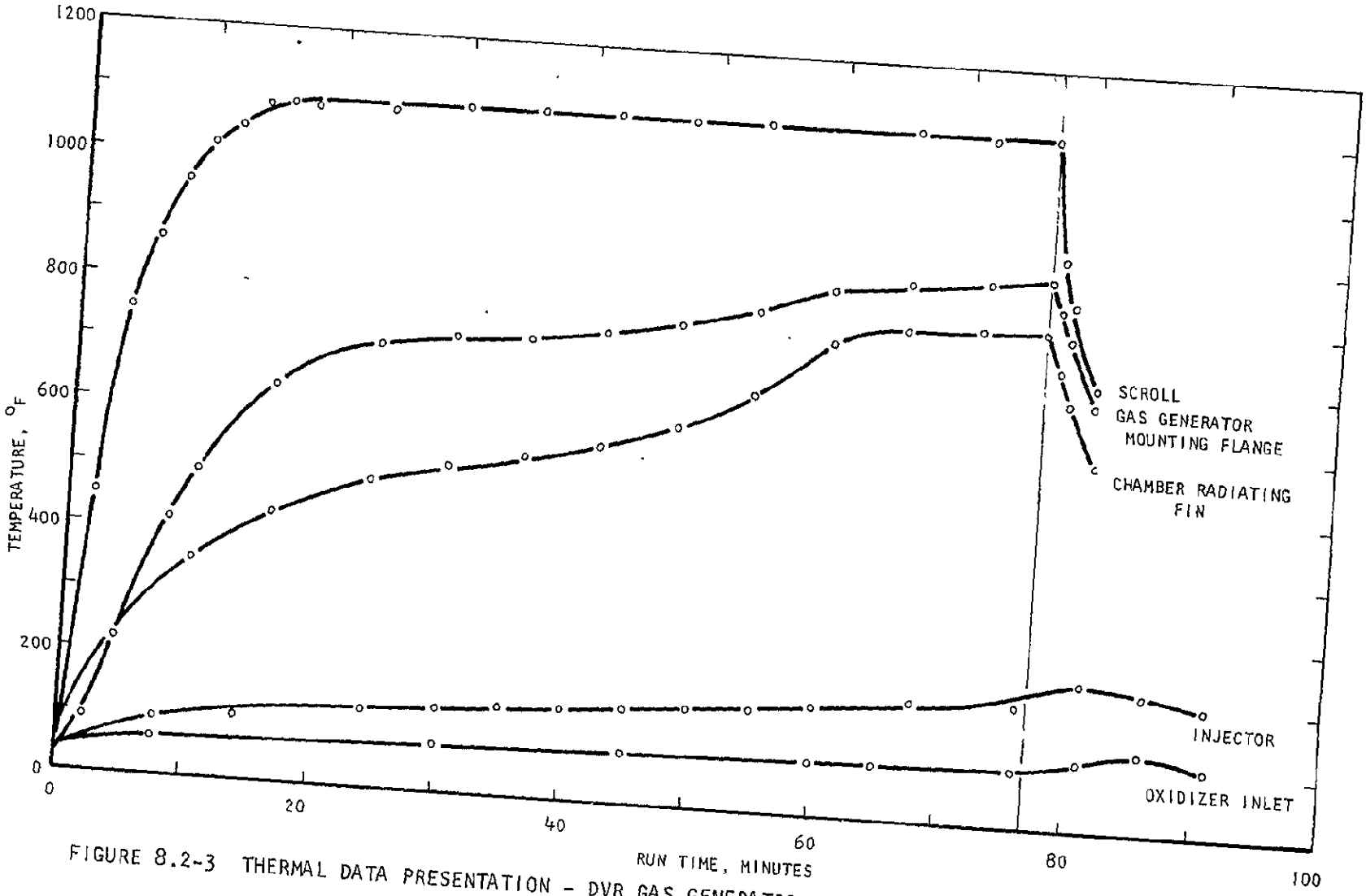


FIGURE 8.2-3 THERMAL DATA PRESENTATION - DVR GAS GENERATOR COMPONENT TESTS (TEST 013) - JAN. 1969

PULSE FREQUENCY: 200MS ON/8.8 SECONDS OFF
0.9 O/F
0.4mm Hg ALTITUDE

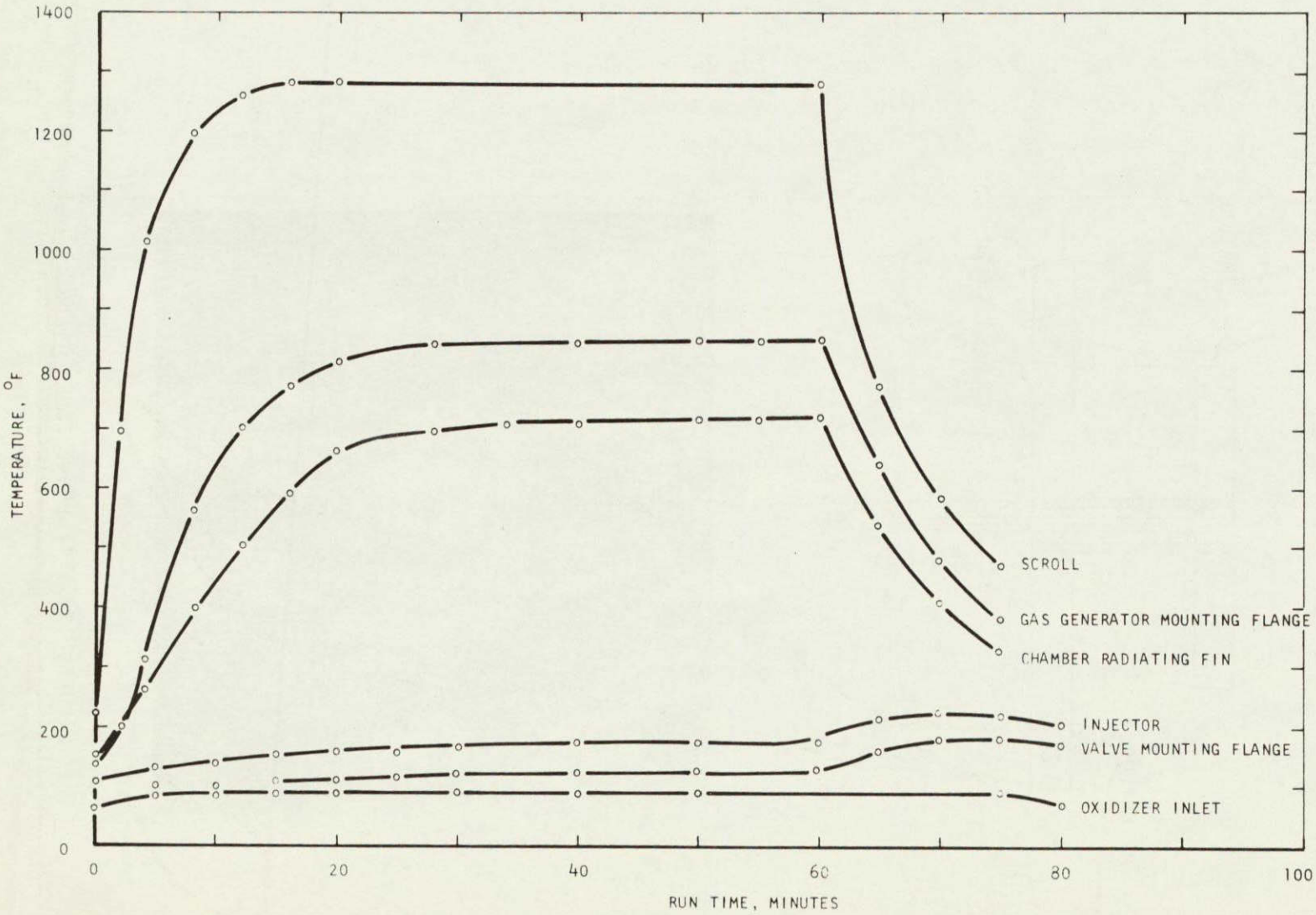
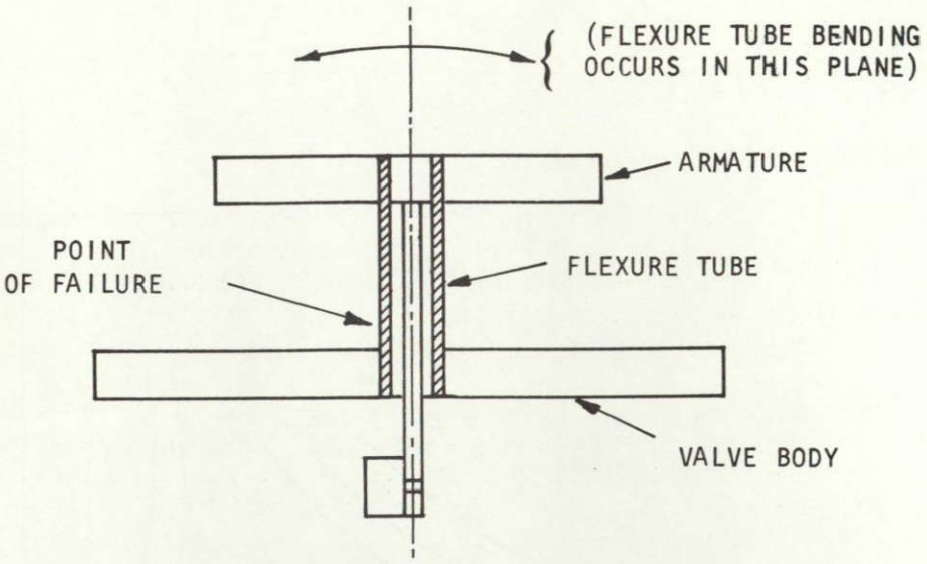


FIGURE 8.2-4 THERMAL DATA PRESENTATION - DVR GAS GENERATOR COMPONENT TESTS (TEST 027) - JANUARY 1969

PULSE FREQUENCY: 200MS ON/8.8 SECONDS OFF
2.0 O/F
0.4mm Hg ALTITUDE



PARTIAL VALVE SCHEMATIC

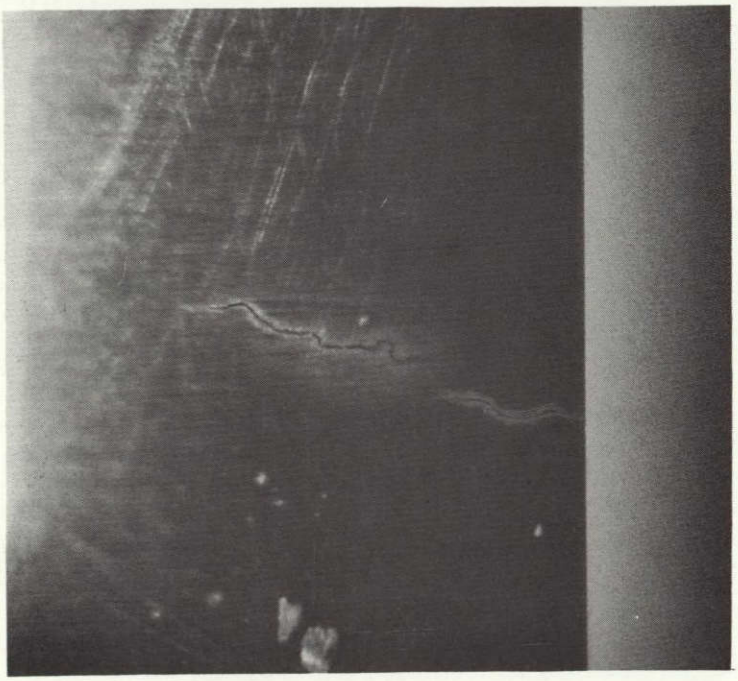


FIGURE 8.2-5 FLEXURE TUBE FAILURE

2. Equal diameter flexure tubes.

3. Equal diameter seats.

8.3 Lubrication System Tests

Lubrication System Development Test

A simulated HEPS lubrication test system was constructed and instrumented so that an oil inventory evaluation could be made for the design under consideration. In addition, the simulated test rig was used for developing the vapor phase separator at TRW Systems. The instrumented test rig is shown in Figure 8.3-1.

The particular supply and scavenge pump used on the test rig was the Phase II shaft driven pump; however, the pump was driven by a Westinghouse 1/3 HP motor at 2900 rpm. A 12-foot copper tube, .5716 inch O.D. was placed downstream of the supply pump to simulate the lube system radiator. A bypass relief valve was inserted between the radiator discharge and the turboalternator oil supply inlet. The bypass flow from the relief valve was returned to the separator. Downstream of the bypass relief valve, the flow split into three components: roller bearing supply, ball bearing supply, and alternator cavity supply. A 27 in^3 plexiglas chamber was used to simulate the gearbox and roller bearing volume in the turboalternator. The roller bearing cavity was fed through two .025-inch diameter orifices which simulated the turboalternator oil jets. The ball bearing supply was fed through two .025-inch diameter orifices into a 4.5-in^3 plexiglas volume. An alternator housing was utilized for system simulation of the alternator cooling jacket. The alternator cooling jacket flow was discharged into the gearbox cavity. Both bearing cavities were then connected to the scavenge pump for return to the oil supply tank. The vapor separator was simulated with a one gallon plexiglas container that was sealed. A vent valve was inserted into this tank to simulate the pressure control on the phase separator.

Tests were conducted with three different fluids simulating the MIL-L-23699 oil viscosity at 20°F, 77°F and 400°F oil temperature. High oil radiator pressure drops at the low temperature condition occurred with .250 inch O.D. tube size. This pressure drop was reduced from 190 psi to 56 psi with .3125 inch O.D. tubing. At 400°F the radiator pressure drop was 21 psi with the .250 inch O.D. tubing.

Tests to determine lube system flow and flow distributions were conducted with .035 inch and .025 inch jets in the bearing feed lines. An oil relief valve was developed to relieve oil system

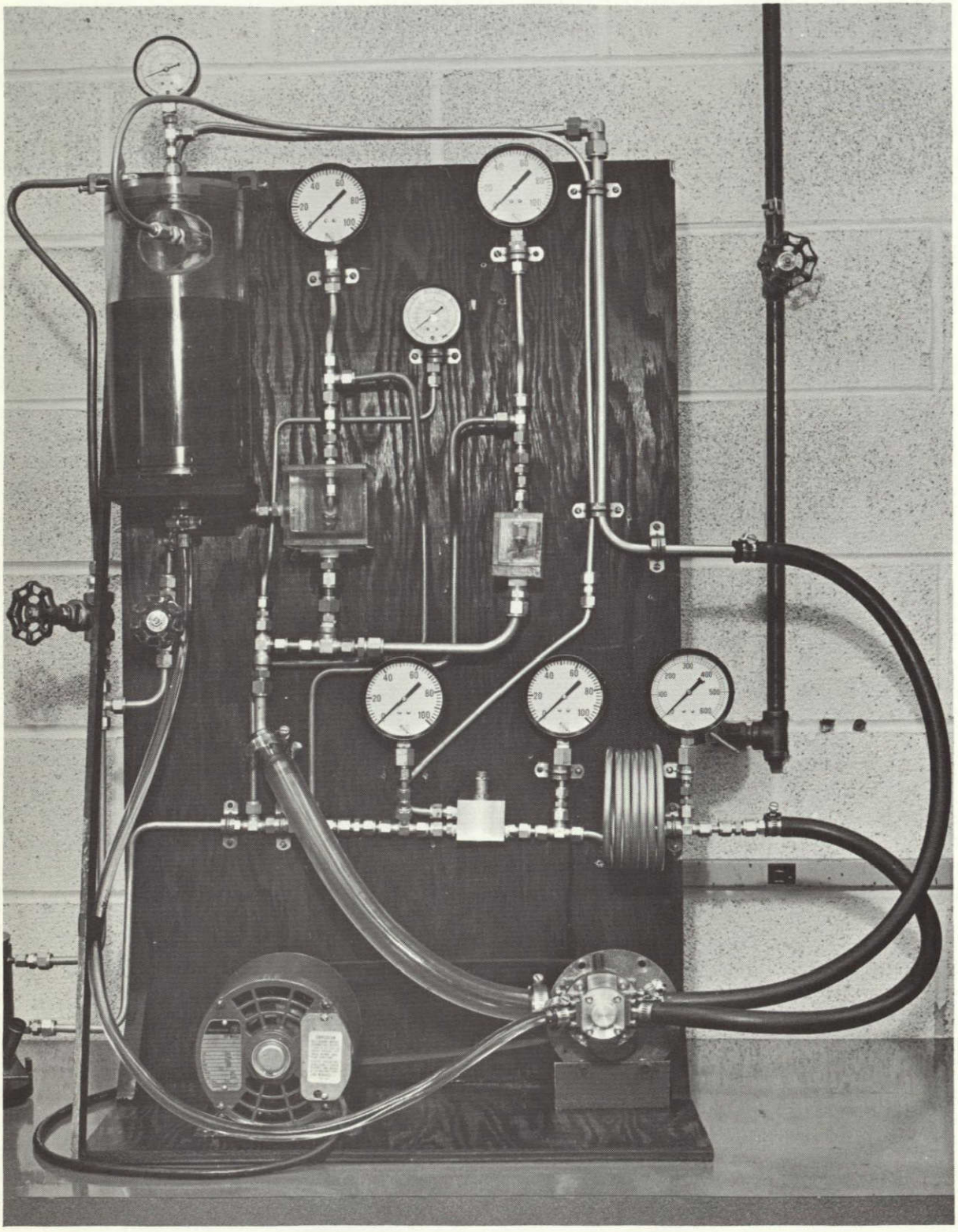


FIGURE 8.3-1 HEPS LUBRICATION SYSTEM SIMULATION

pressure during the cold start condition. This valve was installed downstream of the oil radiator.

These tests established the basic radiator tube and orifice jet sizes.

Alternator Mechanical Loss Tests

Summary

The tests conducted on the HEPS alternator during Phase II showed very high friction and windage losses. The losses measured during tests varied from 1050 to 1500 watts. To investigate these losses, a number of tests were conducted on a HEPS alternator previously used in Phase II tests. Before modifications of the alternator, the mechanical losses at rated shaft speed were 1290 watts.

During these tests the following modifications were made:

1. Additional outlet was provided to eliminate accumul lation of oil in alternator cavity.

2. The size of orifices for oil jets was reduced.

3. The oil jets flow pattern was changed to reduce oil flow through the bearings.

4. New shaft seal (Clevite Co.) was used.

The mechanical losses after the alternator modifications were reduced to 570 watts at 140-180°F oil temperature and to 390 watts at 370°F oil as shown in Figure 8.3-2. To evaluate shaft seal and bearing performance at actual operating temperatures, high temperature tests were conducted. Test results are summarized in Figure 8.3-4. No visual changes were observed in the shaft seal and bearings after high temperature tests. All parts were in excellent condition.

Test Configuration

A 30 KVA alternator driven by a variable speed DC motor was installed in the test cell to provide a variable frequency power source for a dynamometer drive motor. This arrangement provided unit speed regulation between 6000 and 36,000 rpm.

A HEPS alternator used in Phase II testing was mounted on the dynamometer test stand. A lubrication, cooling and scavenge system was integrated into the system. A photograph of the alternator installation is shown in Figure 8.3-3. The schematic

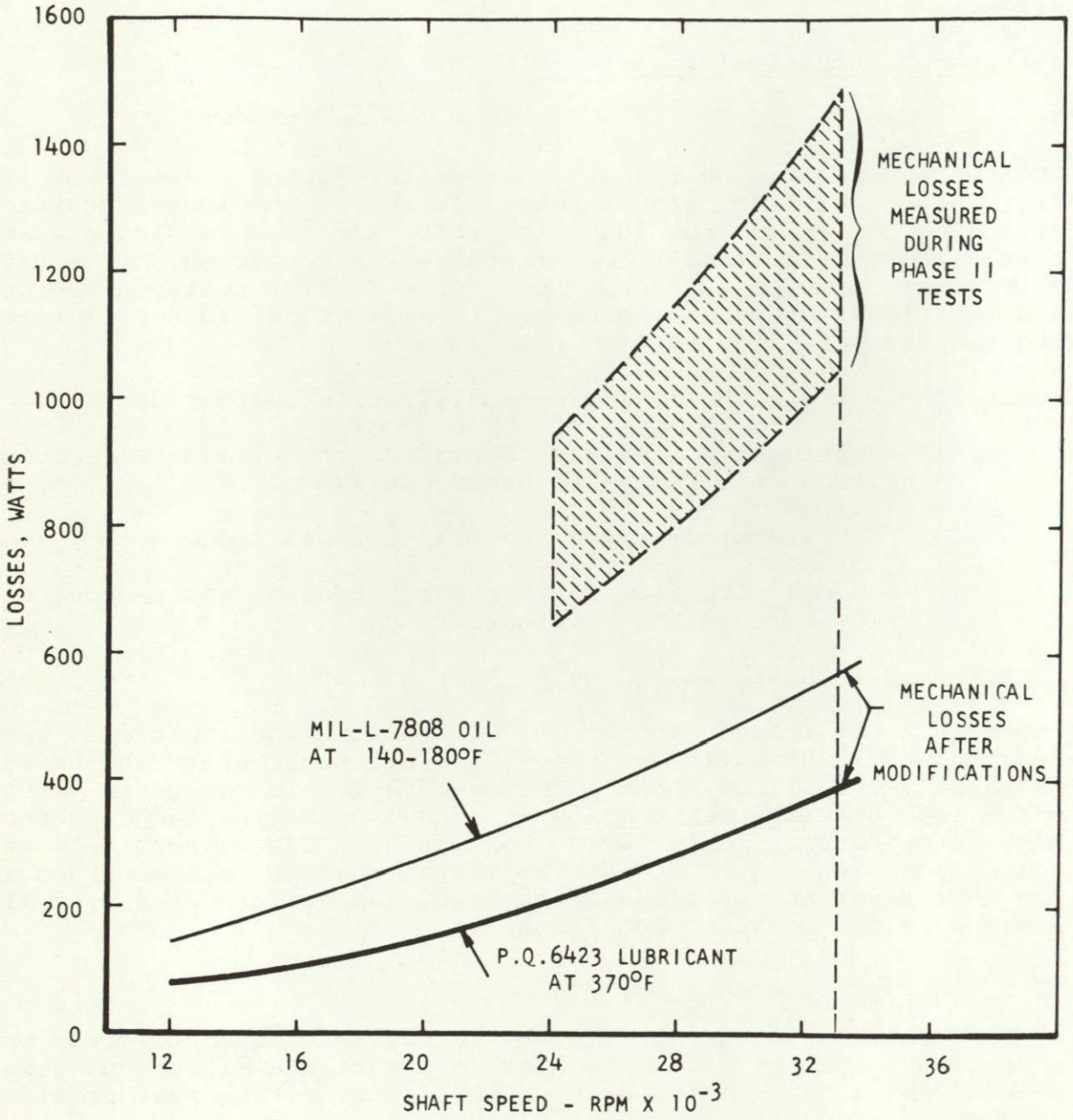


FIGURE 8.3-2 ALTERNATOR MECHANICAL LOSSES VERSUS SHAFT SPEED

20570

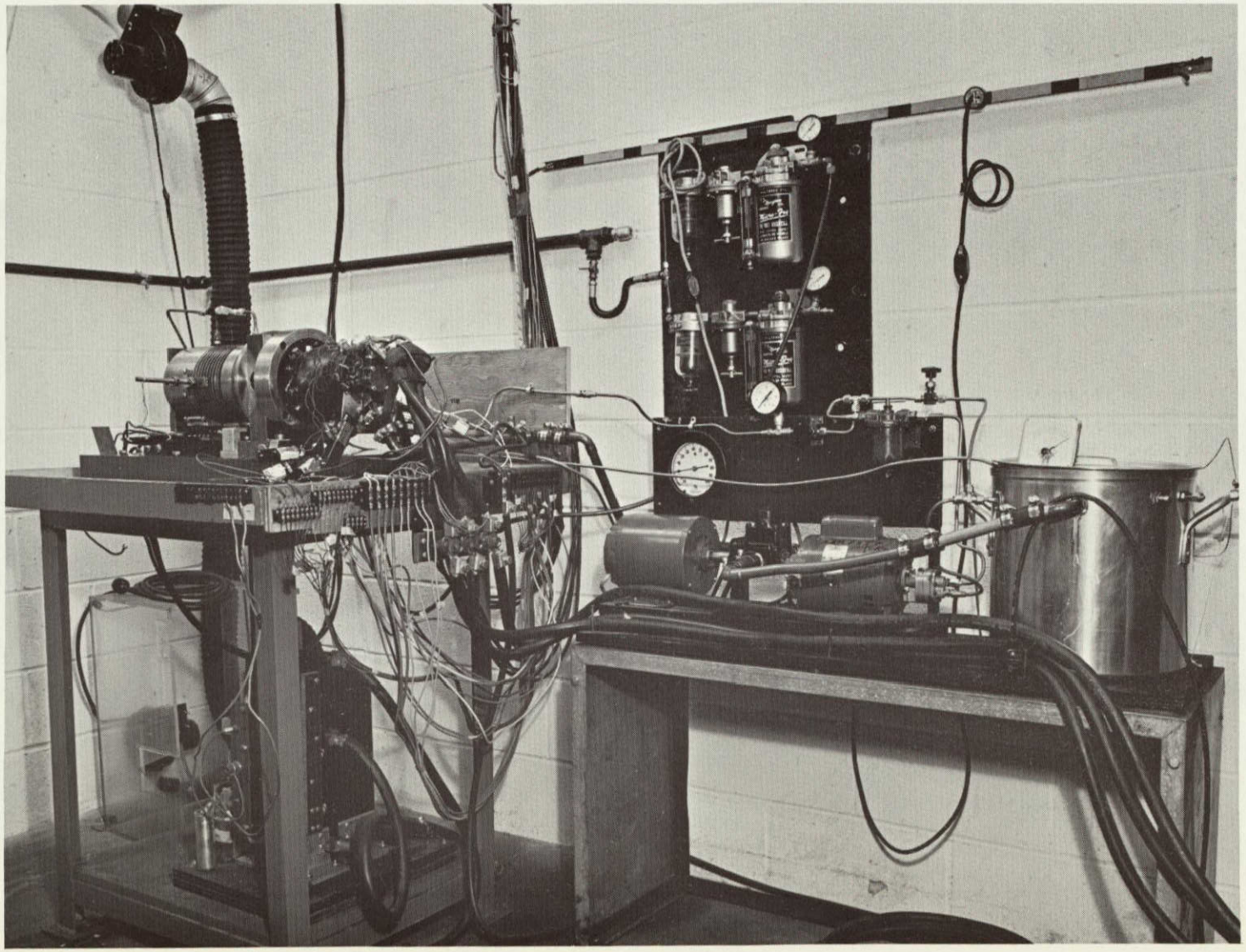


FIGURE 8.3-3 ALTERNATOR/LUBRICATION TEST RIG

REPRODUCIBILITY OF THE
ORIGINAL PAGE IS POOR

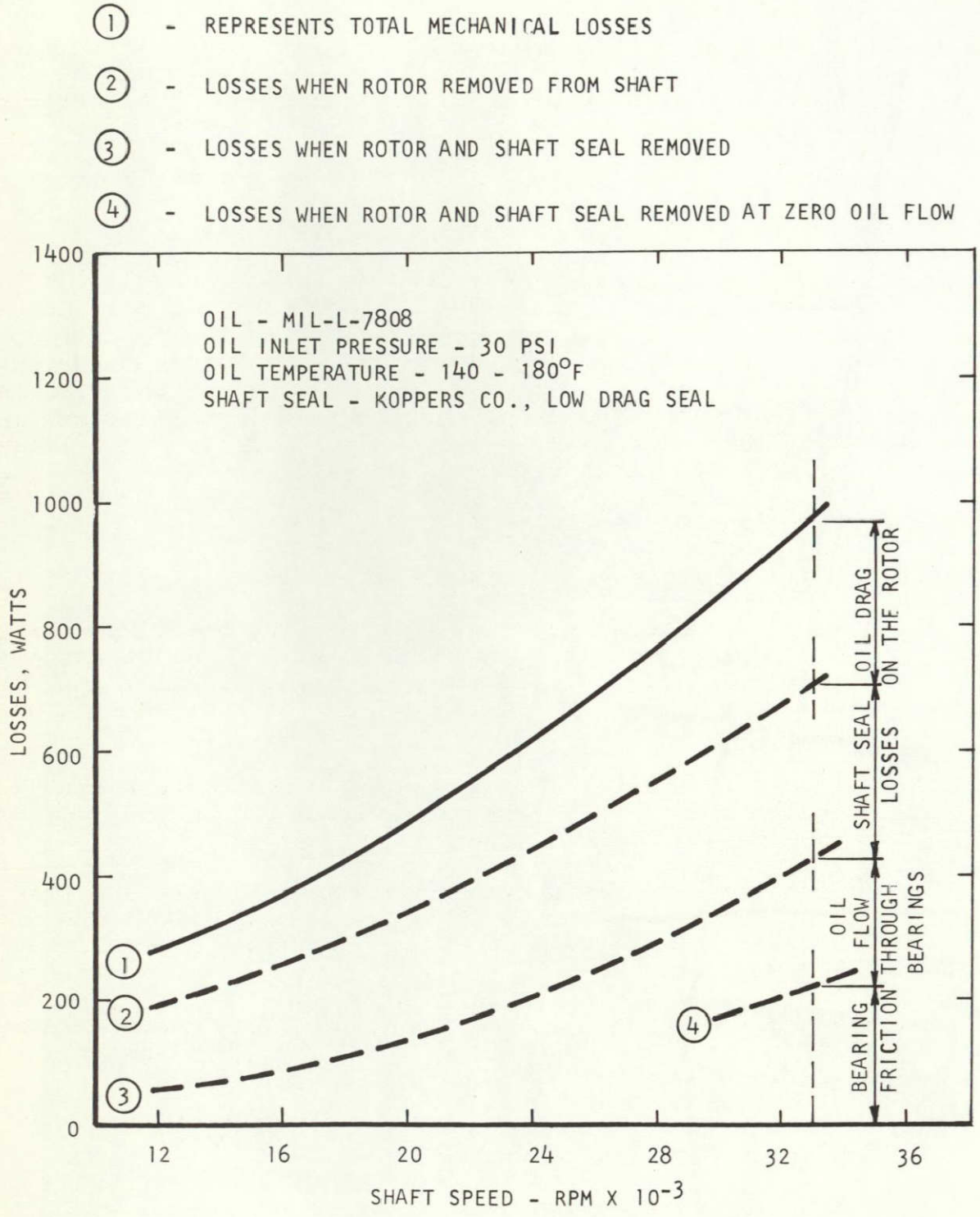


FIGURE 8.3-4 ALTERNATOR COMPONENT LOSSES VERSUS SHAFT SPEED

of the lubrication and cooling system is presented in Figure 8.3-5.

The oil flow through the alternator has three distinct functions:

1. Lubrication and cooling of the turbine end ball bearing and shaft seal.

2. Cooling of the alternator.

3. Lubrication and cooling of the roller bearing.

Alternator Mechanical Losses Before Modification

The alternator was driven without excitation and the input power was measured at shaft speeds from 12,000 to 33,000 rpm. Figure 8.3-6 shows variation of alternator friction and windage losses versus shaft speed. At rated speed the mechanical losses are 1290 watts. The shaded area represents mechanical losses measured during Phase II test runs.

First Modification of the Alternator

The following changes were made in the alternator:

1. An additional outlet was provided within the alternator to eliminate accumulation of oil in the alternator cavity. This eliminated the possibility of the alternator rotor acting as a large journal bearing when submerged in oil as shown in Figure 8.3-7.

2. To reduce oil flow rate through the alternator the orifices of oil jets were reduced from .035 to .025 inches.

3. The force produced on the carbon face by the shaft seal bellows was reduced by inserting shims between the seal housing and the bearing support as shown in Figure 8.3-7.

To separate the mechanical losses, the input power was measured when the alternator was in the following state of assembly:

1. Without the rotor.

2. Without rotor and shaft seal.

3. At zero oil flow when rotor and shaft seal were rem moved. The results of loss separation tests are summarized in Figure 8.3-4.

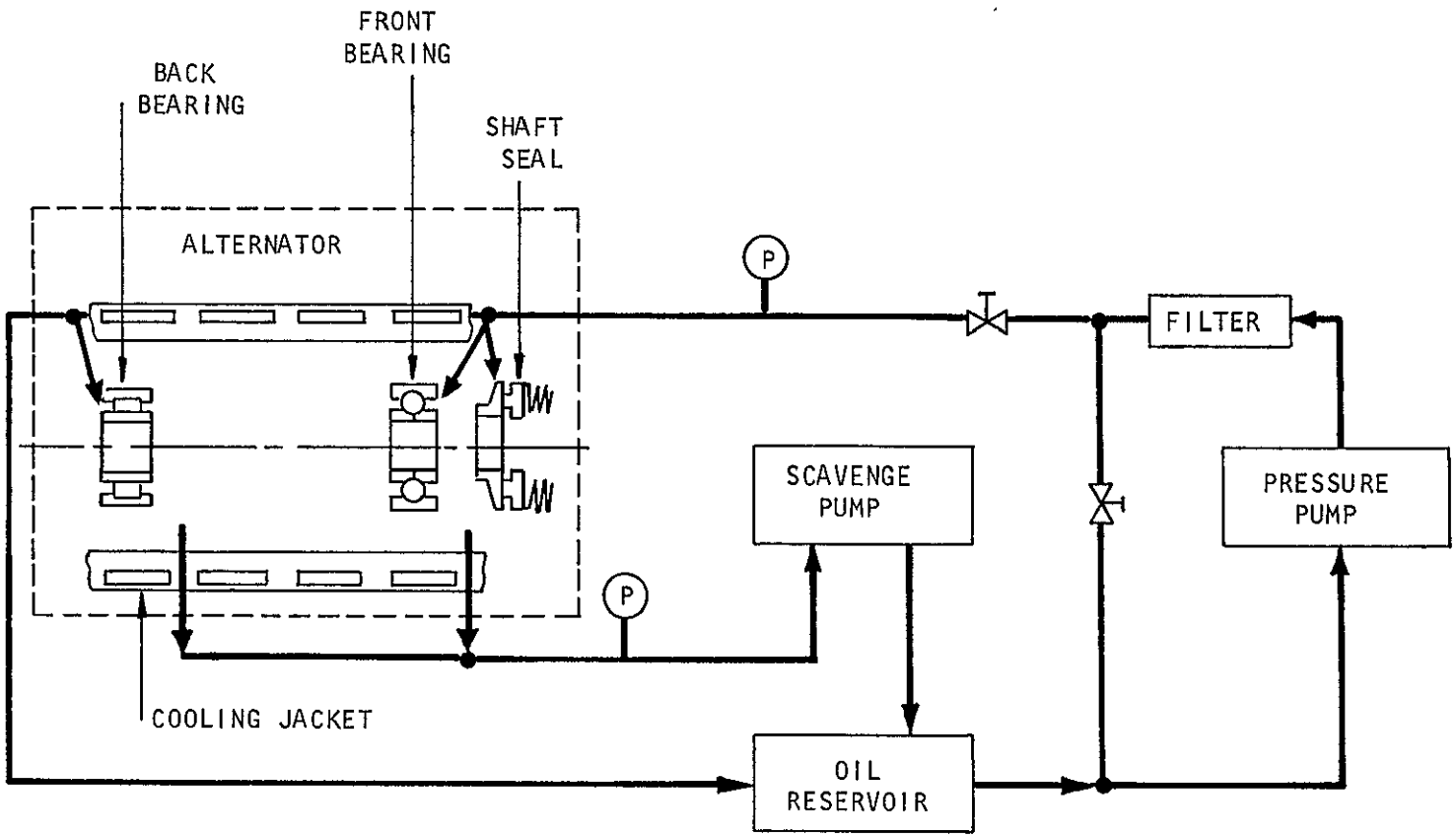


FIGURE 8.3-5 ALTERNATOR LUBRICATION AND COOLING SCHEMATIC

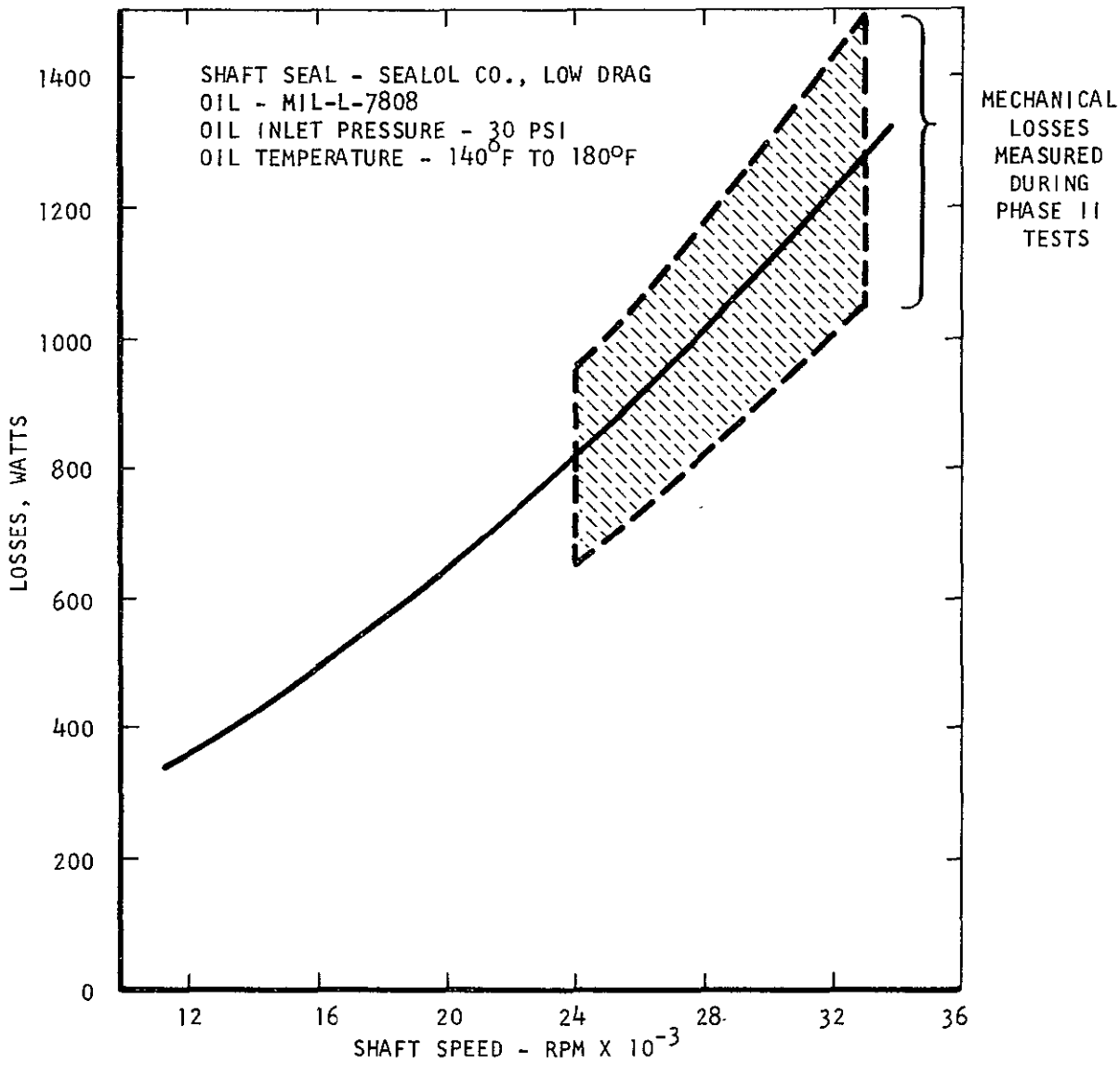


FIGURE 8.3-6 ALTERNATOR MECHANICAL LOSSES VERSUS SHAFT SPEED (FOR PHASE II)

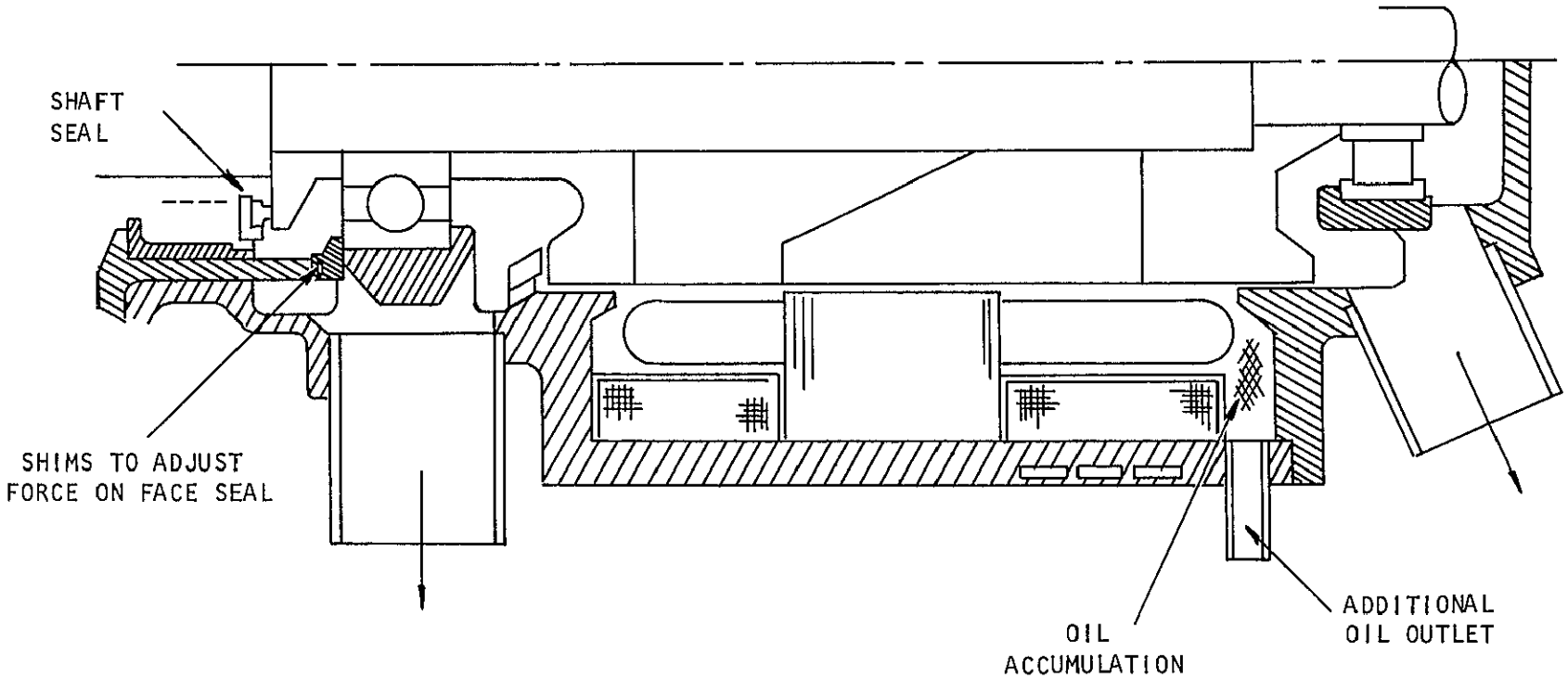


FIGURE 8.3-7 ALTERNATOR COMPONENT TEST CONFIGURATION

At rated shaft speed before modifications, the total mechanical losses consisted of the following:

Bearing Friction Loss	225 watts
Loss Due to Oil Flow Through Bearings	200 watts
Shaft Seal Loss	285 watts
Oil Drag on the Rotor	260 watts
Total	970 watts

Second Modification of the Alternator

After the loss separation tests, the following changes were made in the alternator:

1. The oil jets were arranged as shown in Figure 8.3-8. The oil flow through the bearings was reduced to minimize bearing losses and oil drag on the rotor.

2. A new Clevite Company seal (B-108215) was installed. Minimum diameter of carbon face was used in the new seal. This reduced the contact area and surface velocity of that area. The spring force in the seal was also reduced.

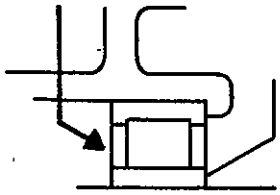
Figure 8.3-9 represents test data after alternator modifications. Test results show lower mechanical losses and at rated shaft speed the losses were:

Bearing Friction Losses	225 watts
Loss Due to Oil Flow Through Bearings	90 watts
Shaft Seal Loss	100 watts
Oil Drag on the Rotor	155 watts
Total	570 watts

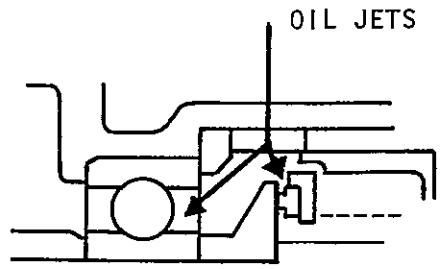
High Temperature Test Runs

High temperature tests were conducted at actual operating conditions to predict alternator shaft seal and bearing performance after modifications. During the tests the alternator mounting flange temperature was maintained between 700 and 750°F. The electrical and magnetic losses in the alternator during these tests were kept to approximately 750 watts to simulate losses

BEFORE MODIFICATION

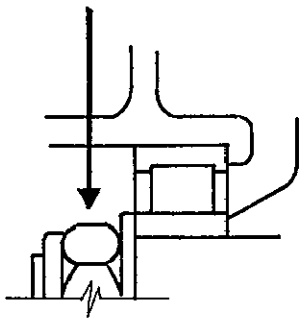


2 - .035 INCH DIA. JETS
. LOCATED 180° APART

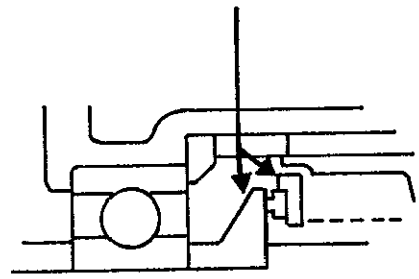


4 - .035 INCH DIA. JETS
LOCATED 180° APART

AFTER MODIFICATION



2 - .025 INCH DIA. JETS
LOCATED 180° APART



4 - .025 INCH DIA. JETS
LOCATED 180° APART

FIGURE 8.3-8 MODIFICATIONS OF ALTERNATOR OIL JETS

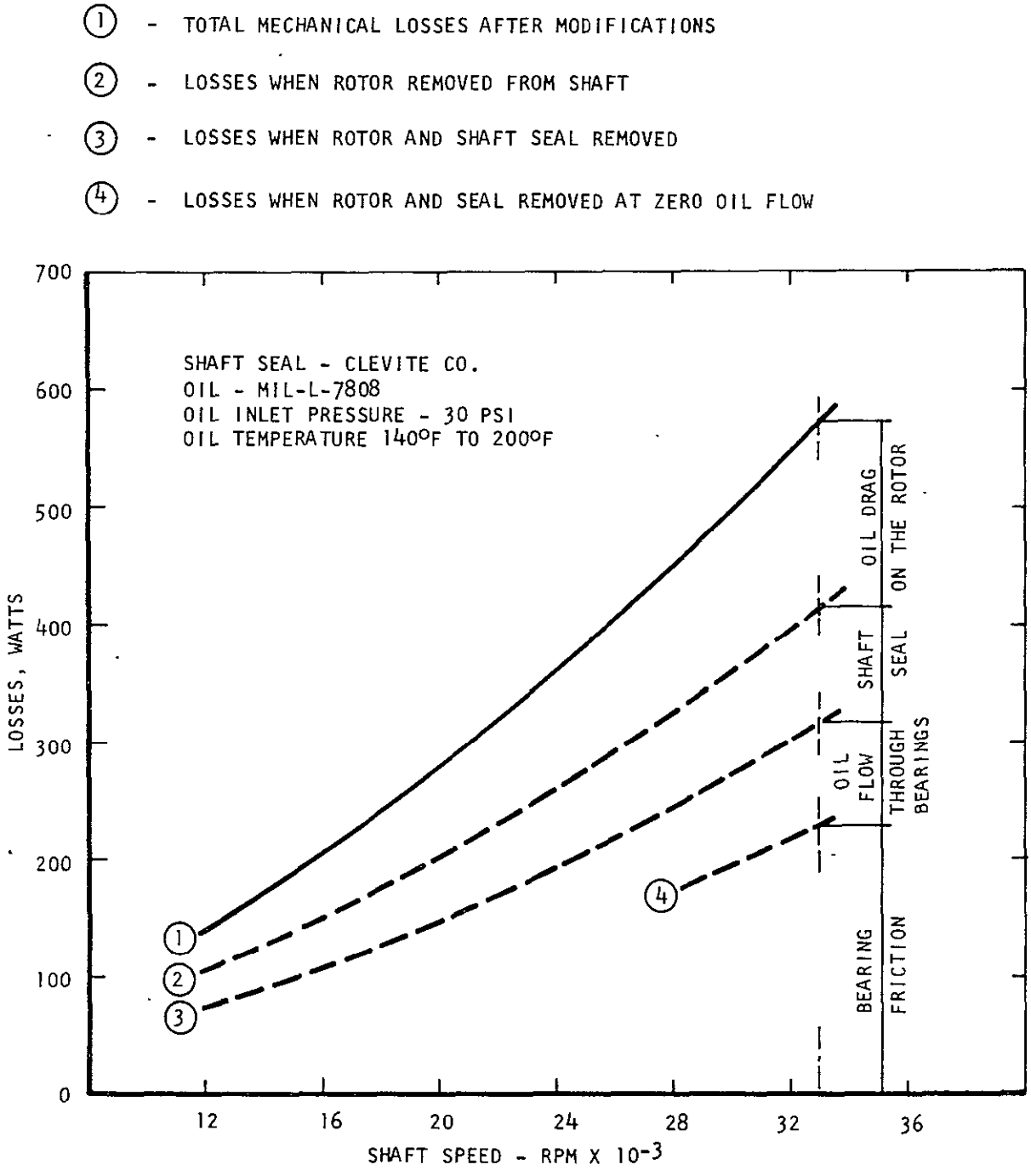


FIGURE 8.3-9 ALTERNATOR MECHANICAL LOSSES VERSUS SHAFT SPEED (AFTER OIL JET ADJUSTMENT)

produced in the alternator at 6 KVA output and rated voltage. To protect the alternator drive motor from overheating, the required alternator losses were produced by operating the alternator over-excited at no load.

The radial and axial magnetic pull on the rotor due to over-excitation was higher when compared to values at rated load.

Thermocouple location and the alternator mounted on the test stand are shown in Figure 8.3-10.

The test data at high temperatures are summarized in Figure 8.3-11.

In Figure 8.3-12, the bearings are shown after the high temperature tests.

In Figure 8.3-13, the shaft seal is shown after the high temperature tests.

In Figure 8.3-14, the alternator components are shown after the high temperature tests.

Additional Lubrication System Bench Tests

After the phase separator was received, an additional test was conducted to evaluate the closed loop oil system and the horse-power losses. Loads up to 6.0 KW were applied during the test which lasted 691 minutes. An average frictional loss of 677 watts was observed. Data analysis indicated the following component losses when tests were conducted with 265°F oil temperature:

Component	Watts
Pump	30
Gears and Bearings	179
Turboshaft	468
Total	677 watts

The temperature characteristics are shown in Figure 8.3-15. The total horsepower loss is considerably less than the Phase II hot gas test results but slightly higher than the induction motor-driven alternator tests described above.

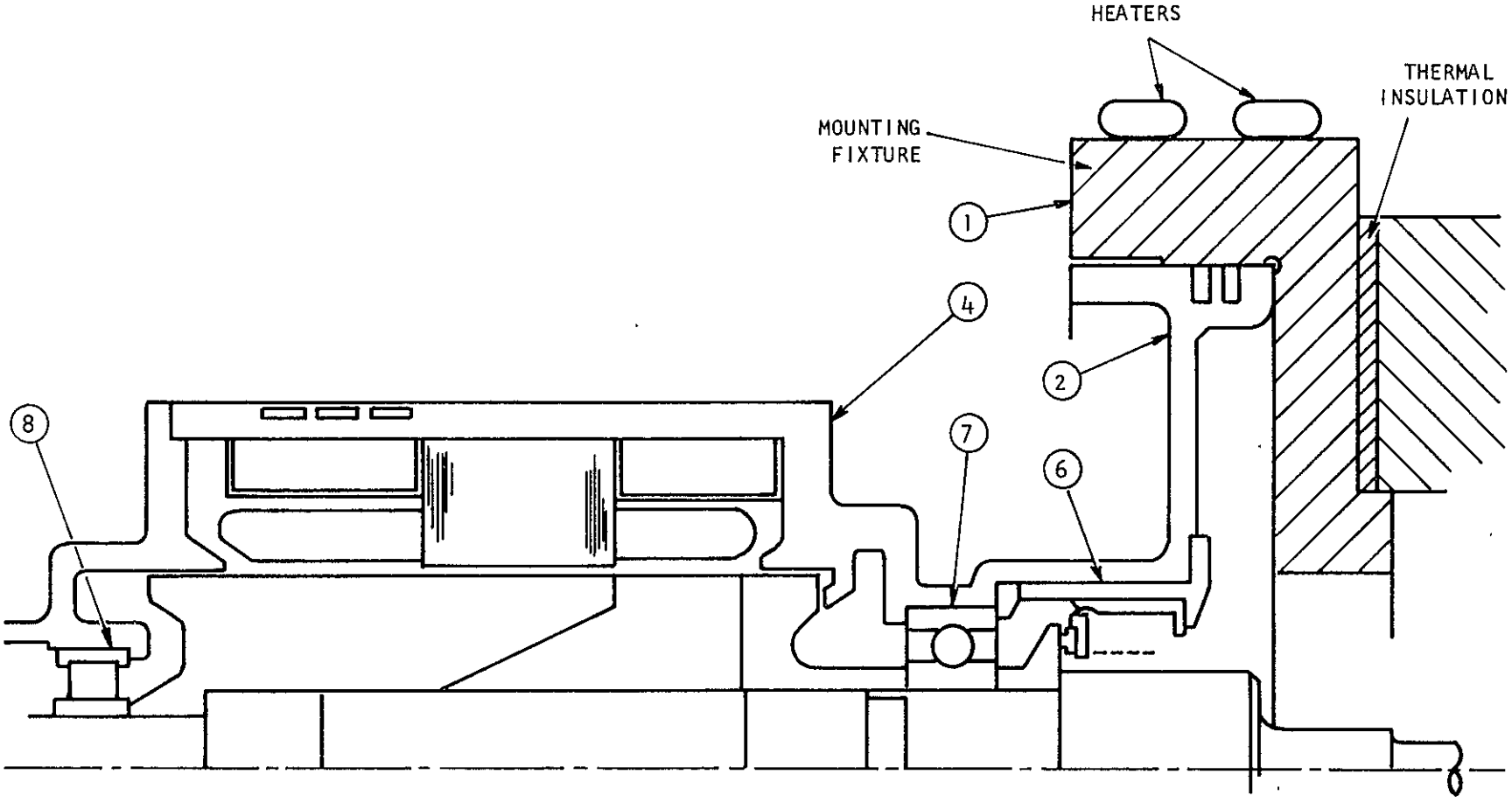


FIGURE 8.3-10 LOCATION OF THERMOCOUPLES FOR THE ALTERNATOR COMPONENT TESTS

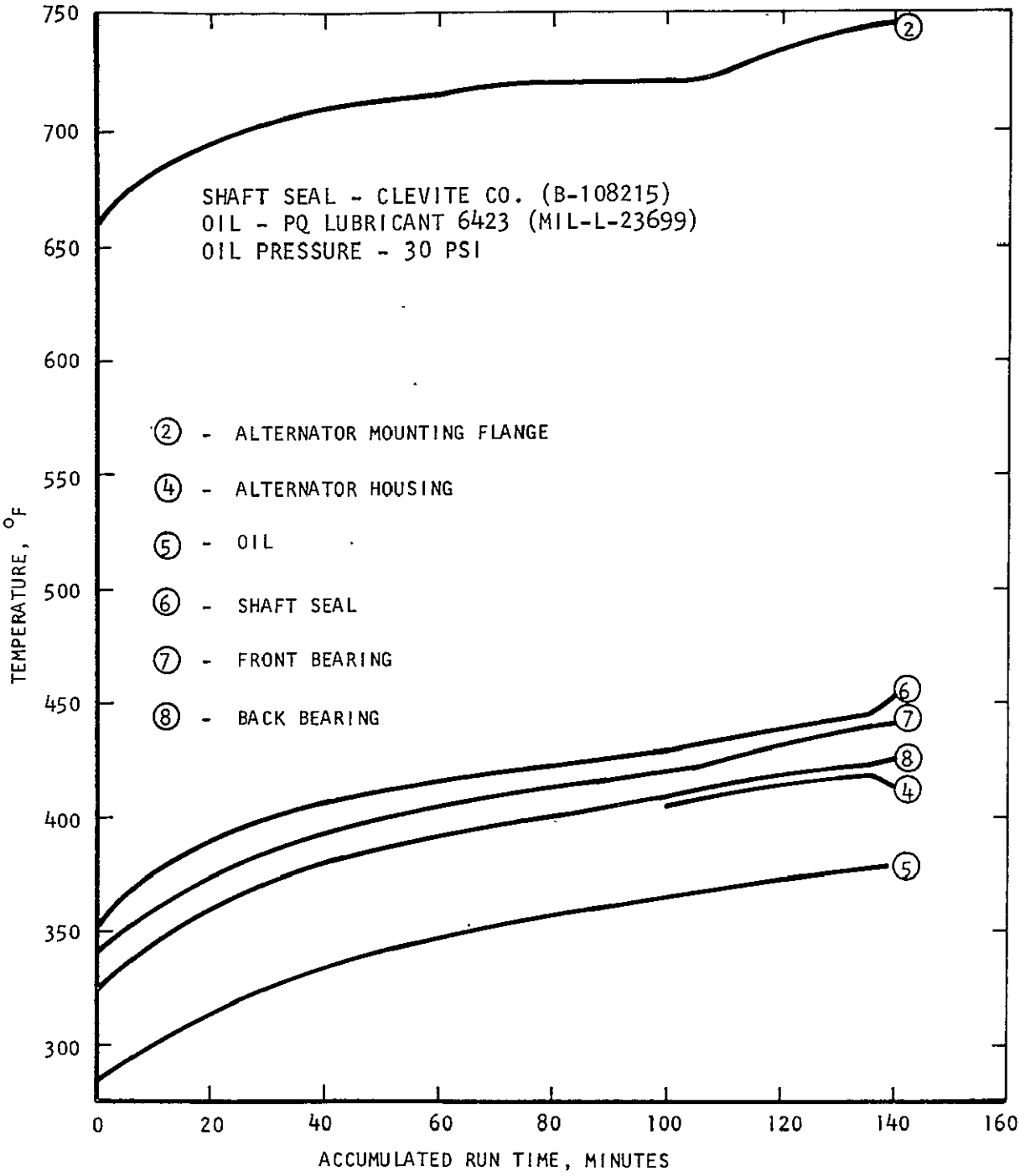
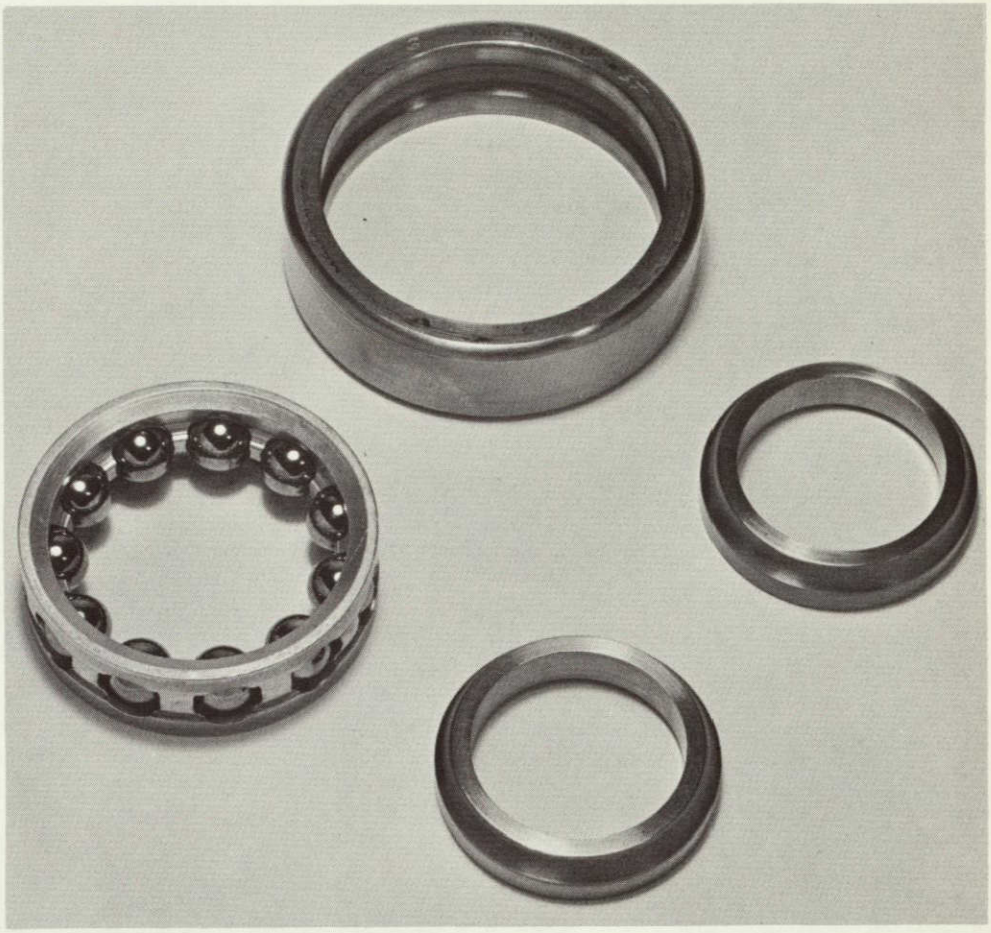


FIGURE 8.3-11 TEMPERATURES IN ALTERNATOR DURING HIGH TEMPERATURE TESTS

REPRODUCIBILITY OF THE
ORIGINAL PAGE IS POOR



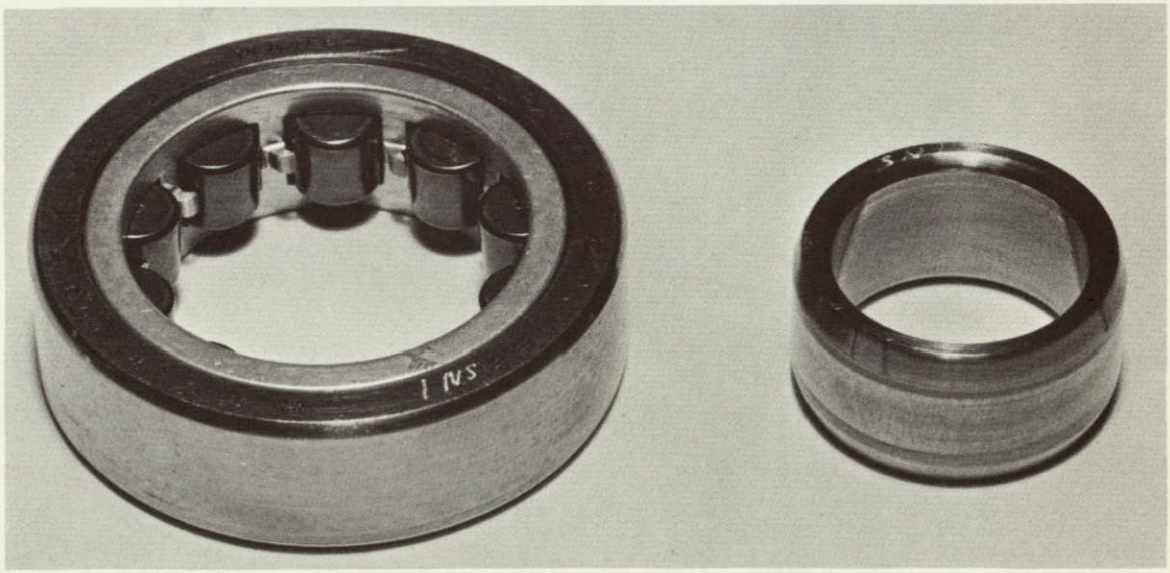


FIGURE 8.3-12 ALTERNATOR BEARINGS AFTER HIGH TEMPERATURE TESTS

REPRODUCIBILITY OF THE
ORIGINAL PAGE IS POOR

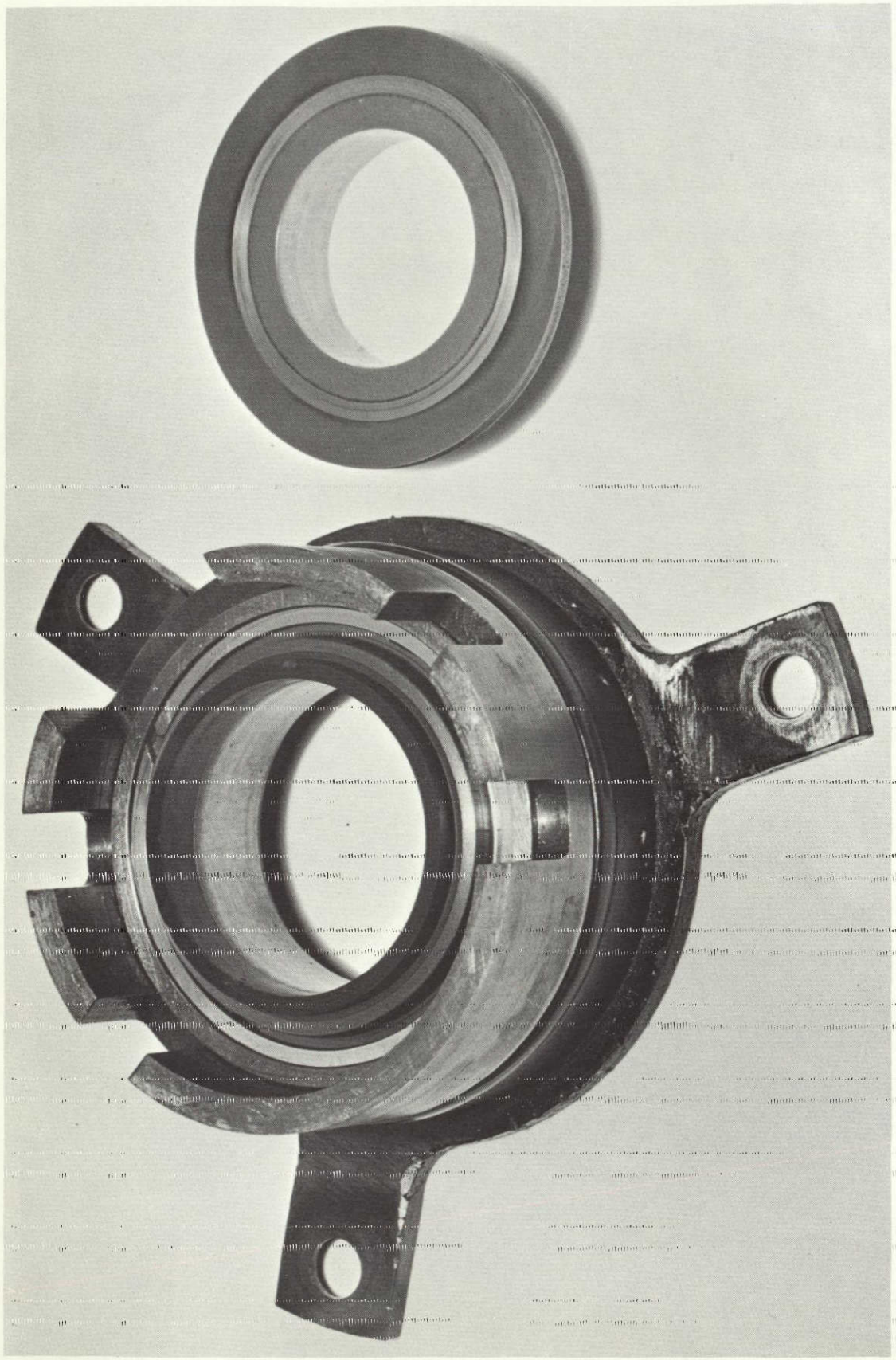


FIGURE 8.3-13 SHAFT SEAL AFTER HIGH TEMPERATURE TESTS

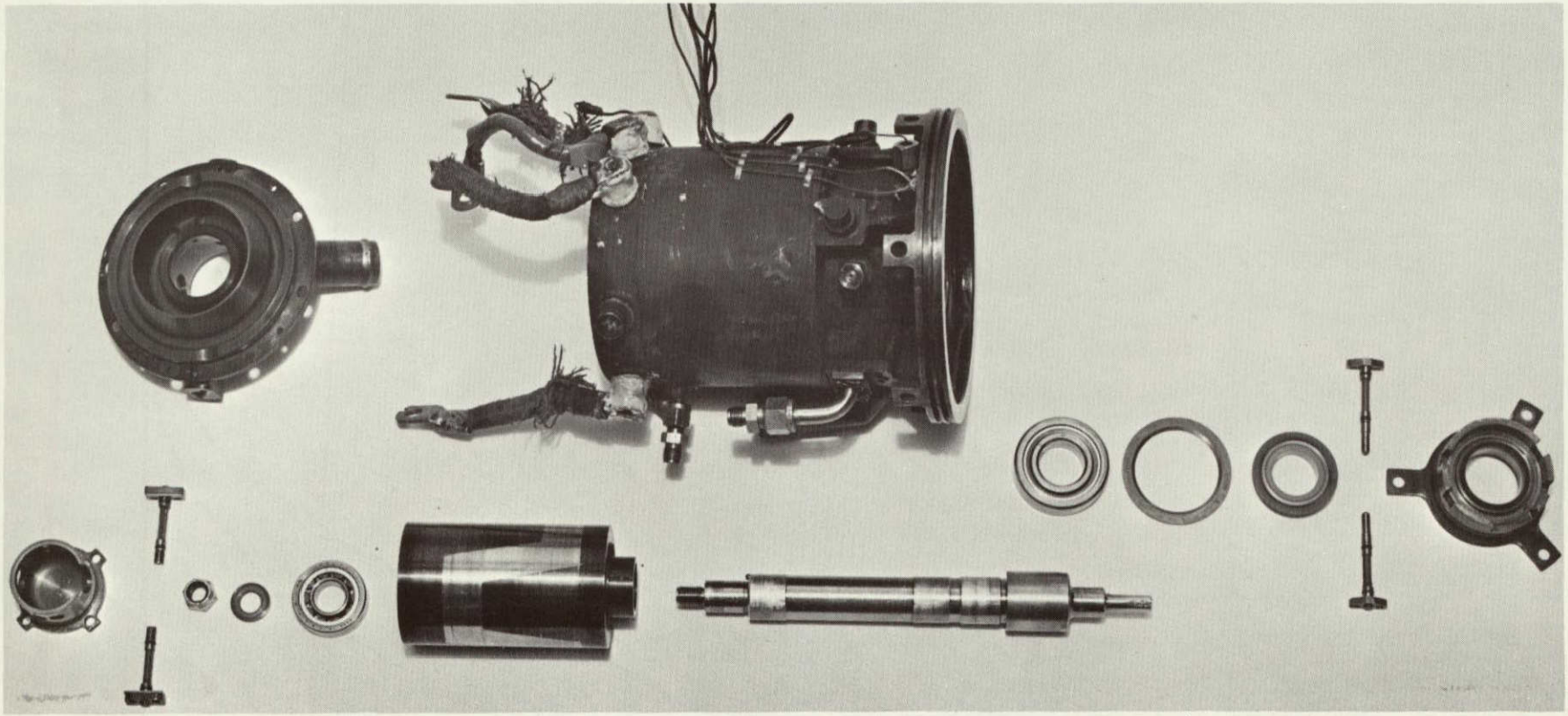


FIGURE 8.3-14 ALTERNATOR COMPONENTS AFTER HIGH TEMPERATURE TESTS

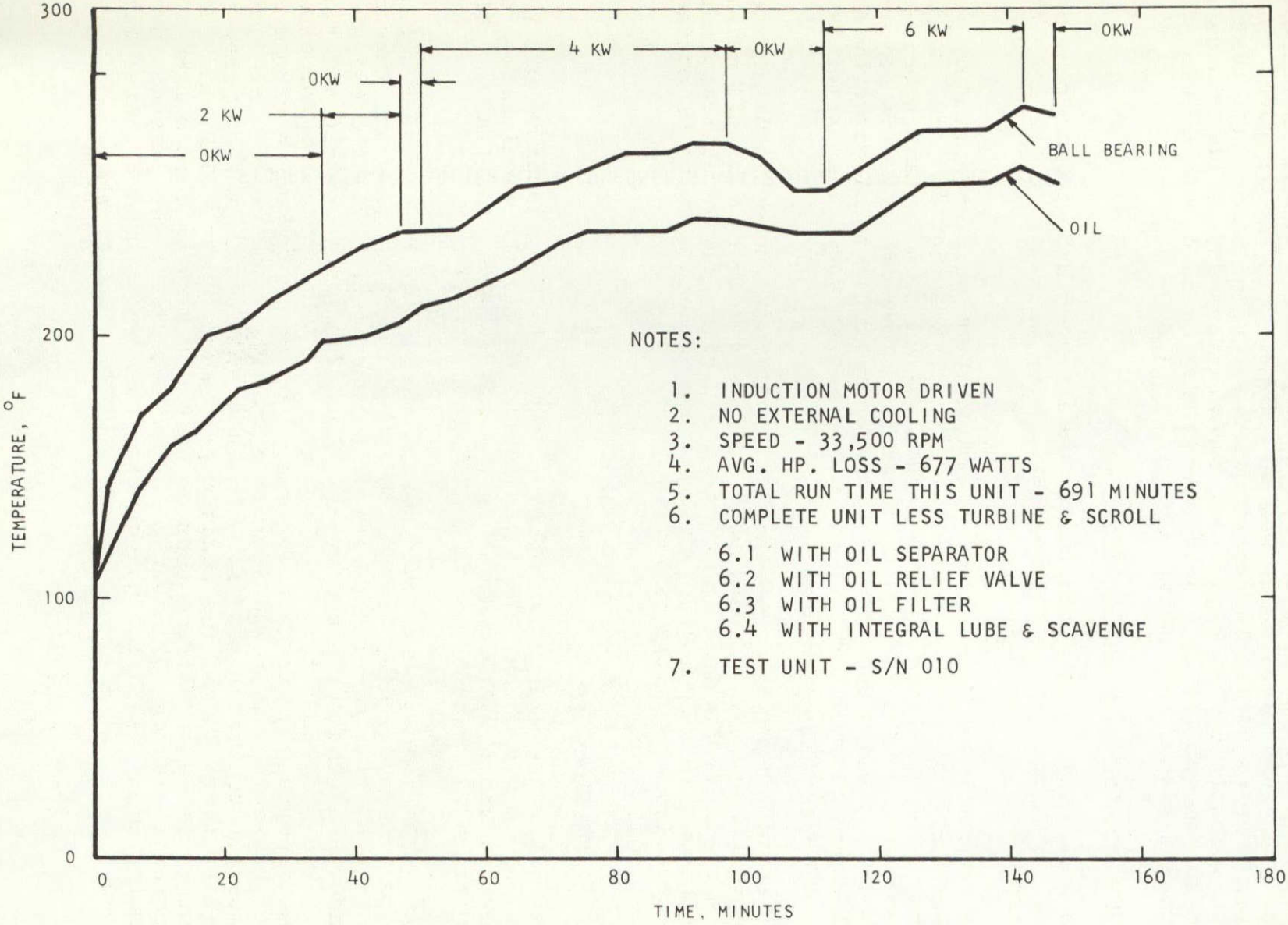


FIGURE 8.3-15 LUBE SYSTEM TEMPERATURE PROFILE

During DVR testing at Roanoke, the estimated total horsepower loss was 480 watts which was determined from the improved coast time. The reduction in frictional loss during hot gas testing was a result of: 1) higher oil temperatures and 2) the discovery and subsequent fix of a 0.005-inch shaft misalignment within the turboalternator test unit.

Phase Separator Component Tests

Several tests were conducted to obtain needed design information and, upon fabrication of the breadboard unit, to evaluate the performance of the unit.

The density of MIL-L-23699 oil as a function of temperature was determined by weighing a small vial containing an oil sample after the oil and vial had been heated to a certain specified temperature. The results of these tests are presented in Figure 8.3-16. Also presented is a room temperature value given by the oil manufacturer, American Oil Company. A two-percent error band is included in the graph for reference.

The surface tension of MIL-L-23699 oil was determined at ten temperatures between 20°F and 400°F. The height of an oil column in a small (0.010 inch diameter) bore, clean glass capillary tube submerged in a pool of oil was used to obtain a value of surface tension from the expression:

$$\sigma = \frac{r\rho g h}{2}$$

where r is the radius of the capillary, ρ is the density of the oil as a function of temperature, g is the acceleration of gravity, and h is the height of the oil in the capillary. The experimental results are shown in Figure 8.3-17.

Flow rate versus pressure drop tests for MIL-L-23699 oil at temperatures of 20°F, 68°F, 200°F, and 350°F flowing through stainless steel screen samples of pore diameters 35μ and 60μ were conducted. The test results are shown in Figures 8.3-18 and 8.3-19. The position of the 300°F curves relative to those for other temperatures in both figures is thought to be due to errors in the pressure or temperature recording equipment at oil temperatures above 200°F. In any case, for the purposes of conservative design, the maximum pressure drop at 20°F and the minimum value of surface tension at 400°F were used to design the separator screen element. In Figure 8.3-19, the pressure drop results from the following equation (see reference 8) are also shown.

$$\Delta p_{fs} = \frac{1.3 \beta u^2 f}{g_c \epsilon^2 D}$$

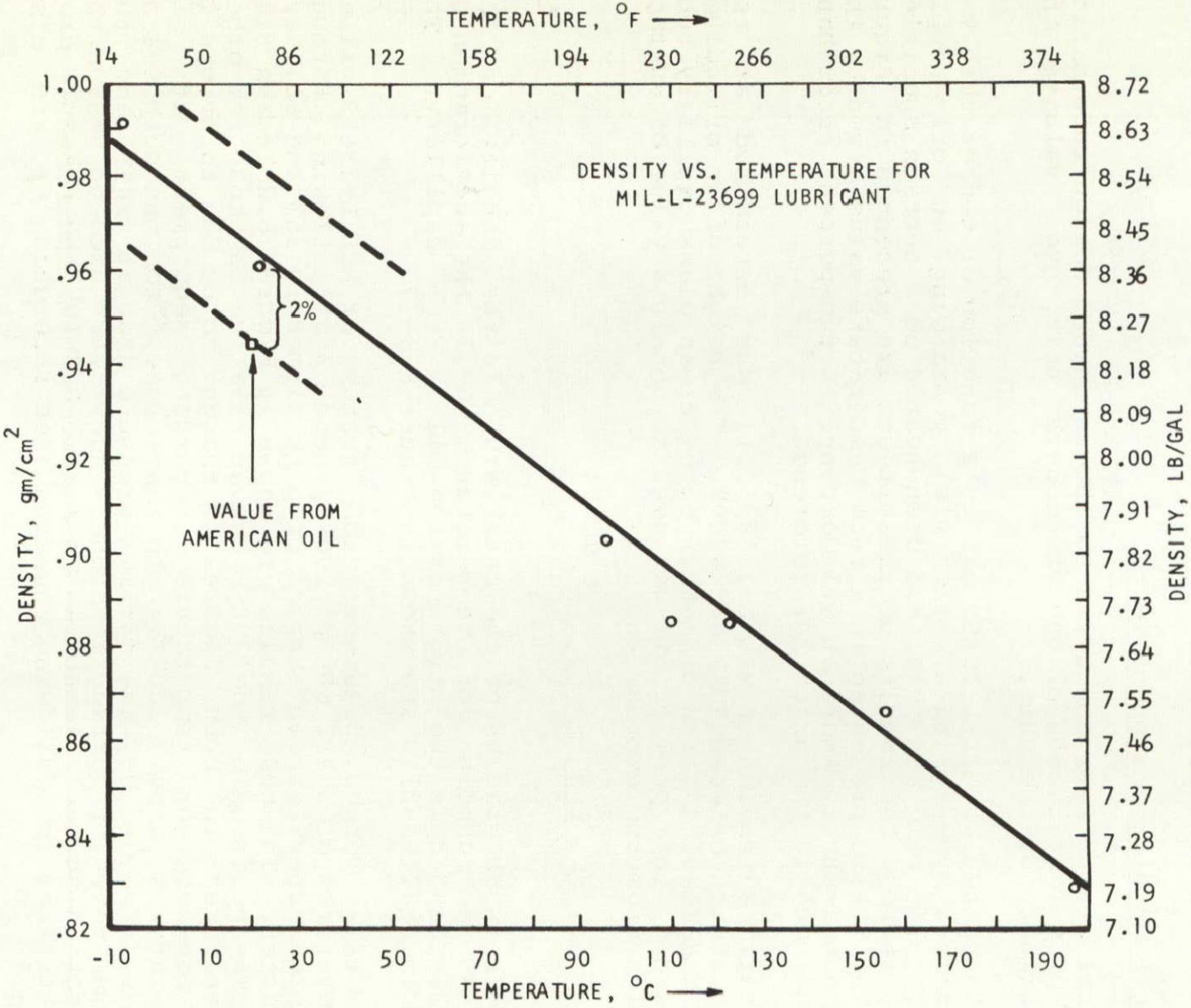


FIGURE 8.3-16 DENSITY VERSUS TEMPERATURE FOR MIL-L-23699 OIL

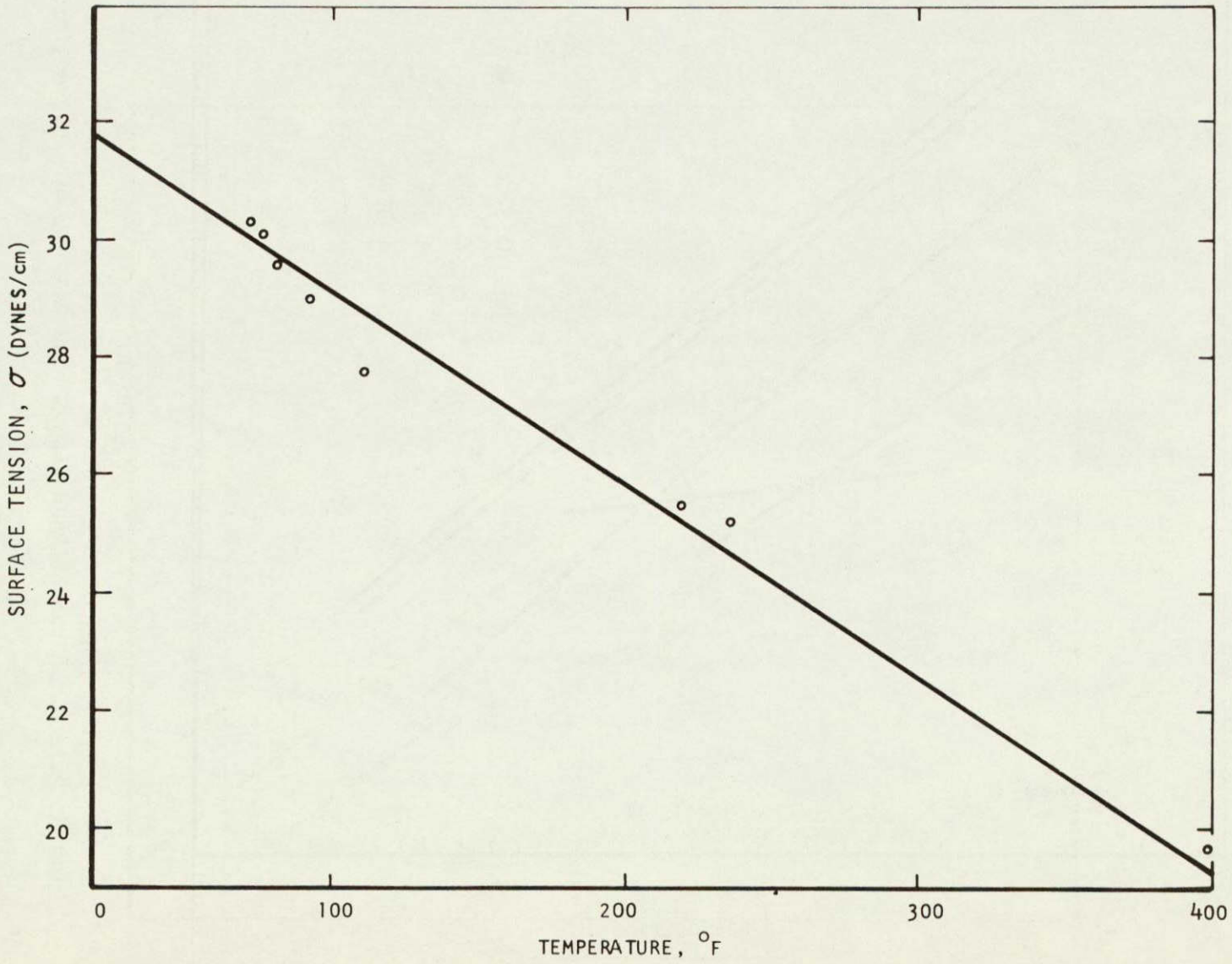


FIGURE 8.3-17 SURFACE TENSION VERSUS TEMPERATURE FOR MIL-L-23699 OIL

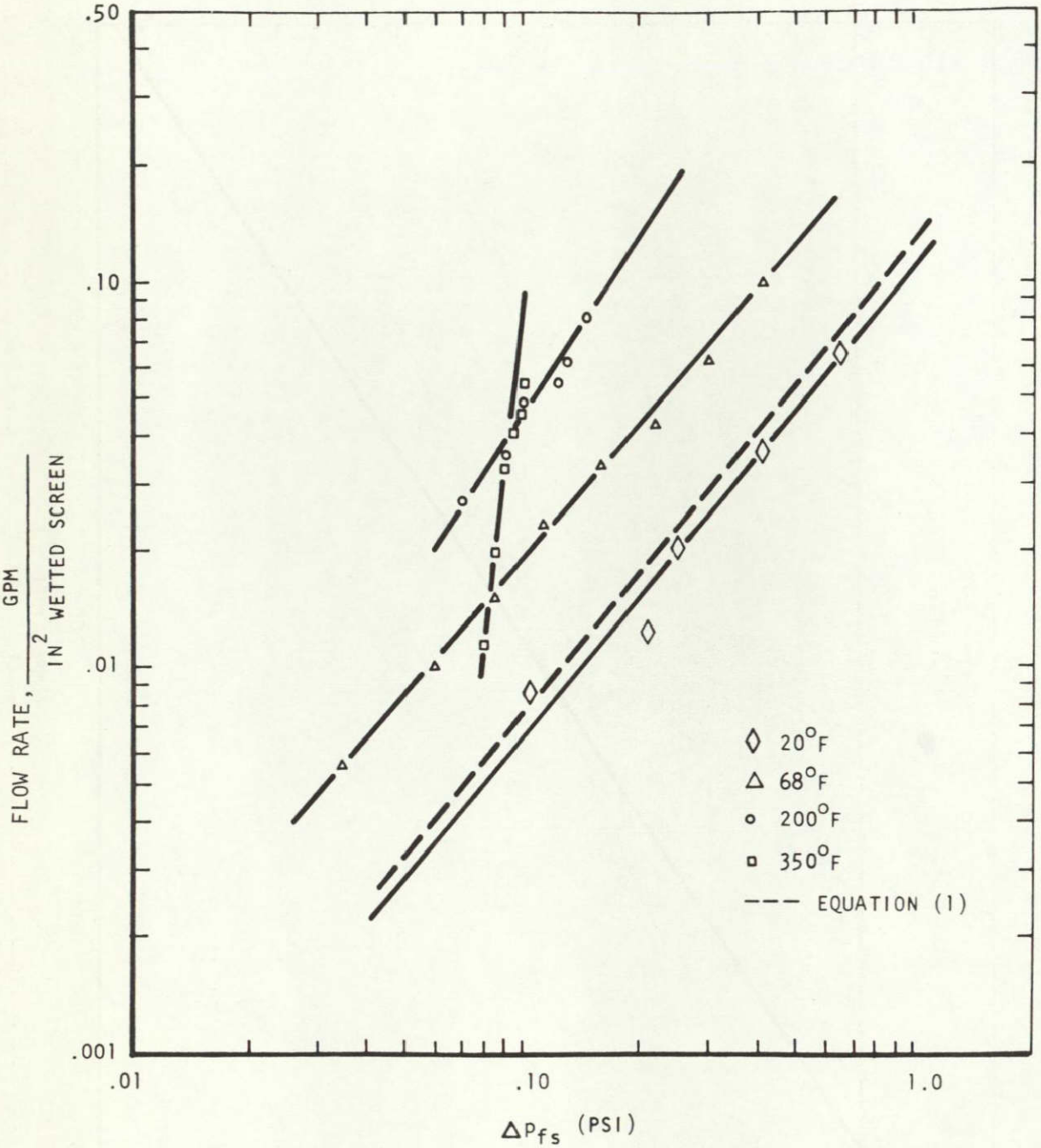


FIGURE 8.3-18 PRESSURE DROP VERSUS FLOW RATE FOR MIL-L-23699 OIL AND 35 μ SCREEN

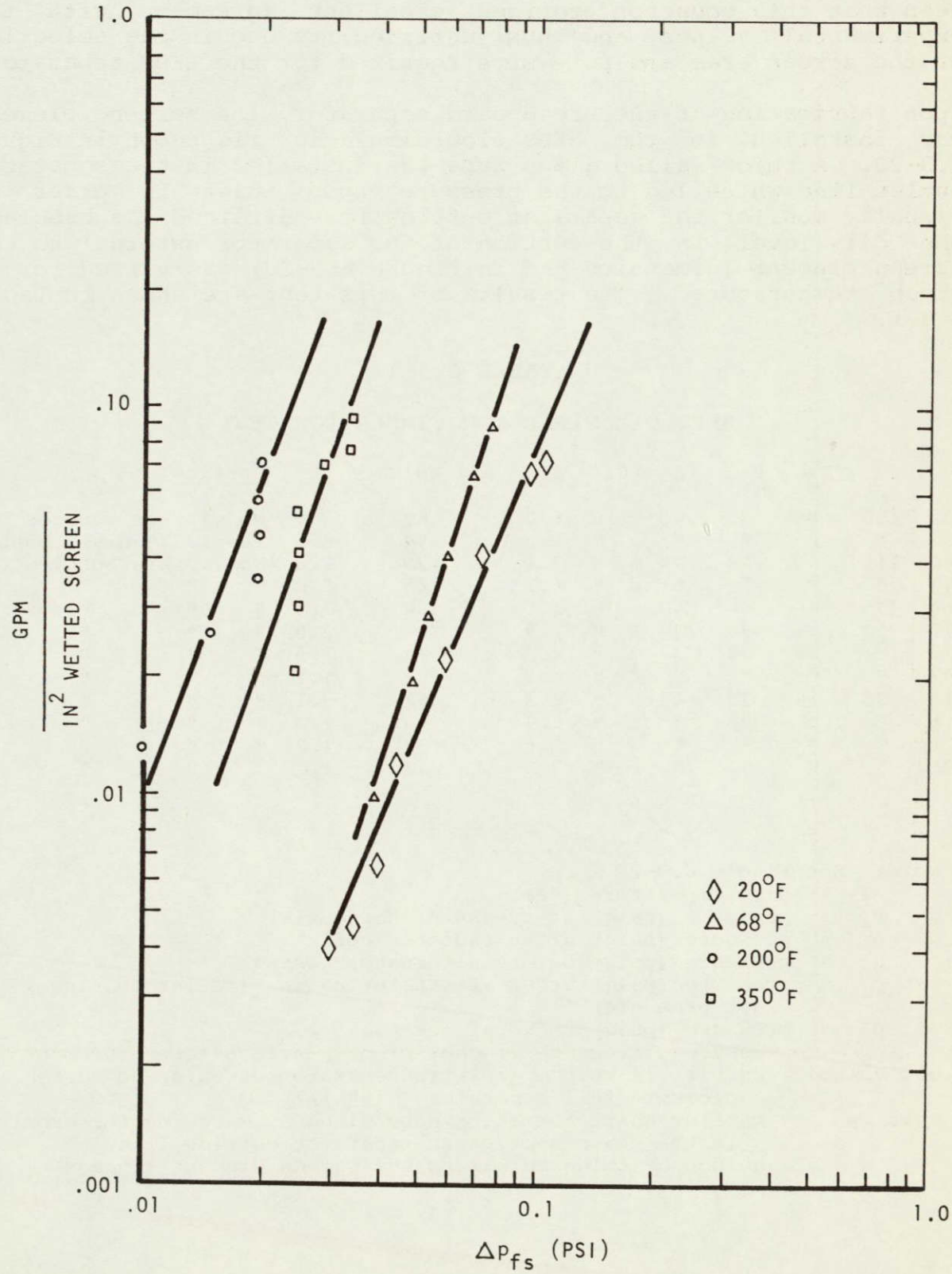


FIGURE 8.3-19 PRESSURE DROP VERSUS FLOW RATE FOR MIL-L-23699 OIL AND 60μ SCREEN

where the various terms are as defined in Section 4.2. It is seen that this equation provided excellent agreement with the experimental values and thus justified its use in the selection of the screen area and pore size required for the HEPS separator.

Upon fabrication of the breadboard separator, the screen element was installed in the HEPS flow simulation rig shown in Figure 8.3-20. A thick-walled glass tube was installed in the separator outlet line which led to the pressure pump inlet in order to visually monitor the separator outflow for entrained gas bubbles. The oil level in the portion of the separator external to the screen element (dimension "h" in Figure 8.3-20) was varied for a given temperature. The results of this test are shown in Table 8.3-1.

TABLE 8.3-1

HEPS OIL SEPARATOR SIMULATION TEST

T	P_1	P_2	P_3	P_4	P_5	ΔP_S	Oil Volume	h	Outflow
33	150	46	45	40	0	6.0	60	2.0	No visible bubbles
33	"	"	"	"	"	9.2	44	1.5	Few 1/32" diam. bubbles
42	110	50	48	44	"	3.1	79	2.6	No visible bubbles
42	"	"	"	"	"	5.1	65	2.2	" " "
64	75	46	44	40	"	1.5	104	3.5	" " "
77	50	37	36	36	"	1.9	60	2.0	" " "
77	"	36	34	32	"	4.2	44	1.5	" " "
77	"	"	"	"	"	6.9	35	1.2	" " "
116	25	14	13	12	"	0.2	94	3.1	" " "
116	"	"	"	"	"	0.4	60	2.0	" " "
121	"	"	"	"	"	1.8	37	1.2	" " "
121	"	"	"	"	"	9.5	33	1.1	" " "

Note: See Figure 8.3-20

T = oil temperature (°F)

P_1 = pressure (psig) at pressure pump outlet

P_2 = pressure (psig) after radiator coil

P_3 = pressure (psig) before alternator casing

P_4 = pressure (psig) after alternator casing (roller bearing jet pressure)

P_5 = pressure (psig) in separator tank

ΔP_S = pressure difference (inches of oil) across screen element

Oil Volume = usable oil volume (in^3) in separator exterior to screen element (full separator = 190 in^3)

Outflow = outflow characteristics determined by watching for bubbles in the glass section on separator outflow line

h = height of oil external to the screen element (inches)

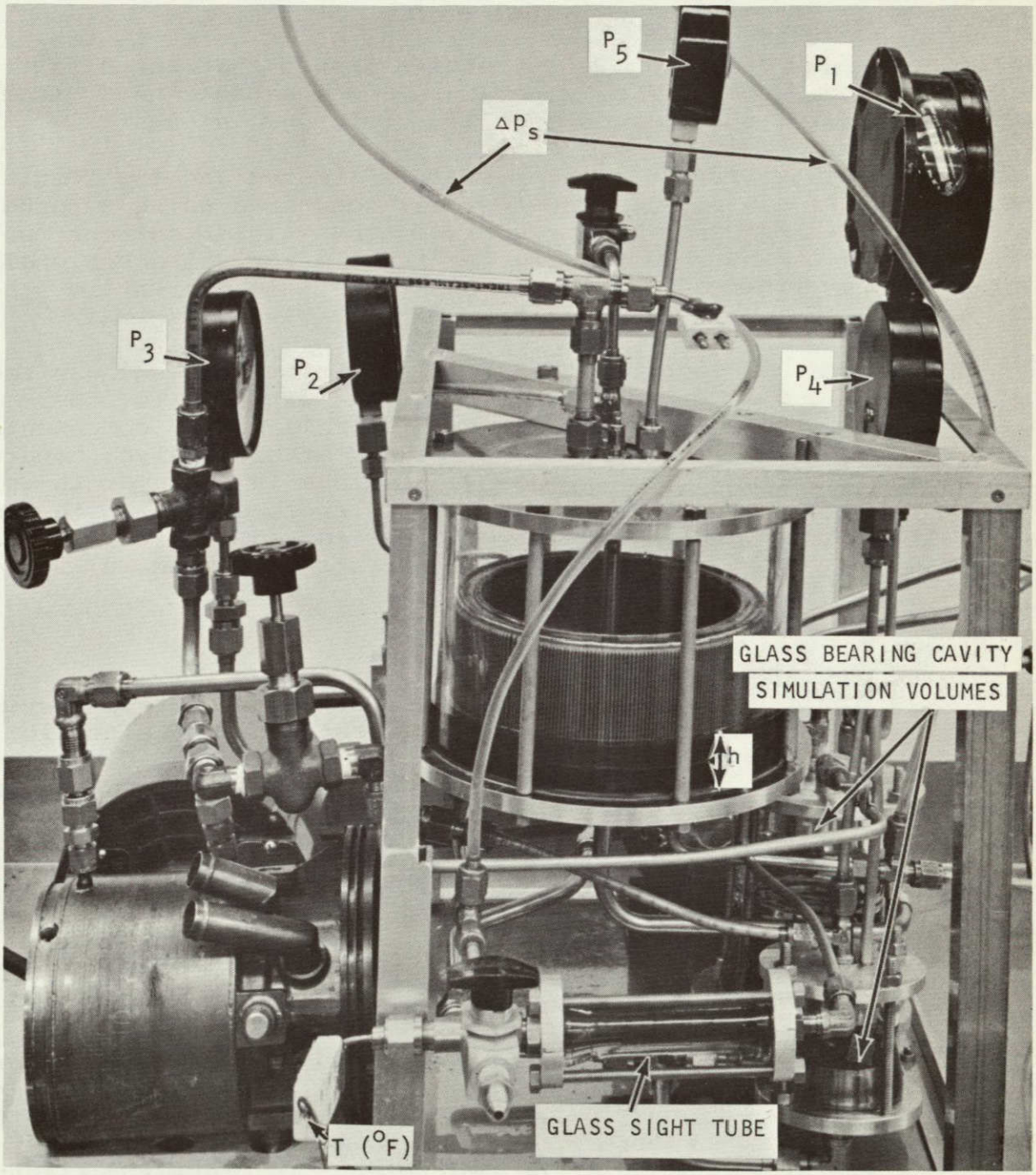


FIGURE 8.3-20 HEPS OIL FLOW SIMULATION SYSTEM

8.4 Electrical System Tests

Breadboard Tests

The voltage regulator and speed control circuits were tested in a thermal environment. Test results showed that the circuits were operational to 230°F. Temperature-compensated zener diodes were required for the voltage regulator reference diodes.

A packaged DVR voltage regulator was also tested and the results are shown in Figure 8.4-1. The test was conducted using a three-phase variable frequency power supply. The field current was maintained constant by varying the input error voltage signal. The deviation required to maintain constant field current is the effect of temperature on the unit.

The speed control required the greatest amount of testing since early Phase I and II breadboards were never exposed to thermal environments. Selection of all new high reliability components also required some circuit changes. Highly stable polycarbonate capacitors were used to reduce variations in pulse width and frequency due to temperature changes. The speed control with its associated startup and safety circuits was tested up to 230°F. Temperature data for various pulse outputs are shown in Figure 8.4-2.

DVR Electrical Component Tests

A packaged voltage regulator, speed control and control panel were not available for the early DVR testing. The electrical system was checked out on the alternator test stand in Cleveland to uncover any problems. The control system performed satisfactorily when checked with a Phase II alternator. Voltage regulator transfer points, field flash, and valve triggering were the types of parameters checked. A regulation curve for the DVR voltage regulator is shown in Figure 8.4-3. Complete electrical system checkout tests will be conducted on the first Qualification Unit.

8.5 DVR Flight Package Development Testing

The DVR unit was assembled in Cleveland prior to shipment for testing at VPI-Roanoke. The front view of the unit was previously shown in Figures 4.1-2 and 4.1-3. The rotor and shaft assembly are shown in Figure 8.5-1. The DVR unit is shown in Figures 8.5-2 through 8.5-6. The rectifier cold plate and flight package are shown in the deployed mode. In the altitude cell, the flight package was attached to a platform that simulated the LM SEQ bay. The frame assembly was cantilevered on fixed length extension members. The details of the extension members and

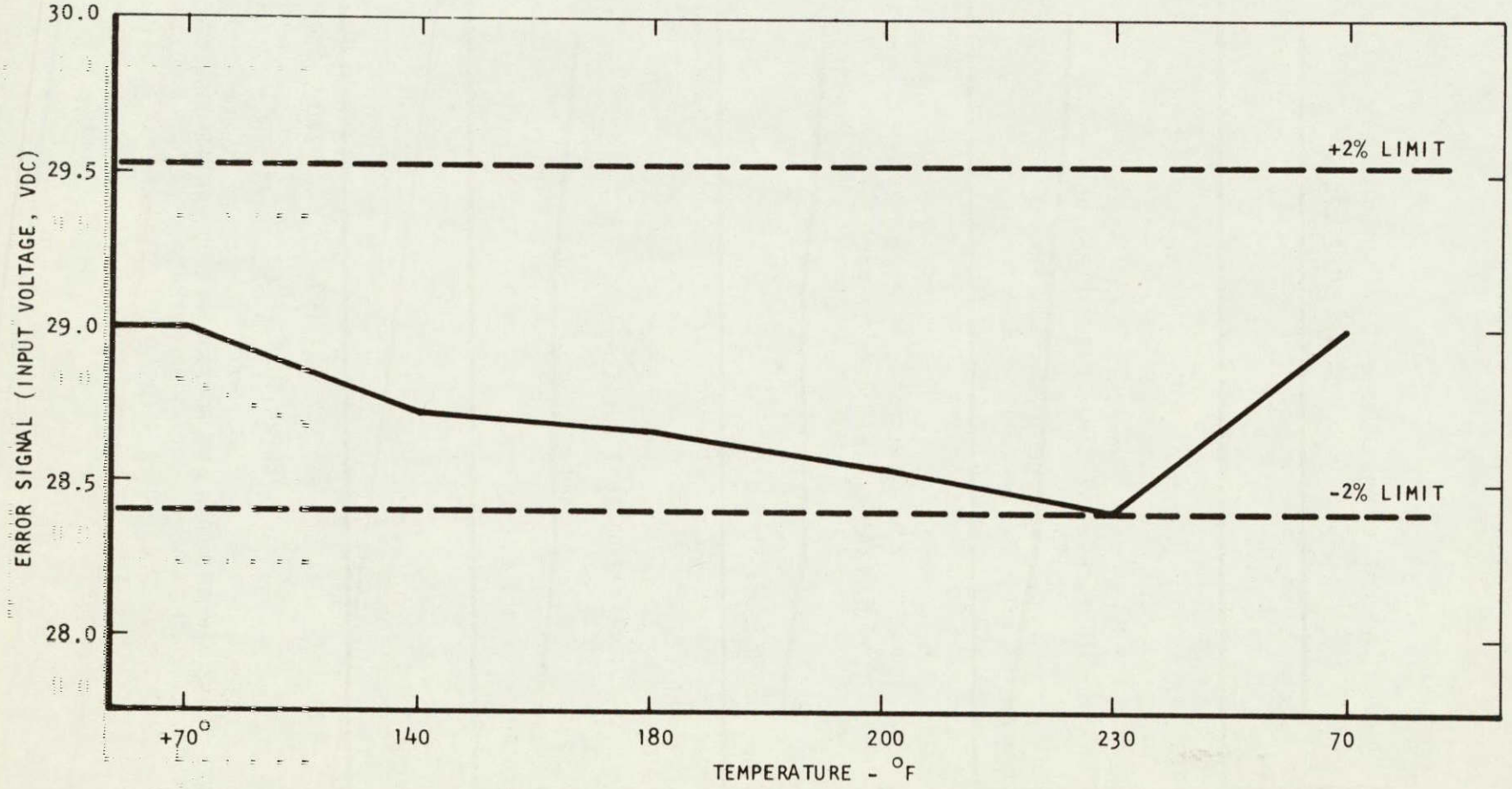


FIGURE 8.4-1 VOLTAGE REGULATOR DRIFT CONSTANT I_{FIELD} = 1.5 AMPERES - DVR UNIT 010

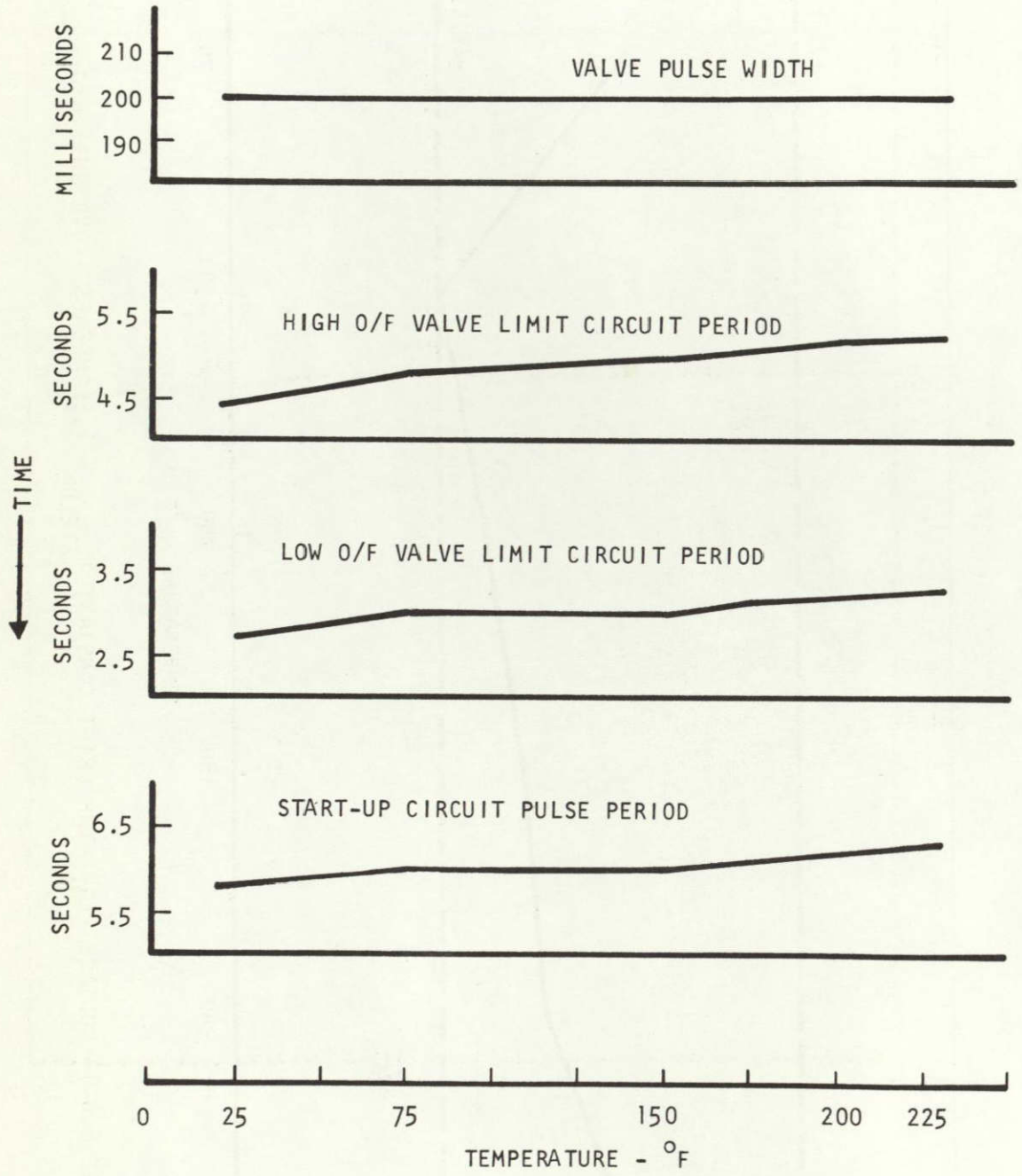


FIGURE 8.4-2 PULSE WIDTH AND PULSING PERIOD VARIATIONS WITH TEMPERATURE

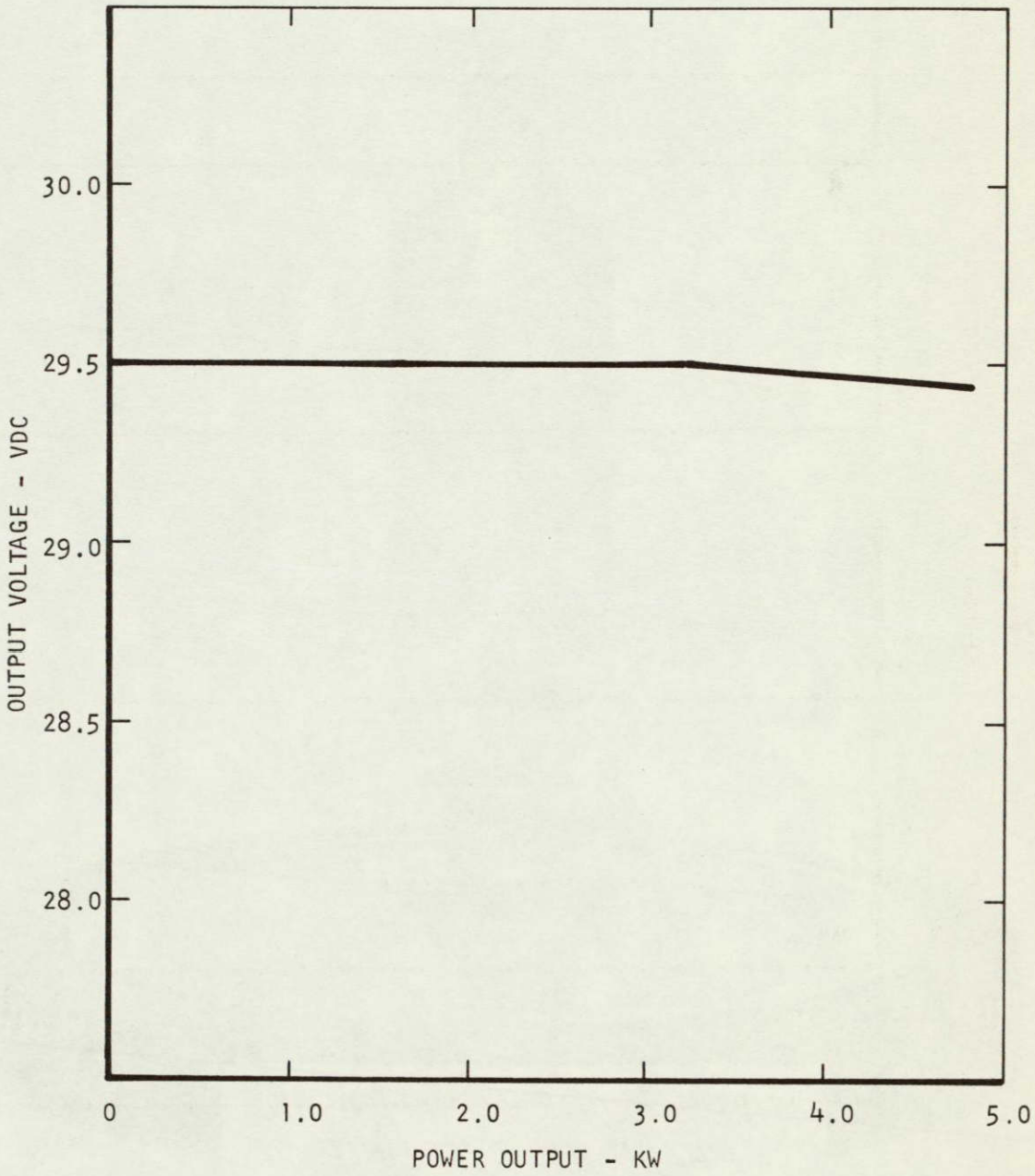


FIGURE 8.4-3 VOLTAGE REGULATION CHARACTERISTIC
VOLTAGE REGULATOR S/N 010



FIGURE 8.5-1 DVR ROTATING ASSEMBLY

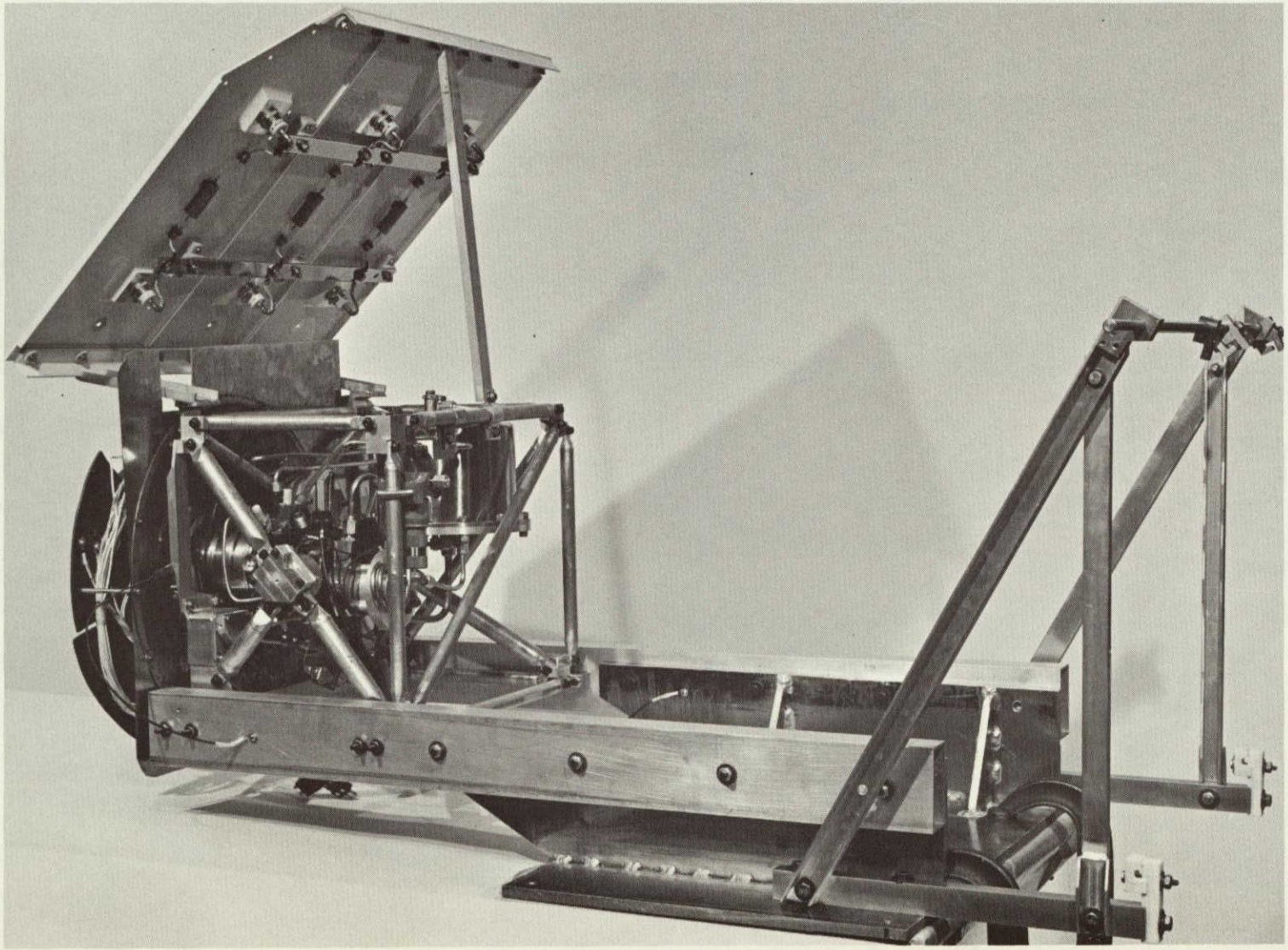


FIGURE 8.5-2 DVR UNIT - RIGHT SIDE

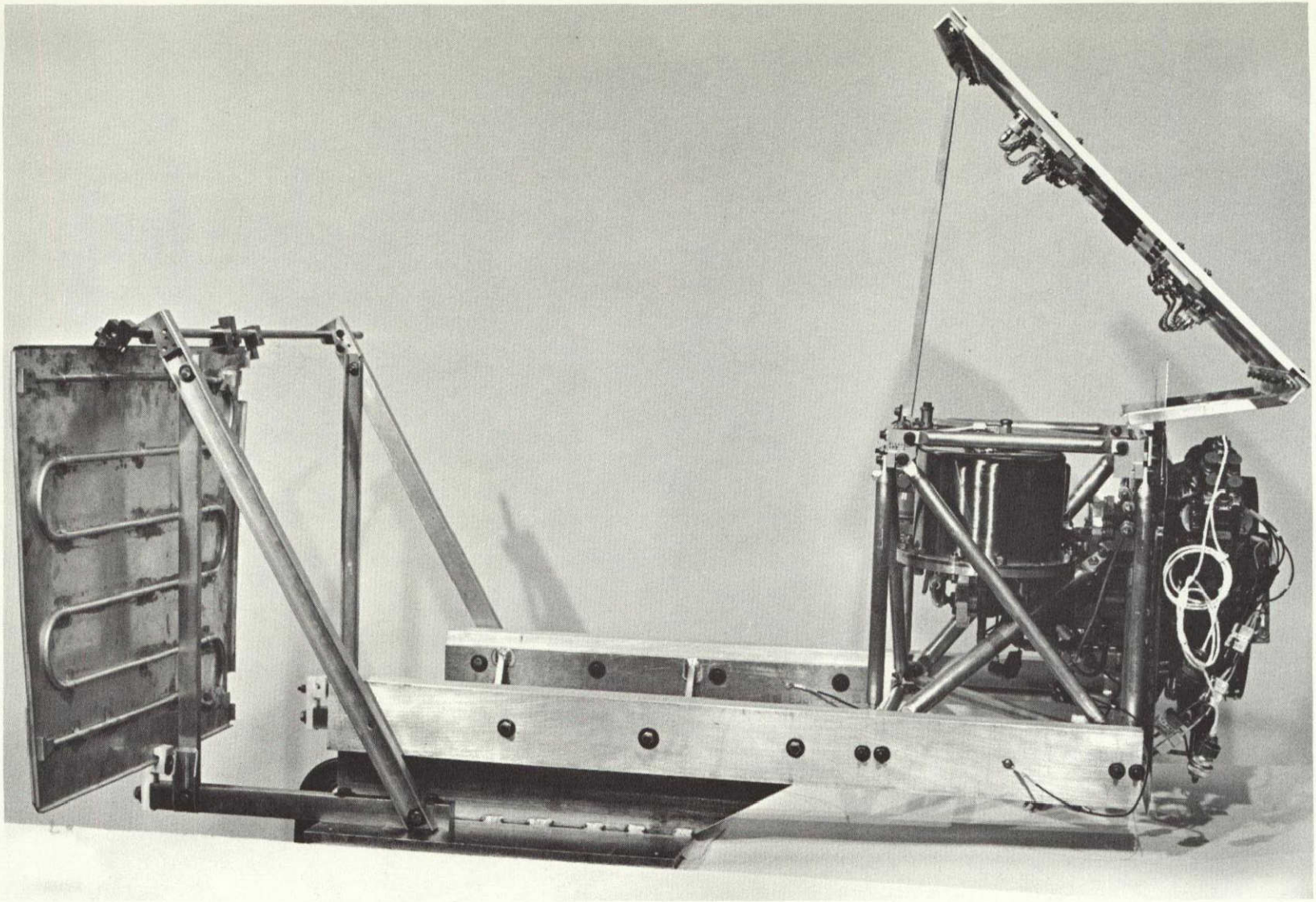


FIGURE 8.5-3 DVR UNIT - LEFT SIDE

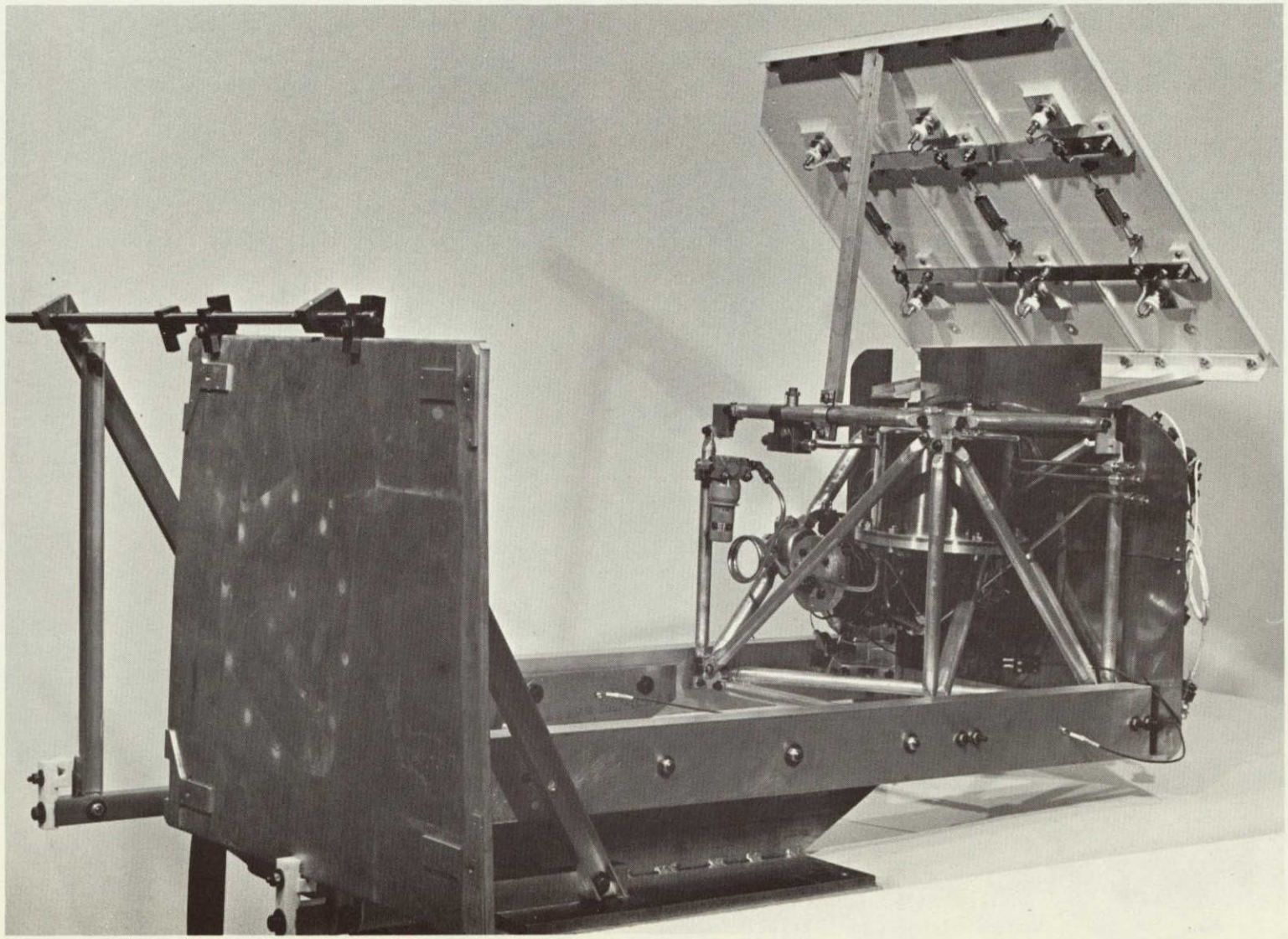


FIGURE 8.5-4 DVR UNIT - LEFT REAR

REPRODUCIBILITY OF THE
ORIGINAL PAGE IS POOR

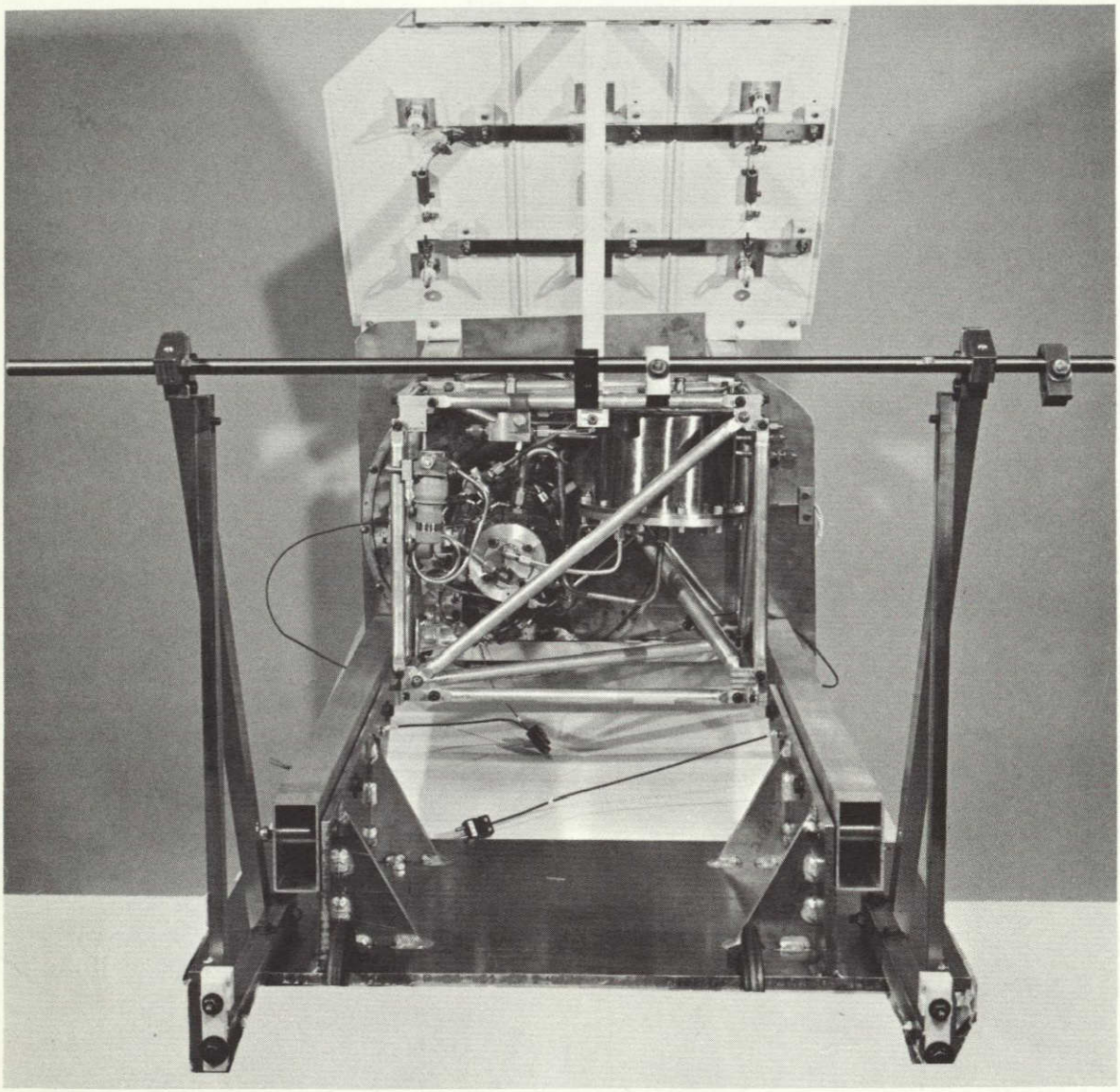


FIGURE 8.5-5 DVR UNIT - REAR

REPRODUCIBILITY OF THE
ORIGINAL PAGE IS POOR

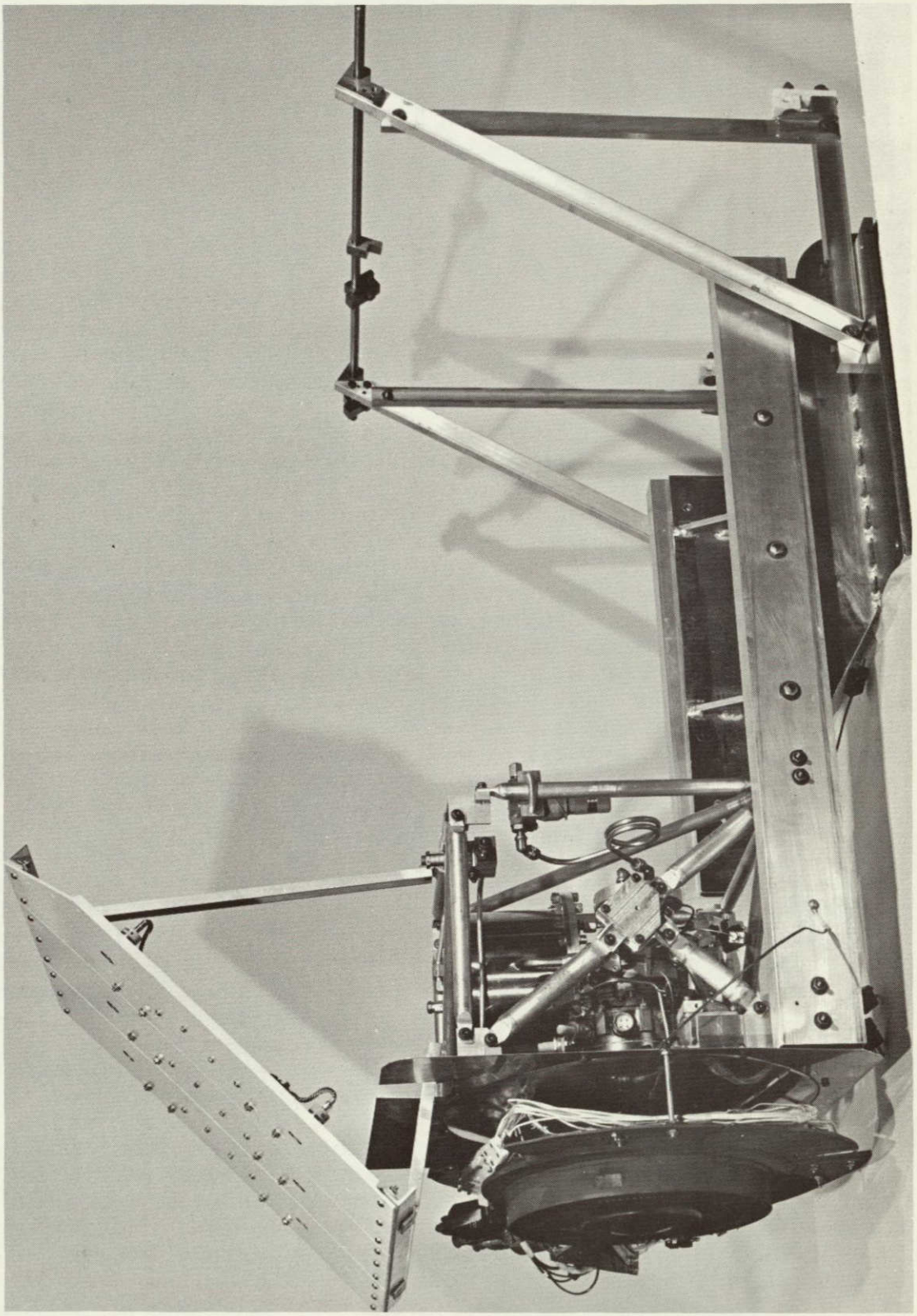


FIGURE 8.5-6 DVR UNIT - RIGHT FRONT

REPRODUCIBILITY OF THE
ORIGINAL PAGE IS POOR

C-3

mounting platform are shown in Figures 8.5-2 through 8.5-6. In Figure 8.5-3, a typical radiator panel is shown mounted in the rear section. After arrival at the test site, the radiator panels were attached to the frame. The radiator placement in the rear of the package was a condition imposed by the limited space in the altitude chamber.

Specific Propellant Consumption

The Phase III DVR performance curves are shown in Figures 8.5-7 through 8.5-11. In Figure 8.5-7 the Phase II and III coast times are compared. For low O/F ratio operation at 3.0 and 0 KW load, a 62% and 118% increase in coast time was realized, respectively. Similarly, for high O/F operation at 3.0 KW and 0 KW load, an increase of 35% and 123%, respectively, was realized. A composite SPC curve comparing high and low O/F ratio data for Phases II and III is shown in Figure 8.5-8. The maximum and minimum SPC values are shown together to prevent distortion of the data. The data scatter was created by erratic flowmeter outputs. However, the SPC limits as shown are considered to be realistic because the flowmeter data correlated closely with density-corrected water flow test data. The low O/F ratio operation SPC comparison curves are presented in Figure 8.5-9. At 3.0 KW and 1.0 KW, the SPC performance improvement was 37% and 87%, respectively, for the maximum (worst) Phase III SPC values. SPC comparison curves for high O/F operation are shown in Figure 8.5-10. For the maximum (worst) Phase III SPC values, the performance improvement at 3.0 KW and 1.0 KW was 26% and 40%, respectively. Consideration for the minimum (best) Phase III SPC values would show an additional performance improvement of 5-10%. Lunar staytime extension curves for various quantities of residual propellants are shown in Figure 8.5-11. The primary reason for the performance improvement was the reduced frictional losses. A detailed discussion of losses for Phases II and III was presented in Section 8.3. Another explanation for the improved performance was the reduced dribble volume in the gas generator. This was a minor improvement compared to the frictional loss reduction. Improved pulse efficiency was another minor factor that contributed to performance improvement. This was accomplished by increasing the system response so that the chamber pressure rise and decay time were 15-20 milliseconds maximum. The chamber pressure overshoot at pulse initiation was followed by a steady pressure and a rapid decrease at pulse termination. Phase II pulse traces showed that the chamber pressure and system response was too slow to provide a simulated step function on the pressure trace. A step function trace would indicate a 100% pulse efficiency. Data scatter due to erratic flowmeter behavior prevented performance comparison between high and low O/F ratios; however, the coast time data indicated that

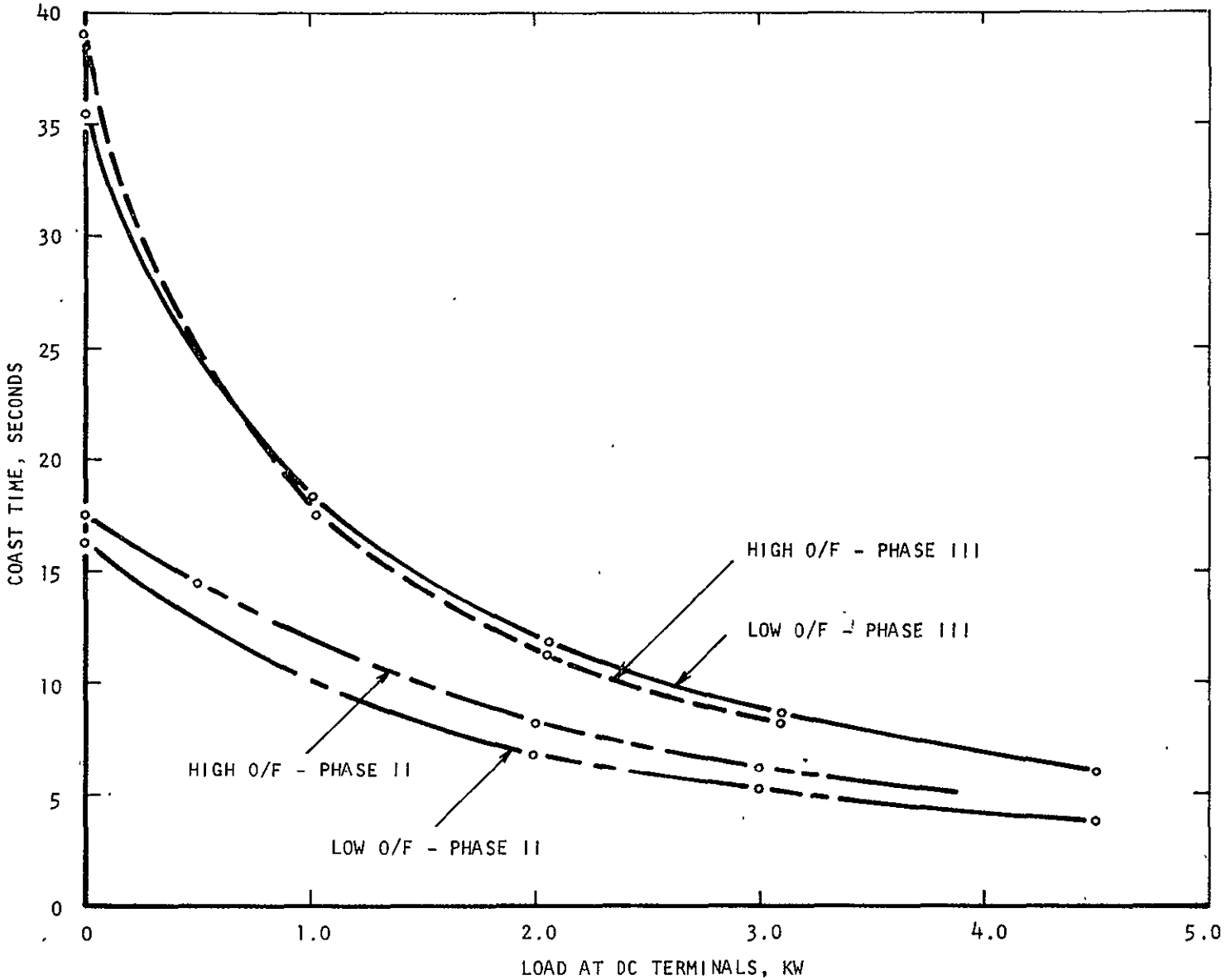


FIGURE 8.5-7 PHASE II & III COAST TIME COMPARISON

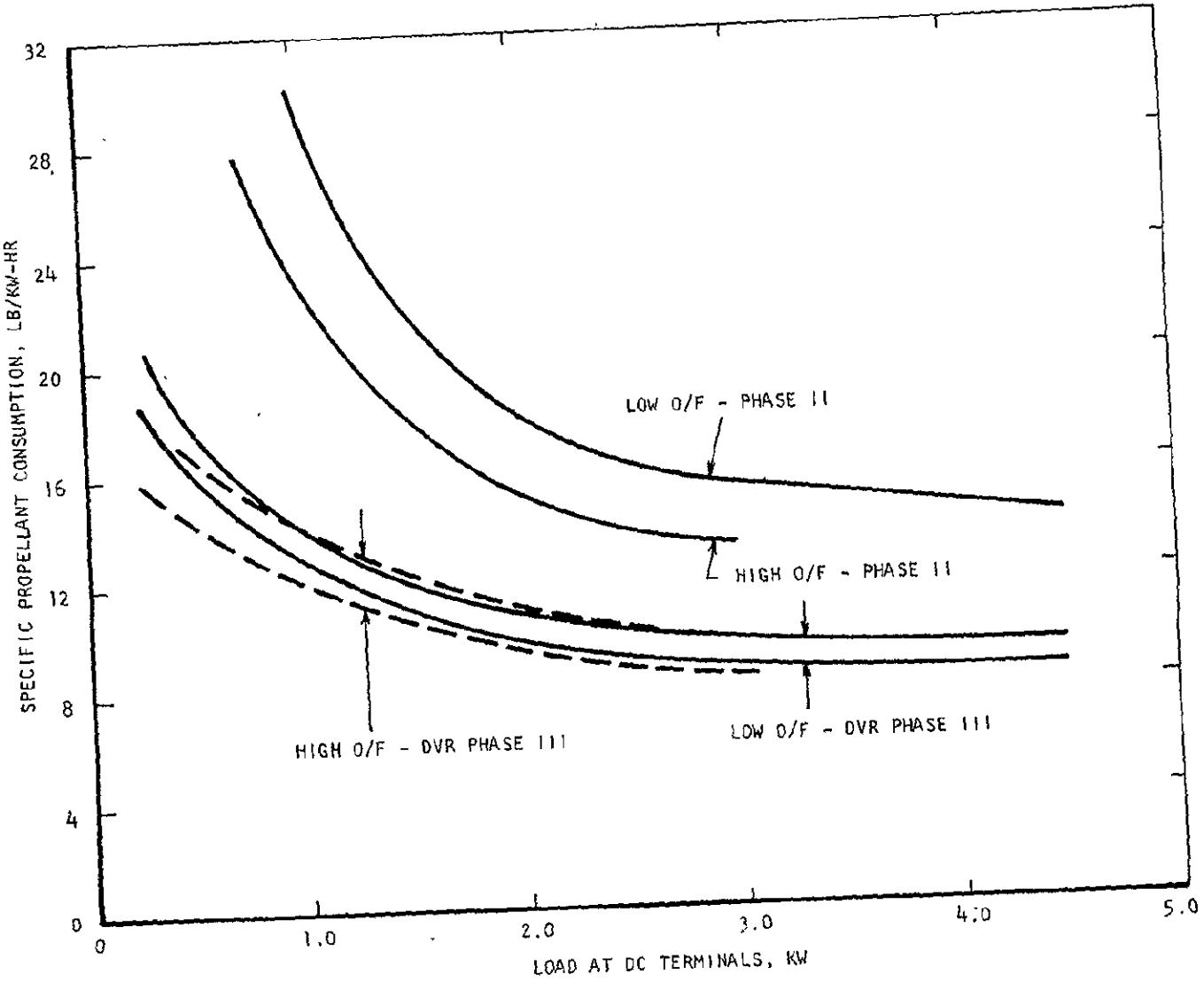


FIGURE 8.5-8 PHASE II & III SPC COMPARISON

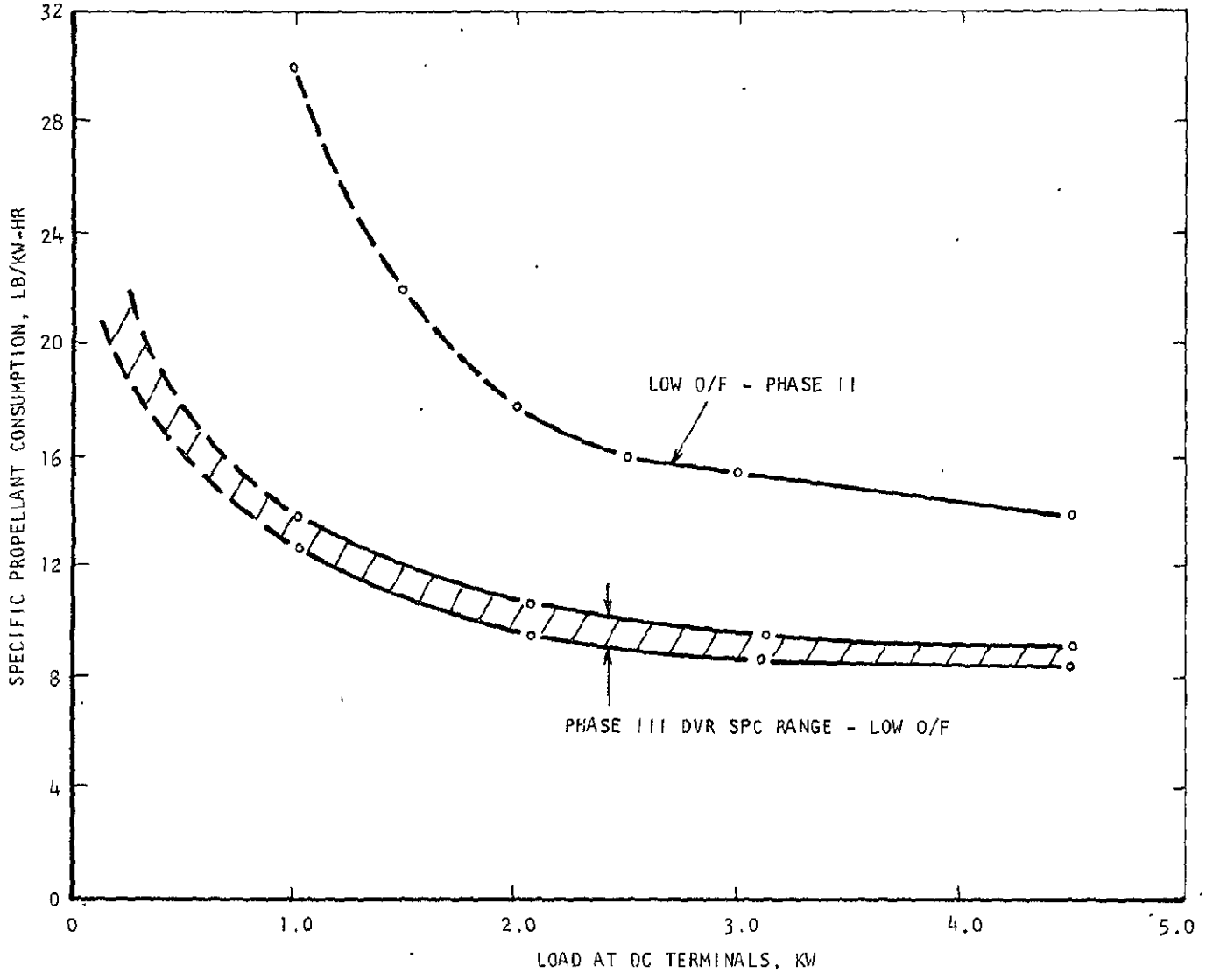


FIGURE 8.5-9 SPECIFIC PROPELLANT CONSUMPTION - LOW O/F - DVR TESTS - PHASE III
(010-4.1-017, -018)

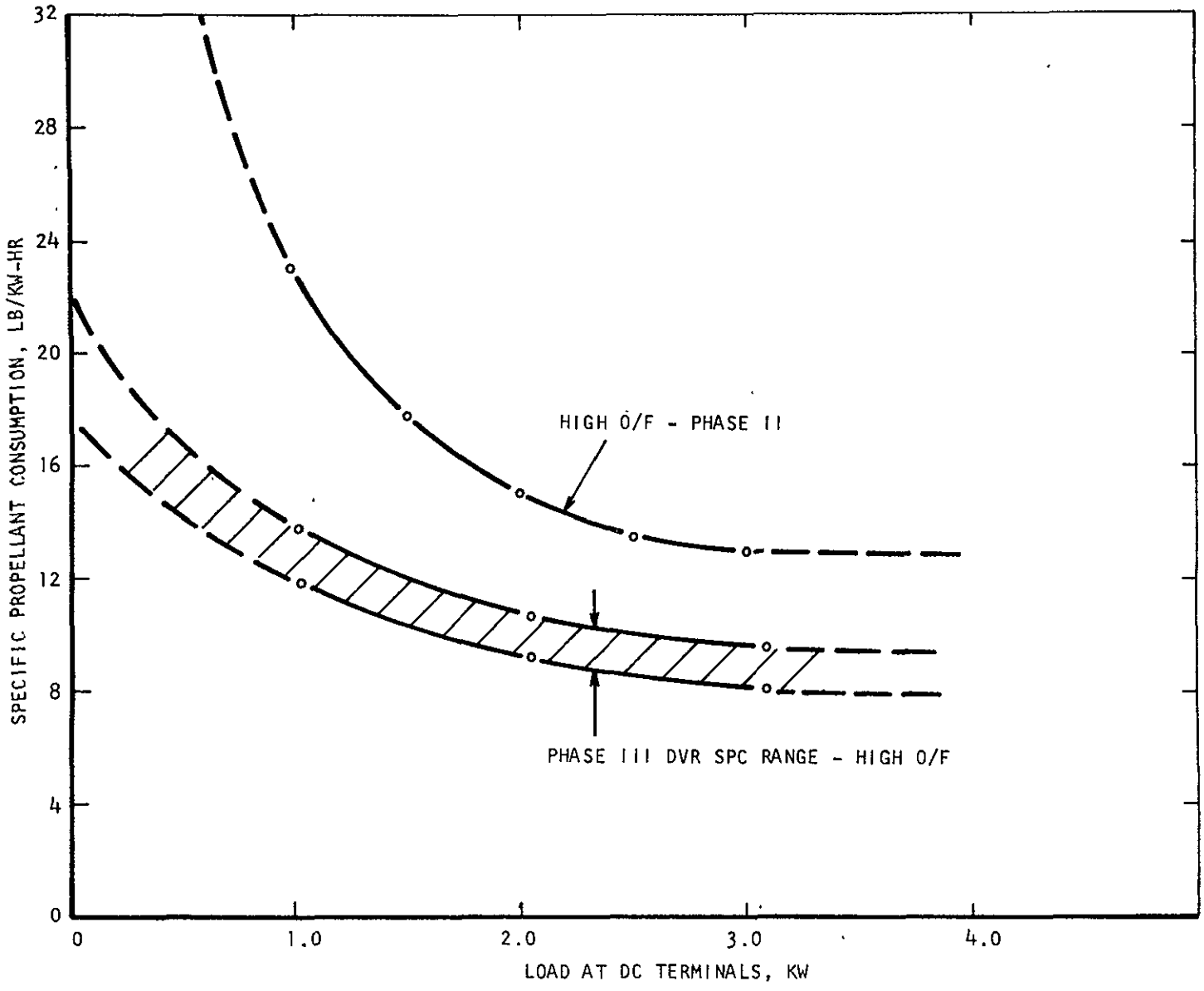


FIGURE 8.5-10 SPECIFIC PROPELLANT CONSUMPTION - HIGH O/F - DVR TESTS - PHASE III (010-4.1-017,-018)

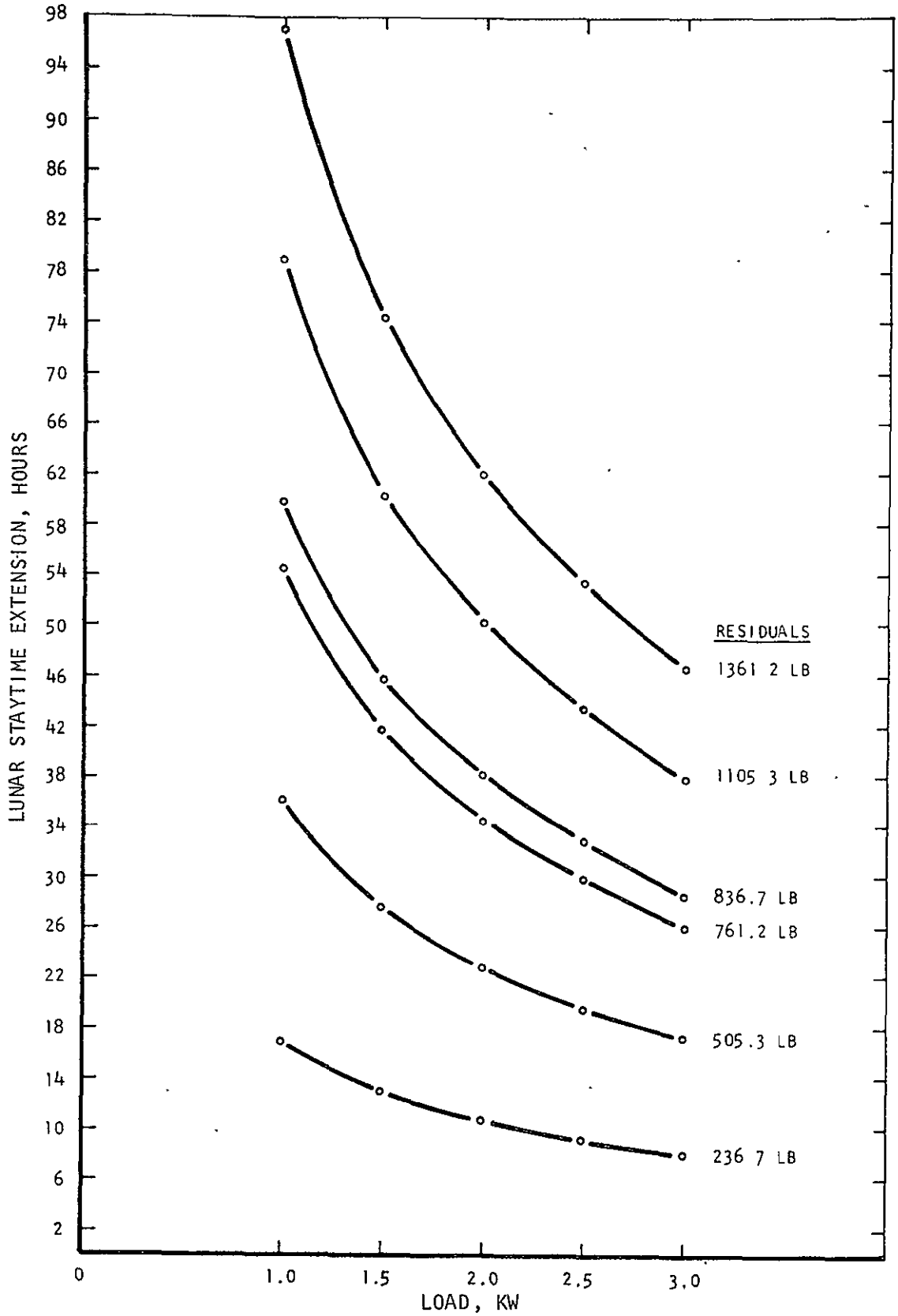


FIGURE 8.5-11 LUNAR STAYTIME VERSUS LOAD, DVR - PHASE III (USING WORST SPC)

the performance at the high O/F ratio was better than for low O/F ratio operation.

DVR Lubrication System Performance

Pressures were measured at the locations shown in Figure 4.2-1 in order to evaluate the flow/pressure drop characteristics of each component. The curves presented in Figures 8.5-12 through 8.5-15 show pressure versus run time. The oil temperature is also shown on these figures to illustrate the relationship between oil viscosity and overall pressure levels. In Figure 8.5-12 it is shown that the pressure drop across the radiator was 4 psi after the oil temperature had stabilized at 377°F. In addition, note that a 15% decrease of radiator inlet pressure accompanied the 80°F oil temperature rise. Similar data for other lube system components are shown in Figure 8.5-13. The scavenge pump inlet maintained a constant scavenge pressure of 2.75 psia. Test 017 was conducted with the altitude chamber wall temperature (heat sink) at 160°F. Test 018 was conducted with a wall temperature of 20°F. The data from Test 018 is presented in Figure 8.5-14. The oil temperature increase from 150°F to 330°F caused the radiator inlet pressure to drop 37% from 46 to 29 psia. The initial oil pressure in the lube system prior to startup was 15 psia during Tests 017 and 018. Prior to Test 019, the oil system pressure was decreased to 2-3 psia. This was accomplished by utilizing a vacuum pump. The cell pressure was then reduced to 0.4 mm Hg for a simulation of a lunar startup. Test 019 continued for 13 minutes before shutdown. Although system oil pressure remained low, there was evidence that startup had occurred. The test was terminated because the oil flow distribution was upset by the low pressure drop that existed across the ball bearing. A greater portion of the flow was induced to flow through the alternator cooling jacket which now had a reduced back pressure in the oil separator from 15 to 1.0 psia. Pressure dependency on oil viscosity is clearly shown in Figure 8.5-15. The overall lubrication system performance is shown in Table 8.5-1.

DVR Thermal Results

The test summary presented in Table 8.5-2 correlates the thermal profile figure and test parameters. The oil temperature in and out of the radiator is shown in Figure 8.5-16 as a function of load. At 3 KW load, the oil temperature drop across the radiator was 12°F. Oil temperature at the radiator inlet was decreased 51°F when the altitude chamber wall temperature was decreased from 160 to 20°F. Typical radiator performance is presented in Figure 8.5-17. DVR test results showed that the radiator was 95% efficient. Bearing and face seal temperatures as a function of load and ambient cell temperatures are shown in Figures 8.5-18

and 8.5-19. The maximum face seal and bearing temperatures are 520 and 400°F, respectively. The difference in temperatures existed because the primary heat source of the face seal was conduction from the scroll. The bearing temperatures were approximately the same.

TABLE 8.5-1

HEPS LUBRICATION SYSTEM PERFORMANCE

1. Pressure Lube Pump	280 psia (maximum) @ 20°F - 1.0 gpm capacity 50 psia (maximum) @ 400°F - 1.0 gpm capacity
2. Scavenge Pump	2.75 psia - 2.0 gpm capacity
3. Oil Filter	Particle removal - 10 micron nominal with a bypass when ΔP = 60 psi
4. Oil Relief Valve	25-50 psia - adjustable
5. High Speed Roller Bearing	.11 gpm with ΔT = 60°F
6. High Speed Ball Bearing and Seal	.23 gpm with ΔT = 70°F (oil to bearing) ΔT = 80°F (oil to seal)
7. Alternator Cooling Jacket	.66 gpm
8. Oil Separator Vent	18 psia
9. Oil Radiator	ΔP = 5 psia @ 370°F oil temp. Maximum ΔT recorded 12°F Heat rejection = 2250 Btu/hr
10. Oil Separator	Capacity = 190 in^3 of MIL-L-23699 Oil (PQ 6423)

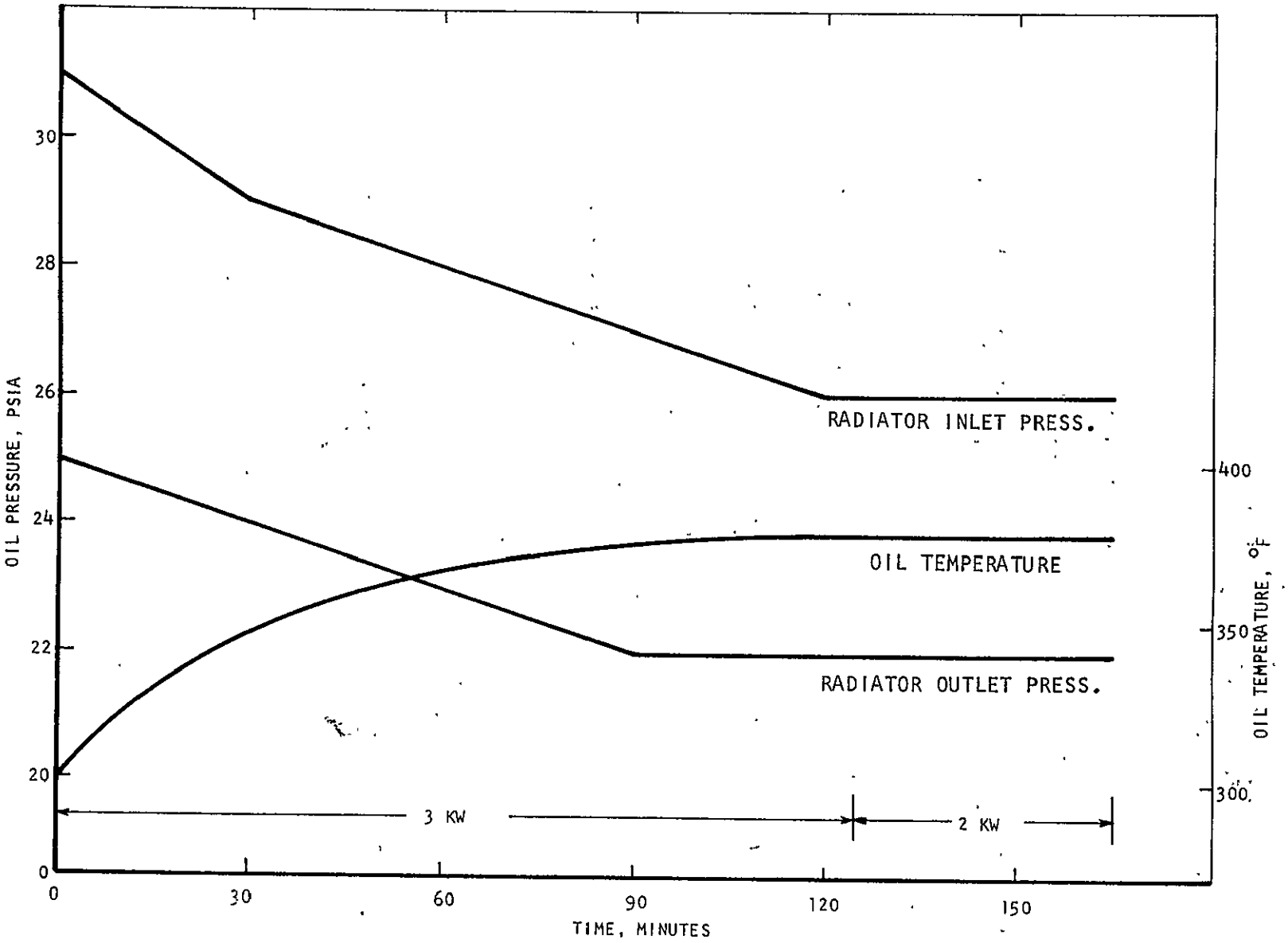


FIGURE 8.5-12 TEST 010-4.1-017 - 160°F AMBIENT - OIL FLOW: 0.9-1.0 gpm

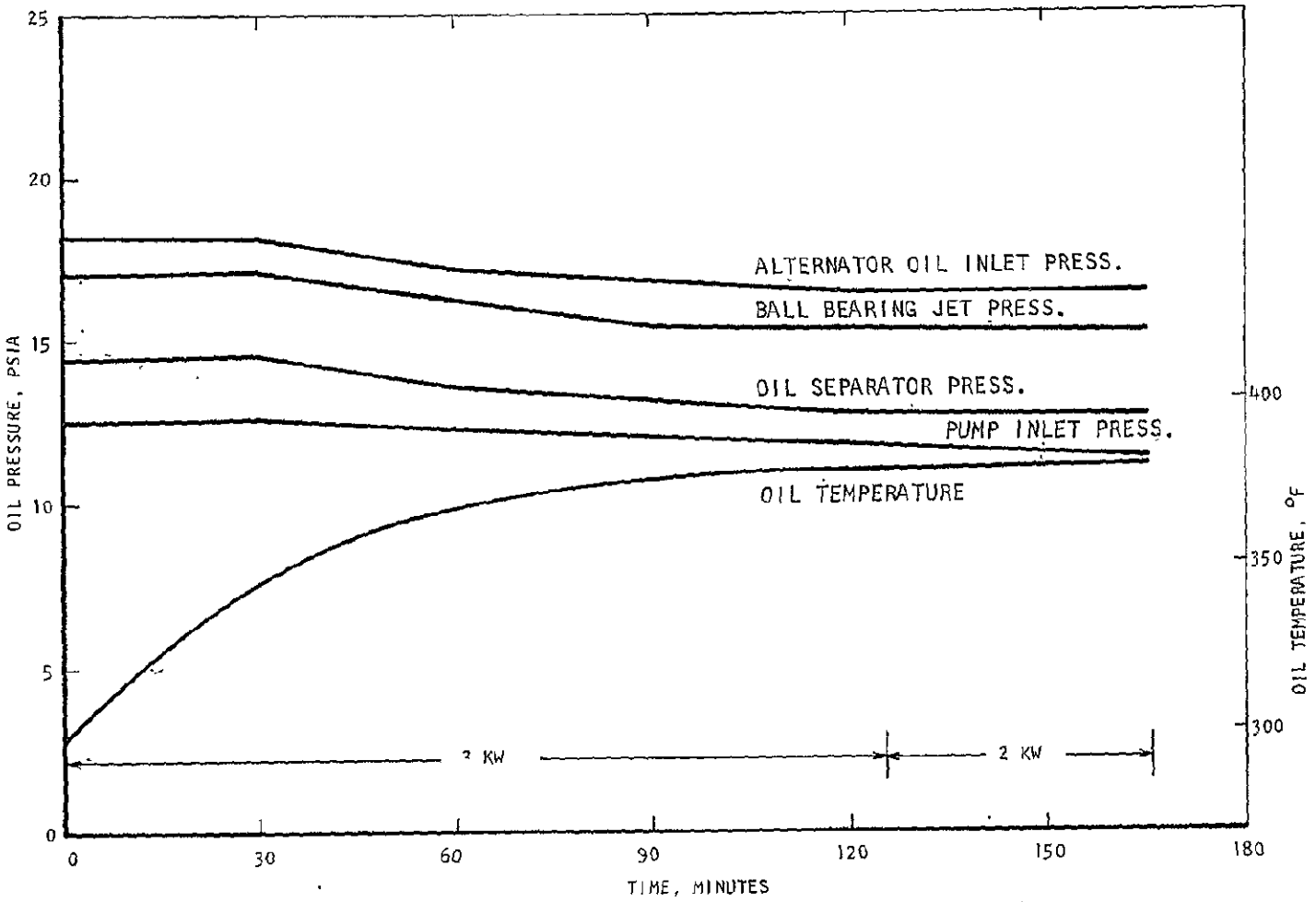


FIGURE 8.5-13 OIL PRESSURE AND TEMPERATURE VERSUS TIME

TEST 010-4.1-017
160°F AMBIENT
0.9-1.0 gpm OIL FLOW

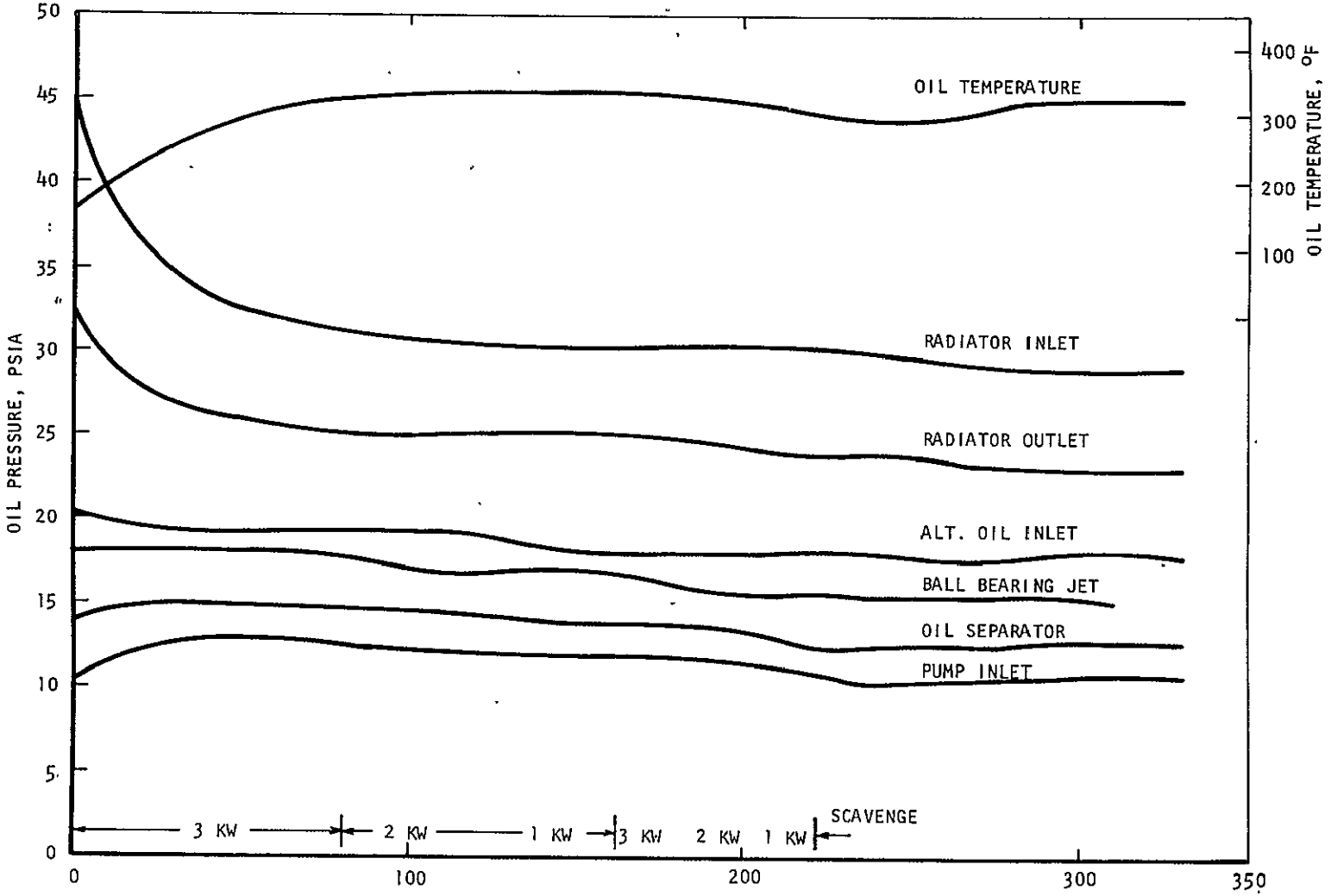


FIGURE 8.5-14 OIL PRESSURE AND TEMPERATURE VS. TIME

TEST 010-4.1-018, -019
20°F AMBIENT
1.04-1.09 gpm OIL FLOW

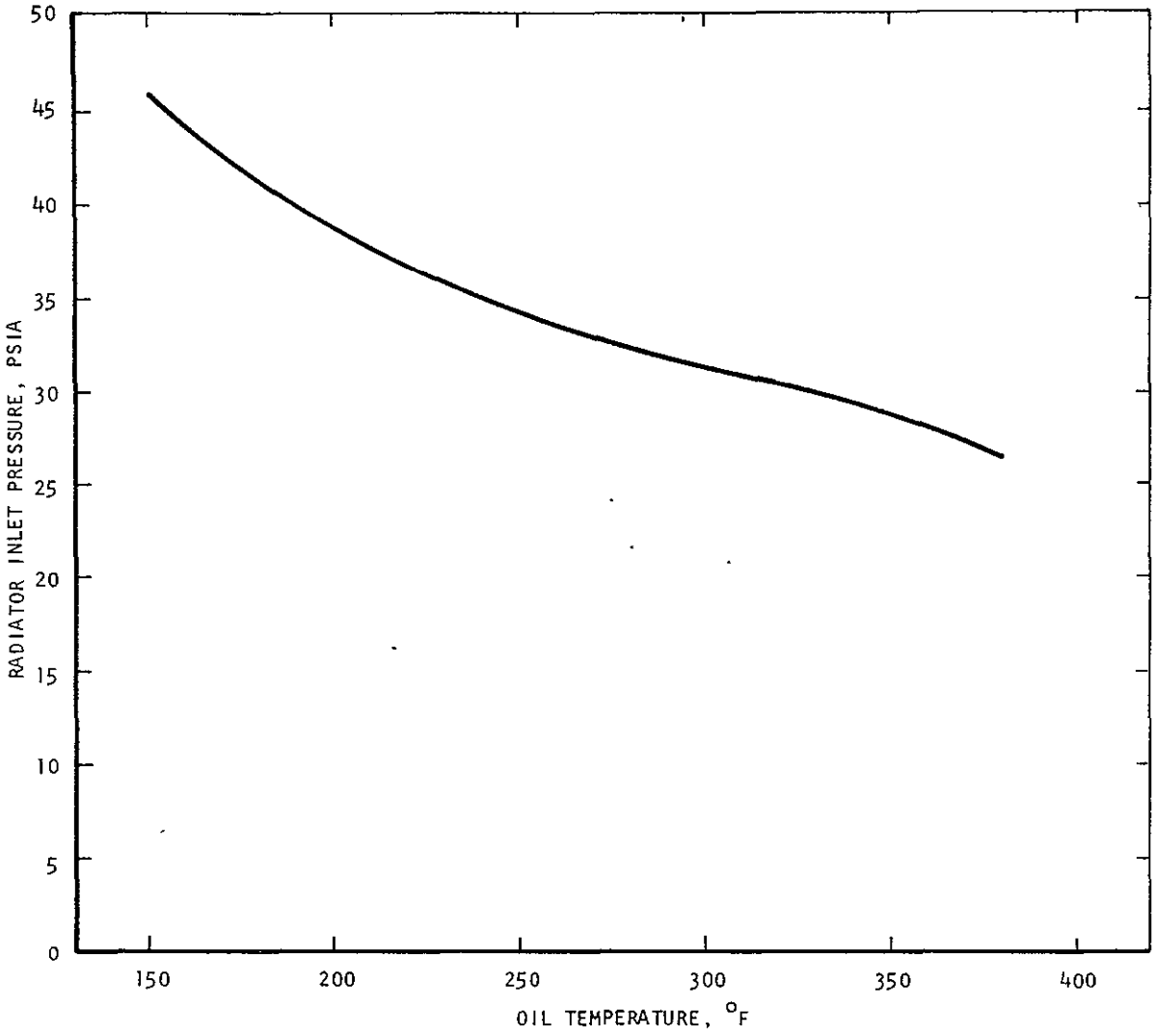


FIGURE 8.5-15 RADIATOR INLET PRESSURE VERSUS OIL TEMPERATURE
DVR SYSTEM TEST 010-4.1-017,-018
OIL FLOW: 0.9-1.09 gpm

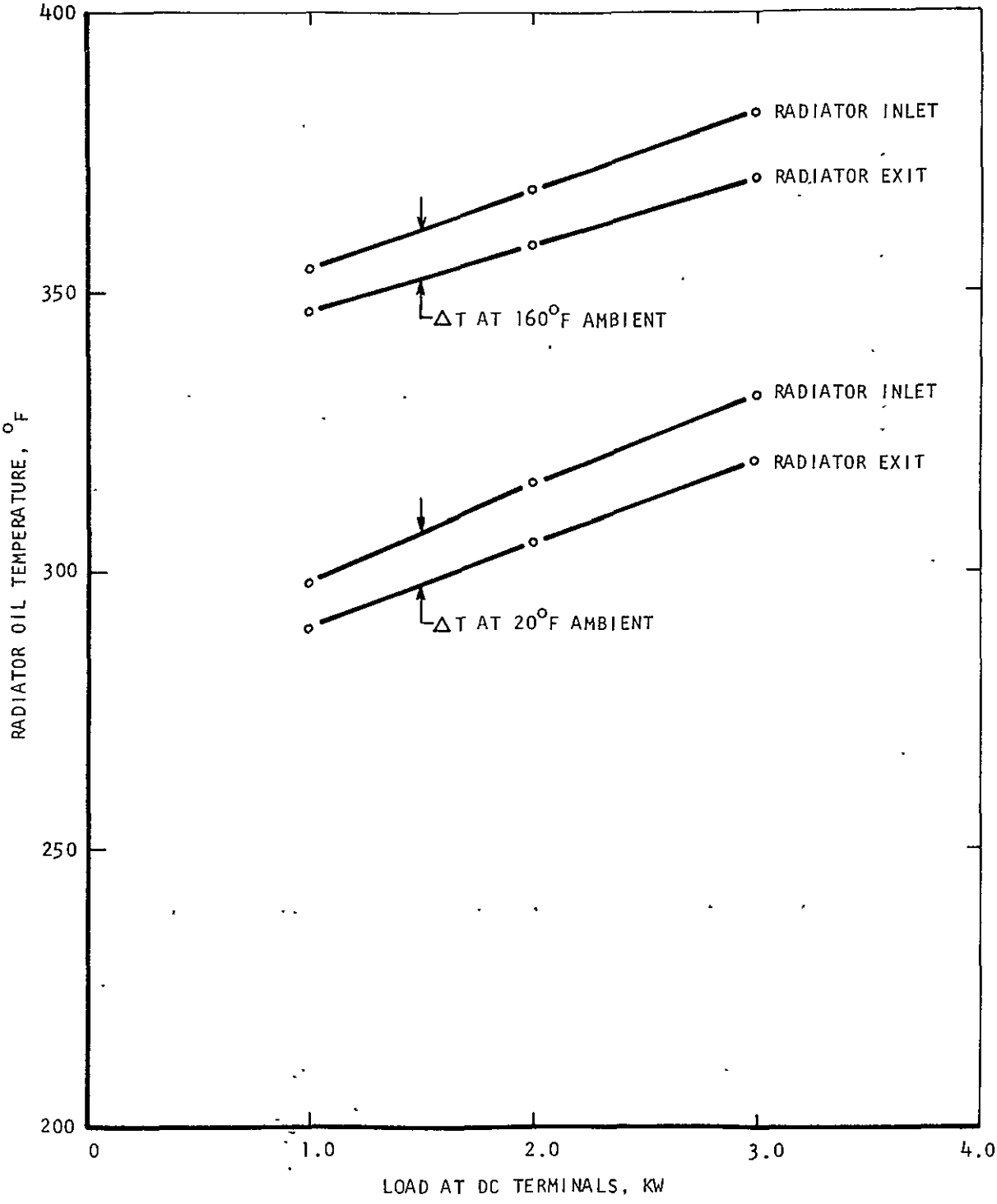
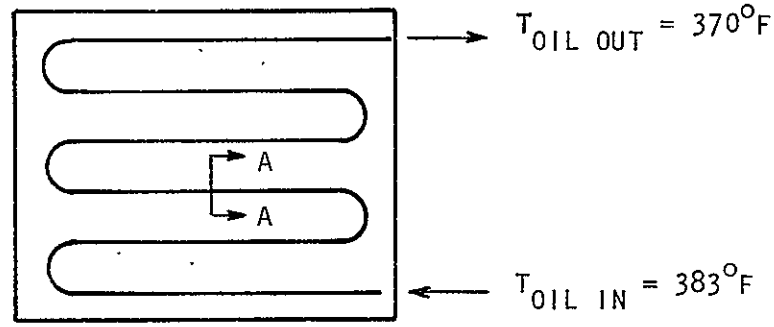
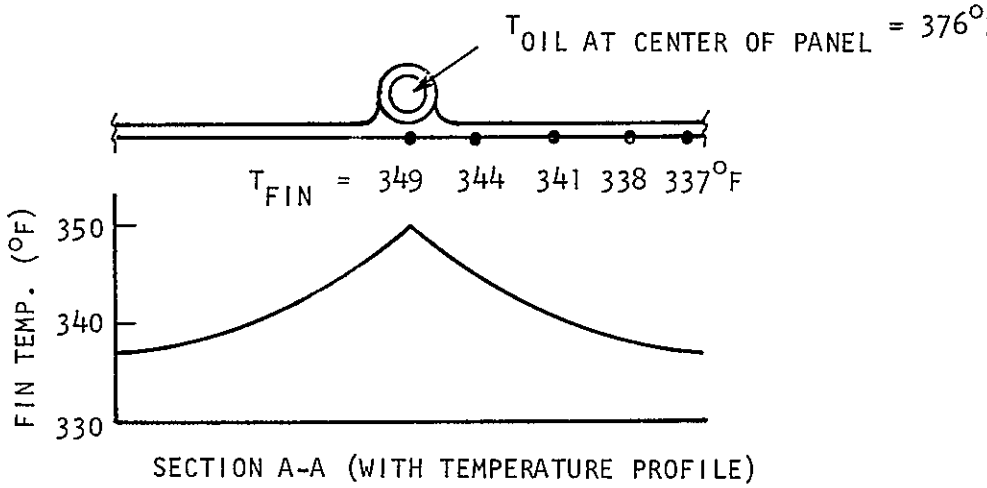


FIGURE 8.5-16 OIL TEMPERATURE VERSUS LOAD

3KW LOAD
160°F AMBIENT TEMPERATURE
APPROX. 0.9 gpm OIL FLOW
SINGLE RADIATOR PANEL





SECTION A-A (WITH TEMPERATURE PROFILE)

BASED ON THE FIN TEMPERATURE PROFILE, THE FIN EFFICIENCY IS: $\eta_F = 0.95$

TOTAL HEAT REJECTED FROM SINGLE RADIATOR PANEL IS:
Q_T = 2470 BTU/HR

FIGURE 8.5-17 OIL RADIATOR TEMPERATURE PROFILE AND PERFORMANCE

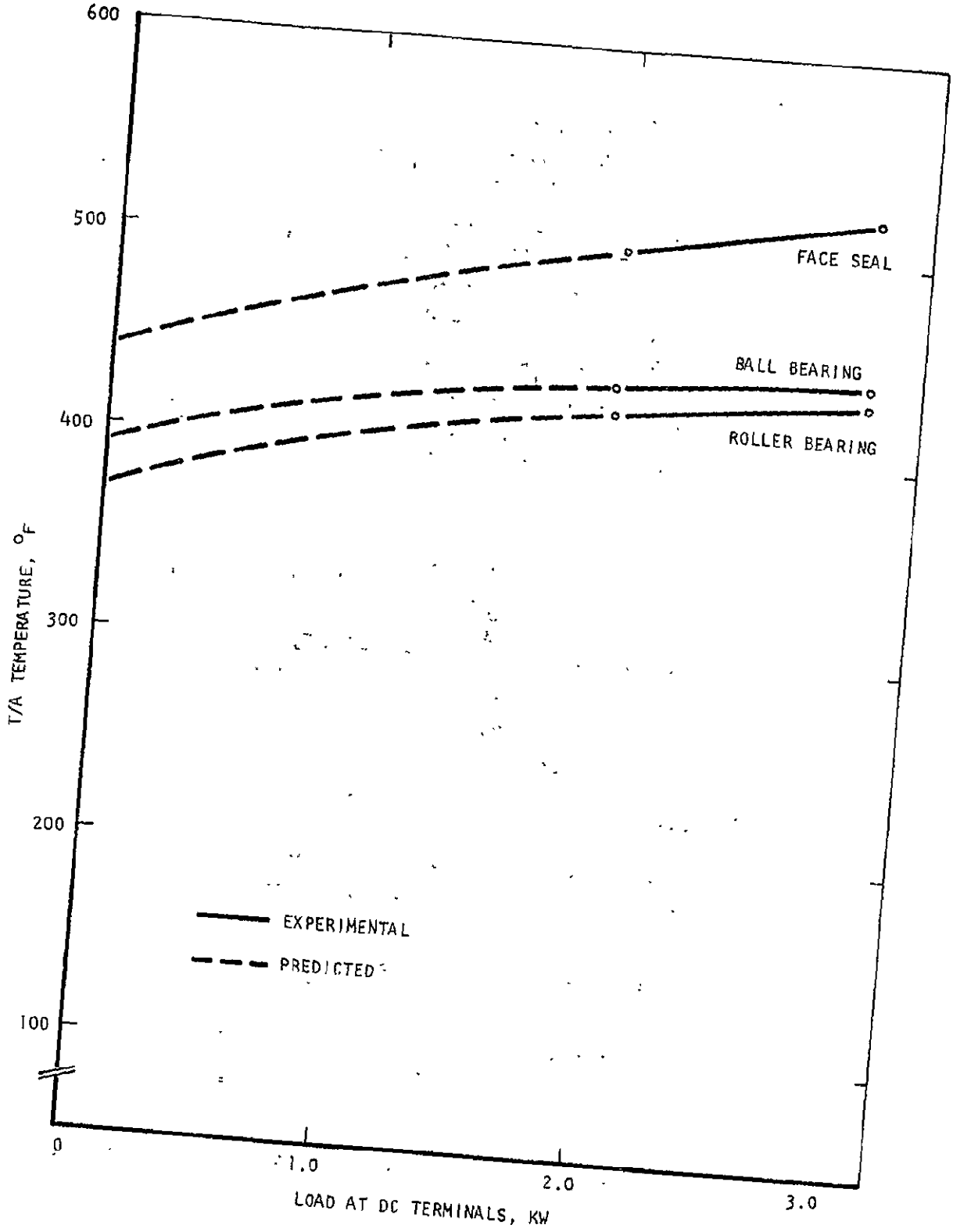


FIGURE 8.5-18 T/A TEMPERATURE VERSUS LOAD (160°F AMBIENT)

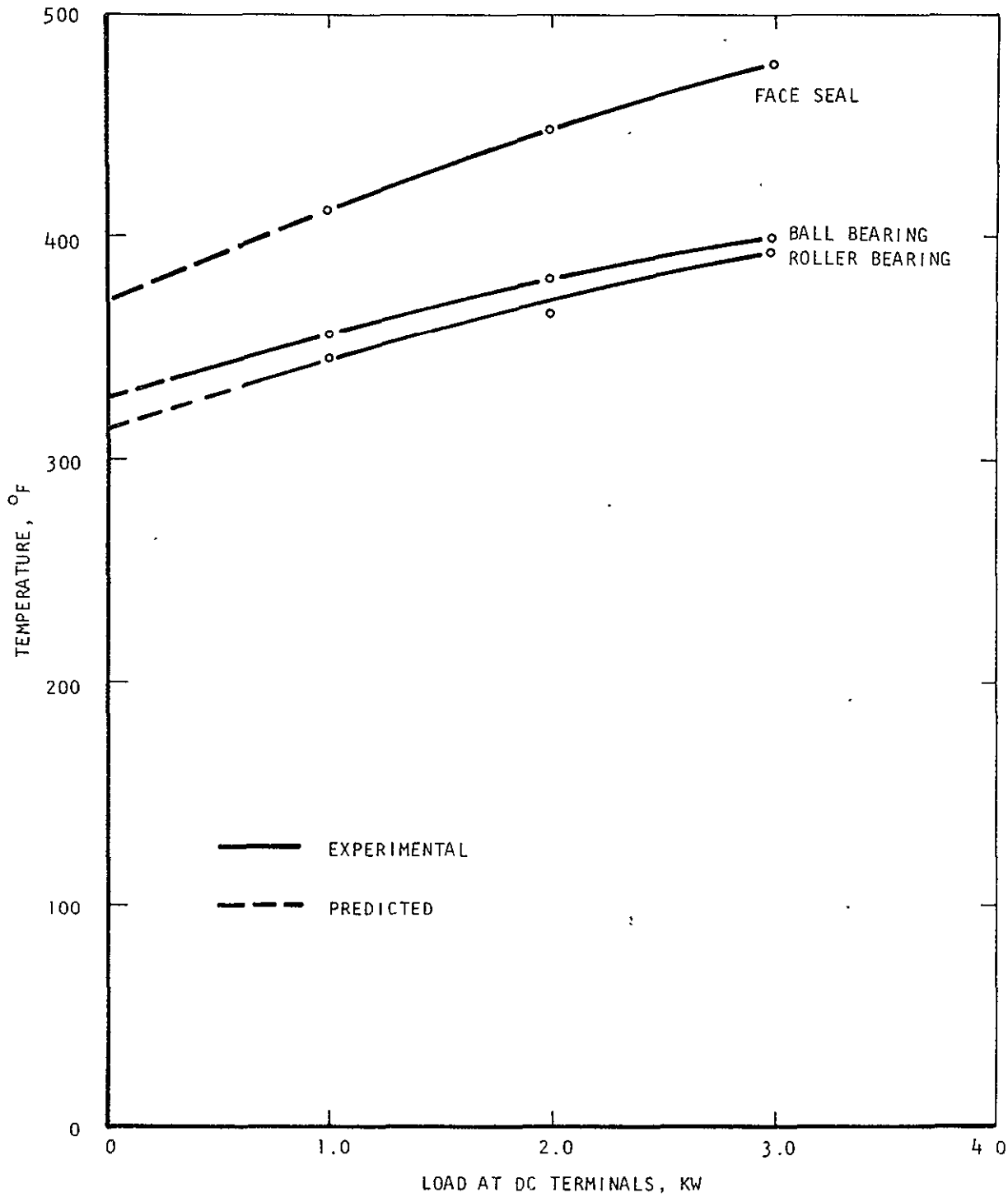


FIGURE 8.5-19 TEMPERATURE VERSUS LOAD (20°F AMBIENT)

TABLE 8.5-2

DVR TEST AND DATA CORRELATIONS

Test No.	Altitude mm Hg	Propellant Pressure	O/F Ratio	No. of Pulses	Plate Coil Temp. °F	Corresponding Figures 4.5-
010-4.1-001	0.35	200 psig	Low	8		
010-4.1-002	0.35	200 psig		15		
010-4.1-003	0.35	200 psig		15		
010-4.1-004	0.3	200 psig		15	Plate	
010-4.1-005	0.3	200 psig		8	Coil	
010-4.1-006	0.4	200 psig		10	Cooling	Transient
010-4.1-007	0.6	200 psig		16	Not	Temperature
010-4.1-008	0.45	200 psig		70	Used	Data
010-4.1-009	0.45 to 0.55	200 psig		85		
010-4.1-010	0.44 to 0.5	200 psig		70		
010-4.1-011	0.5 to 0.95	200 psig	Low & High	013		
010-4.1-012	0.8 to 1.35	200 psig	Low & High	1080		
010-4.1-013	0.35 to 0.6	200 psig	Low & High	113		
010-4.1-014	0.29 to 0.45	200 psig	Low & High	308		
010-4.1-015	0.25 to 0.95	200 psig	Low & High	1620	70	
010-4.1-016	0.36 to 0.65	200 psig	Low & High	--	160	16,17,22,23,24
010-4.1-017	0.35 to 0.8	200 psig	Low & High	--	160	16,17,21,22,23, 24,26,27
010-4.1-018	0.55 to 0.85	200 psig	Low & High	2175	20	16,18,22,23
010-4.1-019	0.4 to 0.65	200 psig	Low	28	--	

The thermcouple locations and temperature profiles for the alternator mount and mounting rail are shown in Figures 8.5-20 and 8.5-21, respectively. The alternator attachment arm temperature was 450°F under the most severe test condition. The rectifier cold plate thermocouple location is shown in Figure 8.5-22. The mid-panel lower diode stud temperature was selected for presentation because its thermal level was representative of the entire cold plate temperatures. Also, it was the most critical item on the cold plate because of its temperature limitation. The diode stud temperature versus load profile is shown in Figure 8.5-23. The relocation of the cold plate resulted in a 36°F decrease. The effect of the chamber ambient temperature was to decrease the stud temperature 64°F when the ambient decreased from 160 to 20°F.

Gas generator and scroll temperatures are presented in Figure 8.5-24. At 3.0 KW the injector temperature was 246°F. Also, at 3.0 KW, the radial temperature difference from the extreme inner edge to the extreme outer edge in the scroll fin was 85°F. The heat reflector thermocouple locations and temperature profiles are shown in Figures 8.5-25 and 8.5-26. At 3.0 KW, the resultant temperatures were 650, 870 and 1120°F from the outer radius to the inner radius. Results indicated that the heat reflector was successfully shielding the alternator and other components that operated at a considerably lower temperature level. The 400°F temperature drop from the inner radius of the heat reflector to the outer radius showed that the path of thin stainless steel prevented conduction and promoted heat removal by radiation. The large temperature differential that was observed between the scroll and the fin shown in Figure 8-5-24 indicated that additional heat could be rejected from the scroll for a cooler operation. The higher scroll heat rejection either by conduction or radiation would decrease the scroll temperature. Representative frame temperatures are presented in Figure 8.5-27. The maximum temperature of 340°F is considerably below the allowable level dictated by material stress/temperature characteristic.

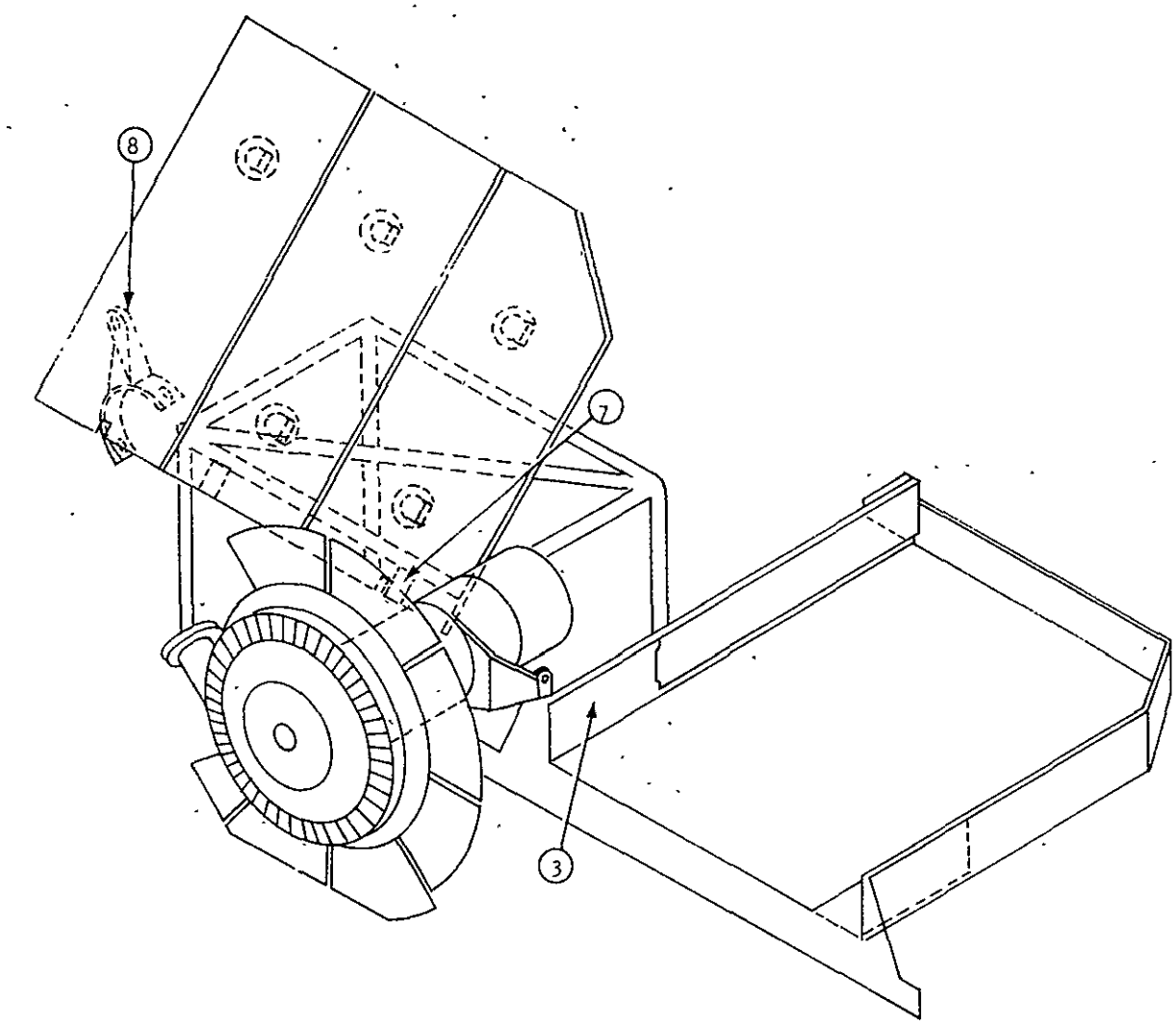


FIGURE 8.5-20 ALTERNATOR MOUNT AND MOUNTING RAIL THERMOCOUPLES

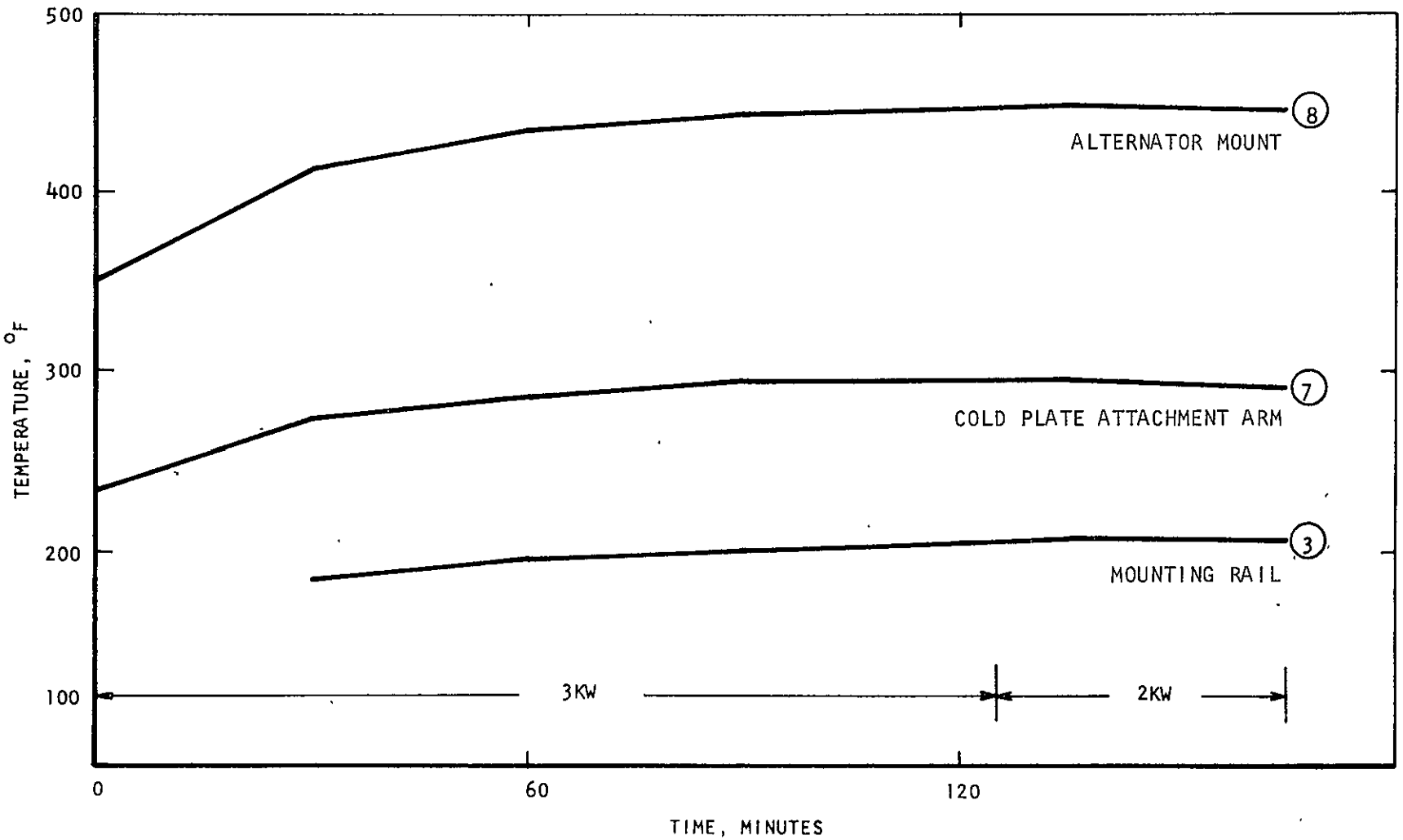


FIGURE 8.5-21 ALTERNATOR MOUNT AND RAILS TEMPERATURE PROFILE (SEE FIGURE 8.5-20)

TEST 010-4.1-017
160°F AMBIENT

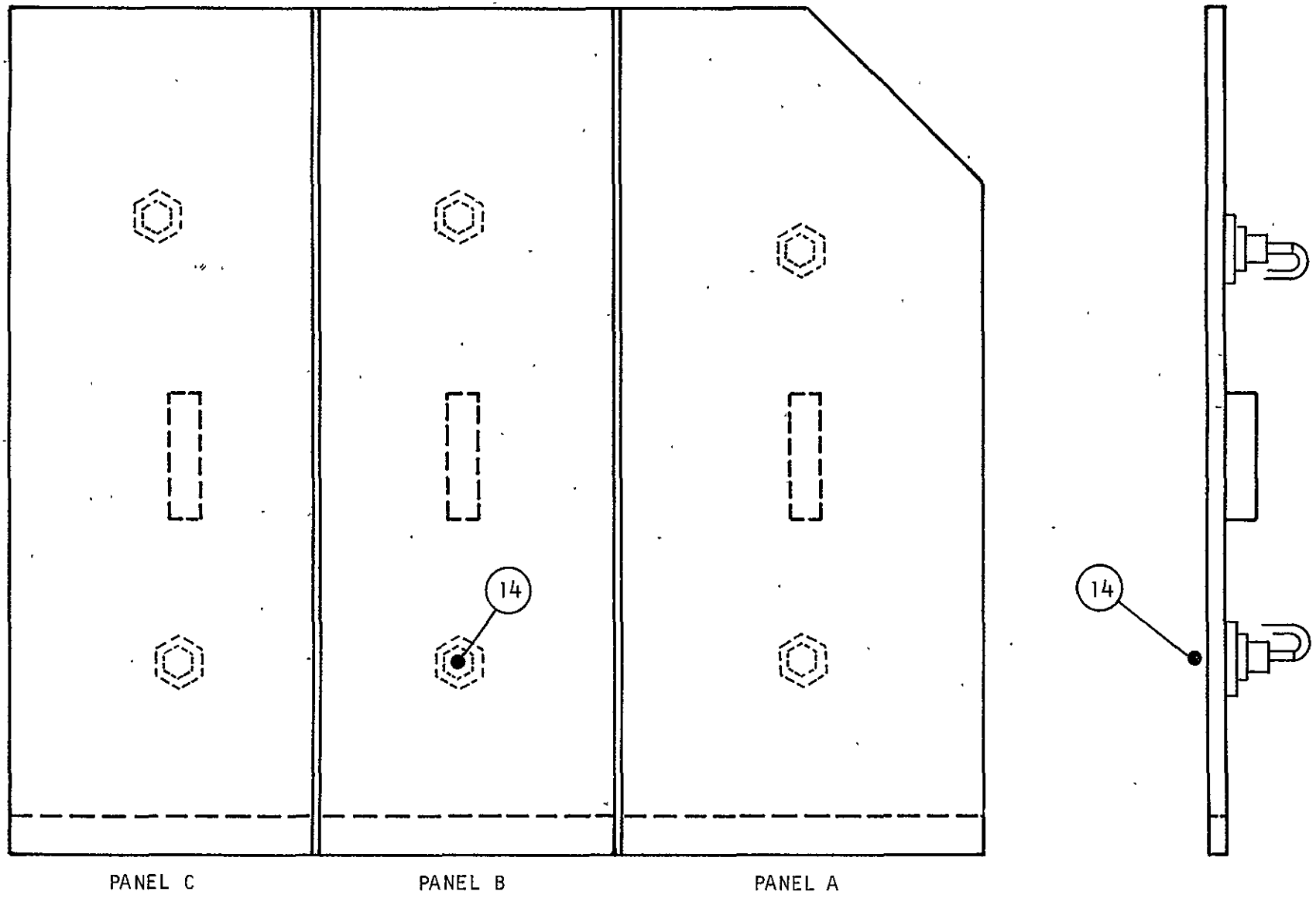


FIGURE 8.5-22 RECTIFIER COLD PLATE THERMOCOUPLE

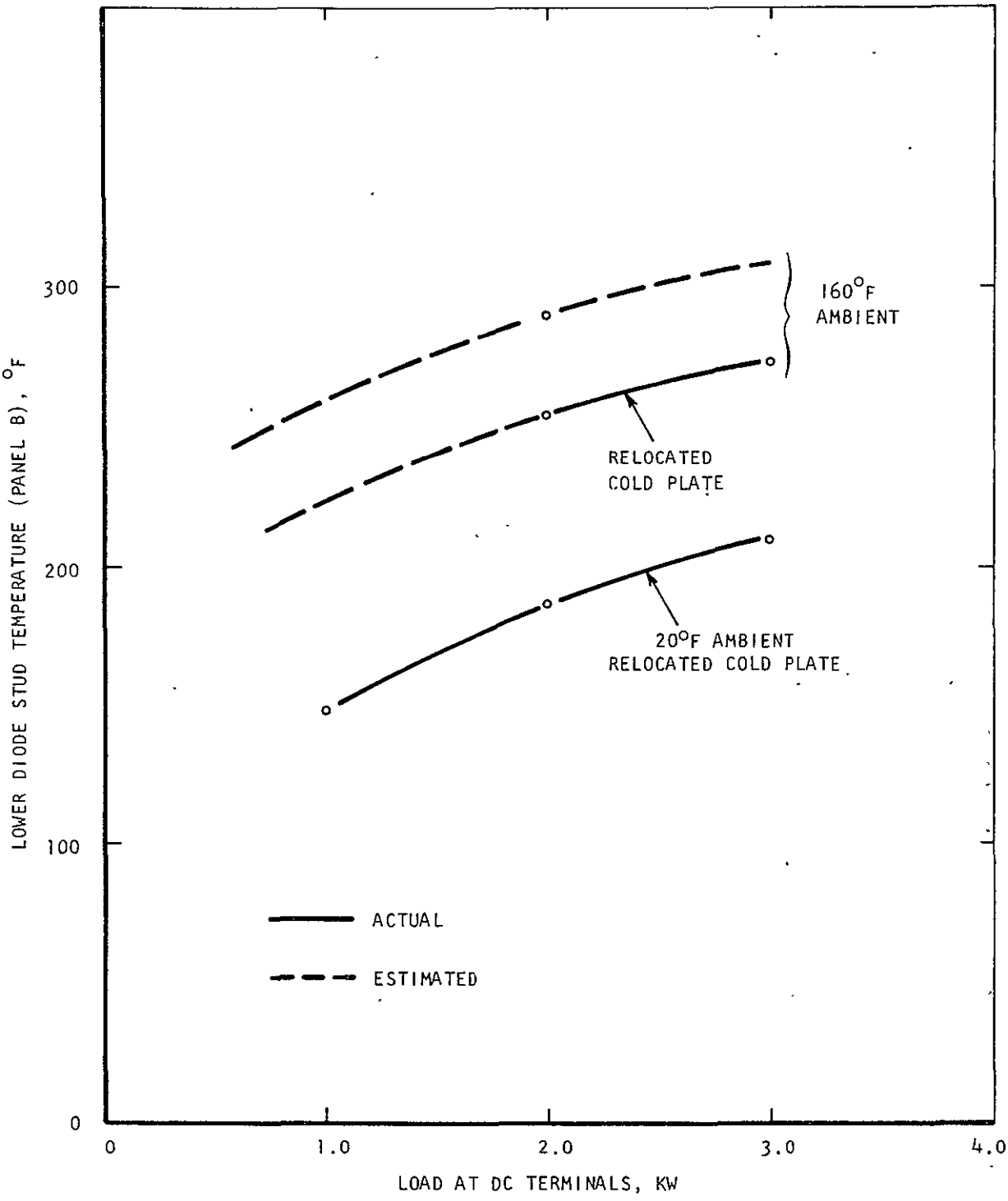


FIGURE 8.5-23 LOWER DIODE STUD TEMPERATURE VERSUS LOAD (THERMOCOUPLE NO. 14 - SEE FIGURE 8.5-22)

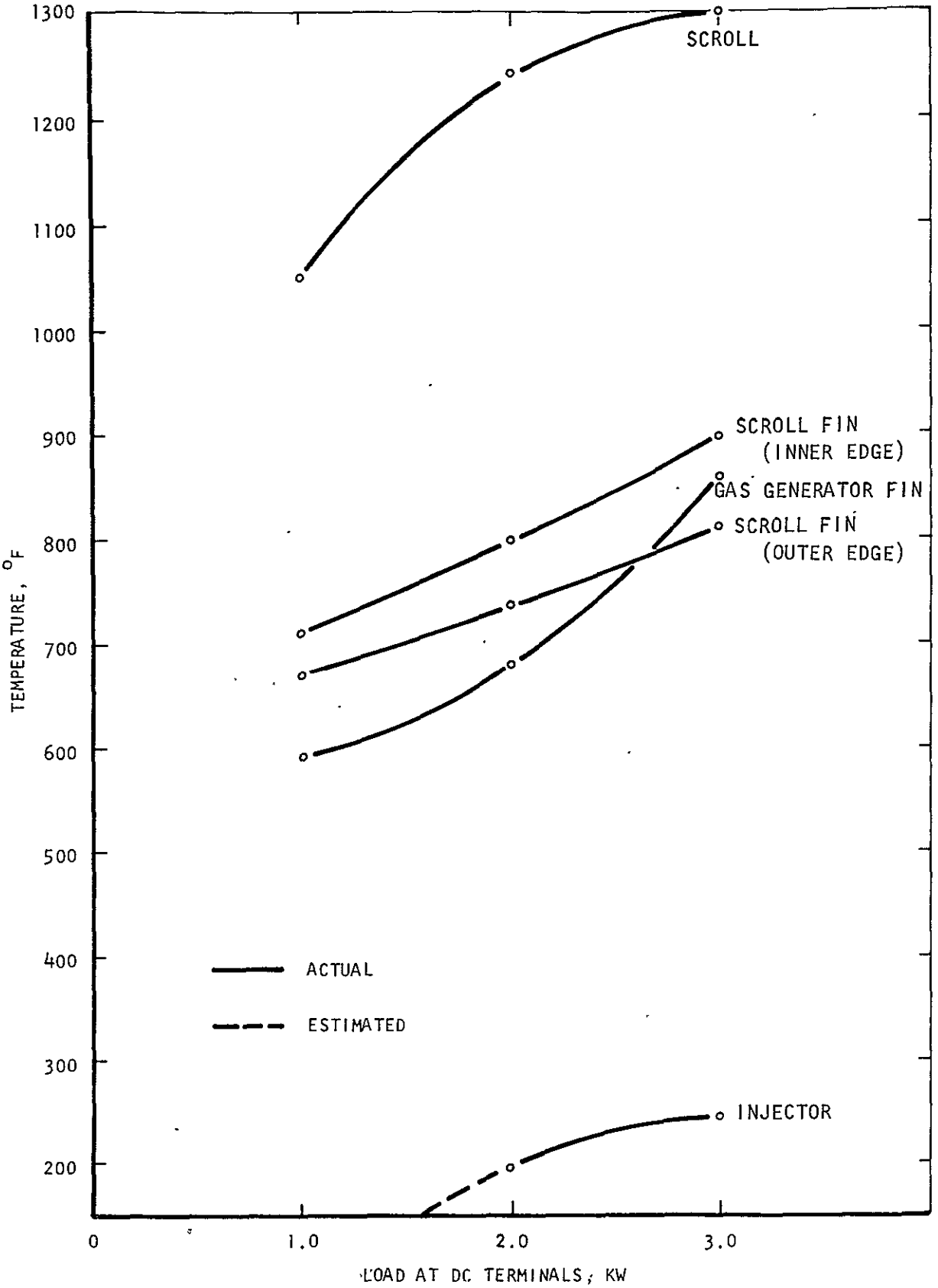


FIGURE 8.5-24 TEMPERATURE VERSUS LOAD

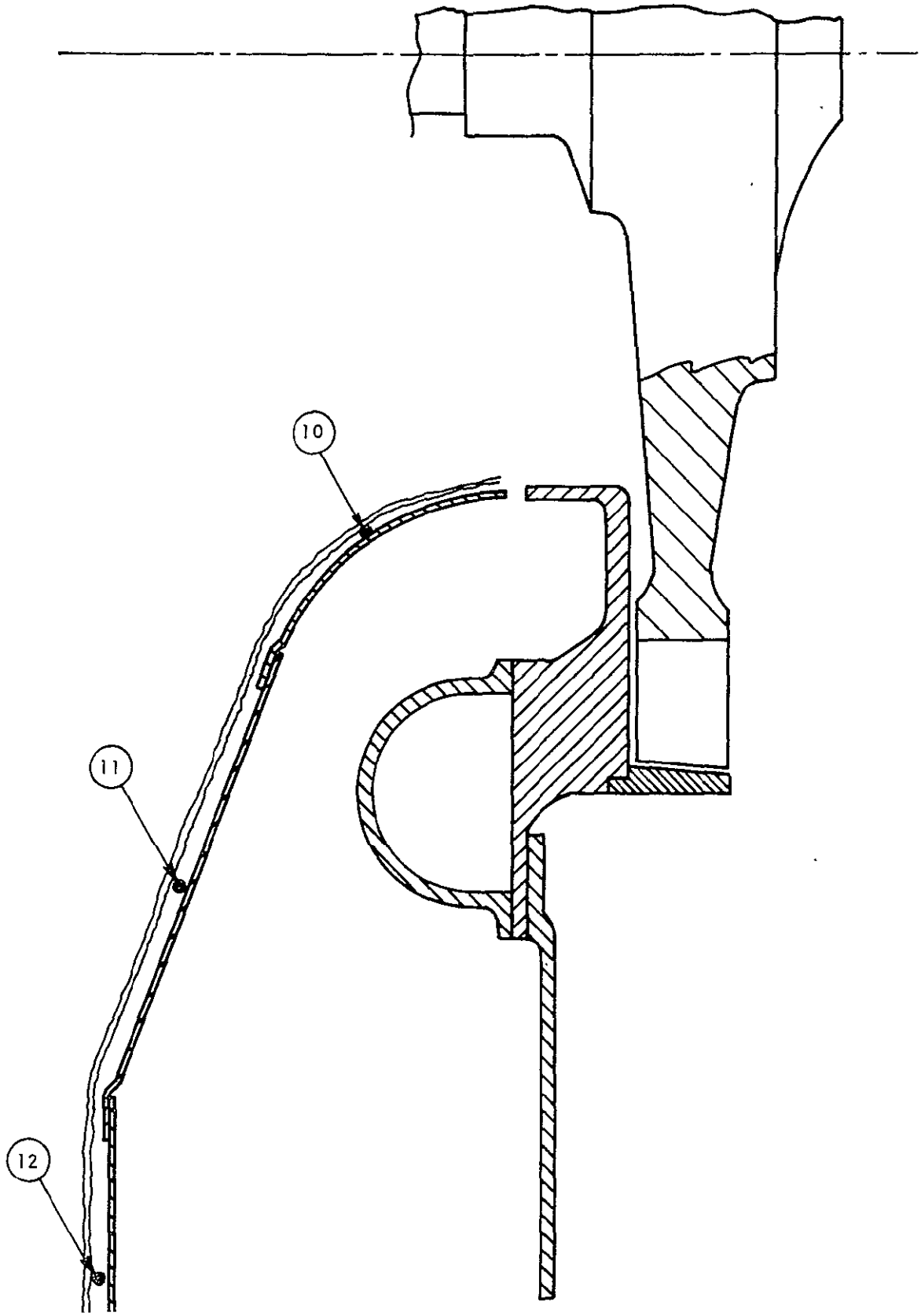


FIGURE 8.5-25 HEAT REFLECTOR THERMOCOUPLES

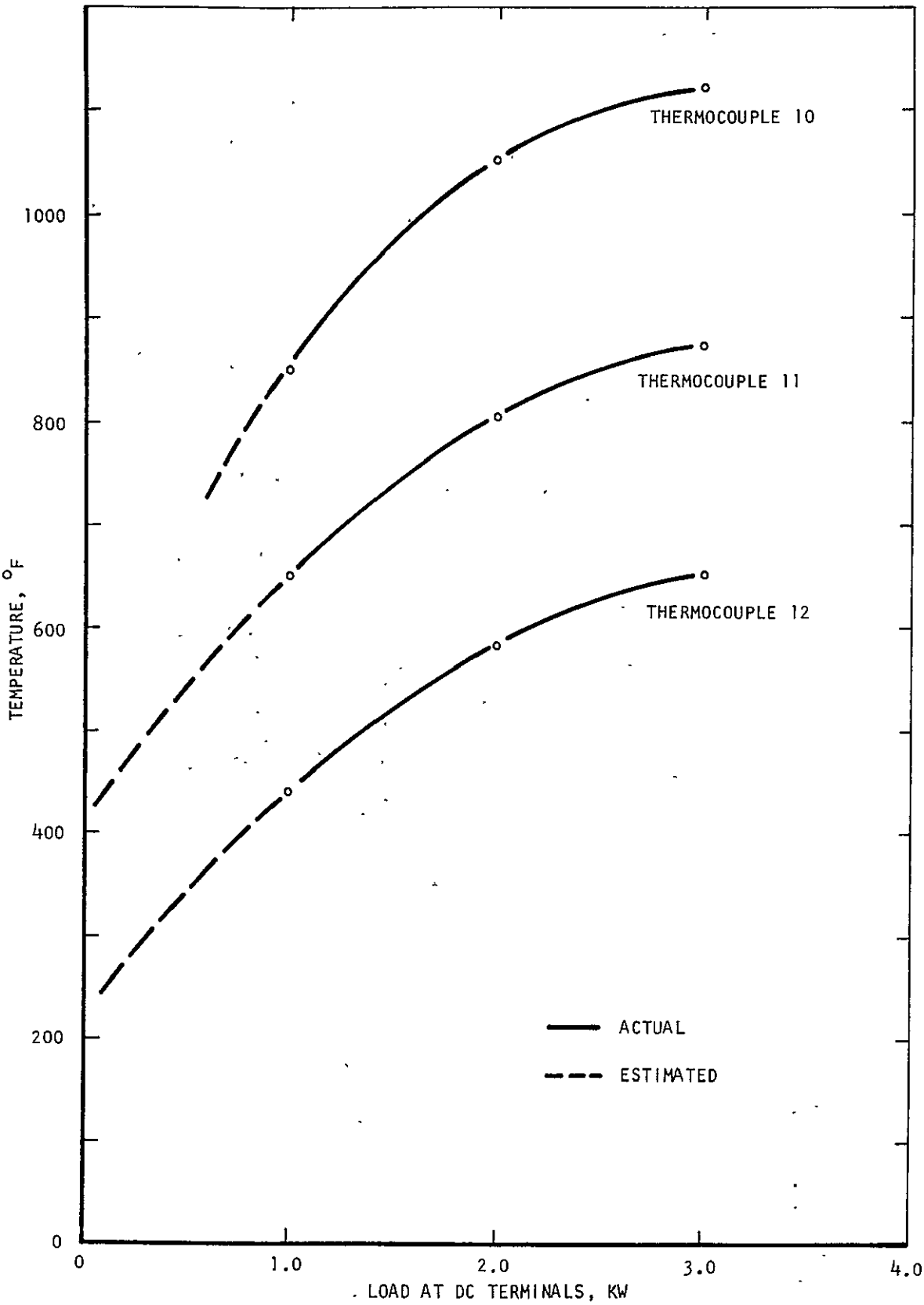


FIGURE 8.5-26 REFLECTOR TEMPERATURE VERSUS LOAD

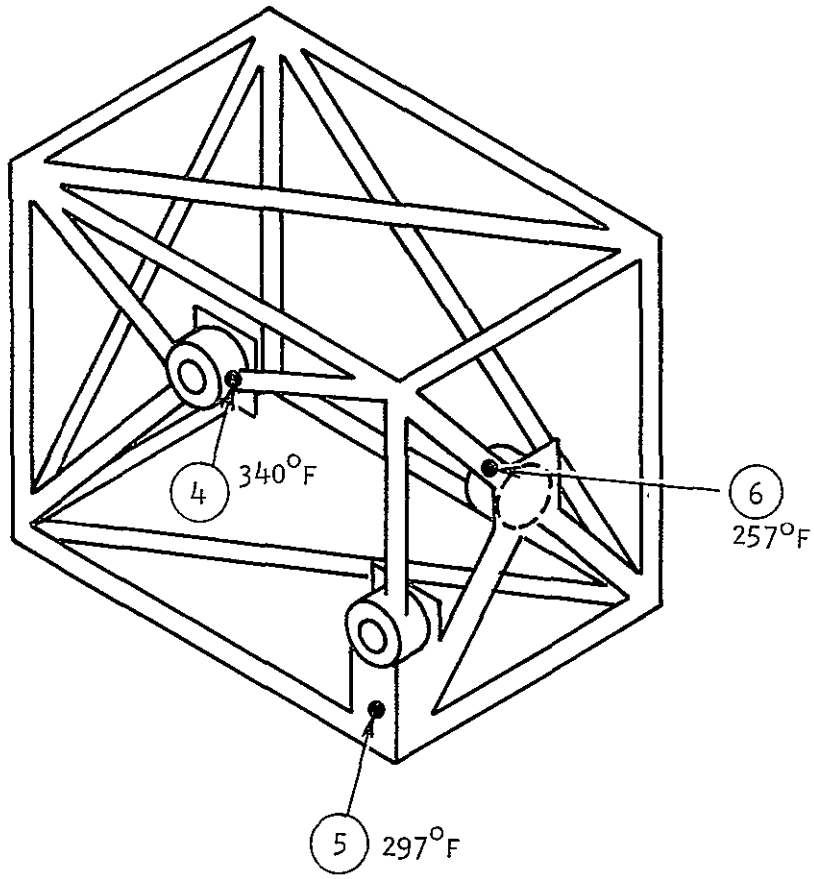


FIGURE 8.5-27 FRAME TEMPERATURES AT 3KW

PRECEDING PAGE BLANK NOT FILMED.

9.0 QUALIFICATION PROGRAM

Prior to the scope of work change, the Phase III program plan included a Qualification Test program. Two Qualification Units were to be fabricated, assembled, and Tested in accordance with the Qualification Test plan. Subsequently, a single Qualification Unit will be fabricated and subjected to the Acceptance Tests only. The following Section 9.1 is a discussion of the intended Qualification and Acceptance Tests.

9.1 Qualification and Acceptance Tests

The Qualification Tests were to be conducted in the following sequence:

Startup
Acceptance
Humidity
Vibration
Acceptance
Shock
Acceptance
Acceleration
Acceptance
Thermal Vacuum
Endurance

The Acceptance Test is an operational test conducted for the purpose of establishing and comparing performance before and after the Qualification Tests. The test was to be conducted at altitude and 77°F ambient with 0-4.5 KW loads being applied.

The Humidity Test was to be performed in accordance with MIL-STD-810B, Method 507, Procedure 1. The minimum and maximum test temperatures were 40 and 110°F, respectively.

The Vibration Test consisted of sinusoidal and random vibration combinations that simulated ground handling, launch, spaceflight and lunar landing that would be experienced during a LM lunar landing mission. The vibration schedules were consistent with the work statement requirements. The schedules are itemized in the DVR test plan (see reference 9).

The Shock Test was to be conducted in accordance with MIL-STD-810B, Method 516, Procedures I and II. The shock pulse shape was a sawtooth with 10 to 12 millisecond rise and 0 to 2 millisecond decay with a 30 g peak value.

The Acceleration Test as defined in the DVR test plan (see reference 9) was a simulation of the expected environment for a lunar mission.

The Startup Test was to be conducted for the evaluation of the system operation and performance over a wide speed range so that system shutdown or failure could be avoided at rated speed. The startup test sequence is shown in Table 9.1-1.

Thermal Vacuum testing was to include system operation over a 0-4.5 KW load profile with ambient temperatures of 20°F, 77°F and 160°F.

The Endurance Test for the Qualification Units was to be a 100 hour continuous test during which time the load profile shown in Figure 9.1-1 was to be followed.

9.2 Quality Assurance

The Quality Assurance effort was two-phased: the specification and control of product quality and the verification of product quality conformance to design requirements. In effect, the quality assurance plan (reference 10) delineated the quality activity associated with establishing the configuration requirements, controlling the manufacturing processes to meet the requirements, and the verification and documentation that the requirements were met.

9.3 High Reliability Parts Program

A NASA/MSC high reliability parts program was implemented on the HEPS Phase III program and was applicable to the electrical and electromechanical component parts for a qualification build of a flight-type HEPS unit (see reference 11). However, the Moog bipropellant valves were excluded. The parts program included a statement of quality and a parts requirements list. Prior to HEPS program changes, 95% of the electrical components were fully controlled by the conditions described in the parts program.

Statement of Quality

All purchased electrical and electromechanical parts were governed by vendor quality requirements (VQR) guaranteeing workmanship, quality and traceability. Such guarantees were verified by certificates of conformance.

TABLE 9.1-1

STARTUP TEST SEQUENCE

Test No.	Minimum Altitude, ft	Propellant Pressure, psig	O/F Ratio	No. of Pulses	Speed, rpm	Load, Kw	Chamber Temp., °F	Test Time, min.
1	120,000	200 ± 2	0.9	10	10,000	0	77 ± 5	<1
2	"	"	"	20	20,000	0	"	<2
3	"	"	"	25	25,000	0	"	<3
4	"	"	"	30	30,000	0	"	<4
5	"	"	"		33,000	0	"	<5
6	"	"	"		33,000	1	"	<5
7	"	"	2.0		33,000	2	"	<5
8	"	"	0.9		33,000	3	"	<5

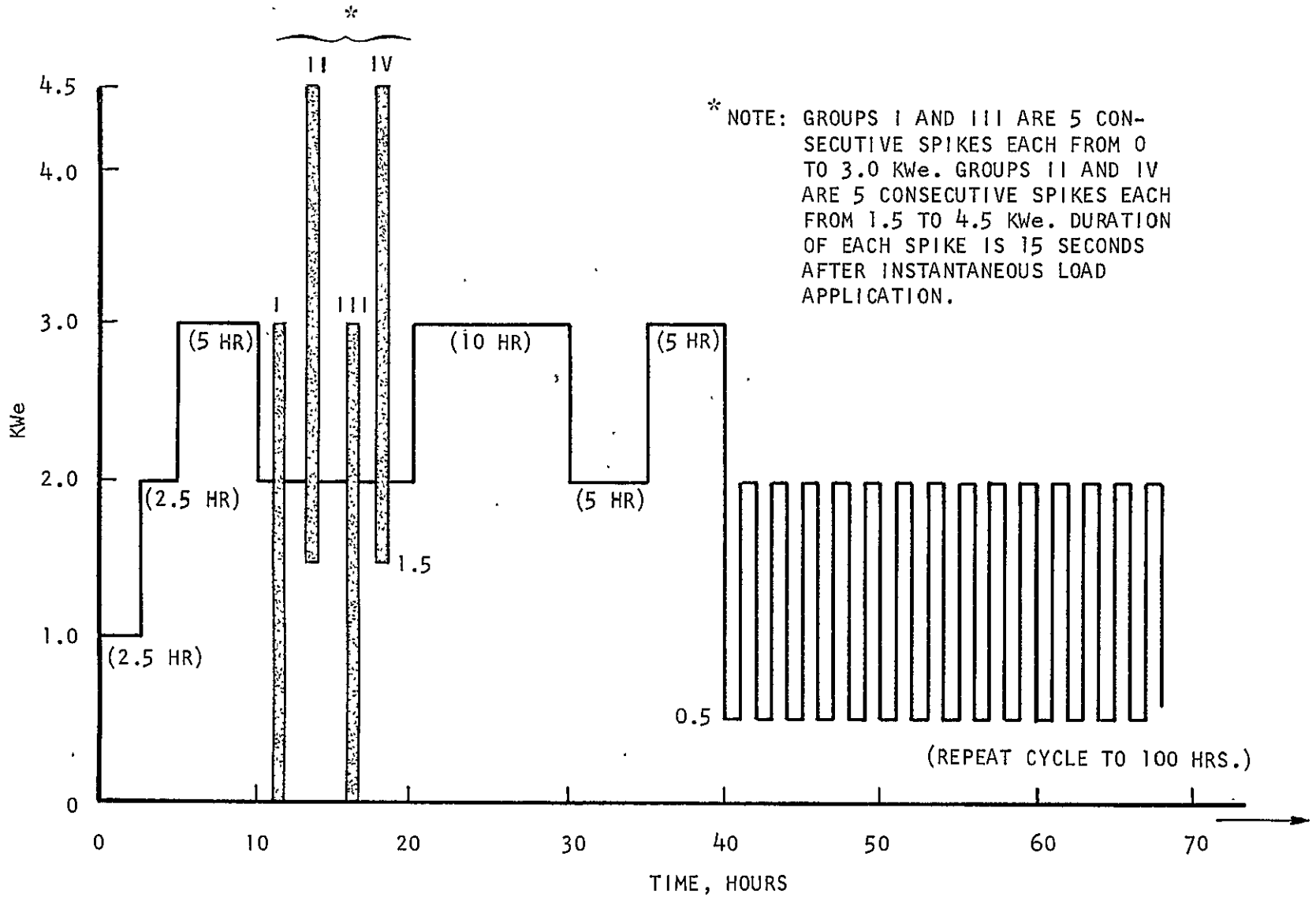


FIGURE 9.1-1 POWER PROFILE

Parts Reliability Requirements List

Approximately 95% of the purchased electrical and electromechanical components were screened and successfully passed burn-in acceptance tests on all electrical parts. The screen tests were in accordance with MSC-A-D-66-8, Revision A, Apollo Spacecraft Qualified Parts List.

A part selection report was completed for each dissimilar component and submitted with the component detailed drawing to NASA/MSC for approval. Upon approval the component description and electrical characteristics were entered in the approved parts list and the part ordered. This list was updated on a monthly basis and submitted to NASA/MSC for review (see reference 12).

PRECEDING PAGE BLANK NOT FILMED.

10.0 RELIABILITY

The HEPS incorporates a pulse-driven turboalternator to provide up to 4.5 KW DC electrical power on the lunar surface. The turbine wheel speed is regulated by the electrical control subsystem which regulates the pulsing rate of the bipropellant valves. Safety shutdown features located in this subsystem will shut down the system when activated automatically. To restart the HEPS after an automatic shutdown, the astronaut must reset the circuits within the electronic control subsystem and then continue with the startup procedure sequence. An automatic shutdown is initiated by any one of the following conditions: turbine wheel overspeed, under voltage-frequency circuit, over temperature, under oil pressure and over voltage. These safety features prevent the loss of the turbine wheel or system destruction caused by certain malfunctions.

The reliability of the current HEPS design is 92.2% for a 50 hour mission. With slight modification of the propellant control valves, the system reliability could be increased to 98.8%.

10.1 Failure Modes and Effects Analysis

A Failure Modes and Effects Analysis (FMEA) was completed to the piece part level (see reference 13). The analysis was basically in two sections, one section for the electronic sybsystem and the other for the mechanical subsystems. The latter subsystems include the turboalternator, lubrication subsystem, the gas generator and the flight package. If a component malfunctions in the HEPS, one of the following events will result: 1) system fails to start, 2) system fails to restart, 3) system remains operational, 4) system shuts down in a safe condition, and 5) system is permanently disabled. These system failure modes were ranked according to their criticality, I being the most critical resulting with possible loss of personnel, II being the next most critical which requires the HEPS to be shut down and not restarted, and III the least critical type of failure mode. All of the types I and II failure modes were thoroughly investigated analytically or by tests. All of the failure modes were grouped in the above listed five categories and are shown in Figure 10.1-1 as a percent of the total failure modes.

The number of all electrical and mechanical failure modes by Type I, II and III for each of the failure mode categories are shown in Table 10.1-1. For most malfunctions, the reset indicator light on the control panel will be on; however, there are a few instances where there is no indication of a malfunction. The state of indicator lights for failure mode types and categories is shown in Table 10.1-2.

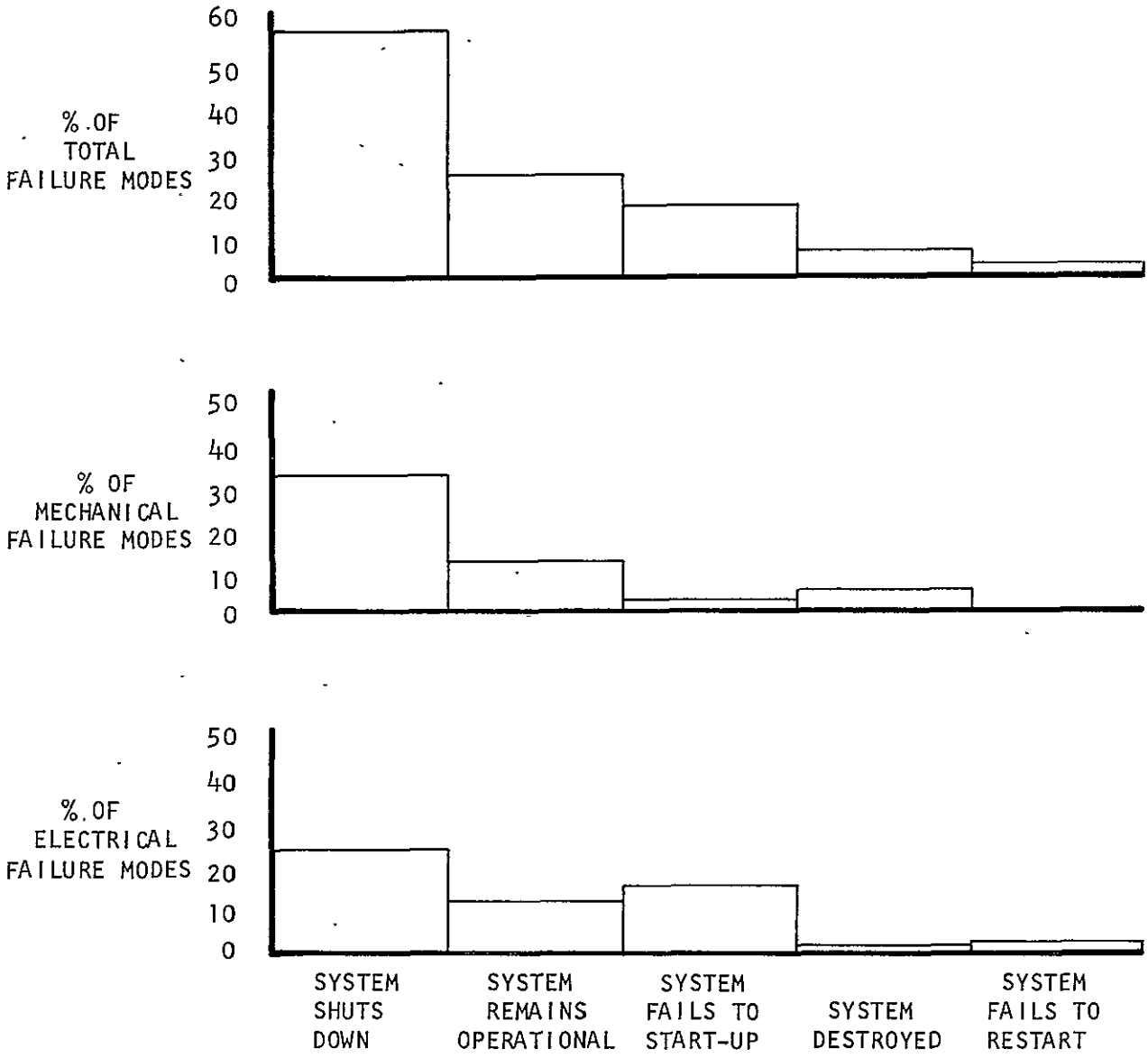


FIGURE 10.1-1 PERCENTAGES OF TOTAL FAILURE MODES FOR VARIOUS SYSTEM CONDITIONS

TABLE 10.1-1

SUMMARY OF TYPE FAILURES FOR VARIOUS SYSTEM CONDITIONS

	Failure Mode Type	System Shuts Down		System Remains Operational		System Fails To Start-Up		System Destroyed		System Fails To Restart	
MECHANICAL FAILURE MODES	I	2	0	0	0	0	0	0	9*	0	0
	II	1	1*	1	0	1	0	0	3*	0	0
	III	59	10*	22	2*	6	1*	0	0	0	0
ELECTRICAL FAILURE MODES	I	0	0	0	0	0	0	0	2*	0	0
	II	1	0	0	0	0	0	0	0	0	0
	III	53	1*	27	0	29	0	0	0	2	0
TOTALS:		116	12*	50	2*	36	1*	0	14*	2	0

*Number of failure modes that exist for each type and category where HEPS start or restart is not recommended.

TABLE 10.1-2

STATE OF INDICATOR LIGHTS FOR VARIOUS SYSTEM CONDITIONS

Category	System Fails to Startup			System Shuts Down			System Fails to Restart			System Remains Operational			System Destroyed		
Type	I	II	III	I	II	III	I	II	III	I	II	III	I	II	III
Armed Indicator Lignt DS1 Remains On		1	22			3					1				
Reset Indicator Light DS2 Is On			1*	1	2 1*	79 9*						1*	2*		1*
DS2 Remains On			1			1			2						
DS2 Will Not Light												3			
Transfer Indicator Light DS3 Is On At Startup												1			
Power Output Indicator Light DS4 Is Not On			1												
DS4 Remains On						1									
All Indicators Are Off			2	1		29 2*						45 1*	7*	2*	2*

*Number of failure modes that exist for each type and category where HEPS start or restart is not recommended.

DS1, DS2, DS3, DS4 defined in Figure 4.3-3.

10.2 Critical Components

There are certain components that are classified as "critical" based on system dependency. The failure modes and criticality are discussed in reference 14. The two most critical components are the bipropellant valves and the turbine wheel.

If a bipropellant valve fails open, the turbine wheel speed will increase; if a flexure tube fails, it may cause the valve to rupture. The turbine wheel speed increases 1400 rpm during a 200 ms pulse. Therefore, for the wheel speed to equal or exceed its burst speed, which is 50,000 rpm, the valve must be open for approximately 2.4 seconds. For this reason, there are two automatic overspeed shutdown circuits that are included in the electronics which operate independently of each other.

The probability of the turbine wheel rupturing in 50 hours is 0.00016 (see reference 15). However, rupture may still be caused by other mechanical and/or electrical failures. Therefore, a loss of turbine wheel failure mode fault tree was constructed (see reference 13). The fault tree clearly shows the criticality of possible failures in the electronic control subsystem. The design of this subsystem is such that two failures among the safety shutdown circuits must occur to be detrimental to the safety of the astronauts.

10.3 HEPS Reliability Analysis

The HEPS reliability analysis considered the following basic subsystems: turboalternator, lubrication system, gas generator, electrical control system and the flight package. The corresponding reliabilities of these subsystems were designated R_T, R_L, R_G, R_E and R_F, respectively. Components within each of these subsystems were considered to constitute a mathematical series function. The total HEPS reliability, R_H, was equal to the product of the startup, operation and shutdown reliabilities given by R_S, R_O and R_D, respectively. Certain components in the electrical control subsystem were operating during all three phases and, therefore, were included in the appropriate phase reliability computation. Furthermore, since some of the components were pulse operated, the corresponding reliabilities were given by the binomial probability function for zero failures. The remaining components were under stress at all times during startup, operation and shutdown and were given by the normal exponential time dependent function. The number of pulses or cycles and the time was considered for startup, operation and shutdown, and the associated component reliabilities evaluated. These results were then used to evaluate R_S, R_O and R_D.

The total HEPS reliability is:

$$R_H = R_S \times R_O \times R_D = 92.2\%$$

10.4 Redundant Bipropellant Valve Assembly

The bipropellant valves in the current gas generator design were physically mounted in parallel with only one employed at a time. Automatic shutdown due to overspeed of the turbine wheel will be initiated if an unused valve leaked propellants to the injector. From a failure mode analysis and reliability viewpoint, the valves were considered to be connected in series. This yielded a low reliability for the gas generator and thus for the complete system. An increase in the system reliability could be realized if the two propellant shutoff solenoid valves are replaced by four solenoid valves. The solenoid valves would be arranged in parallel at the inlet to each bipropellant valve. This would make the unused bipropellant valve completely isolated. The gas generator model is shown in Figure 10.4-1. With bipropellant valve A in operation, valve B is considered standby redundant. The gas generator reliability function is now given by:

$$R_G = R_R R_I R_C \left\{ 1 - \left[(1-R_A R_{S_1}) R_A R_{S_1} (1-R_{S_1}) + (1-R_A R_{S_1})^2 \right] \right.$$

where R_R, R_{S_1}, R_C, R_A and R_I are the propellant flexible lines and fittings, the valves electrical switching, combustion chamber, propellant valve and injector reliabilities, respectively. The system reliability for a 50-hour mission using this arrangement would be 98.8% (see reference 16). Figure 10.4-2 shows a graph of the system reliability as a function of system operating time for the HEPS system for the redundant and nonredundant bipropellant valves.

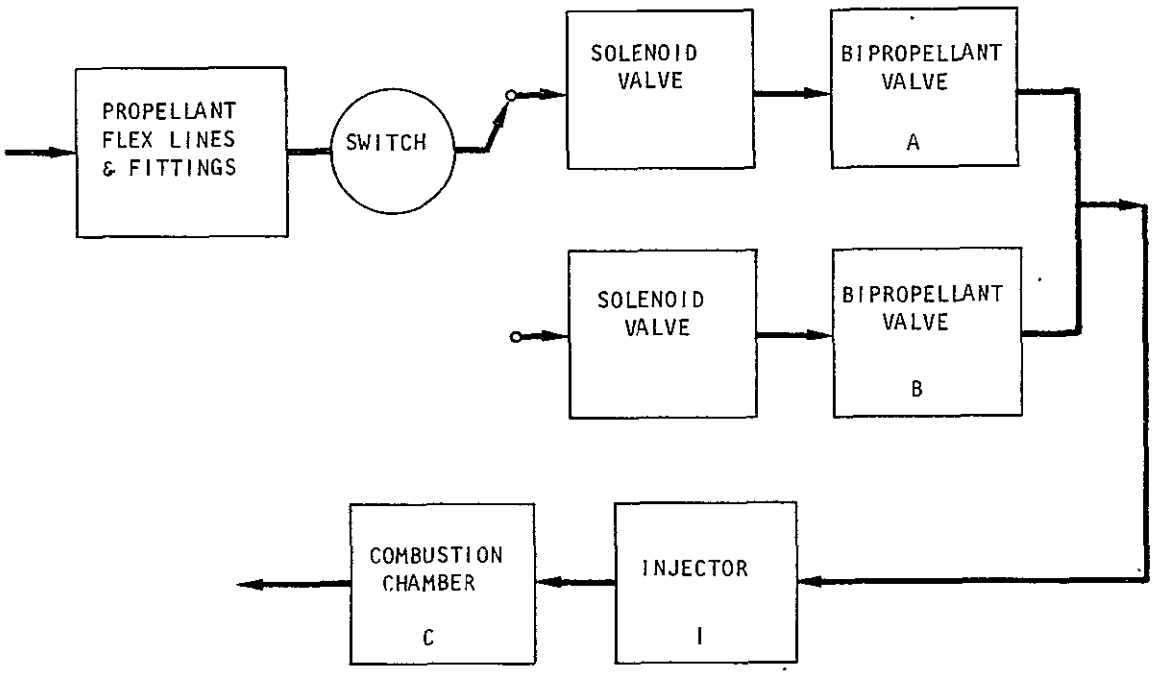


FIGURE 10.4-1 A FUNCTIONAL BLOCK DIAGRAM OF A MODIFIED GAS GENERATOR ASSEMBLY

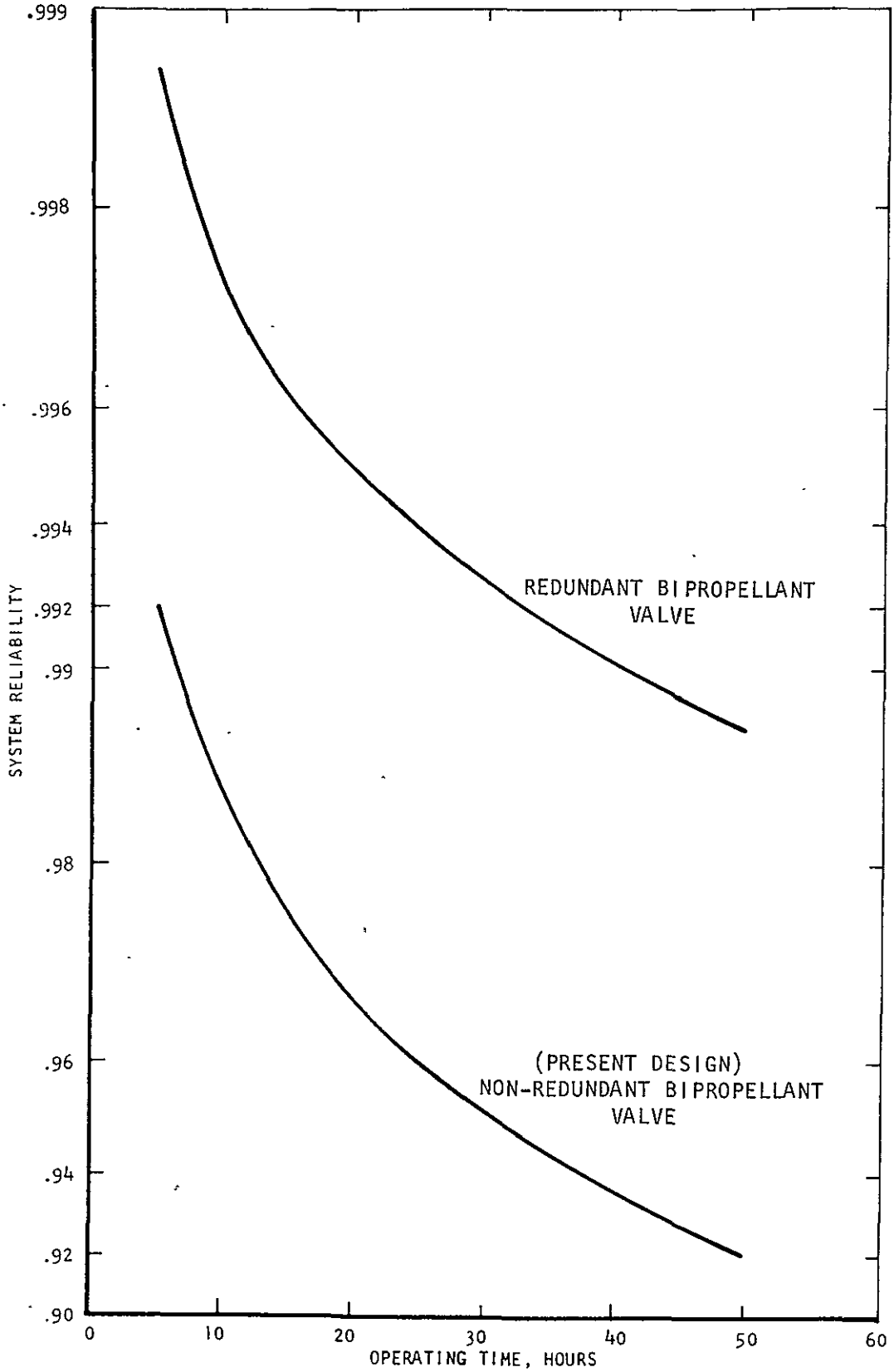


FIGURE 10.4-2 SYSTEM RELIABILITY VERSUS TIME

APPENDIX

HEPS TEST LOG

Early tests were conducted with various orifice combinations to establish the design propellant flow rates. The tests were run at an average altitude chamber pressure of 0.45 mm Hg. Each test consisted of approximately ten pulses during which time three pulses were recorded on a CEC oscillograph. The propellant inlet pressures were set at 200 psig. Prior to testing, 2.5 quarts of turbo-oil were added to the phase separator. In addition, the lube system and propellant lines were leak checked prior to start. The resultant propellant flows and orifice combinations are as follows:

	LOW O/F	HIGH O/F
w_f	.174 lb/sec (no orifice)	.1100 lb/sec (.069 in. dia.)
w_{ox}	.165 lb/sec (.071 in. dia.)	.2250 lb/sec (no orifice)

REPRODUCIBILITY OF THE
ORIGINAL PAGE IS POOR

Test 011-4.1-001, 002	The altitude chamber pressure was 0.4 mm Hg. Preliminary testing to set O/F ratios began. However a pulse did not occur even though the N system was energized properly. An unnecessary attempt was made to restart. It appeared as though the electrical system was not functioning properly. The system was shutdown to allow visual inspection. The altitude chamber was 1/3 full of ice which had condensed from the steam ejector system and drained into the chamber. The deployed speed control assembly was 1/3 submerged in ice. The plate coil temperature was increased to melt the ice and dry the unit. Three pulses were fired on the low O/F side. No speed indications were observed. Three pulses were then fired on the high O/F side and once again, the speed indicator was not functioning. However, the scroll temperature was 325°F. The pickup connector was wired to the wrong pins. The connector was modified and orifice changes were made.
Test 011-4.1-003 10/2/69	The cell pressure was reduced to 0.35 mm Hg. Three pulses were fired at the low O/F and at high O/F ratios. The oxidizer flowmeter amplifier was not connected and no flow output was observed. The speed was approximately 8000 RPM and the oil flowmeter had started to indicate flow.
Test 011-4.1-004 10/2/69	The chamber pressure was reduced to 0.35 mm and three pulses were fired on both the high and the low O/F ratio sides. Total flow measured was 0.06 lb/second. The scroll temperature was 450°F. In order to increase the total flow, the inlet pressures were increased to 215 psig.
Test 011-4.1-005 10/2/69	The altitude reading was 0.35 mm Hg when firing commenced. Three pulses were fired on both the high and low O/F ratio

825
PRECEDING PAGE BLANK-NOT FILMED

sides. The oil flow was 0.11 gpm and the scroll temperature was 620°F at a speed of 10,000 RPM.

The fuel and oxidizer propellant inlet pressures were set at 200 psig.

Test 011-4.1-006
10/3/69

Three pulses were fired at both 0/F ratios. The results were:

Altitude:	0.35 mm Hg
Scroll Temperature:	520°F
Speed:	9500 RPM
Oil Flow:	.085 GPM

Test 011-4.1-007
10/3/69

An .086 inch diameter orifice was installed on the oxidizer 0.9 0/F side. Testing was initiated following Test No. 1, Paragraph 4.1 of the Acceptance Test Plan. The cell pressure was reduced to 0.55 mm Hg and ten pulses were fired.

The scroll temperature was 620°F at 12,000 RPM. The oil flow was 0.23 GPM.

Test 011-4.1-008
10/3/69

The orifice in the low 0/F oxidizer side was changed from .086 to .076 inch. Three pulses were fired at the low 0/F ratio. The altitude reading was 0.9 mm Hg. The scroll temperature was 250°F at 6000 RPM.

The oil level was checked at the end of the last test and refilled prior to starting Test 011-4.1-008. Inspection revealed no leakage. 500 milliliters had been added. The fuel inlet pressure was increased to 215 PSIG.

Test 011-4.1-009
10/3/69

Test #5 of Table 1 was conducted. The altitude was .35 mm Hg. The scroll temperature was 1050°F. The oil flow was .95 GPM after 25 pulses. The speed control transferred and the unit shutdown. The vibration levels on all channels were 50 g's.

Test 011-4.1-010 10/6/69	The low 0/F oxidizer orifice was reduced to .060 inches. The Kistler pressure transducer was installed in the oxidizer inlet line. Fuel inlet pressure was 215 psig and oxidizer inlet pressure was 200 psig. The axial accelerometer was moved to the upper right gusset of the frame reading in the horizontal plane. The altitude was 0.3 mm Hg. The scroll temperature was 810°F after 32 pulses. The speed control transfer occurred. The field flash occurred at the 20th pulse and was on automatic at the 30th pulse, however the unit shut down on the first speed control pulse. The oil flow was 0.85 GPM.
Test 011-4.1-011 10/6/69	Same conditions and results as Test 011-4.1-010. The low 0/F oxidizer orifice was increased from .060 to .071 inches diameter. Also, the overvoltage shutdown circuit was disabled.
Test 011-4.1-012 10/7/69	The altitude was 0.35 mm Hg when pulsing commenced. The startup was automatically terminated by a safety circuit after the 12th pulse. The low pressure oil switch was disconnected.
Test 011-4.1-013 10/7/69	The unit shut down on the first pulse after transferring from the startup mode to the speed control mode.
Test 011-4.1-014 10/7/69	Reconnected building ground and tested. The unit shutdown on the first pulse after transfer.
Test 011-4.1-015 016 017	Unit shut down after first pulse after transfer.
Test 011-4.1-018 10/8/69	The magnetic pickup connection to the speed control was disabled and the unit operated successfully. A normal shutdown was initiated after 46 pulses.

The voltage regulator was reconnected but the magnetic pickup to the speed control was still disabled.

Test 011-4.1-019
10/8/69

The cell pressure was reduced to 0.55 mm Hg. At no load operation, the voltage output was 29.5 VDC. The field voltage and current were 6 volts and 5.3 amps respectively. Intermittent loads of 0.5, 1.5, 3.0, 4.0 were applied. The unit operated satisfactorily. After 28 minutes or 85 pulses of operation, the unit was shut down.

The pressure switch was reconnected. However, the pressure switch delay circuit was changed by removing the 274K ohm resistor. The over voltage safety circuit was armed and the magnetic pickup was backed out approximately 1/4 turn but was not connected to the speed control circuit. The axial accelerometer was relocated in the right front alternator mounting bracket.

Test 011-4.1-020

The unit shut down on the 20th pulse.

The pressure switch was disconnected.

Test 411-4.1-021
10/8/69

A normal run was conducted consisting of 52 pulses or 10 minutes of running.

The unit was returned to Cleveland for disassembly made necessary by imbalance. The electrical safety circuitry problems were reviewed and corrected by adjusting the gap between the magnetic pickup and the pickup gear. The gap was set at .030 inches.

The rotating assembly was rebalanced on a Bear balancing machine at 3500 RPM and checked out in the fully assembled condition at 15,000 RPM. The HEPS was reinstalled at Roanoke. The instrumentation was connected and 2.5 quarts of oil were added to the separator.

Test 011-4.1-022
10/30/69

The cell pressure was reduced to 0.55 mm Hg and testing commenced. Total test time was 10 minutes or 42 pulses.

The unit was shut down to add oil and to alter the gap setting of the magnetic pickup. Vibration levels on all three axes was 44 g's maximum occurring at the time of the pulse. The magnetic gear gap was set at .023 inches and one quart of oil was added to the system (3.5 quarts total).

Test 011-4.1-023
10/30/69
10/30/69

Cell pressure was reduced to 0.55 mm Hg. The unit was pulsed at no-load for 41 minutes or 116 pulses with a normal shutdown occurring. The vibration levels were 45 g's in all axes.

The front of the HEPS was braced to the bottom of the altitude chamber in the vertical plane. The horizontally measuring accelerometer was repositioned on the frame (near rear shock mount) to measure vertical accelerations. In order to evaluate system stiffness, a shock load was applied by tapping the top edge of the cold plate. The vibration output was 20 g's. After adding the vertical brace, the same shock load yielded only 1.0 g's.

Test 011-4.1-024
10/31/69

The cell pressure was reduced to 0.55 mm Hg. The unit was started and transfer occurred at thr 28th pulse. The following test profile was used:

10:00 Hrs.	Normal start
10:09 Hrs.	Applied 1.0 KW load
10:33 Hrs.	Dropped off 1.0 KW load
10:35 Hrs.	Normal shutdown after 35 minutes or 151 pulses running time

A side brace was added to decrease horizontal vibration levels. The brace con-

nected the cell wall to the right top frame member.

Test 011-4.1-025
10/31/69

The cell pressure was reduced to 0.50 mm Hg prior to start. The following sequence of events followed:

13:04 Hrs.	Normal start
13:20 Hrs.	Applied 1.0 KW load
13:38 Hrs.	Dropped load and shutdown after 34 minutes or 128 pulses running time

The vibration level remained at 40-50 g's. The oil flow to the bearings was altered so that oil flow influence on vibration levels could be evaluated.

The relief valve was set to allow maximum bypass flow at 25 PSIG inlet pressure to the relief valve. The side brace was removed.

Test 011-4.1-026
11/3/69

The cell pressure was reduced to 0.45 mm Hg. The unit was started with transfer occurring after 24 pulses. After seven minutes or 34 pulses the unit was shut down. No improvement in vibration levels were noted with a 20% reduction in flow to the bearings.

The braces were removed and the pressure relief valve was readjusted to 40 PSIG bypass pressure.

Test 011-4.1-027

The cell pressure was reduced to 0.45 mm Hg and the unit was run for 44 minutes or 270 pulses. The test sequence was as follows:

15.33 Hrs.	Normal start
15.39 Hrs.	No load operation
15:40 Hrs.	1.0 KW load applied
15.47 Hrs.	2.0 KW load applied

15:56 Hrs. 3.0 KW load applied

16:12 Hrs. All load dropped

16:17 Hrs. Shutdown

Test 011-4.1-028
11/5/69

Cell pressure was reduced to 0.35 mm Hg. The following test schedule was followed:

11:09 Hrs. Normal start

11:25 Hrs. 3.0 KW load applied

11:31 Hrs. Load removed

11:34 Hrs. Normal shutdown

The test was 25 minutes or 112 pulses duration.

Test 011-4.2-001
11/5/69

The cell pressure was reduced to 0.45 mm Hg. This test was the Acceptance Test for the Qualification Unit. The testing was done in accordance with ER-7380, "TRW Acceptance Test Plan for the Qualification Unit". The wall temperature in the altitude chamber was maintained at 77 ± 5°F. The test duration was two hours, 44 minutes or 829 pulses.

Test 011-4.2-002
11/6/69

The cell pressure was reduced to 0.85 mm Hg. The unit was operated for 3.5 hours at 1.0 KW low O/F at which time thermal stability was established. Operation was switched to the high O/F ratio at 1.0 KW and run for an additional 1 hour, 18 minutes for a total run time of 4 hours and 43 minutes or 1163 pulses.

The visual inspection of the unit rev vealed that pin hole leaks existed in two places on the oxidizer manifold tube at the weld joint. Also, the pump inlet lube line was rubbing on the rear vertical frame member. The oil line was bent away from the frame and an adapter piece replaced the oxidizer manifold.

Test 011-4.2-003
11/7/69

The cell pressure was reduced to 0.5 mm Hg. The following test sequence was followed:

12:54 Hrs. Startup on low O/F

13:10 Hrs. Added 1.0 KW load

13:20 Hrs. 2.0 KW load applied

13:30 Hrs. 3.0 KW load applied

13:50 Hrs. 2.0 KW load applied

14:00 Hrs. 1.0 KW load applied

14:09 Hrs. Shutdown

The unit was shut down because of low oil pressure and flow. A broken oil line was found and replaced. The apparent cause of failure was fatigue from the high vibration levels. The oil lines between the rotating assembly and the frame were replaced with flexible teflon lined lines. An .031 inch diameter orifice was inserted in the roller bearing line.

Test 011-4.2-004
-005
-006

The cell pressure was reduced to 0.55 mm Hg. The following test sequence was followed:

09:00 Hrs. Startup and shutdown because overspeed pickup was inadvertently not connected

09:11 Hrs. Startup

09:27 Hrs. Shutdown-No vibration level changes resulted from reduced roller bearing oil flow. The alternator cooling jacket orifice was increased from .055 to .070 inches diameter to evaluate redirected oil flow effect.

10:06 Hrs. Startup

10:15 Hrs. Applied 1.0 KW at low O/F

10:32 Hrs. Shutdown to repair oil leak in roller bearing area.

11:42 Hrs. Startup

11:46 Hrs. Applied 1.0 KW at low O/F

11:56 Hrs. Applied 2.0 KW at low O/F

12:17 Hrs. Applied 3.0 KW at low O/F

12:27 Hrs. Applied 2.0 KW at low O/F

12:32 Hrs. Shutdown

The oil was drained from the unit and the propellant system was purged. After removal from the altitude chamber the the unit was shipped to Cleveland.

Total running time was 14 hours.

Two pulses were fired on the low 0/F side.

Test 018
1/30/69 Two secondary tanks were precharged to 75 psig. Two pulses were fired on each side, T_f = 63°F; T_{ox} = 62°F; $P_f = P_{ox}$ = 200 psig.

Test 019
1/30/69 The secondary tanks were precharged to 100 psig with N_2. Two pulses were fired on each side.

Inlet pressure: 200 psig

Inlet temperature: 64°F

Test 020
1/30/69 The secondary tanks were precharged to 100 psig with N_2. Inlet pressures and temperatures were introduced at 200 psig and 65°F, respectively. Fired 17 pulses on the low 0/F side and recorded pulses 12 and 16. Fired 15 pulses on high 0/F and recorded pulses 8 and 15. The altitude during the test was 0.55 mm Hg (166,000) ft). The results were:

Side	$\dot{\omega}_{Ox}$, lb/sec	$\dot{\omega}_{Fuel}$, lb/sec	0/F	Pc, psia
Low 0/F	.147	.175	.84	97
High 0/F	.223	.112	2.0	123

Test 021
1/30/69 The following orifices were installed:

	Ox	Fuel
Low 0/F	-8(.089)	-11(.1405)
High 0/F	-12(.161)	-3(.076)

The secondary tanks were precharged with 100 psig N_2 and the inlet pressures were 200 psig.

Pulsing was initiated on the low 0/F side.

Pulse 14 - T_f = 84°F, T_{ox} = 91°F

Pulse 21 - T_f = 90°F, T_{ox} = 100°F

Shutdown after 21 pulses and commenced firing on the high 0/F side.

Pulse 7 - T_f = 91°F, T_{ox} = 99°F

Pulse 13 - T_f = 94°F, T_{ox} = 95°F

Pulse 22 - T_f = 95°F, T_{ox} = 92°F

Shutdown after 26 pulses.

The resulting data was:

Side	$\dot{\omega}$ Ox, lb/sec	$\dot{\omega}$ Fuel, lb/sec	O/F
Low O/F	.1680	.1610	1.045
High O/F	.2320	.1100	2.11

Test 022
1/30/69

The orifices were changed as follows:

	Ox	Fuel
Low O/F	-6(.082)	-12(.161)
High O/F	-11(.1405)	-3(.076)

Pulsing was initiated on the low O/F side at altitude. The inlet temperatures were 70°F. At shutdown-T_f = 80°F, T_{ox} = 80°F. During the test, pulsing was changed to the high O/F side.

The secondary tanks were prepressurized to 100 psig N_2. The inlet pressures were 200 psig. The results were:

Low O/F	High O/F
Fuel = .1745 lb/sec	Fuel = .112 lb/sec
Ox = .140 lb/sec	Ox = .2250 lb/sec

Test 023

The prepressure on the oxidizer secondary tank was changed to 150 psig N_2. The fuel was unchanged. Pulsing was started on the low O/F side. Recorded one pulse on both sides. Changed to high side pulsing at No. 17 pulse. At No. 24: T_f = 75°F, T_{ox} = 80°F. Shutdown at pulse No. 25. The results were:

Low O/F	High O/F
Fuel = .1745 lb/sec	Fuel = .112 lb/sec
Ox = .140 lb/sec	Ox = .12250 lb/sec
O/F = 0.802	O/F = 2.01

Test 024
1/31/69

The orifices were changed to

Low O/F	High O/F
Fuel = -12(.161)	Fuel = -3(.076)
Ox = -7(.086)	Ox = -11(.1405)

The secondary tanks were precharged to 100 psig N_2. The main tank pressure was 200 psig. The test was run at altitude with automatic pulsing. Inlet temperature: 62°F.

The unit was started on the low 0/F side.

Pulse No. 1 - 67° and 65°F temperature (propellant)

Pulse No. 2 - T_f = 71°F, T_{ox} = 65°F

Altitude: .15 mm Hg.

The unit was then pulsed on high 0/F side where two pulses were recorded.

Pulse No. 6 - T_f = 72°F, T_{ox}= 75°F (low 0/F pulsing)

Pulse No. 9 - T_f = 79°F, T_{ox}= 80°F (high 0/F pulsing)

Test 025
1/31/69

The secondary tanks were bypassed. Tank pressure was 200 psig. The same orifices were used as in Test 024.

Pulse No. 6 - T_f = 75°F, T_{ox}= 80°F (low 0/F pulsing)

Pulse No. 6 - T_f = 76°F, T_{ox}= 81°F (high 0/F pulsing)

Test 026
1/31/69

The main tanks were bypassed and the pressure source was the secondary tanks. Same orifices were used as in Test 025.

Pulse No. 8 - T_f = 70°F, T_{ox}= 81°F (low 0/F pulsing)

Pulse No. 13 - T_f = 71°F, T_{ox}= 83°F (high 0/F pulsing)

Test 027
1/31/69

High 0/F ratio temperature stabilization test.

Altitude: 0.52 mm Hg.

Automatic pulsing: 0.2 sec. on, 8.8 sec. off.

Inlet pressures: 200 psig

Secondary tanks were prepressurized to 100 psig N_2.

Pulse No. 39 - $T_f = T_{ox} = 83^oF$

Pulse No. 134 - $T_f = 85^oF$, $T_{ox} = 88^oF$

Pulse No. 397 - $T_f = 85^oF$, $T_{ox} = 90^oF$

Shutdown after 398 pulses.

Temperatures were monitored for heat soakback. The injector temperature reached a maximum of 220°F. The plate coil water flow was utilized for heat sink during this test.

After Test No. 027 the chamber was opened and the gas generator inspected. There was evidence of a propellant leakage around the Moog valve. The valve assembly was removed from the gas generator and disassembled. The cover on the high O/F valve was removed. It was found that the cavity was filled with oxidizer. Testing was stopped and the Moog valve was returned to Cleveland. The gas generator and scroll assembly were also removed from the chamber and returned to Cleveland.

APPENDIX B

DVR SYSTEM TESTS

Prior to operation of the complete system, checkouts will be performed on the subsystems and components. The unit was installed in the altitude chamber and all instrumentation was readied.

Test 010-4.1-001
3/21/69

The altitude chamber pressure was reduced to 0.35 mm Hg. Startup procedure was initiated. Gas generator chamber pressure pulse was not observed. After shutdown a relay with dirty contacts was found to be the problem. After cleaning, the unit was restarted. Eight pulses were fired at the low O/F ratio. The turbine speed was 12,000 rpm. Visual inspection after shutdown indicated no difficulties.

Test Running Time - 0.8 minutes

Accumulated Running Time - 0.8 minutes

Test 010-4.1-002
3/21/69

The unit was started again at 0.35 mm Hg pressure. The turbine speed was 22,000 rpm after 15 pulses. Visual inspection revealed no difficulties.

Test Running Time - 1.5 minutes

Accumulated Running Time - 2.3 minutes

Test 010-4.1-003
3/21/69

Fifteen pulses were fired at the low O/F ratio. The H-P meter reading was compared to the AC frequency meter. The two readings were in agreement. The oil flow and pressures appeared to be low from the indicated readings when compared to previous readings. The turbine wheel coasted 20 minutes after shutdown. Visual inspection revealed that the orifice in the scavenge line was missing.

Test Running Time - 1.5 minutes

Accumulated Running Time - 3.8 minutes

Test 0.0-4.1-004
3/21/69

Fifteen pulses were fired at the low 0/F ratio. The turbine speed was 23,000 rpm. Altitude for this test was 0.3 mm Hg.

Test Running Time = 1.5 minutes

Accumulated Running Time - 5.3 minutes

An .080 inch diameter orifice was inserted in the oil scavenge line.

Test 010-4.1-005
3/26/61

The altitude chamber pressure was reduced to 0.3 mm Hg. Eight pulses were fired at the low 0/F ratio. The turbine speed was 12,000 rpm. This test was conducted for the purpose of lube system checkout.

Test Running Time - 0.8 minutes

Accumulated Running Time - 6.1 minutes

Test 010-4.1-006
3/26/69

Altitude chamber pressure was 0.4 mm Hg. Ten pulses were fired at the low 0/F ratio to check out lube system performance.

Turbine speed was 16,000 rpm.

Test Running Time - 1.0 minutes

Accumulated Running Time - 7.1 minutes

Test 010-4.1-007
3/26/69

At an altitude of 0.4 mm Hg, 16 pulses were fired at the low 0/F ratio to check out the lube system performance. The turbine speed was 26,000 rpm.

Test Running Time - 1.6 minutes

Accumulated Running Time - 8.7 minutes

Test 010-4.1-008
3/27/69

Altitude chamber pressure was 0.45 mm Hg. The lubrication system was installed with a high pressure vent, a supply line off center of the separator and 1/4 inch diameter line between the separator and pump inlet. The unit was run for 70 pulses with a transfer from the startup circuit to the speed control occurring after pulse number 24.

Test Running Time - 25.0 minutes

Accumulated Running Time - 33.7 minutes

The lubrication system supply line from the separator to the pump inlet was changed from 1/4 inch to 3/8 inch diameter.

Test 010-4.1-009
3/27/69

The altitude chamber pressure was 0.55 mm Hg at the start of the run but decreased to 0.45 mm Hg after 70 pulses. At the 70th pulse, the no-load coast time was 35.0 seconds. The initial coast time was 28.4 seconds. Total number of pulses was 85.

Test Running Time - 33.0 minutes

Accumulated Running Time - 66.7 minutes

The substitution of the 3/8 inch for the 1/4 inch diameter line resulted in oil flows up to 1.0 gpm.

Test 010-4.1-010
3/27/69

The altitude chamber pressure was 0.45 mm Hg at startup. The system transferred from startup to speed control after pulse 23. Seventy pulses were fired.

Test Running Time - 25.0 minutes

Accumulated Running Time - 91.7 minutes

Test 010-4.1-010
3/28/69

Testing was conducted according to the test sequence in the DVR test plan. The altitude reading in the chamber was 0.5 mm Hg. The unit was started up at the low O/F ratio and transferred after the 25th pulse. After pulse 63, the unit was switched to high O/F operation. After pulse 94, the unit was switched back to low O/F operation. At pulse 100, 1 KW

load was applied. At pulse 137 normal shutdown was initiated to check vibration sources and malfunctioning flowmeters.
Test Running Time - 54.0 minutes

Accumulated Running Time - 2 hours - 25.7 min

Many nuts were found to be loose after testing. It was concluded that thermal expansion was the major cause. All connectors and fasteners were tightened prior to further testing.

Test 010-4.1-012
3/28/69

Altitude reading at startup was 0.85 mm Hg but decreased to 1.05 mm Hg after pulse 30. Transfer occurred after pulse 22. The following test schedule was implemented.

1246 hrs - Startup at low 0/F ratio.

1251 hrs - Switches to high 0/F ratio at 28 pulses.

1253 hrs - 1 KW load applied at high 0/F ratio and 32nd pulse.

1338 hrs - 2 KW load applied at high 0/F ratio and 179th pulse.

1408 hrs - 1 KW load at high 0/F and 330th pulse.

1450 hrs - 1 KW load applied at low 0/F pulse.

1501 hrs - 2 KW load applied at low 0/F and 511th pulse.

1530 hrs - Altitude at 1.05 mm Hg.

1555 hrs - 2.5 KW load applied at low 0/F and 814th pulse.

1616 hrs - 3.0 KW load applied at low 0/F and 952nd pulse.

1630 hrs - Dropped load to 0 KW at low 0/F and 1060th pulse.

1640 hrs - Normal shutdown commenced after pulse 1080.

Test Running Time - 3 hrs - 54.0 minutes

Accumulated Running Time - 6 hrs - 19.7 min.

A 20 psi vent valve leakage was corrected and reinstalled in the top of the oil separator. One radiator (number 2) was removed from the lubrication system. The oil will only circulate through the number 1 radiator. The .080 inch diameter orifice in the scavenge line was replaced with a .070 inch diameter orifice. The propellant line orifices were removed from the high 0/F oxidizer side and the low 0/F ratio fuel side.

Test 010-4.1-013
4/1/69

Unit was started at the low 0/F ratio with transfer occurring after 25 pulses. High 0/F ratio operation commenced after pulse 78. System shutdown was initiated after pulse 113.

Test Running Time - 53 minutes

Accumulated Running Time - 7 hours - 12.7 min

Test 010-4.1-014
4/2/69

Unit was started at the low 0/F ratio and transferred to automatic after 25 pulses. Pulsing was switched to high 0/F operation after pulse 77. One KW load was applied at pulse 124. Two KW load was applied at pulse 227. Unit was shutdown after pulse 308 because the thermocouple on the rectifier cold plate diode was loose. The transducer in the gas generator; chamber was found to be leaking through the diaphragm. The transducer was removed and the boss was plugged. The low 0/F oxidizer orifice was changed to 0.1225 in. diameter and the high 0/F fuel orifice was changed to 0.0685 inch diameter.

Test Running Time - 1 hour - 45 minutes

Accumulated Running Time - 8 hours - 57.7 min

Test 010-4.1-015
4/2/69

The altitude varied from 0.3 to 0.9 mm Hg during the test. The testing schedule was as follows:

1433 hrs - Startup at low 0/F and transferred after pulse 21.

1445 hrs - Pulsing was switched to high 0/F operation after pulse 39.

1500 hrs - 2 KW load applied at the high 0/F after pulse 63.

1620 hrs - Unit operation was switched to the low 0/F side with a 2 KW being applied after pulse 471.

1720 hrs - 3 KW load was applied after pulse 776.

1820 hrs - Load was dropped to 2 KW after pulse 1197.

1826 hrs - The load was reduced to 0 KW for 15 seconds, after which followed 3 KW spikes. The spikes were applied on and off for 15 seconds. This procedure was repeated 5 times before a 2 KW load was reapplied.

1835 hrs - The load was dropped to 1.5 KW for 15 seconds and then followed by five 3.5 KW spikes having 15 second on and off times. 2 KW load was then reapplied.

1846 hrs - The load was dropped to 0 KW for 15 seconds after which followed five 3 KW spikes of 15 second duration each. 2 KW was reapplied.

1852 hrs - The load was reduced to 1.5 KW for 15 seconds. Five 3.5 KW spikes were applied for 15 seconds duration each. 2.0 KW was reapplied.

1921 hrs - Shutdown after 1620 pulses.

Test Running Time - 4 hrs - 59 minutes

Accumulated Running Time - 13 hrs - 56.7 min.

The separator vent check valve was inspected and O-ring leakage was found. The O-ring was replaced and the system was pressure checked up to 15 psig at which pressure the valve relieved. The oil level remained the same. The 0.9 0/F oxidizer orifice size was changed from 0.128 to 0.100 inch diameter. New fitting seals were installed to eliminate oxidizer leakage. The Kistler transducer was removed and the port was plugged.

Test 010-4.1-016
4/3/69

The altitude reading fluctuated between 0.38 mm Hg to 0.60 mm Hg during the test. The testing sequence was as follows:

1022 hrs - Startup was initiated with transfer occurring after pulse 23.

1030 hrs - 2 KW load was applied with the low O/F ratio operation after pulse 36.

1130 hrs - 3 KW load was applied. The pulse counter malfunctioned.

1145 hrs - The plate coil temperature was regulated to 160°F. The hose on top of the altitude chamber used for circulating heated water came loose. The heating system was shut down.

1212 hrs - The load was reduced to 2 KW.

1230 hrs - The load was removed from 15 seconds followed by five 3 KW spikes, each spike lasting 15 seconds.

1233 hrs - The load was increased to 2 KW.

1238 hrs - The load was reduced to 1.5 KW for 15 seconds and followed by five 4.5 KW spikes each lasting 15 seconds.

1241 hrs - The load was increased to 2 KW.

1244 hrs - The load was removed for 15 seconds followed by five 3 KW spikes each lasting 15 seconds.

1247 hrs - The load was increased to 2 KW.

1300 hrs - The load was decreased to 1.5 KW for 15 seconds followed by five 4.5 spikes each lasting 15 seconds.

1302 hrs - 2 KW load was reapplied.

1305 hrs - The pulsing mode was transferred to the high 0/F ratio valve and 2 KW load was applied.

1411 hrs - The load was removed.

1422 hrs - Normal shutdcwn occurred.

Test Running Time - 4 hours

Accumulated Running Time - 17 hrs - 56.7 min.

1. Two thermocouple switches and a millivolt readout were installed for measuring the electrically-hct copper/constantan thermocouples on the cold plate.

2. The cold plate was relocated approximately 6 inches back toward the rear of the flight package.

3. The following c/c thermocouples were installed:

   a) Lower Diode - Panel A

   b) Lower Diode - Panel B

   c) Lower Diode - Panel C

   d) Midpoint of Cold Plate Mounting Angle

   e) AC lead at Splice (Diode Side)

4. Installed a 0.055 inch diameter orifice on the high 0/F fuel side.

5. Repaired plate coil thermocouples.

6. Installed an 18-20 psi one-way check valve in place of the separator vent valve.

7. A pressure gage was added to the separator tank at the port marked fill vent located at the bottom of the separator.

8. A new Dynisco pressure transducer was installed in the gas generator chamber (after dead weight calibration).

Test 010-4.1-017
4/10/69

The initial altitude reading was 0.32 mm Hg.

0933 hrs - The system was started and transfer occurred after pulse 23.

0940 hrs - 3 KW load was applied.

1020 hrs - The electrical plug in the over-temperature controller became loose and shut the unit down.

1028 hrs - The unit was restarted even though the turbine speed was 21,000 rpm. Transfer occurred after 10 pulses.

1029 hrs - 3 KW load was applied.

1240 hrs - Pulsing was switched to high 0/F and 2 KW.

1320 hrs - The unit was shutdown to check the injector.

T_{inj} = 193°F

Test Running Time - 3 hrs - 47 minutes

Accumulated Running Time - 21 hrs - 43.7 min.

Visual inspection revealed that both oxidizer and fuel flowmeters were malfunctioning. They were replaced with Flowcon flowmeters that were used in Phase II. S/N 30 and 32 were used in the oxidizer and fuel side, respectively. The gas generator pressure transducer was removed. All accelerometers except those water-cooled were removed because of the high metal temperatures (250°F). The water-cooled accelerometers are located on the pump housing.

Test 010-4.1-018
4/11/69

The chamber altitude reading was 0.75 mm Hg.

0856 hrs - The unit was started and transfer occurred at pulse 23. Pulsing was initiated on the low 0/F side and a no-load condition.

0901 hrs - 3 KW load was applied at low 0/F.

1130 hrs - 2 KW load was applied at high 0/F.

1210 hrs - 2 KW load was applied at low 0/F.

1232 hrs - 1 KW load was applied at low 0/F.

1252 hrs - 1 KW load was applied at high 0/F.

1318 hrs - 3 KW load was applied at high O/F.

1351 hrs - 2 KW load was applied at high O/F.

1420 hrs - 3 KW load was applied at low O/F.

1436 hrs - 1 KW load was applied at high O/F.

1456 hrs - Shutdown after 2175 pulses.

Test Running Time - 6 hours

Accumulated Running Time - 27 hrs. - 43.7 min

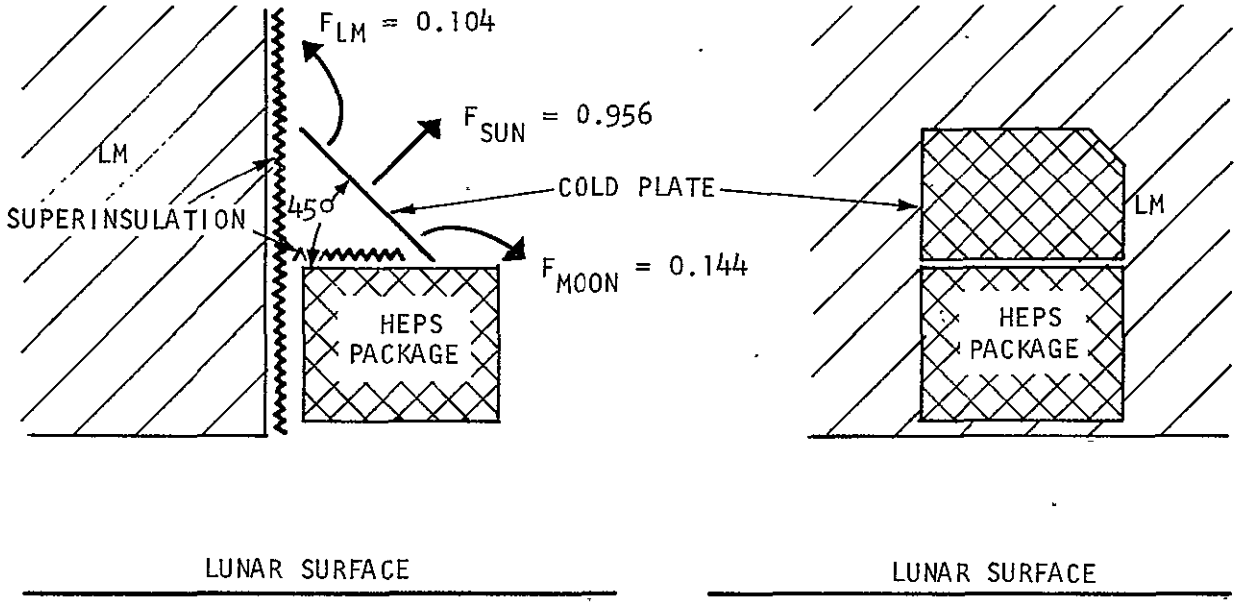
After Test 010-4.1-018, the altitude chamber pressure was held at 0.65 mm Hg and the vacuum pump was used to pump down the lubrication system pressure to 2-3 psia. A simulated lunar startup was planned.

Test 010-4.1-019
4/11/69

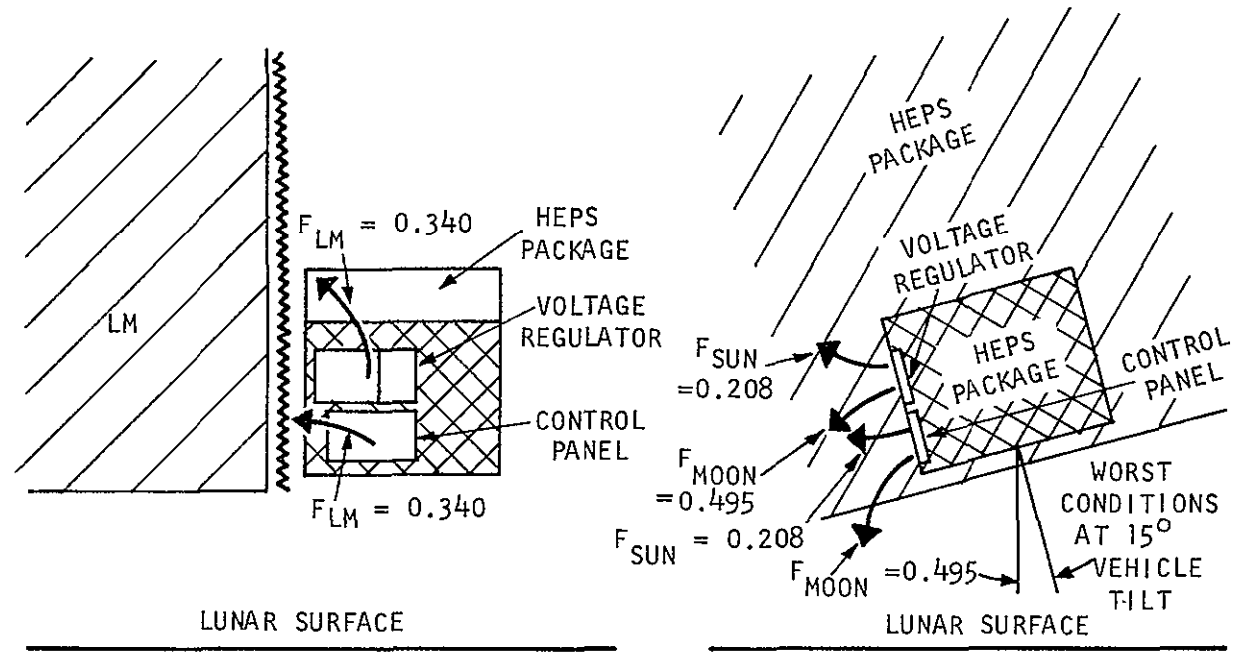
The unit was started at 1529 hours on the low O/F side and no-load. After 28 pulses, the unit was shut down. The oil pressures did not increase but the oil flowmeter indicated that adequate flow was available.

Test Running Time - 7 minutes

Accumulated Running Time - 27 hrs - 50.7 min.



RECTIFIER COLD PLATE



VOLTAGE REGULATOR AND CONTROL PANEL

FIGURE C-1 VIEW FACTORS AND ORIENTATION

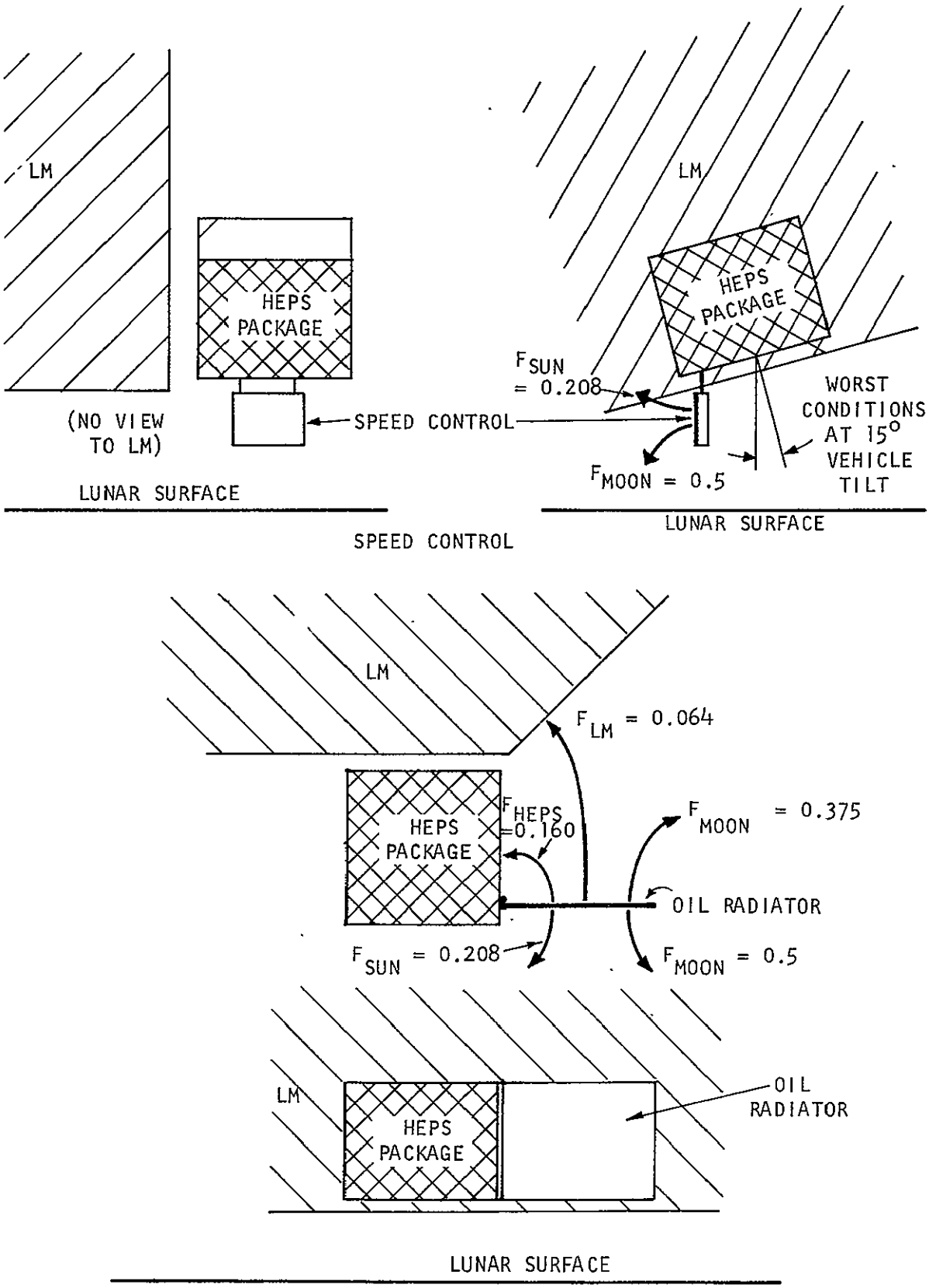


FIGURE C-2 VIEW FACTORS AND ORIENTATION (CONTINUED)

GLOSSARY OF TERMS

O/F	Ratio of oxidizer to fuel flow
DVR	Design Verification Retest
ALSEP	Advanced Lunar Scientific Equipment Package
SEQ Bay	Scientific Equipment Bay
V_D/V_P	Ratio of the dribble volume to the propellant volume per pulse.
V_D	Propellant volume per pulse, in^3
V_P	Dribble volume, in^3, is the volume that exists between the downstream side of the control valve and the combustion chamber.
Phase I	Initial Power System Development Program Contract NAS 9-4820 (1965-1966)
Phase II	Continued Power System Development Program Contract NAS 9-6879 (1967-1968)
Phase III	Power System Qualification Program Contract NAS 9-8247 (1968-1969)
HEPS	Hypergolic Electric Power System
Flight Package	Structural members that form an envelope for the HEPS components
DVR Unit	The prototype hardware that simulated the final configuration which was development tested
Qualification Unit	The assembly that consisted of hardware in the final configuration which was Acceptance Tested
DVR Tests	A series of Development Tests that simulated end use
Acceptance Tests	A series of tests that were representative of the end use and were designated as the criteria for unit acceptance
N_2O_4	Nitrogen Tetroxide, oxidizer

Aerozine-50	50% Hydrazine and 50% Unsymmetrical Di-Methyl Hydrazine by weight, fuel
GAEC	Grumman Aircraft and Engineering Corporation
VQR	Vendor Quality Requirements
NASA/MSC	National Aeronautics and Space Administration - Manned Spacecraft Center
SPC	Specific Propellant Consumption, LB/KW-HR
CEC	Consolidated Electronics Corporation
LM	Lunar Module
Hard Points	Pins located in the SEQ Bay of the LM that provide attachment points for the HEPS unit
Electrical System Efficiency	Efficiency of the alternator and rectifier filter
P	Pressure, psig
ΔP	Pressure drop, psi
ΔP_{fs}	Pressure drop across the phase separator screen, psi
ΔP_h	Hydrostatic pressure drop in phase separator, psi
f	Phase separator screen friction factor
ΔP_σ	Surface tension pressure drop, psi
g_c	Gravitational constant, $\frac{Lb_m\text{-ft}}{Lb_f\text{-sec}^2}$
ρ	Density, lb/in^3
η	Efficiency
σ	Surface tension of phase separator screen
μ	Dynamic viscosity

D	Phase separator screen pore diameter
β	Screen thickness of the phase separator, in
ϵ	Void fraction in the phase separator screen
A	Surface area to volume ratio for phase separator screen
U	Fluid approach velocity, in/sec
α	Solar absorptance
ϵ_1	Emissivity
(Q/A)	Incident Energy transferred to a component, Btu/hr-ft^2.
F	View Factor
I	Emitted energy from source
T	Temperature, ^{0}F
k	Thermal conductivity, Btu/hr-ft-^{0}R
t	Plate thickness, ft
L	Generalized length parameter
l	Plate length, ft
σ_1	Stefan-Boltzmann constant, Btu/hr-ft^2-^{0}R^4
Q	Heat rejection rates Btu/hr
mm Hg	Millimeters of mercury, mm
RPM	Revolutions Per Minute
$\dot{\omega}_f$	Fuel flow rate, lb/second
$\dot{\omega}_{ox}$	Oxidizer flow rate, lb/second
FMEA	Failure Mode and Effects Analysis
R_T	Turboalternator Reliability
R_L	Lubrication System Reliability

R_G	Gas Generator Reliability
R_E	Electrical System Reliability
R_F	Flight Package Reliability
R_H	HEPS Reliability
R_S	Startup Reliability
R_O	Operation Reliability
R_D	Shutdown Reliability
R_R	Flex Hose Reliability
R_{S_1}	Valves Switching Reliability
R_C	Combustion Chamber Reliability
R_A	Propellant Valve Reliability
R_I	Injector Reliability
DS1	Indicator light on control panel
DS2	Indicator light on control panel
DS3	Indicator light on control panel
DS4	Indicator light on control panel

LIST OF REFERENCES

1. ER-7249, "Continued Development of a Hypergolic Electrical Power System, Final Final Report", Contract NAS 9-6879, TRW Equipment Laboratories, March 1968.

2. "Surveyor Spacecraft Model A-21 Equipment Specification 224832," pg 3-23.

3. "Thermal Control Design Manual," TRW Systems, July 8, 1966.

4. "Radiant Interchange Configuration Factors," D.C. Hamilton & W.R. Morgan, NACA TN 2836.

5. "Analysis of Temperature Distribution and Radiant Heat Transfer Along a Rectangular Fin of Constant Thickness," S. [illegible], NASA TN D-194.

6. "BTR Elastomeric Mountings," Bulletin No. 501, Lord Manufacturing Company.

7. "Determinations of the Emissivity of Materials," Report PWA 3278, Final Report, Contract NAS 3-4174, June 30, 1968.

8. "Fluid Flow Through Porous Systems," [illegible] Mount, M. W. Cannon, AIChE Journal, Vol. 12, No. 3, p. 611, May 1968.

9. ER-7247, "Design Verification Retest Plan for Hypergolic Electrical Power System," TRW Inc., November 1968.

10. ER-7270-1, "Final Quality Assurance Plan for Hypergolic Electrical Power System," Contract NAS 9-8247, TRW Inc., August 1968.

11. ER-7270-3A, "HEPS High Reliability Parts Program," Contract NAS 9-8247, TRW Inc., November 1968.

12. ER-7270-5B, "Approved Parts List for HEPS," Contract NAS 9-8247, TRW Inc., April 30, 1969.

13. ER-7270-2B, "Failure Modes and Effects Analysis for the HEPS Program," TRW Inc., Contract NAS 9-8247, April 15, 1969.

14. ER-7270-7C, "Critical Items for HEPS," TRW Inc., Contract NAS 9-8247, April 1969.

15. ER-7181, "Turbine Wheel Failure Rate Analysis for the HEPS Program," TRW Inc., Contract NAS 9-6879, July 22, 1967.

16. ER-7270-8, "Reliability Analysis for the HEPS," TRW Inc., Contract NAS 9-8247, June 9, 1969.

17. "KAPTON," Tradename for a Polyimide Film manufactured by the Du Pont Company, Wilmington, Delaware.

TRW®

MECHANICAL PRODUCTS DIVISION

TRW®

MECHANICAL PRODUCTS DIVISION